Senescence of human skeletal muscle derived cells

Francis, Thomas

Awarding institution:
King's College London

SENESCENCE OF HUMAN SKELETAL MUSCLE DERIVED CELLS

A thesis submitted for the degree of Doctor of Philosophy at King's College London

Thomas Francis

Centre for Human & Applied Physiological Sciences

School of Basic & Medical Biosciences

Faculty of Life Sciences & Medicine

King's College London

· 2020 ·

Abstract

Cellular senescence is a cell fate characterised by the permanent arrest from the cell cycle with an altered, mainly proinflammatory, secretory phenotype. Although, a positive process in development and regeneration, the accumulation of senescent cells, as seen in tissues of aged humans, can cause many negative effects. Within skeletal muscle the resident stem cells, $Pax7^{+ve}$ and $CD56^{+ve}$ satellite cells / muscle precursor cells (MPCs), are essential for muscle maintenance and repair following damage. Impairments either in their inherent behaviour, such as by being senesced, or by being negatively influenced by their environment, such as by the senescence associated secretory phenotype (SASP) of local senescent cells, may impair muscle regeneration in later life and contribute to the age-related loss of skeletal muscle mass, sarcopenia. Furthermore, regeneration is also dependent on the interaction of MPCs with other key cell types in muscle, principally fibroblasts, therefore understanding the senescent characteristics of both cell types is essential to gain further insight into skeletal muscle ageing. Currently, little is known about the senescent phenotype of human skeletal muscle derived cells.

The aim of the work in this thesis was thus to investigate the senescent phenotype of human primary skeletal muscle derived MPCs and fibroblasts in a primary cell culture system. Once characterised this phenotype would then be used to investigate senescence within skeletal muscle cells obtained from very old and frail hip fracture patients. MPCs were sorted using $CD56^{+ve}$ magnetic beads after extraction and expansion from muscle biopsy samples taken from young healthy male volunteers (n=6, 22±1 years). Fibroblasts were derived from the negative fraction. In the first series of experiments cumulative population doublings (CPD) across multiple passages was used to induce cellular replicative senescence (RS). In the second, cells were treated with Doxorubicin (DOX; 0.2 μM) for 24h to induce a senescent phenotype and then investigated at a number of timepoints up to 35 days post treatment. In both approaches, senescence was determined by the presence of senescence-associated β-galactosidase (SA β-gal) and the protein expression of p16, together with the absence of proliferation marker, Ki67. With expression determined using custom built cell-by-cell image analysis programs. The mRNA levels of established SASP factors (e.g. PAI-1, TGF-β1, IL-8 and IGFBP-3, amongst others) were also measured as was the differentiation capacity of MPCs for myogenic fusion.

In the RS study only two of the six MPC populations remained highly myogenic through to RS. Senescence of these two populations of MPCs was shown by increased number of SA β-gal-positive and p16 expressing cells, and decreased Ki67 expression. The senescent, late passage MPCs showed a markedly reduced myogenic fusion index, compared to proliferative MPCs. The fibroblast experiments were terminated at the same time as the equivalent MPC cultures reached senescence. At this point, none of the fibroblast populations had reached RS, as evidenced by no changes in SA β-gal or p16, although there was a trend for slower population doubling times when compared to early passage rates and significantly decreased Ki67. When both MPCs and fibroblasts were exposed to DOX for 24h, senescence was demonstrated shortly after, with 99% of both cell types being SA β-gal-positive four days after DOX treatment, Ki67 expression markedly reduced and MPCs being less able to fuse and form myotubes. SASP factor (i.e. IGFBP7, PAI-1, IGFBP3) mRNA expression from this 4-day time point until 35 days post-DOX treatment varied over time and magnitude in both MPCs and fibroblasts. MPCs isolated from skeletal muscle of old (82±9 yrs) hip fracture patients showed significant differences

in senescence marker and SASP factor expression, compared to young donor cells after a similar time in culture.

In conclusion, RS is hard to achieve in human primary muscle cultures because even highly purified MPCs populations can eventually be overrun by initially small populations of fibroblasts, whilst the sorted fibroblast cultures, from the same biopsy samples, appear to take a much longer time to reach RS than the MPCs. DOX treatment allows a synchronised and rapid induction of senescence in both cell types eliminating these problems. Here the results showed both varying temporal and quantitative responses of the different SASP factors between the two cell types. The data highlight the complexity and dynamism of the senescent state within different cell types derived from human skeletal muscle. When myoblasts are taken from a very elderly frail human population undergoing hip fracture surgery, markers of senescence are elevated compared to young myoblasts after similar exposure to cell culture. These findings suggest that cellular senescence may start to be an issue within skeletal muscle cells very late in life. Therefore, this work could contribute to supporting research into healthy human ageing by investigating strategies which prevent the accumulation, or remove, these senescent cells.

Acknowledgements

My first and most sincere thanks must go to Professor Stephen Harridge for his unwavering support throughout my PhD. His commitment to my development as a scientist and trust in my ability when I lost my own were crucial to me staying on track. I cannot thank Steve enough for the incredible opportunities he has exposed me to and the level of responsibility he entrusted to me within his research group. I would like to thank Dr Oihane Jaka for making this easier by being an excellent mentor in the lab and teaching me primary cell culture. I have learnt so much about ageing and research from discussions with Professor Norman Lazarus which have helped me to grow as a scientist, I look forward to having many more of them. I would also like to thank Professor Georgina Ellison-Hughes for instilling high standards and pushing me to achieve more. I am grateful to Lindsey Marjoram for her technical support and always getting things done. I was fortunate to be associated with the BBSRC LIDo Doctoral Training Programme which provided many great opportunities to develop holistically alongside my PhD and a cohort of extremely talented students to share the ride with. I am grateful to Nadine Mogford for making LIDo such an asset to my training and encouraging me to take an active role within the programme. The staff and students of CHAPS have always supported, guided and laughed with me over the last four and a half years; a special mention must go to Dr Yotam Levy for the hours of scientific discussions and close friendship we developed over our PhDs.

Alongside my PhD I was honoured to captain GHRFC, the oldest rugby club in the world, albeit briefly until that day in Oxford. Every PhD has its challenges but a six-month interruption for concussion was a new one even for Steve to deal with. I must thank him again for his patient support as I dealt with the fallout. I must also thank my friends, who bore the brunt of me during this time, for continuing to support me through the good times and the pain. You held me together when I felt like I was falling apart and stuck with me as I rebuilt. My final thanks go to my family for all they have done and sacrificed to help me get here. I would not have made it this far without your unconditional love and support for which I am incredibly grateful. I love the five of you very much.

This chapter has provided many challenges and I have learnt through many mistakes along the way. Yet, looking back at the experiences, opportunities and personal achievements I have accomplished I am proud and feel better prepared to deal with any challenges the future presents. I am very excited and privileged to be able to continue to work with and learn from both Steve and Norman in my first Post Doc. What's Next?

Table of Contents

Table of Figures

Table of Tables

Abbreviations & Acronyms

ADP	Adenosine diphosphate
ANOVA	Analysis of variance
ATM	Ataxia telangiectasia mutated kinase
ATR	Rad-3 related kinase
ATTAC	Inducible Casp8 apoptosis cassette
BrdU	Bromodeoxyuridine / 5-bromo-2'-deoxyuridine
BSA	Bovine serum albumin
CCD	Cooled charged coupled device
CD56 / NCAM	Neural cell adhesion molecule
CDK	Cyclin dependent kinase
cDNA	Complementary DNA
CHK	Checkpoint protein kinase
c-Met	Tyrosine-protein kinase Met
CPCs	Cardiac progenitor cells
CPD	Cumulative population doublings
CXCL-5	C-X-C motif chemokine 5
DAPI	4’,6-diamidino-2-phenylindole
DDR	DNA damage response
DMD	Duchene’s muscular dystrophy
DMF	Dimethylformamide
DNA	Deoxyribonucleic acid
DOX	Doxorubicin
ECM	Extracellular matrix
FACS	Fluorescence-activated cell sorting
FAPs	Fibro adipogenic progenitor cells
FGF2	Basic fibroblast growth factor
FIJI	Fiji Is Just ImageJ
FOV	field of view
GAPDH	Glyceraldehyde-3-Phosphate Dehydrogenase
GLUT4	Glucose transporter type 4
HF	Hip fracture
Hgf	Hepatocyte Growth Factor
ICC	Immunocytochemistry
IF	Immunofluorescence
IGF-1	Insulin-like growth factor 1
IGFBP-3	Insulin-like growth factor-binding protein 3
IGFBP-7	Insulin-like growth factor-binding protein 7
IHC	Immunohistochemistry
IL-18	Interleukin 18
IL-6	Interleukin 6
IL-8	Interleukin 8

LED	Light-emitting diode
MACS	Magnetic-activated cell sorting
MHC	Myosin heavy chain
MMPs	Matrix Metalloproteinases
MPCs	Myogenic precursor cells
MRF4	Myogenic regulatory factor 4
MRF6	Myogenic regulatory factor 6 / herculin
MRFs	Myogenic regulatory factors
MRI	Magnetic resonance imaging
MYF5	Myogenic factor 5
MyoD	myoblast determination protein 1
PAI-1	Plasminogen activator inhibitor-1
Pax7	Paired box protein 7
PBS	Phosphate-buffered saline
PDGFRα	Platelet Derived Growth Factor Receptor Alpha
PDs	Population doublings
PFA	Paraformaldehyde
RB	retinoblastoma protein
RNA	Ribonucleic acid
ROI	region of interest
RS	replicative senescence
RT q-PCR	real time quantitative polymerase chain reaction
SA β-gal	senescence associated beta galactosidase
SASP	senescence associated secretory phenotype
SD	Standard deviation
SPRTY-1	Sprouty RTK Signalling Antagonist 1
TGF-β	Transforming growth factor beta
TNF-α	Tumour necrosis factor alpha
VSMC	Vascular smooth muscle cells
γH2aX	H2A histone family member X

Introduction

On the subject of ageing, increased life expectancy of the global population is largely a result of advances in public health and medicine over the last 100 years. However, just living for longer is not always beneficial if the additional years are not accompanied by prolonged healthspan, the period of life where individuals are independent, active and disease free. In the UK, men and women are, on average, living 16-19 years in ill health at the end of their lives leading to poor quality of life, declining function and frailty (ONS, 2019; Harper, 2014). These issues also create significant challenges for relatives and states to provide medical and social care emphasising the importance of understanding what mechanisms are behind this age associated decline.

Ageing humans show a deterioration in skeletal muscle mass and quality, termed sarcopenia. Skeletal muscle is a key contributor to the loss of independence in older adults due to its role in locomotion allowing people to perform tasks of everyday living, such as shopping and attending social activities, that maintain good quality of life. Therefore, skeletal muscle ageing is an important area to research which is likely to prolong the period of healthspan. It is argued that sarcopenia is mostly mediated by physical activity into later life, however even in highly active individuals there is still an observed age-related decline in mass and function suggesting an inherent age process in this tissue (Pollock *et al.*, 2015; Lazarus & Harridge, 2017).

With regards to tissue ageing, the process of cellular senescence has been implemented as a key contributor to the age-related decline. Cellular senescence was first discovered in the early 1960s when Hayflick and Moorhead showed that cells in culture could undergo a finite number of divisions before entering a state of proliferative arrest (Hayflick & Moorhead, 1961). But it then took 50 years for a causal effect of cellular senescence to ageing to be confirmed when it was shown that the global removal of senescent cells improved the healthspan of wildtype mice (Baker *et al.*, 2016). The treated mice showed improvements across many tissues showing improved structure, function and regenerative potential, as well as, compressing end of life morbidity. These results have increased the search for senolytics, agents that selectively target and kill senescent cells without affecting non senescent cells (Kirkland & Tchkonia, 2017). Some of these senolytics are currently in human clinical trials and the preliminary results are promising.

The improvements shown in skeletal muscle in the senescent cell depleted mice were seen in strength and endurance performance, as well as, muscle quality and regeneration (Xu *et al.*, 2018). Thus, suggesting that cellular senescence may be linked to age related skeletal muscle loss. However, most work with human primary skeletal muscle cells has not found increased senescence cell burden in older adults (Alsharidah *et al.*, 2013; Barberi *et al.*, 2013; Bigot *et al.*, 2015). This discrepancy could be due to skeletal muscle being a tissue comprised of many different cell types that integrate to perform its function. Therefore, there are many contributing mechanisms to its worsening ageing phenotype. Breakdown in any of these mechanisms could result in the ageing skeletal muscle phenotype but the focus of this thesis is on the potential contribution of senescent cells within the resident stem cell populations.

To investigate senescence and ageing in skeletal muscle, animal models and human cell lines have been important for observing mechanistic changes and conserved biology during skeletal muscle ageing. However, because cell lines are fundamentally altered, they may respond differently to and lack the heterogeneity of human primary cells. The use of primary cells, whilst providing a more appropriate model, is more technically challenging. The heterogeneity introduces biological and methodological challenges which make human primary work technically difficult, yet these experiments are imperative to understanding the ageing phenotype within human skeletal muscle. Previous studies in human cells have been clouded by mixed cell populations and only focus on the myogenic satellite cell progeny, myogenic precursor cells, also known as myoblasts. However, skeletal muscle fibroblasts have been shown to play key roles in development and regeneration of skeletal muscle, such as providing the extracellular scaffolding to hold the muscle fibres, and it is therefore also important to understand what age-related changes are occurring within this cell population in parallel with the myogenic precursor cells. Very little is known about the senescent phenotype of either cell type, especially when derived from human sources, therefore it is of importance to understand the senescent phenotype of these populations, as well as, if cells with this phenotype are present in human skeletal muscle *in vivo*.

The overall aim of this thesis is therefore to investigate and characterise the senescent phenotype of the two main precursor cell populations found within adult human skeletal muscle, namely skeletal muscle myogenic precursor cells and skeletal muscle origin fibroblasts, using a primary cell culture model.

Chapter 1: Literature review

1.1. Skeletal muscle

Skeletal muscle is derived from myogenic progenitor cells found in the myotome of somites in the developing embryo (Ito *et al.*, 2012). Skeletal muscle development then occurs in successive phases from the embryo through to adult skeletal muscle with discernible populations of myoblasts at each stage (Hutcheson et al., 2009). Embryonic myogenesis establishes the basic muscle pattern as embryonic myoblasts differentiate into primary fibres. During the foetal and neonatal stages of myogenesis muscle growth and maturation is accelerated as foetal myoblasts fuse together with primary fibres to make secondary fibres whilst rapidly increasing myonuclear number (Biressi *et al.*, 2007). Over time these fibres develop into adult muscle as their gene expression changes with the help of skeletal muscle origin fibroblasts and other cell types present in the surrounding environment (Mathew *et al.*, 2011).

Adult skeletal muscle accounts for between 30-40% of body mass, making it the most abundant tissue by weight within the human body (Janssen *et al.*, 2000). Skeletal muscle is not only required for its main purpose of producing movement and force through contraction but also for its roles in posture, breathing and thermoregulation. Skeletal muscle is also the most metabolically active tissue consuming up to 80% of ingested glucose and storing 50-75% of the body's total protein (Frontera & Ochala, 2015). The overall size of a skeletal muscle varies depending on its anatomical attachment sites and movement requirements, but is ultimately determined by the number and size of its constituent muscle fibres (Frontera & Ochala, 2015). The individual muscle fibres of skeletal muscle are organised into bundles known as fascicles. Within each muscle fibre are many myofibrils that are tightly packed with sarcomeres, the smallest contractile unit of skeletal muscle (Mukund & Subramaniam, 2019; Figure 1.1).

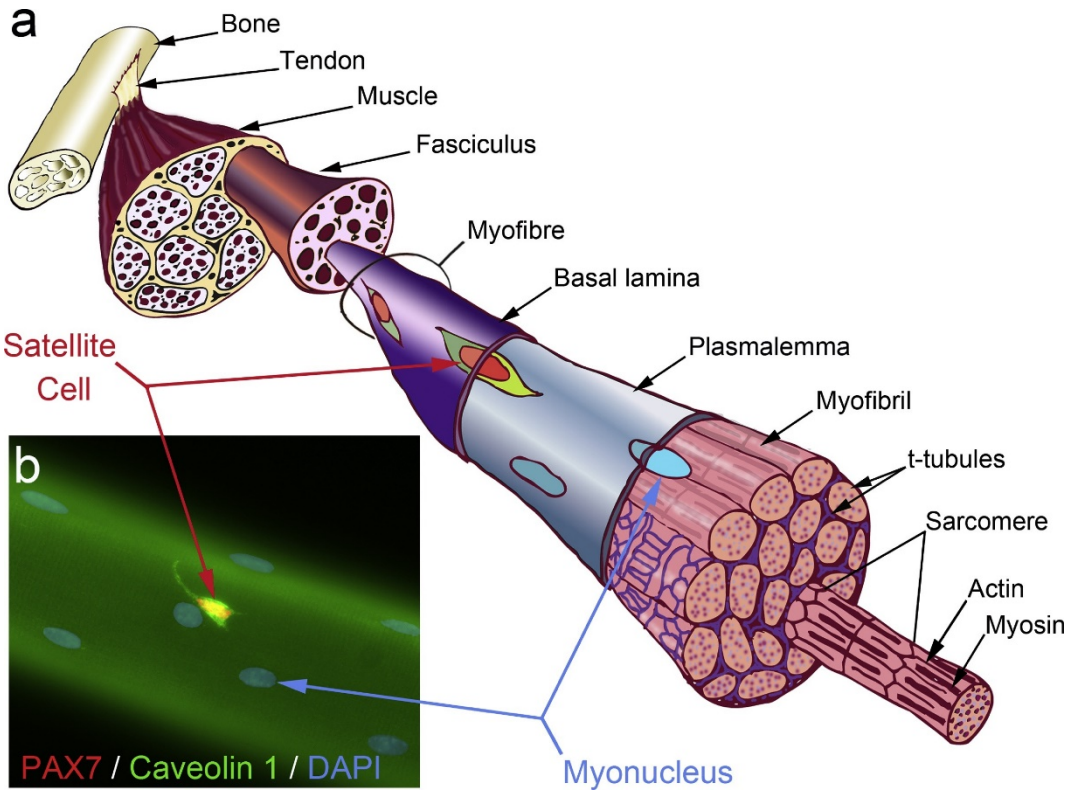

Figure 1.1. Muscle structure and the satellite cell niche.
Schematic showing the structure of skeletal muscle. The satellite cell niche is on the plasmalemma of the myofibre, beneath the surrounding basal lamina (a). A quiescent murine satellite cell retained in its niche on a myofibre isolated from the extensor digitorum longus muscle of an adult mouse (b). The satellite cell has been co-immunolabelled for Caveolin 1 (b; green) and the transcription factor PAX7 (b; red-nuclear). DAPI counterstaining reveals the myonuclei of the myofibre. Reproduced from Zammit, (2017).

Muscle fibres do not necessarily span the whole length of the muscle but are embedded within a connective tissue matrix which is continuous throughout, attaching to bones *via* fibrous collagenous connective tissue called tendons (Jones *et al.*, 2004). This connective tissue is continuous through the whole muscle surrounding each muscle (epimysium), fascicle (perimysium) and muscle fibre (endomysium; Passerieux *et al.*, 2007; Gillies & Lieber, 2011). Force produced within the muscle fibres is therefore transferred to the bones through this connective tissue structure.

Force is generated within skeletal muscle by the transmission of a voluntarily innervated electrical signal from the somatic nervous system through chemical energy into mechanical work via the sliding filament model (Huxley, 1957; Huxley & Simmons, 1971). The axons of α-motor neurons synapse on the neuromuscular junction of extrafusal muscle fibres on the motor end-plate, all innervated fibres by a single α-motor neuron are collectively called a motor unit. The post synaptic activation of nicotinic acetylcholine

receptors causes a depolarisation potential that opens voltage gated Ca^{2+} channels releasing calcium ions (Ca^{2+}) from the sarcoplasmic reticulum into the sarcomeres (Rebbeck *et al.*, 2014). The release of Ca^{2+} reveals myosin binding sites on actin filaments by moving the troponin - tropomyosin complex. Thus, allowing the formation of cross bridges between myosin heavy chain heads and the uncovered actin filament binding sites. Once an inorganic phosphate ion is released from the ATP molecule bound to myosin heavy chain the power stroke is initiated as the myosin head pulling on the actin filament, reducing the distance between the z discs, shortening the length of the sarcomere by pulling "sliding" of the actin filaments towards the M-line (Gautel & Djinović-Carugo, 2016). The myosin heads then detach with the release of the ADP molecule returning to their rigor state completing one cross-bridge cycle. The cross-bridge cycle is then repeated with the myosin head reattaching further along the actin molecule further shortening the sarcomere length (Fitts, 2008).

There are different types of myosin heavy chain (MHC) that are determined by their enzymatic activity (Brooke & Kaiser, 1970). The different MHCs vary in their speed of ADP release slowing the time between power-strokes because whilst ADP is still attached to the myosin head it prevents it from reattaching further along the actin molecule (Caremani *et al.*, 2015). Although most human fibres contain a mix of myosin heavy chains muscle fibres are often classified by their predominant myosin heavy chain as type I (slowest), IIa (fast) and IIx (fastest; Harridge *et al.*, 1996; D'Antona *et al.*, 2006).

A single muscle fibre is a single cell which contains many nuclei spaced along its length. Muscle fibres are considered post mitotic cells as their myonuclei are terminally differentiated and unable to divide to produce new nuclei (Moss & Leblond, 1970). To maximise cytoplasmic space for the contractile apparatus within non-regenerating adult fibres the myonuclei are located on the periphery of the fibres (Roman *et al.*, 2017). These nuclei are long lived in humans, with a report utilising the peak in ^{14}C availability after the post-war nuclear bomb tests being incorporated into DNA to date nuclei suggesting myonuclei survive upwards of 15 years (Spalding *et al.*, 2005). It has also been suggested that this is a conservative estimate and that survival of human myonuclei could conceivably be lifelong (Gundersen, 2016). The main role of myonuclei is to maintain the contractile apparatus of the muscle fibres via the regulation of protein synthesis and breakdown. The contractile filaments can be damaged by being lengthened under tension or sarcomeres popping from forces which rips apart the myosin-actin cross bridges. This

minor damage can be repaired by increasing transcription of the contractile proteins from the myonuclei that surround the fibre. However, when further damage is caused muscle regeneration is required by activation of the skeletal muscle stem cells, satellite cells (Zammit *et al.*, 2006).

1.2. Skeletal muscle regeneration

Muscle regeneration was first described in animals and humans in the 1800's by observations of proliferating cells in areas of diseased muscle, repairing muscle after injury and muscle fibres forming in tumours (Valentin, 1835; Schwann, 1839 cited in Scharner & Zammit, 2011). The extraordinary regenerative potential of muscle was shown *in vivo* when a finely minced sample of a rat's gastrocnemius muscle regained its original structure soon after being put back into the animal (reviewed in Carlson, 1973). Further studies have shown that complete ablation of a mouse skeletal muscle *via* snake venom toxin-induced injury can be fully restored within ten days (Yan et al. 2003; Otto et al. 2008). Although, it was noted that the final size and functional capacity were almost always less than that of the original muscle.

The first reported *in vitro* muscle regeneration experiment was described in 1917 where myotubes, multinucleated cells resembling primitive muscle fibres, were formed by cells seen to be explanting from embryonic chick muscle (Lewis & Lewis, 1917). This finding was then also reported from adult human muscle explants (Pogogeff & Murray, 1946). It was unclear as to what cells were involved in muscle regeneration and the topic was hotly debated. Competing theories suggested that new myofibres were formed from the splitting or budding from old myofibres, that dedifferentiating myonuclei were responsible, that circulating cells could fuse with remaining fibres or form new muscle, as well as, the possibility that skeletal muscle had its own stem/progenitor cells (reviewed in Scharner & Zammit, 2011).

1.2.1. Satellite cells

A candidate muscle stem/progenitor cell was first described by Mauro in 1961, corroborated by Katz et al., in the same year (Katz, 1961) when they discovered a mononucleated cell occupying a unique position between the basal lamina and the

sarcolemma of the muscle fibre in frog muscle using electron microscopy (Figure 1.2; Mauro, 1961). These cells were called satellite cells due to their anatomical location on the periphery of muscle fibres. Satellite cells were subsequently shown to be present in fruit bats and white mice with additional description that they had centrioles, Golgi apparatus and a few small spherical mitochondria (Muir *et al.*, 1965). Moss & Leblond, (1970) confirmed that satellite cells were capable of undergoing mitosis by observing the incorporation of labelled DNA nucleotide, thymidine-^{3}H, into satellite cells of rat *Tibialis Anterior* muscles and not into true myonuclei.

Figure 1.2. Satellite cell in its anatomical niche.
Electron micrograph of the first mammalian satellite cell observed in rat sartorious muscle. The membrane of the satellite cell (sp) can be seen between the muscle cell membrane (mp) and the basement membrane (bm). Reproduced from Mauro, (1961).

At first it was only possible to identify satellite cells *in situ* by their anatomical niche location between the basal lamina and the sarcolemma using electron microscopy. However, since then molecular markers have been identified to label satellite cells. Paired box protein 7 (Pax7) is widely accepted as the definitive satellite cell marker and has been found to be an important regulator for the maintenance of the satellite cell pool, with a subset also expressing the paralogous Pax3 (Seale & Rudnicki, 2000; Seale, 2000; Buckingham & Relaix, 2007). Roughly 96% of human satellite cells were Pax7^{+ve} whilst the remaining cells expressed combinations of the cell-surface markers CD34, CD31 and CD45 (Charville *et al.*, 2015). The key marker of human satellite cells used throughout this thesis is neural cell adhesion molecule (NCAM), also known, and subsequently in this thesis, as

CD56. The location of CD56 on the cell surface makes it an ideal marker for viable cell sorting. Whereas, Pax7 as a nuclear transcription factor is unable to be used as the marker for cell sorting of viable cell populations. Although these markers are common to most cells that populate these niche locations, there is still a large heterogeneity in their wider marker expression (for review see Boldrin *et al.*, 2010).

Genetic ablation studies have provided evidence that satellite cells are sufficient and essential for the regeneration of skeletal muscle fibres (Sambasivan *et al.*, 2011; Lepper *et al.*, 2011). Although the vast majority of cells that regenerate muscle fibres are of satellite cell origin, there are groups of cells that have been shown to be able to also differentiate into myotubes in culture e.g. mesenchymal derived stem cells (Jankowski *et al.*, 2002), endothelial-associated cells (De Angelis *et al.*, 1999) and bone marrow cells (Asakura, 2012). However, their contribution to overall myogenesis *in vivo* was suggested to be minimal (Sherwood *et al.*, 2004; Yin *et al.*, 2013). $Pax7^{-ve}/PW1^{+ve}$ Interstitial progenitor cells, termed PICS, have also been suggested to harbour myogenic potential in mice and pigs however they are as yet undescribed in humans (Mitchell *et al.*, 2010; Lewis *et al.*, 2014; Cottle *et al.*, 2017).

Stem cells are often found within anatomical niches which are microenvironments that maintain the stem cells in a quiescent state, as well as, protecting them from DNA damage and other signals that could cause them to become faulty or unnecessarily activated (Yin *et al.*, 2013). The satellite cell niche architecture is provided by a network of collagen IV containing laminins which anchors the satellite cell through interaction with alpha 7/beta 1-integrins on the cell surface (Blanco-Bose *et al.*, 2001). But also contains additional extracellular matrix proteins such as fibronectin, decorin glycoproteins and other proteoglycans that bind inactive growth factor precursors and buffer the effects of signalling (Montarras *et al.*, 2013). The niche maintains satellite cells in a mitotically quiescent (G_0 phase) state where satellite cells have minimal metabolic activity and therefore undergo very little intrinsic stress.

Quiescence is not a passive state but is tightly regulated by high transcriptional activity involving the up regulation of notch signalling, cyclin-dependent kinase inhibition, regulation of G-protein signaling and Sprouty 1, as well as, many microRNAs (Shea *et al.*, 2010; Cheung *et al.*, 2012; Mourikis *et al.*, 2012; Bjornson *et al.*, 2012). The culmination of these signals result in low expression of cyclins, cyclin dependent kinases and

checkpoint kinases preventing cell cycle progression (Fukada *et al.*, 2007). However, the niche does not keep satellite cells in a quiescent state permanently.

The niche structure allows for mechanical signals from the sarcomeres to be translated into intracellular chemical signals (Boppart *et al.*, 2006). Additionally, extrinsic signals can reach thresholds which result in the activation of the satellite cells when muscle is damaged sufficiently to require repair (Comai & Tajbakhsh, 2014). Satellite cells have also been found in a G_{ALERT} state where they are still quiescent although they enter the cell cycle more quickly than G_0 cells. This primed state is thought to be induced by hepatocyte growth factor (Hgf) in tissues that were not primarily damaged as an expectation for further damage (Rodgers *et al.*, 2014).

When muscle fibres are damaged the chemical and physical damage signals are transferred to the quiescent satellite cells in the niche and a very rapid activation process occurs (Cooper *et al.*, 1999). Key activators of satellite cells are the expression of fibroblast growth factor 2 (FGF2), Insulin like growth factor-1 (IGF-1) and Transforming growth factor beta (TGF-β) (Yablonka-Reuveni *et al.*, 1999*b*; Crown *et al.*, 2000; Seale & Rudnicki, 2000). These signals stimulate the migration of satellite cells to the site of injury and proliferation to produce a pool of muscle precursor cells (MPCs) or myoblasts (Yin *et al*. 2013). Once satellite cells are activated the process of regeneration begins. Firstly, adult satellite cells must divide and expand the population of cells before undergoing differentiation, otherwise there will be insufficient nuclei to support the muscle fibres. Adult satellite cells are thought to divide asymmetrically which also allows for the maintenance of the satellite cell population with a small population of cells ready to take up the niche locations and return to a quiescent state. (Olguin & Olwin, 2004; Collins *et al.*, 2005; Shea *et al.*, 2010; von Maltzahn *et al.*, 2013). The remaining expanded population of cells are thus directed through terminal differentiation under the control of the myogenic regulatory factors (MRFs): MYF5, MyoD, Myogenin and MRF4 (Mice) or MRF6/Hercuin in Humans (Hernández-Hernández *et al.*, 2017; Zammit, 2017).

1.2.2. Myogenic regulatory factors

The MRFs are a family of basic helix–loop–helix central domain transcription factors, which drive myogenesis, the expression sequence of which is outlined in Figure 1.3. They are involved in both protein interactions to form heterodimers and in DNA binding to

transactivate muscle-specific genes (Hernández-Hernández *et al.*, 2017). The satellite cell marker Pax7 can directly regulate the expression of the earliest marker of myogenic commitment, Myf5 and MyoD, which occurs promptly after activation of the satellite cells (Cornelison & Wold, 1997; McKinnell *et al.*, 2008; Buckingham & Relaix, 2015). These MRF genes are so critical to the muscle lineage that the activation of the Myf5 gene in a wide range of cultured cells induces the expression of MyoD and drives the cells to become myogenic cells (Weintraub *et al.*, 1989).

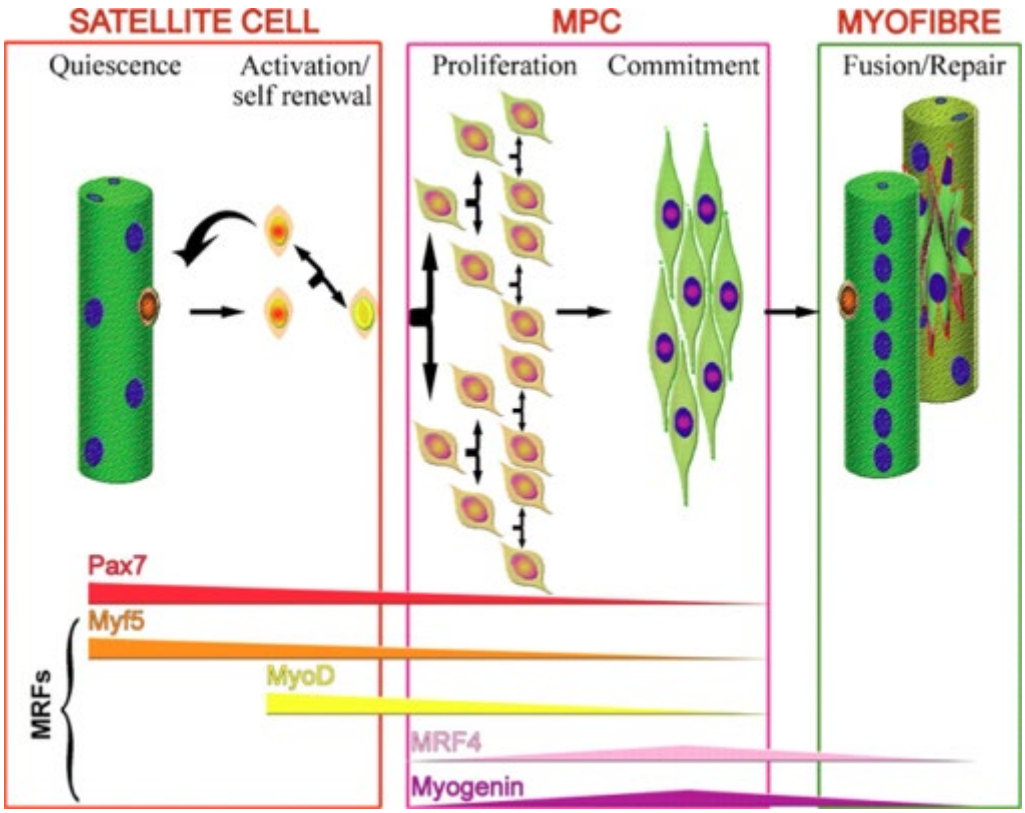

Figure 1.3. Expression of the myogenic regulatory factors during myogenic differentiation. Quiescent satellite cells express Pax7 and Myf5. Upon activation, they upregulate MyoD and start to proliferate creating a pool of muscle precursor cells. Some of the progeny down-regulate MyoD and self-renew to replenish the $Pax7^{+ve}$ satellite cell population. However, the majority differentiate, down-regulating Pax7, Myf5 and MyoD and increasing expression of MRF4 and myogenin. These cells then fuse into damaged myofibers or form new myofibres. Reproduced from Boldrin et al., (2010).

The loss of MyoD expression in adult mice satellite cells results in reduced differentiation capacity and fusion competence (Sabourin *et al.*, 1999; Yablonka-Reuveni *et al.*, 1999*a*). This is because MyoD directly activates its own expression by binding to the DNA immediately upstream of the MyoD gene keeping the gene active (Tapscott, 2005) and also signals the expression of Myogenin, and MRF6 (MYF4 in mice), which is the crucial step in transition from proliferation to differentiation (Grounds *et al.*, 1992; Bigot *et al.*, 2008). There is also evidence to suggest that $Myf5^{+ve}$ satellite cells and $MyoD^{+ve}$ precursor cells are not able to repopulate the satellite cell's anatomical niche therefore MyoD is considered the determinant step in commitment to myogenic differentiation and is upregulated within 24 hours of inducing differentiation in culture (Halevy *et al.*, 1995; Bigot *et al.*, 2008; Wang *et al.*, 2014).

To maintain a satellite cell population there needs to be a fraction of cells that migrate back to the niche location and become quiescent. In cell culture experiments not all cells fuse to form myotubes, the minority of remaining cells are thought of as "reserve cells" which could be representative of the satellite cell population *in vivo* (Zammit, 2006; Bigot *et al.*, 2015). The overexpression of Pax7 is thought to cause satellite cell re-entry to quiescence (Olguin 2004). With Kuang *et al.*, (2007) suggesting that $PAX7^{+ve}/MYF5^{-ve}$ satellite cells divide asymmetrically where one daughter cell remains negative for MRF5 and returns to quiescence whereas the other daughter cell becomes $MRF5^{+ve}$ and becomes committed to differentiation. It is thought that between 10-20% of satellite cells undergo this asymmetric division and return to a quiescent state for future regeneration (Kuang *et al.*, 2007; Bigot *et al.*, 2015).

The $Pax7^{+ve}/MYF5^{+ve}$ satellite cells which are committed to the myogenic differentiation program then expand *via* symmetrical division upregulating proliferating cell nuclear antigen (PCNA) and activation of the Ras-ERK pathway which suppresses the differentiation inducing actions of MyoD and MEF2 (Yokoyama *et al.*, 2007). The interplay between the Notch and Wnt β-Catenin pathways, along with many other possible factors, control the switch from myogenic proliferation into differentiation (von Maltzahn *et al.*, 2012; Agley *et al.*, 2017; Asfour *et al.*, 2018). With regards to the MRFs, this is signalled by the downregulation of Pax7 and upregulation of MyoD, Myogenin and MRF4 in mice, MRF6 in human (Hernández-Hernández *et al.*, 2017). This upregulation of MyoD causes cell cycle exit through the G1 checkpoint initiated by the upregulation of p21, p57, and p19 (Guo *et al.*, 1995; Bigot *et al.*, 2008). Myoblasts also accumulate double strand DNA

breaks via caspase 3 which may be involved in their terminal differentiation (Larsen *et al.*, 2010).

Upregulation of Myogenin allows the non-dividing myoblasts to fuse together or to fuse with the damaged myofibres (Zammit, 2017). Myogenin knockout is lethal perinatally to mice because their myoblasts cannot fuse to form muscle fibres (Nabeshlma *et al.*, 1993). Additionally, two cell membrane proteins, myomaker and myomerger, have also been shown to be essential for the fusion of myoblasts since knockdown of either prevented myoblast fusion (Millay *et al.*, 2013; Leikina *et al.*, 2018). Once fused, the multinucleated cells begin to express contractile proteins, such as myosin heavy chain (MHC). The first types of MHC expressed are embryonic and neonatal forms and as the fibres regenerate they are then replaced by the adult MHC forms, depending on the innervating motor nerve (Carosio *et al.*, 2011).

1.2.3. Fibroblasts

Synthesis, maintenance and repair of the connective tissue layers of skeletal muscle, the epi-, endo- and peri- mysium, is under the control of local stromal fibroblasts and fibro-adipocytes (FAPS; Haniffa *et al.*, 2009). Fibroblasts are mesenchymal cells found within the connective tissue stroma of most organs and there is a large heterogeneity between anatomical locations as they are specialised to their tissue of origin (Chang *et al.*, 2002). Fibroblasts are often identified by elimination of other cell types as non-endothelial, non-epithelial, non-hematopoietic and by the capacity to produce and remodel extracellular matrix (Haniffa *et al.*, 2009). However, TE7, a fibroblast-specific connective tissue protein, has been demonstrated to distinguish fibroblasts in many tissues from other human cell types such as monocyte-derived fibrocytes and endothelial cells (Goodpaster *et al.*, 2008; Pilling *et al.*, 2009). True fibroblast markers that distinguish between sub types are still elusive (Mathew *et al.*, 2011), but human skeletal muscle origin fibroblasts have been shown to express TE7, collagen VI, PDGFRa, vimentin and fibronectin (Agley *et al.*, 2013). There is a potential for these skeletal muscle origin fibroblasts, or a subset, to be undifferentiated bipotent ‘fibro-adipogenic’ precursors (FAPs) which has been found in mouse skeletal muscle (Joe *et al.*, 2010; Uezumi *et al.*, 2010). Although, this relationship between FAPs and fibroblasts is unclear in humans as only some isolated fibroblast populations extracted from human primary muscle biopsies show adipogenic potential (Agley *et al.*, 2013).

During development skeletal muscle fibroblasts play an important role in the organisation of the connective tissue leading to the highly ordered final structure of skeletal muscle (Clase *et al.*, 2000; Kardon *et al.*, 2003). In adult muscle their genetic ablation impaired muscle regeneration *in vivo* (Murphy *et al.*, 2011) which is supported by the observation that their addition enhanced myoblast fusion in culture (Mathew *et al.*, 2011). Fibroblasts and FAPS are known to secrete factors which signal for myoblast terminal differentiation: IGF-1, interleukin-6 (IL-6) and Wnt family proteins Wnt1, Wnt3A and Wnt5A. These factors have a second role as they also initiate extracellular matrix remodelling (Joe *et al.*, 2010; Uezumi *et al.*, 2010; Wosczyna & Rando, 2018). Fibroblasts may also be important for phagocytosis of necrotic debris and respond to immune cell secretions by proliferation before being selectively targeted for apoptosis by macrophage TNF-α secretion (Heredia *et al.*, 2013; Lemos *et al.*, 2015).

Overall skeletal muscle regeneration is a highly integrative process involving multiple cell types including MPCs, fibroblasts and many different blood cells types (Yang & Hu, 2018). The intricate intra- and extra- cellular signalling cascades to coordinate the process which, although complex, is highly effective during development and in young adults (Wosczyna & Rando, 2018). However, the regeneration process may be dysregulated or impaired as organisms age.

1.3. Sarcopenia

Human ageing is the gradual decline in organ and tissue function with increasing chronological time, leading eventually to increased risk of disease, loss of function and death (Kennedy *et al.*, 2014; Lees *et al.*, 2016). Most human physiological systems show peak performance in the third decade of life with declining performance thereafter with the rate of decline accelerating between sixth and seventh decades. This decline is highlighted most elegantly by observing the integrative physiological decline in world record times for master athletes (Lazarus & Harridge, 2017). Within the tissue of interest of this thesis, skeletal muscle, the ageing process manifests itself as an age-related loss of skeletal muscle, which is known as sarcopenia - literally translated as “flesh loss” (Rosenberg, 1997).

Sarcopenia is a geriatric syndrome characterised by progressive and generalised loss of skeletal muscle mass and strength leading to physical disability and poor quality of life

(Cruz-Jentoft *et al.*, 2010). The current clinical definition of sarcopenia is defined by the presence of low muscle mass, two standard deviations below the lean mass of sex-specific healthy young controls, with low strength and a risk of deleterious outcomes, such as frailty, an increased propensity to fall, or the loss of independence (Delmonico *et al.*, 2007; Dennison *et al.*, 2017; Cruz-Jentoft *et al.*, 2019).

A cross sectional study suggested muscle mass loss of between 25-40%, measured by MRI, in both male and females aged 20 to 60 years (Janssen *et al.*, 2000). Longitudinal research suggests that the rate of declines in muscle mass loss is between 1-2% per decade from the age of 50 years and accelerates to as much as 3% per decade beyond age 60 (Hughes *et al.*, 2001; Rolland *et al.*, 2008). The decline in muscle strength is also reported to be 20-40% in the seventh and eighth decades of life (Larsson *et al.*, 1979; Overend *et al.*, 1992), with larger losses (>50%) reported in the ninth decade (Murray *et al.*, 1985). Muscle power (strength x speed) is also reduced with ageing and is strongly associated with functional decline (Bassey *et al.*, 1992). The reduction in muscle power is considerable from the fifth decade of life and is of greater magnitude than decrements in strength (Metter *et al.*, 1997).

The mass and functional loss seen in sarcopenic muscles is most likely due to reduced number and size of myofibers. With a reported 10-40% atrophy in type II fibre atrophy whereas type I muscle fibres appears mostly unaffected by the ageing process (Verdijk *et al.*, 2007; Snijders *et al.*, 2009). The age related loss of fibres is accompanied by an increase in fibrosis, fat accumulation and scar tissue formation (Wagatsuma, 2007; Mahdy, 2018). Scar tissue, in the form of fibrosis connective tissue, accumulates where incomplete or slow muscle tissue regeneration occurs reducing muscle quality. Examples of the quality of aged muscle are shown in Figure 1.4.

There is a growing consensus to better define the ageing population under study because physically active individuals show fewer signs of sarcopenia. Aged exercisers do still have a decline in performance with increasing age, as shown by cross sectional data from age group world record times in sprinting, marathon running and swimming (Lazarus & Harridge, 2017). A study by Pollock *et al.*, (2015) showed a similar trend for declining performance with age in a cross-sectional study of highly active elderly masters cyclists. Masters athletes also show superior muscle strength and power compared to their age-matched non-exercised counterparts (Pearson *et al.*, 2002), although type II fibre atrophy

is evident in master sprinters and therefore may not solely be explained by inactivity (Korhonen *et al.*, 2009). The true extent to which there is a decline in age-related muscle mass and function is masked by inactivity but there are still clear signs of an inherent ageing effect in the highly active.

Skeletal muscle is a multifunctional multi-cell type tissue meaning that there are many potential contributing factors to an age-related decline in muscle mass and function. The prominent mechanisms will be reviewed in brief and focus will be on the possible roles of the MPCs and fibroblasts to the ageing phenotype.

Voluntary skeletal muscle contraction is controlled by the action potentials generated by α-motor neurons. Neuronal cells are not replaced and therefore when they die the fibres of that motor unit are either incorporated into other surviving motor units or are lost to necroptosis (Vandervoort, 2002). This mechanism can account for not only the loss of muscle size with ageing but also functional output because the larger motor unit size causes loss of fine control of muscles. There may also be potentially greater loss of the type II motor units, fast twitch, which could also support the shift in fibre types in older muscles as the motor unit determined fibre type, denervated type II fibres becoming incorporated into type I motor units would cause fibre type switching.

Other external mechanisms include changes in endocrine function (Sakuma & Yamaguchi, 2012), falling circulating levels of anabolic hormones (Wilkinson *et al.*, 2018) and chronic low-grade inflammation known as inflammageing (Franceschi & Campisi, 2014). The circulation of low, but elevated, levels of inflammatory cytokines and chemokines, such as advanced glycation end- products, IL-6, IL-18 and TNF-α, can interfere with regular cellular functioning and potentially impair muscle maintenance, repair and regeneration (Brooks & Faulkner, 1990; Ndip *et al.*, 2016). Old muscle also shows desensitisation to anabolic stimuli such as feeding and exercise, further impairing the ability of the muscle to regenerate (Moore *et al.*, 2015). The impaired repair and regeneration of muscle fibres would support the findings of increased connective tissue fat infiltration into muscles (Mahdy, 2018), as well as, altered protein metabolism (Breen & Phillips, 2011). These mechanisms are likely to impact the phenotype of aged skeletal muscle.

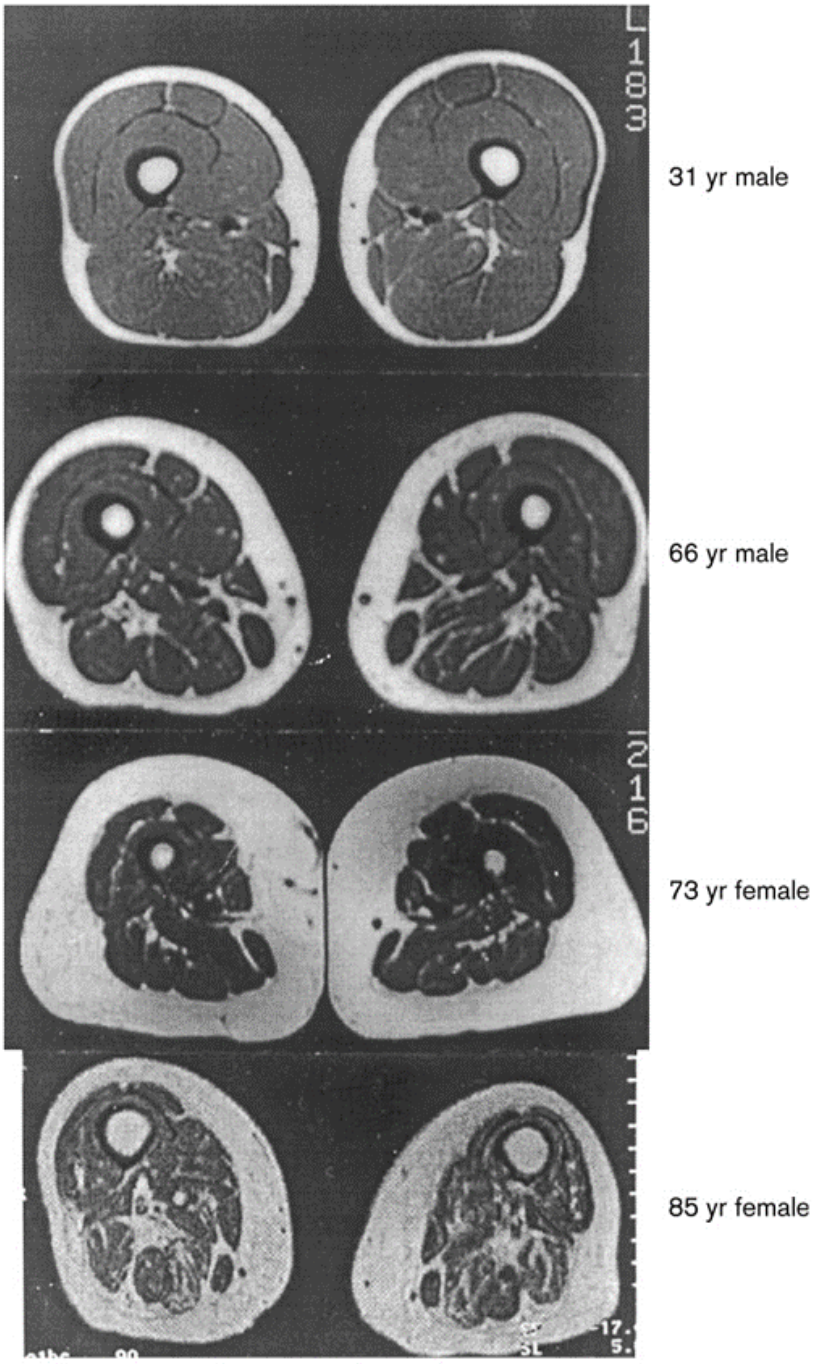

Figure 1.4. Loss of muscle quantity and quality with increased age.
Cross-sections through the upper thigh from a young male and aged men and women show the characteristic decrease in muscle mass and intrusion of fatty connective tissue described by sarcopenia. Images were obtained using computerised tomography where white indicates fat and connective tissue and grey indicates muscle tissue (Parise & Yarasheski, 2000).

1.4. Stem cell loss and dysfunction

Satellite cells are essential for the repair and maintenance of regenerating muscle tissue. Their loss with increasing age could influence the aged phenotype because the remaining populations may not be able to fully repair or regenerate skeletal muscle fibres. In rodent post-natal muscle, roughly 30% of myogenic cells are considered satellite cells with this number decreasing to <5% in adult muscle, accounting for the increased myonuclear number seen during development (Allbrook *et al.*, 1971; Gibson & Schultz, 1983). Snow (1977) showed a further 50% decrease in satellite cell number to 2.4% in soleus muscle of 30-month-old mice and rats compared to 8-month-old animals. Gibson & Schultz, (1983) suggested there may be a difference in relative satellite cell loss between oxidative and glycolytic fibres by showing a decline from 2.9% to 1.9% in extensor digitorum longus muscle compared with a declined from 6.6% to 4.9% in soleus muscle. A more recent study suggests that there is a reduced number of satellite cells in old mice, 20-24 months, compared to young adults, 5-6 month old, but no further loss in very old mice, 28-32 months (Sousa-Victor *et al.*, 2014).

In humans, the results are less clear, an early report showed a reduction in satellite cell number from 4% in young adults to 0.6% in one 73 year old man (Schmalbruch & Hellhammer, 1976). Another study including more older participants showed a less severe decrease in satellite cells from 5% in young to 1.5% in old adults (Renault *et al.*, 2002*a*). Furthermore, while the number of satellite cells as a proportion of myonuclear number was lower in old age, the mean number of myonuclei remained constant. The authors state that over 200 myofibres were analysed per sample but there was no mention of actual number of satellite cells counted per sample. However, another electron microscopy study with 14 young and 15 old participants didn't show a decrease in satellite cell number but the proportion of satellite cells to total nuclei was in the range 1.7-2.8% between the groups (Roth *et al.*, 2000).

Two further studies from a different group (Sajko *et al.*, 2002) claimed that previous studies had not been able to accurately count satellite cells suggesting only 6 satellite cells were counted per participant in the Schmalbruch & Hellhammer, (1976) study and 4.2 satellite cells per participant in the Roth *et al.*, (2000) study. Their later study counted an average of 117 (range 35-200) satellite cells, identified by calcium-dependent cell adhesion molecule M-cadherin staining, within an average of 3824 (1352-5350) myofibres

per muscle, from 6 young and 6 old adults (Sajko *et al.*, 2004). In this thorough analysis they showed that the proportion of satellite cells (per total number of nuclei or myofibres) was higher in young adults, compared to older adults in 10 µm sections. However, over the whole of the 1 mm^3 muscle tissue sample this difference was not significant. This was likely due to high inter-individual variability especially in the young group. Another study from the same year also showed a significantly lower absolute number of satellite cells per muscle fibre in older, compared to younger, women and men (Kadi *et al.*, 2004). They also showed a significantly higher number of myonuclei in older individuals suggesting this could be a compensatory mechanism for loss of satellite cells. The interpretation was further confounded by the finding that the satellite cell population density differed between type 1 and 2 fibres, which previous studies had not determined (Zammit *et al.*, 2002). When satellite cell loss was counted in the specific fibre types there was an age-associated decrease in satellite cell number but specifically in type 2 fibres (Verdijk *et al.*, 2007). Another consideration is that both satellite cell and myonuclear number increase due to exercise training and therefore understanding the lifelong physical activity status of the participants is important to match for activity level (Snijders *et al.*, 2015; Goh *et al.*, 2019).

The lack of consensus on satellite cell loss with age in human studies, even from the same muscles, is likely due to inaccuracies in the measurements (Brack & Rando, 2007). Satellite cells are scarce, even in healthy muscle, and they are counted in human biopsy tissue sections from a very small samples of muscle fibres, which may not be representative of the satellite cell distribution across the whole muscle. Although techniques such as flow cytometry do yield accurate counts of numbers of cells these populations are similarly likely to be biased by the extraction techniques used because digesting the whole muscle may cause loss of cells favouring survival of healthy cells.

Overall, it is most likely that satellite cell number does decrease with age, in common with other stem/progenitor cell populations. Irrespective of this, there seems to be sufficient satellite cells in elderly muscle to rejuvenate muscle effectively (Brack & Rando, 2007). Especially as only a very small number of satellite cells are required to fully regenerate skeletal muscle (Günther *et al.*, 2013). However, this is dependent on the remaining satellite cells being functionally capable of regenerating muscle. One of the key ageing mechanisms that has been associated with reduced stem cell function, and the one that this thesis focuses on, is cellular senescence (Lopez-Otin *et al.*, 2013).

1.5. Cellular senescence

The first studies of cells in culture suggested that when cells were removed from their *in vivo* constraints they could divide and function indefinitely (Carrel & Ebeling, 1921). However, it has subsequently been proposed that the chicken embryo extract used to feed the cells was providing a source of new cells into the cultures (references in Shay & Wright, 2000). It took until the 1960's for a study to convincingly show that normal human cells had a limited replicative capacity in culture. Hayflick & Moorhead, (1961) showed that human foetal diploid fibroblasts could be serially passaged for a consistent number of population doublings (approximately 55 divisions) before reaching proliferative arrest. This finding was interpreted as cellular ageing of mortal cells and that only cancerous cells were immortal (Hayflick, 1965). The limit to proliferative capacity of normal mortal cells became known as replicative senescence and subsequently "the Hayflick limit" after its discoverer. A replicative limit has since been shown in many other cell types, including adult skeletal muscle myoblasts (Decary *et al.*, 1996; Kang, 1998; Spaulding *et al.*, 1999; Wagner *et al.*, 2001; Coppé *et al.*, 2010*b*).

Due to the consistency of the replicative lifespan of the same cell population, even after cryopreservation, it was postulated that there must be some form of mitotic counter remembering how many divisions a cell had undergone. Telomeres, short tandem repeat sequences of TTAGGG nucleotides that cap the end of chromosomes, were suggested to be a likely replicometer (Hayflick, 1965; Blackburn *et al.*, 2015). During chromosomal transcription DNA polymerase cannot fully transcribe the 3′ end of each DNA strand because the enzyme needs nucleotide bases to bind to beyond those being copied (Bodnar *et al.*, 1998; Blasco, 2005). Telomeres provide these additional nucleotides allowing for the full transcription of the last coding gene with the last section of the telomere being lost after each replication resulting in a progressive shortening of the telomere. It has been shown *in vitro* that once telomeres reach a critical length the cell will stop proliferating (Di Donna *et al.*, 2003), with initial telomere length correlating very highly with the cell population's *in vitro* replicative capacity (Allsopp *et al.*, 1992). Additionally, the degree of telomere shortening is roughly proportional to risks of common comorbidities of ageing (Blackburn *et al.*, 2015). However, it was shown that telomere shortening is not always regular because other factors such as DNA damage caused by oxidative stress can cause additional bases to be lost (Von Zglinicki, 2002).

Therefore, telomere length is not necessarily a precise indicator of replicative capacity, but an upper proliferative limit determined by the end-replication problem.

Telomere length can be restored by the ribonucleoprotein enzyme telomerase that extends the 3' end of telomeres and therefore prevents them from reaching a critically short length (Shippen-Lentz & Blackburn, 1990). Telomerase has been found in many other non-human cells and immortal cell lines suggesting the importance of the telomere in retaining proliferative capacity (Shay & Bacchetti, 1997; Blasco, 2005). In normal human cells, telomerase activity has only been found in very few stem cell populations such as foetal tissue, bone marrow stem cells, testes, peripheral blood lymphocytes, skin epidermis and intestinal crypt cells (Broccoli *et al.*, 1995; Wright *et al.*, 1996; Kyo *et al.*, 1997; Calado & Young, 2008). It is important to note that the addition of telomerase is not always sufficient to immortalise human cell populations. The addition of telomerase to normal human fibroblasts increases their proliferative capacity by at least 20 population doublings but they still reached proliferative arrest suggesting that there were other senescence inducing mechanisms (Bodnar *et al.*, 1998). This is supported by rats and mice dying with long telomeres suggesting that other mechanisms are involved in causing cellular senescence (Blasco *et al.*, 1997).

As cell culture is a constant environment with relatively low stress, the number of population doublings that a normal cell can undergo *in vitro* is considered to be an expression of the maximum potential longevity, under those culture conditions. However, in most cases, telomere-driven senescence occurs much sooner due to imperfect protection from damage, which results in accelerated telomere loss (Von Zglinicki *et al.*, 2005). The replicative limit is rarely reached *in vivo* because of the hundreds of molecular disorders that accumulate before the division competent cell reaches replicative capacity causing the cell to either succumb to apoptosis, necroptosis or to organismal death well before telomeres reach a critical length to prevent DNA replication (Hayflick, 1998; Brooks & Myburgh, 2014; Sciorati *et al.*, 2016; Morgan *et al.*, 2018).

When telomeres become critically short or damaged sufficiently there is an induced activation of a sustained DNA damage response (DDR) pathway that leads to a senescent cell cycle exit (Blackburn *et al.*, 2015). The loss of telomeres uncaps the end of DNA which activates a kinase cascade of ataxia telangiectasia mutated (ATM) and Rad-3 related kinase (ATR) followed by checkpoint protein kinase CHK1 and CHK2, resulting in the

stabilisation of tumour suppressor protein, p53, which in turn upregulates p21 causing the inhibition of cyclin dependent kinase (CDK) activity (Cyclin E/CDK2 complex) preventing cell cycle progression as retinoblastoma protein is still in its active, hypophosphorylated, state (Figure 1.6; McHugh & Gil, 2018).

This same cell cycle exit response has been shown to be activated by other damage causing factors that do not necessarily cause DNA or telomeric damage such as epigenetic stress, reactive oxygen species, endoplasmic reticulum stress, proteotoxic stress, nucleolar stress, spindle stress and low BubR1 (Itahana *et al.*, 2004). In these stress-induced incidences the p53/p21 senescence pathway may, or may not, be involved alongside the silencing of INK4a/ARF locus by Polycomb Repressive complexes (Fridman & Tainsky, 2008). This silencing allows the upregulation of p16 which maintains Rb in its hypophosphorylated by inhibition of a different set of CDKs, Cyclin D1, CDK4 and CDK6 (Alcorta *et al.*, 1996). It is difficult to determine exactly how an individual cell became senescent because the pathways converge on a common cell cycle exit strategy. Both p16 and p21 keep retinoblastoma tumour suppressor protein (pRB) in an active, hypophosphorylated form, preventing E2F transcription factor from transcribing genes that are needed for proliferation (Adams, 2009). Although the p53-p21 and p16 cell cycle inhibitor pathways are strongly involved in triggering the senescent cell state, it is suggested that p53/21 is as an indicator of cellular senescence initiation, whereas p16 is expressed throughout cellular senescence maintenance (Stein *et al.*, 1999). However, senescence cells have also been found without the expression of either of these cell cycle inhibitors further confusing the identification of senescent cells (Hernandez-Segura *et al.*, 2018).

The current gold standard marker of senescent cells is the activity of Senescence-Associated β-Galactosidase (SA-β-Gal; Dimri *et al.*, 1995). The heightened activity of lysosomal-origin β-galactosidase is thought to be the result of the expansion of the lysosomal compartment and increased autophagy in senescent cells to compensate for the accumulation of damaged macromolecules and organelles (Lee *et al.*, 2006). SA-βGal has an optimal activity at pH 6, whereas non-senescent cells β-Gal is optimally active at pH 4. However, this upregulation of β-Gal at non optimal pH is not only associated with senescence but is present in some cell types, such as adult melanocytes and sebaceous and eccrine gland cell when still proliferative (Dimri *et al.*, 1995). It is therefore paramount to use multiple markers to determine cells as senescent.

Markers of DNA damage such as the chromatin modifier phosphorylated histone H2aX (γH2aX), that identifies double strand breaks in DNA (d'Adda di Fagagna, 2008), as well as, the cell cycle inhibitors p53, p21 and p16 are often used as markers of senescent cells, but they are not definitive markers of senescence. DNA damage does not always result in senescence and mutations in the cell cycle inhibitors are highly prevalent in immortal cancer cells, as well as in some non-senescent cells (Turgeon *et al.*, 2018). Therefore, combining these markers with direct markers of proliferation, such as Ki67 or BrdU, more clearly identify these cells as senescent. However, this combination of markers could still be marking a quiescent or temporary non-diving cell rather than a permanently arrested senescent cell. The DNA damage response pathways are also the primary trigger for altering the chromatin structure and formation of senescence associated heterochromatin foci (Adams, 2009; Rodier *et al.*, 2009). Senescent cells are also characterised by morphological changes, enlarged and flattened shape distended nuclei, increased microfilament content, prominent Golgi apparatus and increased presence of cytoplasmic vacuoles (Renault *et al.*, 2000; Campisi, 2013).

The most prominent feature of senescent cells is their altered secretory phenotype, known as the senescence associated secretory phenotype (SASP; Coppé *et al.*, 2008). Despite being unable to proliferate, senescent cells remain metabolically active and can display extensive changes in gene and protein expression which is thought to be tissue specific with core common pathways (Tchkonia *et al.*, 2013).

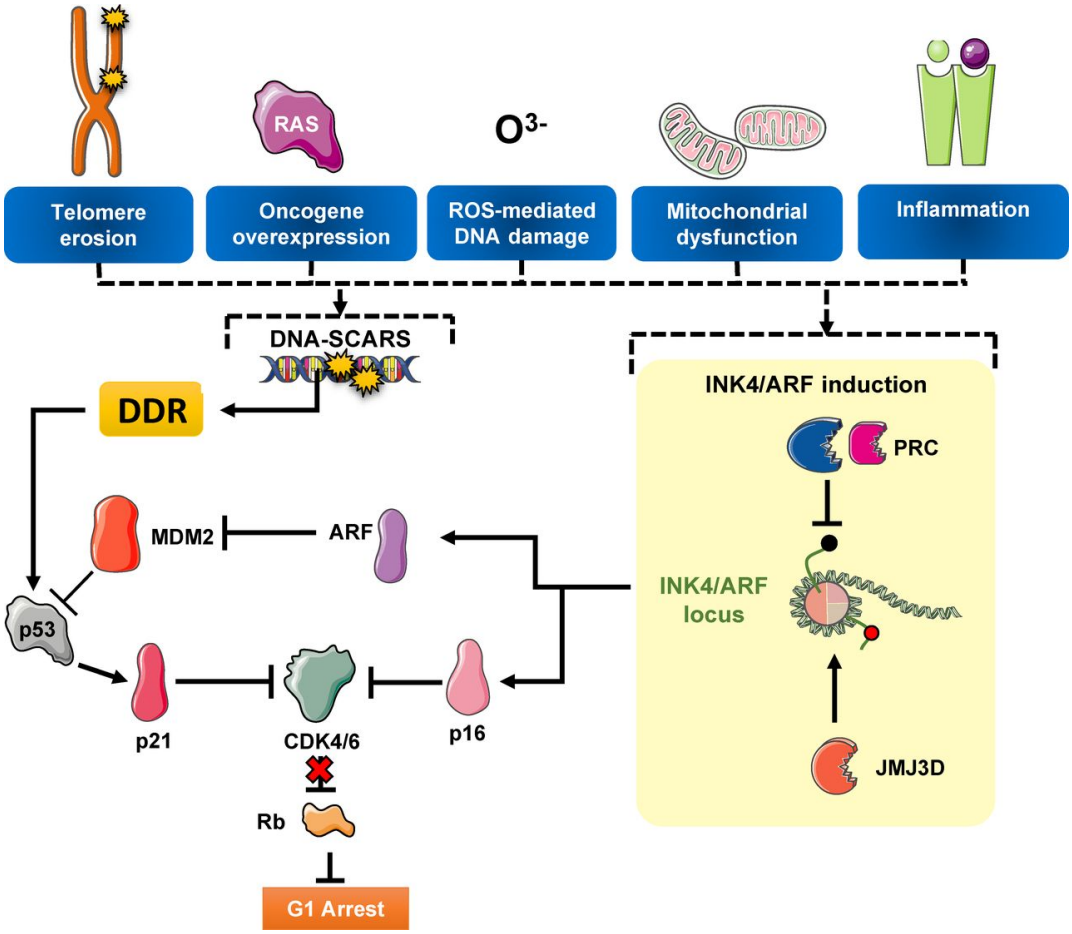

Figure 1.5 Senescence cell cycle inhibitor pathways.
The two main pathways activated in response to stressors are the p53/21 and the p16 pathways. Following activation of the DNA damage response, this activates a kinase cascade of ataxia telangiectasia mutated (ATM) and Rad-3 related kinase (ATR) followed by checkpoint protein kinase CHK1 and CHK2, thereby activating p53. p53 then induces p21 transcription, which inhibits the Cyclin E/CDK2 complex, resulting in hypophosphorylated retinoblastoma (RB) protein and cell cycle exit. p16 and ARF are tumour suppressors residing in the INK4/ARF locus. In response to stressors, the INK4A/ARF locus is silenced by Polycomb Repressive complexes (PRCs) and activated. This activates p16, thereby inhibiting the Cyclin D1/CDK4/6 complex, resulting in hypophosphorylated RB and cell cycle exit. Reproduced from McHugh & Gil, (2018).

1.5.1. Senescence associated secretory phenotype

The SASP is characterised by the secretion of several families of soluble signalling molecules, including cytokines, chemokines and growth factors, together with the secretion of bioactive lipids, proteases and changes in extracellular matrix components (Kuilman *et al.*, 2010; Tchkonia *et al.*, 2013; Malaquin *et al.*, 2016). The key components are listed in Table 1, which is reproduced from (Gorgoulis *et al.*, 2019). However, the exact composition of the SASP varies between cell types and even between different cells within the same cell type, as well as, changing over time (Coppé *et al.*, 2008; Wiley *et al.*, 2017).

Table 1. Senescence Associated Secretory Phenotype (SASP) factor components

Class	Component
Interleukins	IL-6; IL-7; IL-1; IL-1b; IL-13; IL-15
Chemokines	IL-8; GRO-a, -b, -g; MCP-2; MCP-4; MIP-1a; MIP-3a; HCC-4; eotaxin; eotaxin-3; TECK; ENA-78; I-309; I-TAC
Other inflammatory molecules	TGF-β; GM-CSE; G-CSE; IFN-γ; BLC; MIF
Growth factors; regulators	Amphiregulin; epiregulin; heregulin; EGF; bFGF; HGF; KGF (FGF7); VEGF; angiogenin; SCF; SDF-1; PIGF; NGF; IGFBP-2, -3, -4, -6, -7
Proteases and regulators	MMP-1, -3, -10, -12, -13, -14; TIMP-1; TIMP-2; PAI-1, -2; tPA; uPA; cathepsin B
Receptors; ligands	ICAM-1, -3; OPG; sTNFRI; sTNFRII; TRAIL-R3; Fas; uPAR; SGP130; EGF-R
Non-protein molecules	PGE2; nitric oxide; ROS
Insoluble factors	Fibronectin; collagens; laminin

Reproduced from Gorgoulis *et al.*, (2019).

The SASP is thought to be induced in response to senescence *via* a signalling loop involving IL-1α, miR-146a/b, IL-6, C/EBP-β, p38/NF-κB and mTOR-mediated signalling cascades which contribute to the alterations in gene expression (Yoshimoto *et al.*, 2013; Tchkonia *et al.*, 2013; Xu *et al.*, 2015*a*). Part of the SASP's effect is to reinforce senescence-associated proliferative arrest by increased PAI-1, insulin-growth factor binding protein family (IGFBPs), and TGF-β1 alongside reduced levels of IGF-1 and WNT2 (Adams, 2009). PAI-1 is a pro-thrombotic plasma protein that inhibits plasminogen activators, tissue and urokinase plasminogen activators participating in wound healing, angiogenesis and metastasis, as well as interacting with extracellular proteolytic activity (Kortlever *et al.*, 2006; Eren *et al.*, 2014). Moreover PAI-1 is an established p53 target and although it is

mostly regarded as a marker that correlates with senescence, it is also sufficient to drive senescence in fibroblasts (Kortlever *et al.*, 2006). The upregulated IGFBPs sequester IGFs supressing their signalling which also plays a role in regulating p53 expression (Kuilman & Peeper, 2009). MCF-7 cells, human breast cancer cell line, incubated in media containing IGFBP-3 undergo senescence, which is prevented if IGFBP-3 is degraded by tissue plasminogen (t-PA) in the same media (Elzi *et al.*, 2012). IGFBP-3, IGFBP-5 and IGFBP-7 have been shown to interact with an activated BRAF oncogene, upregulating senescence through oncogene overexpression, and aiding apoptosis induction (Wajapeyee *et al.*, 2008). TGF-β is able to reinforce cellular senescence through paracrine mechanisms, by generating reactive oxygen species which interact with nearby cells (Hubackova *et al.*, 2012), and autocrine mechanisms, by establishing a positive feedback loop leading to p21 and p15 induction (McNeal *et al.*, 2015; Tominaga, 2015).

Senescent cells also often express increased amounts of immune-regulatory factors, namely cytokines, chemokines and their receptors (Adams, 2009). These include IL-6 and its receptor IL-6R (Kuilman *et al.*, 2008; Adams, 2009; Kuilman & Peeper, 2009), as well as, the seven-spanning transmembrane receptor CXCR2 and its ligands, IL-8, CXCL1, CXCL5, and CXCL7 (Acosta *et al.*, 2008; Kuilman *et al.*, 2008). IL-6 reinforces senescence-associated proliferative arrest of primary cells in an autocrine manner, as well as, being a potent attractor and activator of immune cells (Kuilman *et al.*, 2008; Tchkonia *et al.*, 2013). Likewise, increased CXCR2 and IL-8 reinforce the senescence program by causing proliferative arrest, promoting angiogenesis and inhibiting differentiation through autocrine mechanisms (Parrinello *et al.*, 2005; Acosta *et al.*, 2008; Orjalo *et al.*, 2009). CXCL5 has also been shown to promote angiogenesis but also cell proliferation, migration, and invasion (Begley *et al.*, 2008; Kawamura *et al.*, 2012). The SASP can also signal the immune system directly via increased natural killer group 2D (NKG2D) ligands, MHC class I polypeptide related sequence A (MICA), UL16-binding protein 2 and IL-15 (Roberts *et al.*, 2001; Xue *et al.*, 2007; Krizhanovsky *et al.*, 2008; Faget *et al.*, 2019). Activation of NKG2D signalling can trigger interferon-g (IFNg) production and cytolytic responses toward target cells (Swann & Smyth, 2007). This is thought to be important for the role of senescence in tumour suppression.

Senescent cells also increase secretion of extracellular matrix (ECM) remodelling factors, such as Matrix Metalloproteinases (MMPs) and decreased expression of fibronectin and collagen (Krizhanovsky *et al.*, 2008). MMPs affect the structure of

senesced cells through extracellular degradation and remodelling (Freitas-Rodríguez *et al.*, 2017). Another function of secreted MMPs is to regulate the activity of cytokines, through binding to the cytokines themselves or the ECM (Page-McCaw *et al.*, 2007; Adams, 2009).

Acutely, a SASP may be beneficial in allowing damaged cells to communicate their compromised state to neighbouring cells and facilitating their immune-mediated removal or to instigate tissue regeneration (Coppé *et al.*, 2010*a*; Freund *et al.*, 2010). Their distinct secretome attracts immune cells to the area to dispose of these damaged cells, reducing the risk of oncogenic transformation and stimulating surveillance and clearance of senescent cells by the immune system (Campisi & d'Adda di Fagagna, 2007; Freund *et al.*, 2010; Byun *et al.*, 2015). However, when senescent cells are not cleared and start to accumulate, such as in ageing tissues, the chronic expression of SASP factors can lead to tissue dysregulation and start a cycle of inducing further senescence. This senescence bystander effect is thought to be a contributing factor to the tissue deterioration seen during the ageing process.

1.5.2. Cellular senescence and ageing

Cellular senescence is a cell fate characterised by the cessation of cellular division whilst maintaining metabolic activity and having an altered, inflammatory, secretory phenotype. It is thought to be a positive evolutionary adaptation because it prevents damaged cells from continuing to divide thereby acting as an anti-tumorigenic mechanism promoting survival in young organisms (Von Zglinicki, 2002). The temporary presence of senescent cells in development and adult wound healing suggests that their pro-inflammatory state may be beneficial in development and regeneration processes before being cleared by the immune system *via* apoptosis. However, with increasing age most senescent cells become resistant to apoptosis and start to accumulate within several tissues, including skeletal muscle. Small numbers of these apoptosis-resistant senescent cells are present in the early adult years but are not thought to cause problems to homeostasis. However, there becomes a threshold where the pronounced and chronic SASP expression from the accumulated senescent cells can induce local and systemic inflammation, increasing risk of cancer, impairing tissue homeostasis and inducing secondary senescence in nearby cells through paracrine-mediated mechanisms, termed the senescent bystander effect (Coppé *et al.*, 2010*a*; Kuilman *et al.*, 2010; Nelson *et al.*,

2012). It is unclear why some senescent cells are not cleared by apoptosis or necroptosis but, it could be affected by either desensitisation of immune cells to the SASP, senescent cells entering a state whereby they oppose apoptosis or reduce their SASP so they become undetectable (deep senescence), or immune cell deficiency (Hampel *et al.*, 2005; Serrano, 2014). Overall, it is most likely to be that the accumulation of senescent cells does not cause negative effects until after reproductive ages and therefore cellular senescence is a neutral process unaffected by natural selection.

As organisms age the proliferative capacity of cells should theoretically decrease as the cells undergo more divisions over time. These cells are also more likely to accumulate random mutations and DNA damage due to more divisions but also due to increased cumulative exposure to radiation, free radicals and other environmental toxins. It is most likely that regenerative tissues such as the skin, liver and haematopoietic system are most likely to accumulate senescent cells as they require more frequent repeated cell divisions to maintain tissue functioning by replacing old or damaged cells even though these stem cells possess telomerase activity. Skeletal muscle is also a highly regenerative tissue however it may be slightly less affected due to the relatively few times it is called upon to undergo regeneration rather than micro-damage 'wear-and-tear' repair.

Indeed, there is a strong correlation between number of senescent cells and chronological age in many different organs and tissues including adipose tissue, skin, cardiac and skeletal muscle cells analysed both in mice and humans (Krishnamurthy *et al.*, 2004; Martin *et al.*, 2014). In humans, this has been shown in many tissues including cardiac progenitor cells, adipose tissue and potentially in skeletal muscle (Sousa-Victor *et al.*, 2014; Xu *et al.*, 2015*a*; Lewis-McDougall *et al.*, 2019). The causal role of senescent cells in ageing and declining tissue function was confirmed when evidence for the beneficial effects of senescent cell removal was shown by the clearance of $p16^{+ve}$ cells, *via* drug induced apoptosis, significantly increasing lifespan and healthspan in both BubR1 and chronologically aged wild type mice (Baker *et al.*, 2011, 2016).

Baker and colleagues showed this by genetically inserting an inducible Casp8 apoptosis cassette, known as "ATTAC", into the $p16^{Ink4a}$ promotor region to create "INK-ATTAC". Whereby apoptosis could only be activated in cells which expressed p16 after the systemic introduction of drug AP20187. The drug activated Casp8 by dimerizing the membrane-bound myristoylated FK506-binding-protein–caspase 8 (FKBP–Casp8) fusion

protein leading to Casp8 induced apoptosis (Baker *et al.*, 2011). The treated wild type mice showed reduced senescence cell burden and functional improvements in adipose, kidney and heart tissues. But, most relevant to this thesis, they also showed increased movement compared to untreated aged matched controls suggesting improvements to skeletal muscle when $p16^{+ve}$ cells were eliminated (Baker *et al.*, 2016). This was also supported by decreased mRNA for senescence associated genes, p16 and p21, in the whole gastrocnemius muscle tissue of these mice (Baker *et al.*, 2016). However, these studies were reducing the global level of $p16^{+ve}$ senescent cells and not targeting muscle tissues specifically. Therefore, the benefits to skeletal muscle may not be due to the removal of senescent cells within skeletal muscle tissue itself but due to the removal of senescent cells from other tissues improving the systemic circulatory environment. Moreover, there are different cell types within human skeletal muscle which may be contributing to the senescent marker expression that are not satellite cells. It is thus important to better understand the impact of senescent cells specifically within skeletal muscle to determine what impact they may have on the ageing phenotype of skeletal muscle.

1.6. Cellular senescence and skeletal muscle

The first experiments to observe human muscle cell behaviour *ex-vivo* were performed by Pogogeff & Murray, (1945) who observed the explant expansion of cells from muscle tissue which fused to form myotubes. The key work to develop a reproducible *in vitro* primary muscle cell culture was performed by (Blau & Webster, 1981). Thus laying the foundations for the first studies to investigate senescence and ageing in human primary skeletal muscle culture in the late 90's (Decary *et al.*, 1996, 1997). This first series of studies investigated the difference in telomere length and proliferative capacity of cell populations extracted from different chronologically aged humans. It was hypothesised that cells from older humans would have undergone more divisions during life and therefore would have a reduced proliferative capacity and shorter telomeres.

Cells were allowed to explant from muscle biopsies samples until they reached proliferative arrest from a 5-day, a 5-month-old infant, 9- and 15-year-old children, as well as, eight adults aged between 26 and 86 years (Decary *et al.*, 1996, 1997; Renault *et al.*,

2000). Skeletal muscle cells from a 5 day old infant could divide 55-60 times which quickly declines to 15-20 population doublings in cells extracted from all adult aged donors (Renault *et al.*, 2000). Although the total proliferative capacity was similar across the adult samples, the cells from older adult donors took longer to grow out of their explants and had a higher percentage of non or slow dividing cells, as measured by BrdU incorporation, suggesting some internal differences persisting in these cells post isolation. These cells also showed a down-regulation of skeletal muscle cytoplasmic structural protein desmin as the cells approached senescence, as well as, an increase in the number of desmin negative cells which are most likely to be skeletal muscle origin fibroblasts. The finding of no difference in adult aged cells replicative capacity were mirrored by the initial mean telomere length of the cell populations showing no difference between young and old adult donors (Decary *et al.*, 1996; Renault *et al.*, 2002*b*). However, when assessing minimal telomere length a decline with increasing age in extracted muscle cells was shown (Decary *et al.*, 1996; Renault *et al.*, 2002*b*). Even though minimal telomere length was significantly decreased the telomeres were still sufficiently long to allow for multiple rounds of replication, as shown by there being no difference in the cumulative population doublings.

These studies were limited by small sample sizes, not accounting for potential sex differences and not taking into account the health and physical activity status of the subjects. The muscle samples used in these studies were acquired during surgery or autopsy thus not from healthy participants which could impact their findings. Characterization of the subjects' physical activity levels is important, as overtrained endurance athletes have shown abnormally short telomeres in the vastus lateralis (Collins *et al.*, 2003), whereas the minimum telomere length within skeletal muscle of power-lifters tended to be longer than that in untrained young subjects (Kadi *et al.*, 2008). When accounting for these factors mean and minimum telomere length was unchanged in the vastus lateralis of active aged men and women (Ponsot *et al.*, 2008) suggesting that proliferative potential is not an issue in healthy older skeletal muscle.

In a condition where there is excessive proliferation of satellite cells, such as Duchene's muscular dystrophy (DMD), telomere loss was 14-time greater in dystrophic muscle compared to aged matched healthy controls (Decary *et al.*, 1997). The regenerative decline in these diseased muscles is attributed to replicative senescence of the satellite cells induced by their excessive proliferation during repeated cycles of

degeneration and regeneration (Decary *et al.*, 2000). Most importantly the telomeres of the aged adults were sufficiently longer, 10-12 kb, than the suggested critically short length, 7-9 kb for human muscle cells (Di Donna *et al.*, 2003). However, the early studies calculated telomere length of all nuclei within muscle tissue not just satellite cells and as satellite cells are <5% of myonuclei, not considering the other cell types in skeletal muscle, it would be unlikely to see a significant reduction (Decary *et al.*, 1996; Renault *et al.*, 2002*b*).

Lorenzon *et al.*, (2004) extracted cells from the skeletal muscle of a 2, 21, 48 and 76-year-old, all of which had high initial percentages of desmin^{+ve} cells (~90%). All three adult samples showed variability in number of population doublings, 18-24, 13-19 and 6-12 from the 21, 48 and 76-year old respectively, suggesting a reduced proliferative capacity with increasing age. Schäfer *et al.*, (2006) analysed cell populations extracted from 12 skeletal muscle biopsies spanning an age range of 2-82 years. All samples started with desmin^{+ve} cells percentages above 70%, however some cultures did not maintain this initial desmin expression through to replicative senescence becoming overrun with other cell types, most likely to be skeletal muscle origin fibroblasts. The populations that lost desmin expression divided more than their age matched populations which maintained desmin. However, all populations reached replicative senescence within 50 days of thawing with cumulative population doublings ranging from 8-26 doublings. When only considering the cell populations that started with high desmin expression, 80% or above, the authors suggest there may be a slight decline in proliferative capacity with increasing age although the *n* number was reduced to only seven samples spanning the adults years and included a sample from a two year old which could skew the correlation as it has previously been shown that young children have much higher population doublings than adults. Using their correlation, with the limitations discussed, the authors suggest that for every 10 years of life senescence occurs two population doublings sooner (Schäfer *et al.*, 2006).

These early studies all used few samples to span the whole lifespan. More recently, studies employing larger grouped sample sizes have shown that the proliferative capacity of adult human stem cells in culture was unaffected by donor age (Pietrangelo *et al.*, 2009; Alsharidah *et al.*, 2013; Barberi *et al.*, 2013; Bigot *et al.*, 2015). Pietrangelo *et al.*, (2009) compared the replicative capacity of skeletal muscle derived cells from 6 males, aged 38.0 ± 4.1 years with 5 females and 5 males aged 78.5 ± 7.7 years. There was no difference in

population doublings achieved with the young adult cells stopping dividing after 17–20 PDs compared to the elderly 15–20 PDs. However, this study was limited by very varied initial desmin expression, between 32.6% and 76% across all ages. Alsharidah *et al.*, (2013) showed no difference in the number of population doublings achieved between young (aged 20–25 years) and elderly people (aged 67–82 years). There was no difference in starting percentage of desmin positive myogenic cells between young or old donors, however it was variable with cell population desmin purities between 50-95%. Some populations lost desmin expressing cells with time in culture, irrespective of initial desmin expression percentages whereas one sample was initially 50% desmin positive yet maintained this level of expression through to replicative senescence. Those populations which maintained desmin expression underwent 5-12 population doublings whereas those which lost desmin expression underwent 15-20 population doublings. Barberi *et al.*, (2013) compared five young (age range 15–24-year-old), and 10 old subjects: five old sedentary (age range 72–80 year-old) and five old active (age range 68–79 year-old). All samples showed similar proliferative capacity and mean telomere length. This study did not provide the specific desmin expression percentages of the individual samples but they did mention staining for desmin. Bigot *et al.*, (2015) compared five young (15–24 years old) and ten old (72–80 years old) healthy subjects, most likely the same participants as (Barberi *et al.*, 2013). Here the authors state using a $CD56^{+ve}$ MACS sort of all samples as they showed low initial percentages of desmin expressing cells reporting significantly lower desmin expression (30% $desmin^{+ve}$ cells) in old donor cell populations compared to young (50% $desmin^{+ve}$ cells). MACS sorted young and old groups showed similar early passage mean telomere length, rate of cellular division and maximum population doublings before replicative senescence.

Most studies have low *n* numbers due to the labour intensity of the experiments with some populations requiring over 100 days of continuous culture to reach replicative senescence (Barberi *et al.*, 2013). Therefore, data from all published studies where age of donor, number of mean population doublings and percentage of $desmin^{+ve}$ positive cells were reported have been collated and plotted for mean population doublings against age of donor (Figure 1.6). The drop in proliferative capacity from birth to adulthood is striking compared to the relative stability during the adult years. There are high activity phases for satellite cells during development and through adolescence as skeletal muscle develops and grows. Once into adulthood, proliferative capacity of myoblasts is relatively

stable with no obvious tread for lower proliferative capacity in older adults compared to young adults although there is a large degree of individual variability.

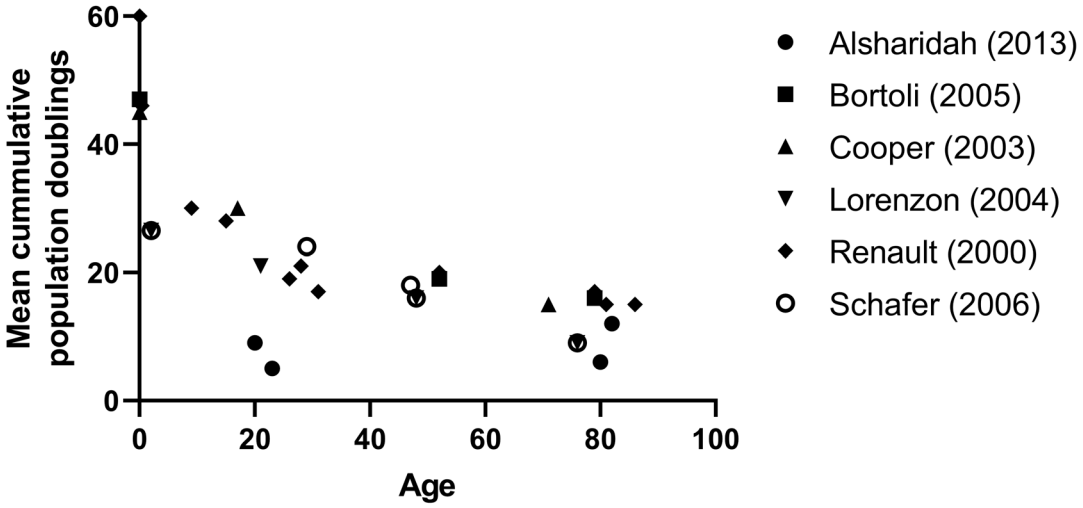

Figure 1.6. Population doubling limits of myogenic skeletal muscle cell populations.
Cumulative population doublings for desmin positive cell populations from all published studies that stated percentage of desmin^{+ve} cells and population doubling numbers. Only samples which where at least 80% desmin at senescence were included here.

It was hypothesised that satellite cells would become exhausted in later life due to the demands of repeated rounds of regeneration accrued across the lifespan. However, this does not seem to be the case, at least at the cell population level. In comparison, young DMD patients show reduced proliferative capacity reaching only 13 PDs compared to 30 PDs from age matched healthy people (Renault *et al.*, 2000). Here satellite cell replicative exhaustion could be potentially reached owing to the requirement of multiple rounds of regeneration due to increased muscle damage caused by their disease. Studies using *in vitro* replicative capacity as a measure of ageing are likely to misrepresent the *in vivo* cell population because any senescent cells extracted will be unable to proliferate and will therefore be rapidly outgrown by the proliferation of healthy, functioning cells. The proliferative capacity of cell populations is also not a very sensitive measure because population doublings are exponential therefore the number of cells after 20 PDs is 100's of millions of cells making any slight differences hard to observe. However, if *in vivo* populations still have such vast replicative capacity irrespective of age there are enough cells to regenerate the whole muscle. It therefore seems that reduced proliferative capacity of satellite cells is not the underpinning factor that causes impaired muscle

regenerative capacity with increasing age and that proliferative capacity of the population is not an issue in current human lifespan.

In vivo, myoblasts are a transient cell population which expand rapidly then terminally differentiate into myocytes. Under cell culture conditions these cells will differentiate and fuse together if left to become confluent in high serum conditions, as well as, at lower confluency in low serum conditions. The myogenic differentiation assay is therefore a model system of the early stages of regeneration and is useful to identify any functional differences *in vitro* which may reflect the *in vivo* phenotype.

As has been suggested, there are considered to be enough cells with proliferative potential *in vivo* to fully regenerate whole skeletal muscles, however they must also be functionally able to differentiate if they are to restore muscle function. The early studies presented previously also looked at differentiation capacity from their different aged human donors. Renault *et al.*, (2000) showed that myotube formation, as measured by fusion index, was not different between different aged adults. Whereas, Lorenzon *et al.*, (2004) did show age related impairment in fusion capacity. Although, this study was using unsorted cells (but 90% desmin^{+ve}) from a 2, 21, 48 and 76-year-old. Cells from the 48-year-old took longer to fuse but eventually formed myotubes whereas cells from the 76-year-old were unable to form myotubes even after 10 days. Although, these cells did show an increase in myogenin, the MRF that signals commitment to differentiation, suggesting these cells may have a very delayed differentiation or an inability to complete fusion. Jacquemin *et al.*, (2004) also showed lower fusion index and fewer nuclei per myotube from unsorted, but with desmin^{+ve} cell percentage above 70%, cells grown from muscle explants from a 65-year-old when compared to a 17-year-old. However, as both studies only used one biopsy per age limited conclusions can be drawn from their findings.

In a study using samples from 3 young (29-48 years) and 6 old (69-87 years) donors Fulle *et al.*, (2005) showed a trend for poorer fusion of myoblasts from older donors 33.7% compared to 56.7% in younger adults. Older donor cells also had a reduced antioxidant activity of catalase and glutathione transferase compared to newborn and younger adults. They exhibited lower membrane fluidity and higher basal cytoplasmic calcium levels. These results suggest that within aged skeletal muscle there is altered antioxidant capacity which could interfere with calcium handling impairing contractile function. However, the conclusions are limited by low numbers of desmin^{+ve} cells, around 60%, in

both young and old adults. Therefore, these results must be taken in a general effect on "muscle mononucleated cells" than on myoblasts specifically. A similar study by Beccafico *et al.*, (2007), also using mixed cell populations from 3 young (~30 years, ~55% desmin) and 3 old (~83 years, ~40% desmin), showed a lower fusion index from old donor cells, ~25%, after 7 days of differentiation than young donor cells, ~45%. Myotubes formed by the old donor cells also showed more oxidative damage in the form of lipid peroxidation. This increase in lipid peroxidation could affect membrane fluidity as reported by Fulle *et al.*, (2005) and explain why they did not see any calcium spike in the old participants, although the poor myotube formation could also explain this.

The first study of differentiation capacity with sizeable groups of participants was performed by Beccafico *et al.*, (2011) who investigated eleven old (77.3±6.4 years) and ten young (28.7±5.9 years) cell populations with over 95% desmin^{+ve} muscle precursor cells, as measured by positive tyrosine-protein kinase Met (c-Met) staining. In this study they showed old cells differentiated less efficiently than young and had lower Pax7 expression, reduced ability to express MyoD, Myogenin and MHC, as well as, lower RAGE and higher S100B levels. Sousa-Victor *et al.*, (2014) also showed lower fusion from older donors but they only measured fusion after 48 hours whereas Beccafico *et al.*, (2011) took their differentiation out to six days. Previous studies have shown that old cells take longer to fuse but do eventually fuse fully therefore this could just be delayed differentiation rather than inability to use. In contrast, Alsharidah *et al.*, (2013) showed there was no difference in fusion index, myotube size or expression patterns of MyoD, myogenin or MHC between different aged donors. Conversely, Bigot *et al.*, (2015) actually showed increased fusion of older donor cells. The authors suggest that there were fewer unfused cells due to epigenetic repression of SPRTY-1 expression preventing the cells ability to return to quiescence. This would leave differences in the reserve cell populations rather than the differentiating populations and could suggest a possible mechanism for the reduced satellite cell number with ageing. Overall, the fusion competence of cells from different aged humans is variable with variably between and within studies, even when percentage of desmin positive cells is controlled for.

A recent meta-analysis looking at senescence burden in aged human tissue highlighted the lack of research into senescence post-mitotic tissues such as skeletal muscle. This meta-analysis found no human skeletal muscle studies which met their entry criteria into the meta-analysis (Tuttle *et al.*, 2020). Within the studies to look at

senescence within human skeletal muscle contradictory results have been reported when analysing expression of the commonly utilised senescent markers. Carlson & Conboy, (2007) show increased whole skeletal muscle tissue protein levels of p21 and p15 but not p16 in older people. Barberi *et al.*, (2013) observed similar results when looking at mRNA in early passage myogenic precursor cells showing increases in p53 and p21 but not p16 mRNA expression in cells from aged donors. Bigot *et al.*, (2015) also showed no difference in p16 mRNA expression or in the number of SA β-gal positive cells in populations of human muscle precursor cells. Whereas, Sousa-Victor *et al.*, (2014) showed an age-related increase in SA β-gal positive cells, elevated p16 and p15, as well as, increased γH2aX expression. Conversely, Alsharidah *et al.*, (2013) found no difference in γH2aX. The conflicting results between these studies could be due to the different age criteria used to define for the aged group. With the Sousa-Victor *et al.*, (2014) study using significantly older donors suggesting that there was a potentially late life decline in these "geriatric" people that was not captured by the previous studies. This could also relate to the physiological function of the individuals as older individuals are more likely to be frail and senescence may be associated with frailty.

The current literature on senescence in human skeletal muscle cell culture studies is conflicting. There are some methodological considerations that could account for these differences in observed results. Satellite cells are maintained in a state of quiescence for most of their life *in vivo*. One of the major problems with *in vitro* studies is that once extracted from a muscle biopsy, quiescent satellite cells become activated and do not naturally re-enter quiescence (Machado *et al.*, 2017). The activated cells start to divide and differentiate, altering their transcriptome and phenotypic markers (Charville *et al.*, 2015). The expansion of the extracted cell populations will affect the detection of senescent cells because senescent cells, by definition, do not divide and cannot re-enter the cell cycle. Therefore, if senescent cells survive the extraction process they will not divide. The expansion of healthy proliferating cells will diminish the percentage of senescent cells within the population which could account for some of the discrepancies in the early passage marker expression due to different extraction methods and different time points used. Therefore, it is important to understand what the phenotype of senescent muscle origin cells are so that they can be identified before being overrun by expanding cells.

1.7. Replicative senescence – ageing in vitro

The early passage comparison of young and old MPCs have shown that old satellite cells function can be restored by removing them from their old environment and replacing them in a youthful environment. This suggests that satellite cells from older individuals are at least mostly able to be rejuvenated. Understanding which factors are causing the impairment as well as which factors have restorative capabilities is a pertinent question. It has been established that extracted cells from old muscle are altered by the culture environment in which they are grown masking or altering their phenotype, although this is encouraging for improving the *in vivo* phenotype, it makes identifying and investigating causal factors difficult. Many different methods could therefore be employed to try to artificially identify these factors and what effects they have on satellite cell functioning. Indeed, many studies have investigated these with animal models, cell lines and primary cell cultures. However, there are key differences between human and mouse physiology down to the cellular level. Therefore, a human culture aged, senescent, cell population may be able to shed light onto specific factors which impact satellite cell functioning, as well as, provide a human model in which to test the effects of such factors.

When culture MPC populations approach senescence their cell morphology starts to change, the cells become larger and flatter with a more pronounced intermediate filament network (Renault *et al.*, 2000). This early study also suggested that the cells started to down regulate desmin expression (Renault *et al.*, 2000). However, later studies using multiple markers show that there is often an increase in TE7 positive fibroblasts as desmin positive myoblasts decrease (Schäfer *et al.*, 2006; Alsharidah *et al.*, 2013).

Analysis of the gene expression changes of senescent cells from one 5-day old, one 52 year old and a 79-year-old has been investigated using cDNA arrays (Bortoli *et al.*, 2003). These were pilot data due to only three participants analysed across a wide age range and the new-born cells were considered early passage after 21 population doublings whereas the older participants were analysed after 1 population doubling. Additionally, comparing new-born to old adults is comparison of development to old adulthood rather than age related changes in adult myoblasts. From this analysis four potential markers of pre senescent myoblasts were identified: up regulation of allograft inflammatory factor 1 and actin alpha 1, as well as, down regulation of serine proteinase inhibitor and colon cancer antigen 7. There was also shown to be a shift in mitochondria

metabolism genes with senescence away from carbohydrate metabolism. The cells from the same 5-day old muscle sample where also analysed *via* proteomics and demonstrated targeted oxidative damage to proteins which were related to impairment in cellular energy metabolism (Baraibar *et al.*, 2016).

Studies with more participants in their comparison groups showed increased p16 mRNA expression and shorter mean telomere length at replicative senescence (Barberi *et al.*, 2013). Another study showed that expression of proliferation marker Ki67 was heterogeneous however the general trend across all populations was for a reduction in expression to zero as the population reached senescence and the number of cells positive for DNA damage increased from less than 10% during early passage to around 90% at senescence (Alsharidah *et al.*, 2013). The main limitation of this study was that some myoblast populations did not maintain their initial high percentage of desmin^{+ve} cells and therefore could not be analysed as senescent myogenic populations. It is unclear why some highly myogenic populations lost desmin^{+ve} cells whereas one cell populations started and reached replicative senescence with 50% desmin^{+ve} cells.

The ability of culture aged cells to differentiate and engraft has also been investigated. Late passage cells from a 5-day old new-born, approx. 10 population doubling before senescent, were less successful at grafting into immune compromised mouse muscle fibres than early passage cells from the same biopsy. Fewer cells were detected but also lower percentages of total cells incorporation into mosaic fibres at both 4 and 8 weeks (Cooper *et al.*, 2003). These results were also seen in cell culture models where senescent cells were less mobile and took longer to differentiate eventually forming thinner, smaller myotubes (Renault *et al.*, 2000). Lorenzon *et al.*, (2004) reported that culture aged myogenic cells from a 2-year-old donor differentiated similarly to freshly isolated cells from a 21 and 48-year-old in terms of fusion index and nuclei per myotube after 10 days. Array analysis of RNA expression of these myotubes showed upregulated pyruvate kinase and GLUT4 down regulation after differentiation of senescent cells in all three participants, one 5-day old, one 52-year-old and one 79-year-old (Bortoli *et al.*, 2005).

Bigot *et al.*, (2008) compared the ability of freshly isolated and senesced myoblasts to form myotubes. Early passage cells formed larger myotubes with 90% of nuclei being incorporated into myotubes containing more than 50 nuclei. Whereas, senescent cells

formed smaller myotubes with only 2% of nuclei being incorporated into myotubes containing more than 50 nuclei and 63% being incorporated into myotubes containing less 25 nuclei. These results were supported by lower and delayed expression of MyoD and myogenin RNA and proteins in the senescent population. This reduced fusion was also the case when senescent cells were plated at density double that of confluence suggesting an inherent defect in differentiation. However, this study only looked at one biopsy from a 5-year-old infant and a 17-year-old.

Using only the cell populations which maintained high desmin expression though to replicative senescence (*n*=5), Alsharidah *et al.*, (2013) showed that as the cells were aged in culture their ability to differentiate gradually declined. Myoblasts were induced to differentiate at early passage, after 16 days and 28 days in culture, then at replicative senescence. Incremental reductions in the expression of MyoD, myogenin and MHC were observed as the number of passages increased suggesting slower differentiation. The size of myotubes formed and percentage of nuclei incorporated into these myotubes, fusion index, were significantly reduced at senescence. This delay in differentiation could be due to the regulatory cytokine TGF-β which was shown to be more concentrated during the first 48 hours of differentiation in senescent compared to early passage myoblasts. TGF-β was confirmed as a transient inhibitor of differentiation with the addition of 300 pg ml^{-1} to early passage myoblasts preventing the expression of Myogenin and MHC seen in differentiation. When the TGF-β concentration was reduced to 100 pg ml^{-1} Myogenin and MHC expression increased, and normal differentiation was restored.

Overall, little is still known about the senescent phenotype of human myoblasts. It is known that their ability to differentiate is impaired, but the underlying mechanisms are not fully elucidated, although TGF-β is known to be involved. Senescent markers at replicative senescence are not well characterised and often only in very low numbers of participants. Such studies have also been hampered by difficulty maintaining high initial desmin expression in these primary cell populations as they become overrun with skeletal muscle origin fibroblasts. This highlights the importance of understanding the contributions of other cell types within skeletal muscle to the tissue's senescent phenotype, as well as, determining if other senescence induction methods could be used to generate senescent populations of primary skeletal muscle cells.

1.7.1. Sorting cell types within skeletal muscle biopsy

Biopsies of skeletal muscle contain many different cell types and therefore yield a mixed cell population of mononucleated cells including muscle precursor cells, fibroblasts, fat cells, blood cells and immune cells. All studies have been confounded by variability within the cell populations myogenic cell proportion and although pre-plating was employed to enrich myogenic cell percentages it was only in recently where studies regularly started using sorting techniques to further enrich myogenic populations (Barberi *et al.*, 2013; Agley *et al.*, 2015; Bigot *et al.*, 2015). Therefore, relatively few studies have been performed on highly enriched cell populations.

The nuclear location of Pax7 make it problematic as a sorting marker of human cells because it requires either genetic labelling of the protein or permeabilization, and therefore death, of the cell population. Any study requiring a viable population of human satellite cells cannot use Pax7 without genetical alteration to the cell and therefore another marker, preferably on the cell surface, must be used. Fluorescence Activated Cell Sorting (FACS) have been used to sort for myogenic cells by positively selecting for $CD56^{+ve}/CD29^{+ve}$ cells (Xu *et al.*, 2015*c*) or negatively selecting for $CD34^{-ve}/CD31^{-ve}/CD45^{-ve}$ cells (Charville *et al.*, 2015). Both methods yielded cell populations with very high $desmin^{+ve}$ percentages. Whilst FACS is a very good sorting method, it requires a large number of cells for positive and negative controls, especially when using multiple markers. The process of forcing cells through high pressure flow is also a stressor for the cells which can reduce the viability of the cell population and affect the cells early behaviour in cell culture (Hines *et al.*, 2014).

Magnetic activated cell sorting (MACS) has been shown to be much gentler on the cells when compared to FACS as well as being a lot easier and quicker to perform in a laboratory setting (Sutermaster & Darling, 2019). A $CD56^{+ve}$ MACS sorting protocol has been developed which has been stringently tested to show that $CD56^{+ve}$ cell sorts produce a 98% $desmin^{+ve}$ population in human myogenic cells (Agley *et al.*, 2013, 2015). They also show that these cells can differentiate into myotubes and are unable to undergo adipogenesis.

Sorted cell populations allow better understanding of the expression of a single cell type that are not confounded by other cell types which may be on different senescent trajectories. The characterisation of senescent populations of skeletal muscle cells could

provide cell type specific markers of senescent cells which could be used for determining the senescent state of *in vivo* populations of cells. Due to the problems and current limitations associated with assessing senescence within populations of aged myoblasts *in vitro* other methods need to be utilised to determine the phenotype and tissue specific marks of cellular senescence within skeletal muscle cell populations. Studies have been mentioned previously that assessed the replicative capacity of human cells in culture as a method for determining if cells from aged people were closer to replicative senescence than younger donor cells. These studies involved passaging cell to replicative senescence. Investigating the phenotype of cells at replicative senescence could help to characterise and develop new markers and greater understanding of the characteristics of senescent skeletal muscle cell populations.

1.8. Aims

The Literature Review has set out to establish the current understanding of ageing and cellular senescence with regard to human skeletal muscle cells and identify gaps in our knowledge. Human primary cells are the chosen model for this thesis and these primary cells were extracted from skeletal muscle biopsies with the myogenic cells originating from satellite cells, which in this work will refer to cells in their anatomical niche location between and underneath the basal lamina (Mauro, 1961). These cells become activated almost instantaneously when the extraction process begins (Machado *et al.*, 2017), and therefore the cells used in these experiments and in this thesis will be referred to either as muscle precursor cells (MPCs), which refers to the activated and partially differentiated cell progeny of satellite cells. The other main mononucleated cell type extracted are stromal fibroblasts which are also present in the skeletal muscle biopsy. The work in this thesis sets out to provide further insight into this area and had the following aims.

1. To develop bespoke automated quantitative image analysis programs to analyse the different type of microscopy images collected throughout this thesis.

2. To characterise and compare the replicative profiles of sorted $CD56^{+ve}$ (myogenic precursor cells) and $CD56^{-ve}$ (fibroblast) cell populations extracted from the same human muscle biopsies in terms of markers of senescence and their SASP expression.

3. To examine the effects of chemotherapeutic drug, Doxorubicin, at inducing premature stress-induced senescence in the two cell types. This again was characterised in terms of markers of senescence and their SASP expression.

Chapter 2: General methods

This chapter outlines the participant classification and recruitment, the muscle biopsy procedure, as well as the previously established core techniques used recurrently across multiple studies in this thesis. These include the cellular extraction, magnetic activated cell sorting and general cell culture. Analysis techniques such as polymerase chain reaction, immunocytochemistry and microscopy. Methods which were required to be developed or enhanced are presented in a specific method development chapter, Chapter 3.

2.1. Participants and ethical approval

Prior ethical approval was obtained from the UK National Health Service Ethics Committee (London Research Ethics Committee) and in accordance with the Human Tissue Act and Declaration of Helsinki. Co-sponsorship for the project was awarded by King's College London and Guy's and St Thomas' Foundation Trust.

Young participants (18-35 years) were recruited using King's College London internal research study circular email. Before visiting the laboratory, they had received a lay overview of the project and completed a pre-screen health questionnaire. On arrival participants were talked through the study by the principal investigator and any questions they had were answered before providing written consent to take part in the study and have the muscle biopsy.

2.2. Muscle biopsy

The muscle biopsy procedure occurred in the muscle biopsy suite situated in Shepherd house of King's College London's Guy's campus. Muscle biopsy samples were always taken from the mid-belly of the *vastus lateralis* of the participant's chosen leg. First a sterile field was created around the participant's leg using sterile surgical drapes. The leg was then shaved, if required, around the site of the muscle biopsy. Chlorohexidine was used to clean the skin of the leg and allowed to dry. Local anaesthetic (2 % lidocaine) was injected into the skin and muscle belly and allowed to infiltrate the surrounding area for

10 minutes. Once the anaesthetic has numbed the area, a sterile scalpel blade was used to make a 1 cm proximal to distal incision in the skin for the Bergström needle to be inserted through. The needle, with additional suction provided by a sterile syringe and connective tubing (Bergström, 1962; Agley et al., 2013), was then inserted into the muscle through the incision site and muscle facia. The window in the needle was then opened and suction applied to draw the muscle tissue into the open window. The window was then closed making a cut through the muscle tissue. After rotating the needle through 90° the cutting was repeated followed by two more rotations and cuts before the needle was removed. The tissue was immediately transferred into a collection tube containing ice cooled basal skeletal muscle growth medium, which had previously been weighed. The tube was then weighed again, and tissue weight was determined by subtracting the weight of tube+media from the weight of tissue+tube+media. The typical muscle wet weight achieved from this laboratory using this technique is 100-200 mg. Ethical approval allows up to three separate needle entries into the muscle, however the laboratory has never needed more than a second pass to collect enough tissue (100-150 mg). Each biopsy sample was anonymised with a code e.g. Y01 which was used throughout all experiments undertaken with the cell populations extracted from that biopsy sample. Due to the labour-intensive protocol no more than two biopsies could be processed and analysed at one time. Therefore, all experiments for Y01 and Y02 were undertaken before biopsies Y03 and Y04 were taken which, in turn, were completed before biopsies Y05 and Y06 were taken.

2.3. Cell extraction

The biopsy samples were transferred into a sterile laminar flow hood, so cells could be extracted under sterile conditions using the published method developed previously (Agley *et al.*, 2015). The muscle sample in solution was tipped into a sterile Petri dish and the basal media was replaced with digestion media (2-3 ml; 2 mg/ml collagenase D, Roche and 2 mg/ml Dispase II, Sigma). Collagenase D and Dispase II were chosen instead of Trypsin or pronase because they are less harsh digestion enzymes and are therefore more likely to preserve cellular functioning and surface marker expression. To negate any differences between enzyme batches new enzymes were ordered then aliquoted into 20x stocks in basal medium and frozen for long term storage at -20°C.

The tissue was then minced into ~1 mm^3 pieces using two sterile surgical scalpels for up to 10 minutes. The minced tissue was then transferred to a sterile 15 ml falcon tube using a 25 ml stripette due to its large bore hole. The petri dish was washed with more digestion media (2-3 ml) 3 times to collect any remaining tissue. The 15 ml falcon tube containing tissue in digestion media (total 10 ml) was placed in a 37°C incubator for 1 hour with trituration, using a 10 ml stripette, every 15 minutes. Once digestion was complete the enzyme reactions was quenched by adding an equal volume of Skeletal Muscle Growth Medium (SKGM, Promocell, Table 2). The cells were reclaimed by centrifugation at 657 g for 6 minutes. No additional debris or cell type removal occurred as it was thought the extra steps could potentially negatively affect cell yield and functioning. The cells were re-suspended in SKGM and plated into a T25 cell culture flask for seven days. After 48 hours the media was removed centrifuged at 657 g for 6 minutes and the cell pellet was re-suspended in fresh SKGM and replaced into the culture flask. A further media changed occurred 48 hours later however, the media was discarded without centrifugation. Any non-adherent cells at this time point are assumed to be dead cells or unwanted cell types such as, red blood cells. Seven days after isolation the cells were trypsinised and prepared for magnetic activated cell sorting (MACS). This cell extraction method yields $2.8 \times 10^6 \pm 8.87 \times 10^5$ cells/g tissue after the 7 day expansion period in SKGM (Agley *et al.*, 2015). This cell yield was sufficient for the experiments undertaken therefore, it was thought that higher enzyme concentrations were unnecessary and could potentially negatively impact cell viability.

2.3.1. Magnetic Activated Cell Sorting

After seven days of culture post biopsy, cells were trypsinised (0.04% Trypsin-EDTA in PBS) and pelleted. The centrifuged cell pellet was re-suspended in 170 µl sterile filtered MACS buffer (1% BSA, 0.05% EDTA, Miltenyi Biotec) and incubated with CD56 magnetic antibody (35 µl, Miltenyi Biotec) for 15 minutes, mixed halfway, in the dark at 4°C. The solution was then diluted with 10 ml MACS buffer, centrifuged (6 min, 657 g, RT) and re-suspended in 1 ml MACS buffer. The MACS column was pre lubricated with 1 ml MACS buffer before the cell suspension was passed through the column followed by three 1 ml washes with MACS buffer. The negative fraction was collected in a tube containing 2 ml MACS buffer. Following the final wash, 2.5 ml was added to the column which was removed from the magnetic field and the plunger applied to dispense the positive cell

fraction into a different tube containing 2 ml MACS buffer. Both fractions were then centrifuged and re-suspended in 1 ml SKGM for haemocytometer counts and subsequently plated at required densities for experimentation. Throughout this thesis the $CD56^{+ve}$ fractions will be referred to with the biopsy sample code and (+), e.g. Y01+. The $CD56^{-ve}$ fractions will be referred to with the biopsy sample code and (-), e.g. Y01-.

Table 2. Cell culture media composition

Media Component	Concentration	Company
Skeletal Muscle Cell Basal Medium	-	Promocell
Fetal Calf Serum	5%	Promocell
Fetal Bovine serum	10%	PAA Laboratories
Fetuin (bovine)	50 µg / ml	Promocell
Epidermal Growth Factor (recombinant human)	10 ng / ml	Promocell
Basic Fibroblast Growth Factor (recombinant human)	1 ng / ml	Promocell
Insulin (recombinant human)	10 µg / ml	Promocell
Dexamethasone	0.4 µg / ml	Promocell
Penicillin	100 U/ml	Sigma
Streptomycin	100 µg/ml	Sigma
L- Glutamine	292 µg/ml	Sigma

2.4. Cell culture

2.4.1. Passaging cell populations

Skeletal muscle myoblasts start to differentiate and fuse to form myotubes when at high density, even if in a high serum medium. Therefore, passaging occurred before cells became 80% confluent, which translates to every 3-4 days. Human skeletal muscle myoblasts will eventually senesce in cell culture and therefore proliferation rate slows over their replicative lifespan which increases the amount of time taken to reach 80% confluence and hence increases the time between passages. For experiments which required a calculation of population doubling time passage time was kept constant at

every 3 days to standardize across all cell populations. Skeletal muscle fibroblasts were also passaged every 3-4 days.

2.4.2. Trypsinisation

The mononucleated cells extracted from a muscle biopsy are adherent to tissue culture plastics. To detach the cells for further applications the culture media was removed and retained in a 20 ml universal tube. The flask was then washed with PBS and incubated with trypsin (0.04% Trypsin-EDTA in sterile PBS) for 3 minutes at 37°C. Once all cells had detached the retained culture media was added to quench the trypsin digestion. The cell suspension was then centrifuged (6 min, 657 g, RT) to pellet the cells. The supernatant was removed leaving a cell pellet ready for resuspension for counting, sorting etc.

2.4.3. Cell counting

To obtain a viable cell count cells were first trypsinised, centrifuged and resuspended in 1 ml SKGM, as described previously. Depending on estimated cell number 10 µl of cell suspension was diluted in a different total volume of counting buffer. Counting buffer contained 10 µl of trypan blue with or without the addition of 30 µl or 80 µl PBS, thus giving a final dilution of cells:counting buffer at either 1:1, 1:4 or 1:9 respectively. The haemocytometer was then set up by breathing moist air onto the coverglass to aid attachment to the haemocytometer. 10 µl of diluted cells were then added to each chamber of the haemocytometer using capillary action to draw the solution under the coverglass. Viable cells, cells which exclude trypan blue, were then counted in the four outer quadrants of the haemocytometer for each chamber using a x10 magnification objective under a light microscope. The average number of viable counted cells of the two chambers was calculated, then divided by the number of chambers counted, 4, then multiplied by the dilution factor in counting buffer, i.e. 2, 5 or 10 depending on volume used, then multiplied by the dilution factor of the resuspended cell sample, i.e. 1 ml, finally multiplied by 10,000 which converts from the volume of the haemocytometer (0.1 mm^3) to 1 cm^3, which is equivalent to 1 ml.

Using the total number of cells in suspension the required volume needed to plate a certain number of cells for experiments can be calculated. The volume of cell suspension

divided by the total number of cells then multiplied by the required number of cells gives the volume of homogenous cell suspension containing that number of cells. The standard plating densities for human skeletal muscle myoblasts in this laboratory are 2,500 cells/cm^2 and 7,000 cells/cm^2 for proliferation and differentiation respectively. However, plating densities differ depending on experiment and are stated for each individual experiment.

2.4.4. Freezing cells

Aliquots of cells ($5x10^5$-$1x10^6$) were frozen down across their replicative time course as backups if populations became contaminated or as cells populations for future experiments. The freezing medium was the same for both myoblast and fibroblast cell populations which was, skeletal muscle basal medium with high serum content (20% FBS and 1% PS). Each aliquot contained 900 µl of freezing medium and 100 µl DMSO, which was added just prior to freezing to prevent cell toxicity. Aliquots were frozen to -80°C slowly at roughly -1°C/minute in an isopropyl alcohol buffered *Mr Frosty™*. Once frozen samples were transferred to liquid nitrogen dewars for long term storage.

2.5. Immunocytochemistry

Cultured cells were either cytospun on to poly-L-lysine microscopy slides or grown on collagen coated coverslips for immunocytochemical analysis. For cytospun samples aliquots of cells were prepared at a density of 10,000-20,000 cells per 200 µl. Double funnel cytospin slide holders were assembled with poly-L-lysine microscopy slides and the 200 µl of cell suspension was added to each funnel. The funnel cassettes were then spun at 600 rpm for 3 minutes at room temperature. The cytospin spots were then either frozen at -80°C or fixed (4% paraformaldehyde in PBS) for 10 min, washed and stored in PBS for no longer than 2 weeks.

Coverslips were used for the myotube formation assay to visual the myotube structures formed. The 1.5 thickness glass coverslips were washed (1% acetic acid, 70% ethanol) for 4 hours with gentle rocking, then air dried overnight in a laminar flow hood with 15 min UV light exposure to sterilise the coverslips. Once dried, coverslips were placed in the bottom of 24 well plate wells and covered with collagen (0.5 mg/ µl in dH_2O).

After 4 hours at room temperature, or overnight at 4°C, collagen solution was removed and stored for future use. Coverslips were then sterilised by exposure to UV light for 10 before being washed with PBS (x3) and stored in PBS+NaN_3 at 4°C until use. When coverslips were to be used the PBS+ NaN_3 was removed and replaced with SKGM. These plates were then allowed to equilibrate in a 37°C incubator for 2 hours before cells were plated onto them. After the experiment had been completed cells attached to coverslips were fixed with 4% PFA for 10 minutes, washed with PBS (x3), then stored in PBS+NaN_3 at 4°C until use.

Once ready to stain both fixed cytospin and coverslip mounted cells had their cell membranes permeabilised (0.1% triton X-100, 1% BSA in PBS) for ten minutes followed by the three PBS washes. Blocking solution (1% BSA in PBS+NaN_3) was then applied for one hour at room temperature before the blocking solution was removed and the samples were incubated overnight in diluted primary antibody solutions at 4°C. Primary antibodies were diluted as per Table 3 in PBS+NaN_3 (1% BSA). Samples were washed three times with blocking solution then incubated with diluted fluorescent secondary antibodies (1:1000) as per experimental requirements for 1 hour at room temperature protected from light. Samples were washed for a final 3 times with PBS+NaN_3 before mounting. Cytospin samples were covered with 1.5 thickness glass coverslips using prolong gold antifade mounting medium. Glass coverslip mounted samples were removed from their wells using tweezers and a needle point. The coverslips were then mounted onto poly-L-lysine microscopy slides using prolong gold antifade mounting medium. If DAPI was not included in the fluorescent secondary antibody mix, prolong gold antifade mounting medium containing DAPI was used.

2.5.1. Senescence associated β-Galactosidase assay

The SA β-Gal staining kit from cell signalling technologies was used as per manufacturer's instructions. The assay utilises the shift in enzyme kinetics that non-senescent cells exhibit β-galactosidase activity optimally at pH 4.0 (Kuilman *et al.*, 2010). The heightened activity of SA β-Gal in senescent cells can be measured at suboptimal pH 6.0. At the end of the specific experiment the SKGM media was removed and cells were fixed for 10 minutes with 1X fixing solution diluted in PBS. They were then washed with PBS (x3) before being incubated with 1 ml of X-gal staining solution (50 µl X-gal (20mg/ml in DMF), 10 µl supplement A, 10 µl supplement B, 930 µl 1X staining buffer, pH 6)

overnight in a humidified 37°C chamber, without added CO_2, in the dark. Cells were then washed twice with PBS followed by a 30 s wash in methanol before washing again with PBS and stored in PBS+NaN_3 at 4°C until imaging. Prior to starting experiments, this SA β-Gal method was adapted to work on cytospin samples so that all image analysis could be performed on cytospun cells. However, technical issues arose with this developed method which affected the first four biopsy samples collected: Y01, Y02, Y03 and Y04. The final two biopsies from the replicative experiments (Y05 and Y06), as well as the hip fracture study were assayed for SA β-Gal using the plated protocol described above. The technical issue was most likely caused by the very small volumes of staining solution used on cytospin samples (200 µl) and therefore any residual washing buffer could affect the very tight pH range required by the assay kit.

Table 3. Immunofluorescence staining antibody dilutions.

Name/antigen	Antibody species and isoptype	Dilution concentration	Company & code
CD56	Mouse mc IgG_1	1:100	BD biosciences 347740
Desmin	Rabbit mc IgG_1	1:250	CST 5332
Desmin	Mouse mc IgG_1	1:250	Dako M076001-2
$MyoD_1$	Mouse mc IgG_1	1:20	Novocastra NCL-MyoD1
Myogenin	Mouse mc IgG_1	1:50	DSHB D7F2
Myosin Heavy Chain 1	Mouse mc IgG_{2b}	1:200	DSHB MF20
Anti-human fibroblast (TE-7)	Mouse mc IgG_1	1:100	Millipore CBL271
Ki67	Rabbit mc IgG_1	1:200	A Menarini Diagnostics MP-325-CRM
γ-H2AX	Rabbit mc IgG	1:500	Cell Signaling Technology 9718
p16	Mouse mc IgG_{2b}	1:50	Abcam ab54210

2.5.2. Microscopy

The SA β-Gal stained cells were imaged using an Olympus bright field microscope equipped with 4x, 10x and 20x air objectives and a colour camera. Cells were identified using the phase contract filter which was removed before image acquisition. Images were acquired using cellSens software to adjust exposure time and to set white balance. Images were analysed with a manual count of number of positive staining cells divided by total number of cells counted.

All fluorescence microscopy took place on an Axiovert upright microscope (Zeiss, Germany) equipped with a 10x, 20x and 40x air objectives with a charge-coupled device (CCD) camera. Images were acquired using Axiovision software (version 4.3.2 Carl Zeiss Microimaging, Germany) on a PC. Fluorescence was detected from emission wavelength in the blue, green, red and far red spectral ranges as per the secondary antibodies. Bespoke image analysis programs were developed in FIJI and python to analyse the fluorescence images for each specific analysis. These programs, as well as a description of quantitative fluorescence microscopy are detailed in the image analysis method development chapter (Chapter 3).

2.6. Q RT-PCR

Prior to each step in the gene transcription analysis the RNA work only bench area and pipettes were cleaned was RNase away to reduce any chance of contamination with RNases which could degrade the RNA. The RNA was extracted from cells using Qiagen RNeasy Plus Mini Kits at room temperature. In preparation for RNA extraction cells were either trypsinised and washed twice with PBS or washed twice in their wells. The washed cells were then mixed or scraped off the wells with 350 µl of Qiagen lysis buffer RLT. Cells were further lysed through QIAshredder spin columns for 2 minutes at 16,000 g. At which point the cell lysates were frozen at -80°C so sample from the same experimental series could be processed together. Once defrosted an equal volume of ethanol (350 µl; 70% in RNAase free water) was added to the lysate. After mixing, 700 µl of the sample was transferred into an RNeasy spin column and centrifuged for 15 seconds at 12,000 g. The flow through was discarded and 700 µl of Buffer RW1 was added to the same RNeasy spin column, the column was again spun for 15 seconds at 12,000 g. The flow through was discarded and 500 µl of buffer RPE was added to the RNeasy spin column, the column was

again spun for 15 seconds at 12,000g. This step was repeated with the centrifugation extended to 2 minutes at 12,000 g to dry out the column. The RNeasy spin column was removed and placed into a fresh 1.5 ml Eppendorf (RNA and DNA free) before 30 µl of RNase-free water was added to the spin column and centrifuged for 1 min at 12,000 g to collect the RNA. Collected RNA was stored on ice and quality and quantity was assessed using a NanoDrop spectrophotometer (NanoDrop Technologies). Firstly, the Nanodrop was blanked using the same RNase-free water RNA was collected in to give the reference intensity to calculate absorbance. RNA concentration of each sample was then measured as well as 260/280 nm and 260/230 nm ratios to determine quality. After quantification, RNA samples were either stored at -80°C for future use or stored on ice if cDNA amplification occurred immediate.

2.6.1. cDNA amplification

For cDNA amplification 1 µg of total RNA was used and therefore the volume of each RNA sample needed to provide 1 µg of total RNA was calculated using the following equation:

1000 ng / measured RNA conc. (ng/µl) = volume needed for 1 µg RNA

A stock of the reverse transcription master mix was assembled from an Invitrogen reverse transcription kit (Table 4). The total volume of the reaction was 100 µl which was made up of the final master mix (61.5 µl), the variable volume of RNA solution and RNase free water as required. The reaction mixed was made on ice in PCR tubes with the addition of the RNA sample last.

Table 4. Reverse transcription mastermix components for a single reaction

Component	Volume	Final concentration
10x RT Buffer	10 µl	1X
25 mM $MgCl_2$	22 µl	5.5 mM
DNTPs mixture (2.5 mM)	20 µl	500 µM/DNTP
Random Hexamers (50 um)	5 µl	2.5 µM
RNase inhibitor (20 U/L)	2 µl	0.4 U/µl

Multiscribe reverse transcriptase (50 U/ul)	2.5 µl	1.25 U/µl
Mastermix Total	61.5 µl	

The reaction mixture tubes were placed in a MyiQ™ single-colour real time PCR detection system (Bio-Rad) which was programmed with the following Reverse Transcription reaction protocol: 10 mins at 25°C, 30 mins at 48°C, 5 mins at 95°C then hold at 4°C to keep samples cold and prevent degradation until collection. Upon completion of reverse transcription, cDNA samples were transferred into RNase free 1.5 ml microfuge tubes and stored at -80°C for later polymerase chain reaction (PCR) analysis.

cDNA samples, iQ SYBR green and forward and reverse primers were thawed on ice and protected from light. Once thawed, master mixes for each gene of interest were made up and stored on ice protected from light. The master mixes contained per well: 7 µl RNase and DNase-free ultra-pure H_2O, 10 µl iQ SYBR green dye (Bio-rad), 1 µl forward primer, 1 µl reverse primer (list of primer sequences are shown in Table 5). Master mixes were made up in excess by three wells per plate to account for loss due to pipetting. 1 µl of sample cDNA was then added to the bottom of each corresponding well in a Bio-rad white plastic 96-well PCR plate on ice. Each sample was analysed in duplicate or triplicate. The required master mix was then added to each well containing cDNA before the plate was sealed with clear plastic film which prevented sample evaporation during the plate run. Plates were then loaded into a Bio-Rad CFX Connect real-time system with Bio-Rad CFX Manager 3.1 software. The sample layout of the plate was transferred into the software for automatic sample recognition in analysis. The qRT-PCR cycling protocol used was: 5 mins at 95°C to denature the cDNA; followed by 40 cycles of 15 sec denaturation at 95°C, 30 sec annealing at 60°C, 30 sec elongation at 72°C. After these cycles the plate was either cooled and stored at 4°C or went through a melt curve protocol to check PCR specificity of 81 cycles at 55-95°C for 30 sec. The Cq values were exported into Microsoft Excel where fold expression values were calculated using the 2-ΔΔCT method using GAPDH and β-actin as reference genes.

Table 5. Table of primers sequences

Gene name	Forward Primer	Reverse Primer
GAPDH	GTCAAGGCTGAGAACGGGAA	AAATGAGCCCCAGCCTTCTC
β-actin	GTGGCATCCACGAAACTACC	GTACTTGCGCTCAGGAGGAG
PAI-1	CATCCTGGAACTGCCCTACC	AGGGAGAACTTGGGCAGAAC
TGF-β	CTCACCAACCAAAGCCCGAC	TCCACATAGGGCTCAACACG
IGFBP-3	GCGCCAGGAAATGCTAGTGAG	CAACTTTGTAGCGCTGGCTG
IL-8	AGAGCCAGGAAGAAACCACC	GGCAAAACTGCACCTTCACAC
p16	GGGTCGGGTAGAGGAGGTG	GCCCATCATCATGACCTGGA
CXCL-5	ACCACGCAAGGAGTTCATCC	GTTCTTCAGGGAGGCTACCAC
IGFBP-7	GGGTGCTGGTATCTCCTCTAAG	TCTGGAGGTTTATAGCTCGGC
MMP-3	TGGACAAAGGATACAACAGGGAC	GGAACCGAGTCAGGTCTGTG
β-Gal	GGAACAGGCAGCAACATCAC	TACAAGTTCACACTCGCCCC
IL-6	ACCCCCAATAAATATAGGACTGGAG	ACCAGGCAAGTCTCCTCATTG
TNF-α	CCCATGTTGTAGCAAACCCTC	GTAGGCCCCAGTGAGTTCTG
p21	GCAGACCAGCATGACAGATTTC	GATGTAGAGCGGGCCTTTGA

2.7. Statistical analysis

Statistical analysis and production of graphs were performed using Prism v8 (GraphPad Software), and included normality tests, t-tests and Analyses of Variance (ANOVAs). The distribution of data can be assessed using normality tests, such as, the Shapiro-Wilk test using the Royston method (Royal Statistical Society, 2019). Where fold change was analysed normality was assessed on the raw values. Parametric tests assume a normal, or Gaussian distribution, however ANOVA's have been shown to be robust to normality violation (Maxwell & Delaney, 1990). When multiple t-tests were performed for gene expression data of the replicative fibroblast experiments the Bonferroni correction was applied to reduce the risk of type 1 errors. For the DOX induced senescence time course studies Dunnett's post-Hoc test was used to determine significant changes relative to baseline expression (Dunnett, 1955). Where data were not normally distributed non-parametric tests were applied. Statistical significance was set to $p < 0.05$. Data are presented as mean ± SD and as individual data points. The specific statistical tests performed are described with each figure.

Chapter 3: Development of automated image analysis protocols

3.1. Introduction

Determining RNA and protein expression by PCR and Western blot typically only explains the expression at the cell population level. For example, if there was an observed increased expression of cell cycle inhibitor p16 via PCR and Western blot it could suggest that the cell population overall had entered a state of cellular senescence. However, for instance elevated p16 expression could be driven by a sub-population of cells. Being able to determine marker expression change within each cell of a population would provide more granularity about the state of individual cells within cell populations.

Microscopy can be used to visualise populations of cells or the subcellular location of target molecules, e.g. transcription regulators in the nucleus or proteins translocated to membranes (Bolte & Cordelieres, 2006). The use of fluorophores, either bound directly to the primary antibody or conjugated to antibodies specific to the host species of the primary antibody, has improved the signal to noise ratio of traditional brightfield microscopy and allow for abundance, as well as, spatial measurements to be made about that molecule (Waters, 2009). However, the resulting digital image is a representation of an optical image of the distribution of the fluorophores (Jost & Waters, 2019). Therefore, to measure abundance, microscopy images must be acquired under certain conditions, discussed in the method section, because it is vital that fluctuations in pixel intensity should reflect changes in antibody abundance, not changes that originate from methodological variability (Agley *et al.*, 2012).

A common practice is the subjective determining of positive and negative cells within images to give a binary count. Which, although time consuming, can be highly accurate for binary analysis, such as determining the cell types within a cell population. However, if the marker expression is not binary but can affect cellular functioning depending on its expression level, the analysis relies on subjective classification of expression level in determining if a cell is positive for that marker. This can lead to inter- and intra-individual variation in classification. Throughout this thesis the senescent markers p16, γH2aX and

proliferation marker Ki67 are being analysed by fluorescent microscopy, all of which have variable expression levels. Using the earlier example of p16 expression in a cell population, with quantitative imaging, the increase in p16 expression could be described at the individual cell level. Therefore, quantitative imaging would provide valuable insight into the expression of these markers and whether the whole cell population was showing signs of becoming senescent.

To quantitatively analyse images requires the use of software to extract the relevant pixel data from the images. There are many image analysis software programmes available both commercially and open source. A manual image analysis method using Adobe photoshop has previously been published from this laboratory (Agley *et al.*, 2012). This method required the user to manual click through steps with subjective selection of segmentation thresholds. Although, this image analysis pipeline is effective and reproduceable, Adobe Photoshop requires a licence and analysing multiple images takes a long time and focused concentration.

The open source software FIJI, which is the upgrade of ImageJ, is the most popular and best supported image analysis software (Arena *et al.*, 2017). FIJI has an underlying scripting language called IJ1 Macro language which is a high-level computer programming language built on Java script. To make it easier for novice programmers to build image analysis programs, called Macros, FIJI has some useful templates and functionality that make the automation of workflows much easier. FIJI also has many plugin programs developed by the user community for a wide range of analysis problems, http://imagej.net/Update_Sites. For example, auto threshold algorithms can binarise grey scale images using global histogram-derived thresholding methods. These binary images can then be fed into other plugins that can count or take measures of regions of interest (ROI) found within these images. Although each individual plugin is a powerful tool it is the combination of these plugins that can lead to very complex and biologically useful analyses. The combination of auto threshold and ROI detection is frequently used to count cells or take measures specifically from ROI measurements intensity of fluorescence. These plugins along with others could be used to analyse the images generated from the analyses in this thesis. The automation of these image analysis pipelines would also save a significant amount of time.

3.1.1. Aims

The aim of this chapter was to develop automated image analysis workflows in FIJI image analysis software for the imaging data acquired in the main thesis chapters.

Programs will be made specifically to determine:

1. Percentage of cell populations expressing desmin or TE7
2. Senescent marker fluorescence intensity within all nuclei, or only within nuclei of a specific cell type
3. The number of nuclei incorporated into myotubes

3.2. Method pipeline for quantitative imaging

To quantitate from fluorescent images there are some key methodological considerations that must be observed in order to minimise errors within the results. The methodology for quantitative imaging is the standard protocol for immunocytochemical imaging but requires several specific conditions within the protocol. The general immunocytochemical methods employed through this thesis are detailed in the general methods chapter (section 2.5). Below are the key steps in the image analysis pipeline that must be incorporated for images to be used for quantitative analysis and not only as representative images.

3.2.1. Sample preparation

Prior to quantitative imaging, all samples that are to be directly compared must be prepared in the same way. The staining protocol (General methods section 2.5) needs to be performed at the same time with the same reagents and incubation times. This is because it is vital that fluctuations in pixel intensity should reflect changes in antibody abundance, not changes that originate from methodological variability (Waters, 2009). One source of variability is that primary antibodies can bind to multiple epitopes of the target molecule. Changes in antibody concentration and incubation conditions such as temperature or length of incubation may incorporate unintentional variability into antibody binding. These factors can vary between different antibody batches therefore when antibodies needed replacing the same batch was ordered wherever possible. If the

same batch was unavailable the new batch was tested alongside the old batch to see if they were comparable. However, as all samples to be directly compared where analysed in a single experimental run batch to batch variability was accounted for.

Background fluorescence should be minimised as much as possible however, background fluorescence is present in all samples to some extent and is unavoidable (Allen *et al.*, 2013). For example, both the fixative and the permeabilization solution contain Aldehyde groups which can auto-fluoresce, so unbound groups need to be removed (García-Plazaola *et al.*, 2015). A minimum of three washes with PBS were performed after each step to minimise possible autofluorescence from the solutions. All samples were blocked with 1% BSA for one hour prior to primary antibody incubation. The incubation with a blocking buffer binds all endogenous floating antibodies and helps both primary and secondary antibodies bind more specifically reducing nonspecific binding and background fluorescence. Between primary and secondary antibodies samples were washed with 1% BSA rather than PBS to maintain blocking solution. Sample preparation is therefore a critical step for reducing error in quantification, all samples that were to be directly compared, i.e. all samples across a time series, were stained at the same time under the same conditions. Once samples were prepared, they were stored in the dark to protect them from photobleaching before they were imaged.

3.2.2. Microscope set up and image acquisition

All fluorescence imaging took place in a temperature controlled dark room with no external light source to reduced light from other sources. Additionally, a black reference image, the image captured after blocking the light path to the camera, was performed to establish the dark noise level within the camera system. The black reference image was then used to apply a correction to all subsequent images acquired within that microscopy session.

Once excited by a narrow band of light wavelengths the fluorochromes release photons which are detected by a cooled charged coupled device (CCD) camera at many individual point locations (pixels; Waters, 2009). The number of photons detected at each individual pixel within the specified exposure time is translated into a grey scale value dependent on the bit depth of the camera. Usually 256 (8bit) or 4096 (12bit) different grey values. Thus, bright pixels will have detected more photons which is translated into

a higher grey value. If the maximum detection limit is reached (pixel saturation) then no differences in intensity can be measured between saturated pixels. It is therefore imperative for quantitative imaging that all pixel intensities fall within the detection limit of the camera. It is also best practise to utilise over 50% of the dynamic range (4096 greys) to provide a degree of tolerance to increases and decreases of intensity between different time points and reduce the impact of background fluorescence in the image (Jost & Waters, 2019). Saturated pixels were prevented by setting exposure times using the sample with highest expression and monitoring the 'overexposure' feature in AxioVision software.

Each pixel captures the local intensity of the fluorophore at the specific site within the sample that the pixel relates to. Using the individual pixel locations and intensity values a grey scale image of the intensity distribution of the fluorophore across the sample is made. Combining fluorophores of different excitation wavelengths allows for multiple target molecules to be visualised in the same sample revealing more about the localisation of molecules relative to each other within the sample.

The light source can introduce noise to the pixel intensity values by fluctuations in the light intensity emitted, this is minimised by using a LED or Laser light source rather than a mercury lamp which is prone to fluctuations in intensity as well as a slow decay in emission over time (Bolte & Cordelieres, 2006). The light source used through this thesis was a white light LED (Excelitas technologies, X-cite 120 LED Boost). White light contains all wavelengths of light which would excite all fluorochromes at once preventing any distinguishing between the fluorochromes used. Although each fluorochrome is excited by a specific spectral range of light wavelengths, there is overlap between these spectral ranges which can results in "bleed-through" of signal into another detection channel (Figure 3.1). This bleed through, or nonspecific excitation, can be reduced by using a light source with a specific tight wavelength range or using sets of band pass filters which only allow a narrow range of wavelength through from a white light source (Pawley, 2006). The filter set used to capture all images in this thesis were: 45 HQ Texas red shift free, 44 FITC special shift free, 49 DAPI shift free band pass filters (Carl Zeiss, Cambridge, UK). Bleed through can also be minimised by imaging in order of longest wavelength to shortest because there is the most bleed through from the DAPI antibody therefore exciting this fluorochrome last minimises the bleed through.

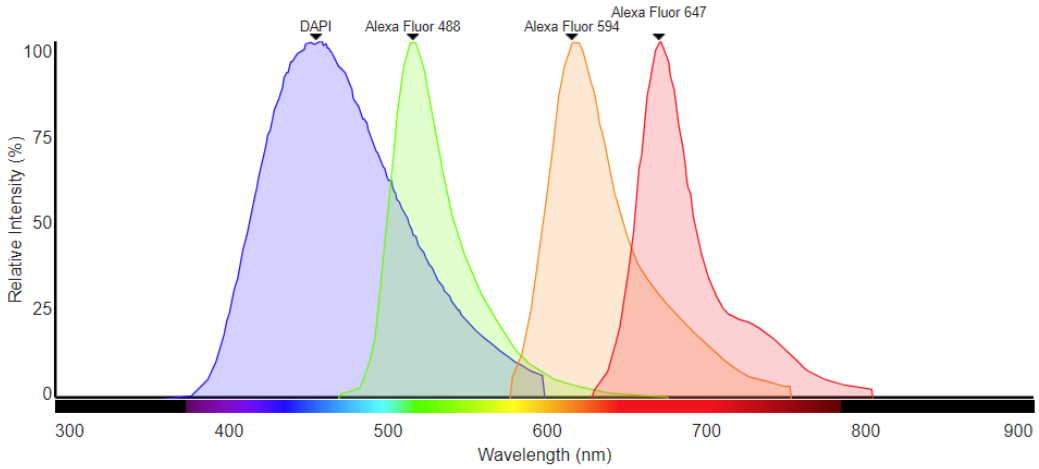

Figure 3.1. Fluorescent spectral emission for fluorescent antibodies used.
Emission spectra for the four fluorophores used throughout this thesis. Data obtained from: https://www.thermofisher.com/order/spectra-viewer (Accessed Jan 2020).

To accurately compare fluorescence images, they must have been imaged in the same microscopy session using the same microscope parameters, light intensities and exposure times (Waters & Wittmann, 2014). Although all these parameters can be recorded and set up again on a different day there is variability in light source power and microscope maintenance etc. that can potentially alter the output from identical settings. Imaging all samples for direct comparison in the same session minimizes the impact of all these variables (Jost & Waters, 2019). Due to the large number of time points and samples taken in this thesis, only two samples time courses could be feasibly imaged in a single microscopy session. Therefore, when all samples are compared the data is presented relative to a reference time point in each individual time course therefore the difference in microscopy setting are eliminated.

Each individual camera has a different density of pixels and total field of view size limiting raw measurements to be made in terms of pixels. For measurements to be made in microns the calibration of the camera, using a graticule of known length, must be performed to determine the number of pixels per micrometre. Once the image had been taken the scale bar was applied in the software so that the scale calibration is stored in the image file's metadata. Then finally, to protect the raw image data and metadata all image files were stored in the raw Zeiss file format, .zvi. This prevents any loss of data through file compression and maintains the file meta data such as microscope information and scale calibration. Once images were saved and transferred to the analysis computer, they could be stored indefinitely for image analysis.

3.2.3. Image analysis

Each type of analysis followed the same four steps pre-processing, image analysis using an automated program, post-processing and then data analysis. Different image analysis programs were built to extract the required data from the raw image files. For a specific analysis all images were processed in the same way using the same macro.

3.2.3.1. Pre processing

Before running images through an image analysis program, the data were pre-processed to remove any raw images that were identified as invalid during the microscopy session such as external light present, overlapping FOV and non-biological debris during acquisition. All images that did not clearly violate these conditions were analysed to prevent bringing subjective bias into the image selection. All images to be analysed where then transferred into a folder named “input” so that they could be analysed as a batch.

3.2.3.2. Image analysis programs

The macros applied to the images depended on what analysis of the data being obtained from that image is required. The specific macros are detailed later however generally each macro can be separated into two sections, segmentation and measurement. Segmentation involves selecting the regions of interest (ROI) within each image from which the measurements should be made (Arena *et al.*, 2017). E.g. selecting only the nuclei so that marker expression can be determined within each individual nucleus or selecting only desmin positive cells. Once the image is segmented into the ROI then the measurements such as cell counts or pixel intensities can be made on the image. The measurements were exported as a single .csv file per run. Each ROI could be identified by its label identifying which image it came from and which ROI within that image it related to.

3.2.3.3. Post processing

Although automatic threshold in a superior unbiased method for ROI selection it does not understand the biology underpinning the image. To check that the thresholds had selected accurately the required ROI quality control images were built into each program. Images of the final ROI selection over the nuclei channel and over the marker of interest

channel were saved into the output folder as .jpeg files. These images could be scanned quickly to determine if any images did not accurately threshold the nuclei. Images which did not threshold due to e.g. excessive background in the nuclei channel where excluded from analysis by removing the ROI associated with that image. However, if nuclei masks were accurate all images were used.

3.2.4. Data analysis

3.2.4.1. Determining cell type percentages and myotube fusion index

To determine the percentage of desmin positive cells within a cell population the ROI counts from both the total nuclei image and then the desmin positive image were recorded in the .csv file. In Microsoft Excel the number of nuclei within desmin positive cytoplasm was divided into the total nuclei count and multiplied by 100 to give the percentage of cells that were desmin positive. This analysis was the same for TE7 positive cells. The same format and analysis method were used for myotube fusion index. The number of myonuclei was divided into the total number of nuclei and multiplied by 100 to give the percentage of nuclei within myotubes.

3.2.4.2. Marker intensity

The raw data recorded from the marker expression analysis created a table with every row representing an individual ROI with all associated measurements in headed columns in the same row. This data needed to be reconfigured to separate the measurements into individual tables and group the ROI from each time point into separate columns. To do this the .csv file was moved into a folder containing a python script which reorganised the data to collate the same measurement on one excel sheet e.g. all individual mean fluorescent intensity measurements were separated onto an individual sheet. Then within this sheet the program separated the nuclei data into the different time points by searching the file makes for time point information. This uses the spaces between sections of the file name e.g. Y05+ DOX D4 Des+p16, this file name has 4 sections separated by spaces. The time point information is in the third section, i.e. D4, therefore the program groups all nuclei with the exact same third section information the column header of the time point name. Separating each timepoint into a new column.

Once reordered the program saved the whole workbook as a .xlsx file. This new format allows simple copy and paste into Graphpad prism software for cell by cell marker expression graphing and statistical analysis.

3.3. Automated image analysis macros

All image analysis programs were created using FIJI ImageJ software. FIJI was chosen because it is opensource, has a wide range of plugins and has a very active online forum support community (Schindelin *et al.*, 2015). FIJI also has easy to use templates and tools to help the novice programmer to write image analysis programs, called macros in FIJI.

The FIJI scripting template "Process Folder" was used to create all macros (Figure 3.2). This template is a generic folder and file scanning tool that searches for image files of a user defined image type e.g. .tif, .zvi, .png, *etc.* within the files of the specified folder. Once the program finds an image of specified type it sequentially opens the file, performs the defined functions then subsequently writes the recorded outputs to a predetermined output file before searching for the next image file. All images used in this thesis were kept in their raw file format .zvi, therefore the file suffix was always set to .zvi (Figure 3.3). The template for Process Folder was adapted so that all results from the processed file were added into a cumulative results table after all analysis steps had been completed. Additional lines were added to clear and close all open windows and print the message "Job done!" once the program had found and processed all files in the folder.

Within the process folder macro is the processFile function. This function is where the same analysis steps are applied to each image that met the process folder criteria. The exact content of the processFile function is dependent on the analysis required from the images which are outlined for each analysis pipeline in the following sections. Therefore, the first step to develop a macro is to plan the sequence of analysis steps to perform within the pipeline. These steps then needed to be coded into the processFile function. To help the novice programmer with coding the steps for each analysis program FIJI has a built-in command recorder found in Plugins>Macros>Record. This Recorder function records in sequence all computer mouse clicks within the FIJI user interface. Therefore, once the steps have been determined to complete the require analysis the user simply opens the recorder then manually clicks through the steps on a sample image.

Every click is recorded in the recorder as the underlying code which can be exported into the process folder script as steps under the processFile function.

Once the code has been copied it then needs to be edited to change options and to allow the program to run smoothly for images with different file names. The iterative debugging of the code with test images allows for testing how the program responds if certain constraints aren't met, e.g. if no ROI are found within an image. Once these debugging steps were performed the programs were tested with different full data sets to determine its efficacy with images taken during different imaging sessions. Once it was shown that the program is robust all images were run through the program and the data exported in .csv files for post processing and subsequent data analysis.

```
/*
 * Macro template to process multiple images in a folder
 */

input = getDirectory("Input directory");
output = getDirectory("Output directory");

Dialog.create("File type");
Dialog.addString("File suffix: ", ".tif", 5);
Dialog.show();
suffix = Dialog.getString();

processFolder(input);

function processFolder(input) {
    list = getFileList(input);
    for (i = 0; i < list.length; i++) {
        if(File.isDirectory(input + list[i]))
            processFolder("" + input + list[i]);
        if(endsWith(list[i], suffix))
            processFile(input, output, list[i]);
    }
}

function processFile(input, output, file) {
    // do the processing here by replacing
    // the following two lines by your own code
    print("Processing: " + input + file);
    print("Saving to: " + output);
}

```

Figure 3.2. Process Folder template script in FIJI.
Screenshot of the Process Folder template available in FIJI, written in IJ1 Macro language. The macro asks for the user for input and output directories as well as file suffix then searches through the input directory for all files that end in file suffix. Then, in turn, applies the processFile function to each image file with the correct file suffix.

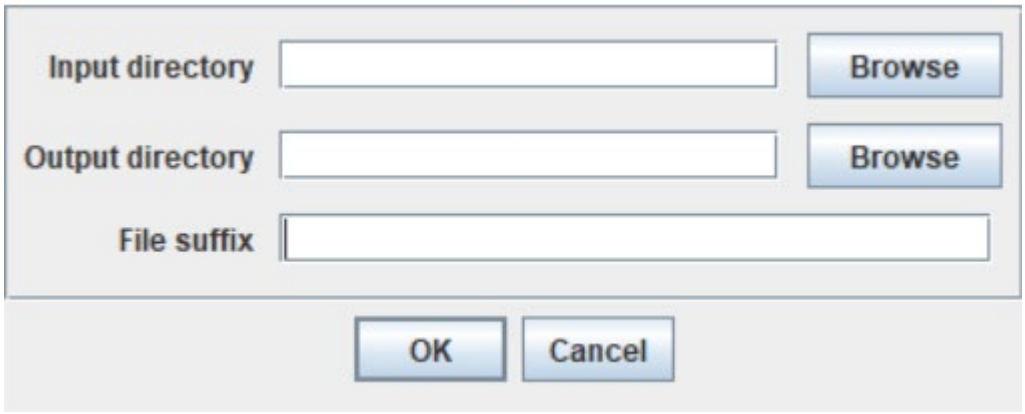

Figure 3.3. Dialog window prompt for Process Folder template.
Screenshot of the dialog box opened when process folder is run. User selects the input directory as the folder containing the images to be analysed and the output directory where the any outputs from the program are saved. The file suffix related to the image file types the program should search for in the input folder to process. File suffix was always .zvi as all images were saved in Zeiss raw file format.

3.3.1. Cell type population percentage Macro

Previous studies have shown that the percentage of desmin positive cells can decrease over time in culture with an increase in TE7 positive fibroblasts overgrowing the myogenic cells (Alsharidah *et al.*, 2013). Therefore, every sample needed to be analysed for desmin expression across their lifespan. An automated image analysis program was built to determine the percentage of desmin positive cells within each cell populations. This program was also used to determine the percentage of TE7 positive cells within the fibroblast populations using the same logic.

The logic behind the program was to first detect all nuclei within the field of view and count them, then to remove all nuclei that were not within desmin stained areas, and then finally to count the remaining nuclei. Counts of the total number of nuclei detected then the number of nuclei after removing non covered nuclei allows for the determination of the desmin^{+ve} cell percentage of these cell populations.

The first step was to create a table for the results to be stored. This table was created at the beginning of the processFolder function before it cycled through the input folder looking for image files so that the results from each image file could be saved into the same table. The for each image processFile created a new line in the table with the image filename as the label. All measurements were reset between each image imported and scaled to the known calibration for the microscope objective used so that these were constant for all images. The image was split into the individual red, green and blue channels ready for segmentation of the desmin cytoplasm and the nuclei.

The selection of nuclei needed to be representative of the actual size of the nuclei as these boundaries would define the area of the nuclei. Firstly, a duplicate image was created so that an image can be saved of the final nuclear selection over the original image to check for accurate nuclei selection in post processing (section 3.2.3.3). To reduced background fluorescence signal rolling ball background subtraction, size 50 pixels, was applied as nuclei are very bright so the rolling ball can distinguish well between nuclei and background fluorescence. The Huang dark auto threshold was applied because it is very good at identifying circular objects like nuclei (Huang, 1995). The post-threshold image may have left some holes within nuclei so they were filled using “fill holes” and then the “watershed” algorithm was also applied to split overlapping nuclei (Figure 3.4B). These

steps are critical because analysis of expression needs to be within whole individual nuclei.

The total number of nuclei within the nuclei mask image was determined using "analyse particles" to count how many objects were detected in the image. Here it is important to have scaled the image so that when analyse particles is run any particles which are obviously not nuclei can be removed by setting size exclusion criteria. Nuclear size and shape are relatively standard however there is variability, especially when culturing to replicative senescence. This step it only to remove particles which are obviously too small or too large to be nuclei. After analysing particles, the FIJI ROI manager contains details of each ROI, i.e. each nucleus, found within that image. Counting the number of ROI in the manager therefore gives a count of the number of nuclei within that image. This ROI count is stored in a column called "TotalCount" in the results table created at the beginning of the program.

The next step was to remove nuclei which were not within desmin positive cytoplasm from the all nuclei mask. To remove the nuclei which were not associated with desmin staining a cytoplasmic selection was created by applying a threshold to the desmin channel that was sufficient to select all desmin positive cells by overlapping with the nuclei of all desmin positive cells. The Otsu threshold (Otsu, 1979) followed by "Fill Holes" was used to create this desmin cytoplasm mask. The resulting binary image can be seen in Figure 3.4C and overlayed onto the nuclei channel in Figure 3.4D.

To remove the nuclei which were not covered the desmin cytoplasm maker a FIJI plugin called BinaryReconstruct_.class, developed by G. Landini was used (the plugin is available from: Landini G. Advanced shape analysis with ImageJ. *Proceedings of the Second ImageJ User and Developer Conference*, Luxembourg, 6-7 November, 2008. p116-121. http://www.mecourse.com/landinig/software/software.htm Accessed last on: 02/07/2019). This is a very powerful morphological operation that reconstructs (retains) 8-connected particles in an image (called mask) based on markers present in another image (called seed). Morphological Reconstruction consists of dilating the seeds inside the mask (so particles that do not have seeds are not reconstructed). In biological terms, all nuclei in the mask image which are within the cytoplasm threshold image (seed image) are retained. All nuclei outside of the cytoplasmic areas, e.g. other cell types, are removed for the nuclei mask.

The resulting reconstructed image is a binary image of only nuclei of a specific cell type (Figure 3.4E). This image is rescaled as it is in pixels rather than converted to micrometres using the same calibration as from the original image so that the same size exclusion criteria can be applied. Analyse particles and ROI manager count are then run to count the number of nuclei within this image to give the number of desmin positive cells. This result is again saved into the results table but in the column called "DesminCount".

This process is completed on all .zvi files found in the input folder and a new row is added to the results table for each image. Once all images have been processed the program saves the results table as a .csv file and is exported to the select output folder for post processing and data analysis as described in sections 3.2.3.3 and 3.2.4.

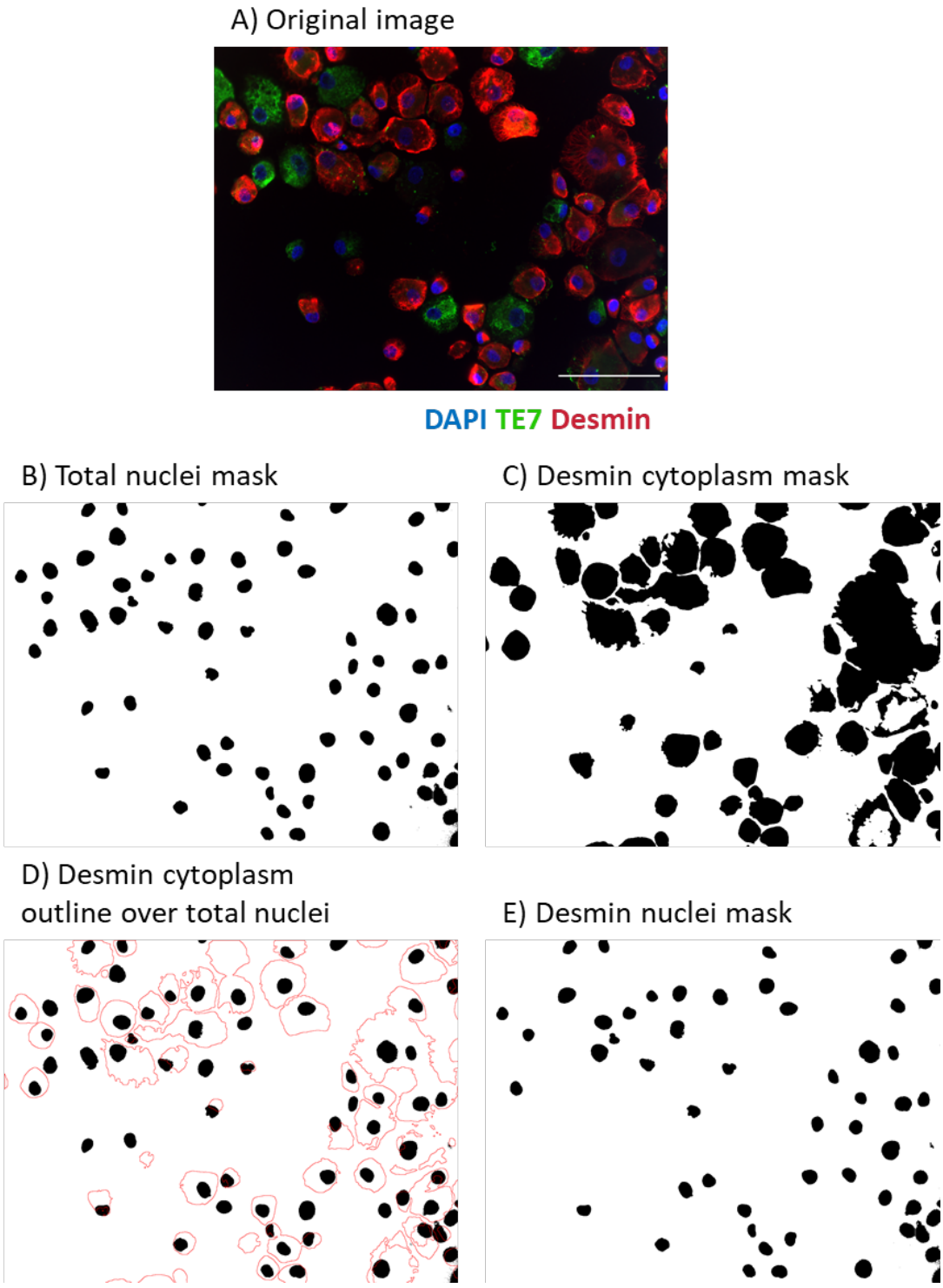

Figure 3.4 The main steps in a macro to determine the percentage of desmin^{+ve} cells from microscopy images.

This macro was developed to determine the number of desmin positive cells within a microscopy image. A) shows the example original three colour microscopy image. B) The resulting mask of all nuclei after automated thresholding on the DAPI channel. C) shows the desmin cytoplasm mask created after automated thresholding of the desmin channel D) shows the outline of the desmin mask overlayed on the same all nuclei mask created previously, where it is evident that not all nuclei are within desmin staining regions. E) shows the resulting nuclei mask when those nuclei that do not have desmin staining are removed. Automated counts of the total and desmin

associated nuclei masks allows for determining the percentage of desmin positive cells from the image.

3.3.2. Nucleic marker expression Marco

The expression of proteins in not always binary, the concentration of the protein can affect the functioning of the protein. It is therefore hard to determine a threshold of expression to determine when a cell is positive for that marker. Subjective counting results in arbitrary thresholding as positive or negative. This type of analysis removes the large area of grey visible within the image. Non bias cell by cell analysis can show the true variability within a cell population for the expression of that marker.

The expression of p16, Ki67 and γH2aX are all within the nucleus and the expression of these markers can be determined by measuring fluorescence within each cell nuclei. However, human primary muscle cell cultures are not always pure populations, so it is important to be able to observe the marker expression within only the cell type of interest in impure cell populations. Therefore, the cytoplasmic selection described in the cell type population percentage macro (section 3.3.1) was used here to remove nuclei that were not of a specific cell type when required.

This program was built to determine the expression of a marker within all nuclei or only within nuclei of cells that express a cytoplasmic marker such as desmin or TE7. The logic behind this program was to first detect all nuclei within the field of view, then, if required, to remove all nuclei that were not within desmin stained areas, and then finally to use the nuclei ROI to measure fluorescence intensity within each ROI from the raw image of the marker of interest channel. The example provided here and in Figure 3.5 & Figure 3.6 are for a program that make nucleus selection in the blue channel, cytoplasmic selection is the green channel and analyse nuclear marker of interest in the red channel. However, a version of this program was also created to make the cytoplasmic selection is the red channel and analyse nuclear marker of interest in the green channel.

For this program no specific results table needed to be created as the built-in results table was able to handle the data created. The first step was therefore to reset all measurements and scale the image so that these were constant for all images. The image was then split into the individual red, green and blue channels ready for segmentation of the desmin cytoplasm and the nuclei.

The creation of the nuclei ROI is the same as described in the cell type population percentage macro (section 3.3.1 & Figure 3.5B). If marker expression was going to be measured in all nuclei then ROI selection was carried out here using the same size exclusion, as previously described (section 3.3.1), with the addition of exclude of edges. Nuclei on the edges where excluded so that only whole nuclei were analysed. All particles which met these criteria were added to the ROI manager. The raw image for the marker of interest, red channel, was selected and "From ROI Manager" was run. This command applies all regions of interest saved in the ROI manager to the selected image (Figure 3.5C). Therefore, the predetermined nuclei locations were superimposed on the marker expression channel. The command ROIManager("Measure") then completed all measurements outlined in the set measurements command at the beginning of the programme, including; mean fluorescent intensity, area of ROI, etc. the results of these measurements were saved into the results table labelled with the source image name and which ROI those measurements related to. If marker expression was only to be carried out on nuclei of a specific cell type, then additional steps were required to remove the nuclei of other cell types before applying the nuclei mask to the marker of interest channel (Figure 3.6). The cytoplasmic selection described in the cell type population percentage macro section 3.3.1 was used to remove the other cell types. As can be seen from the example image in Figure 3.6G the marker expression is visible higher in the nuclei which were lost from the total nuclei image in Figure 3.5C.

Following the measurements within each image, the ROI manager was reset so that all ROI from the image were deleted before a new image was opened so only ROI found within that image were analysed. Once the programme had read through every image in the folder it saved the results table, compiled of all nuclei measurements from all images, to a .csv file into the designated output folder. This .csv file was then ready for post processing and data analysis as outlined in sections 3.2.3.3 and 3.2.4.

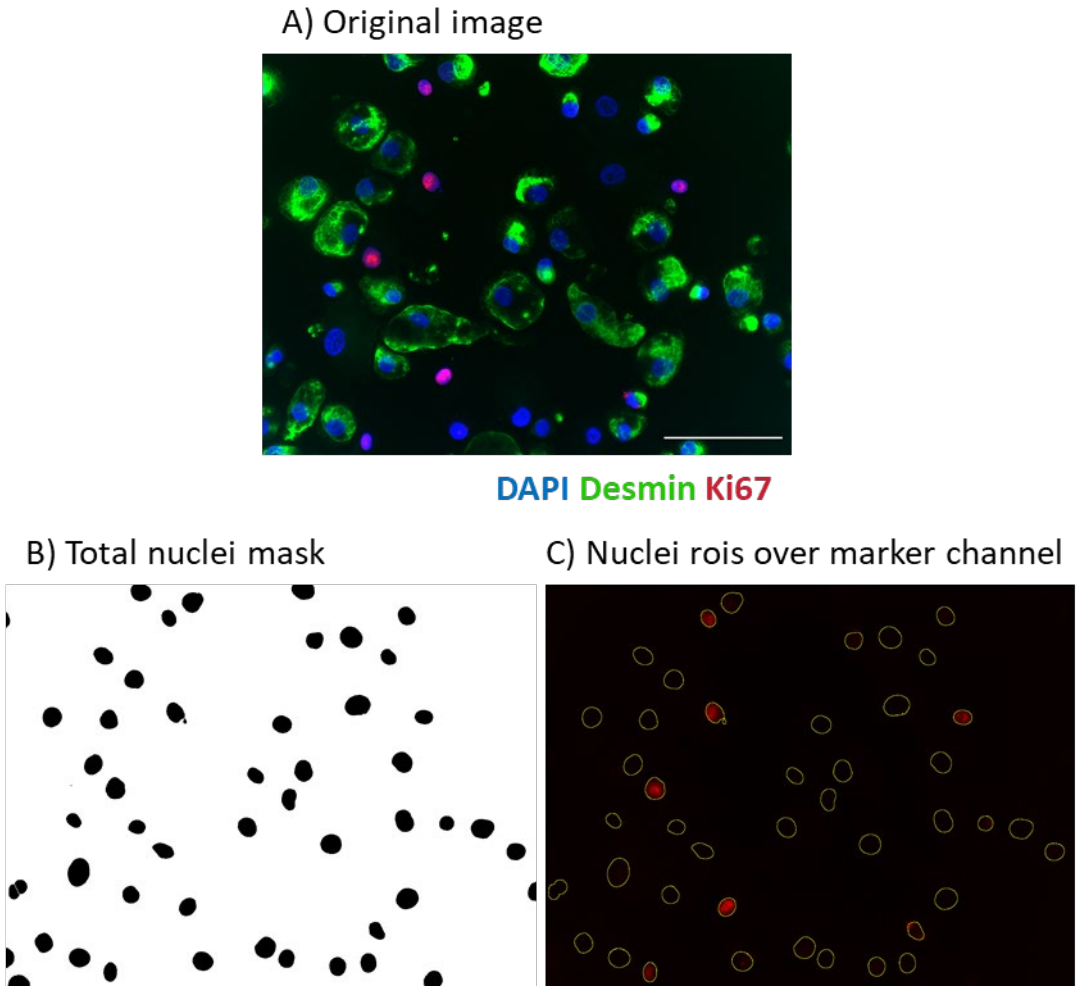

Figure 3.5 The main steps in a macro to determine marker expression within all individual nuclei from a microscopy image.

This macro was developed to measure the fluorescent intensity of a marker of interest within the nuclei of all cells within an image. A) the original three colour microscopy image B) The resulting mask of all nuclei after automated thresholding on the DAPI channel. C) After running ROI selection on the all nuclei mask the ROI are applied over the marker of interest channel and marker expression is measured within each ROI. This macro was used throughout this thesis to determine expression of p16, Ki67 and γH2aX within pure populations of cells. Figure 3.6 describes additional steps to only measure expression in nuclei of a specific cell type.

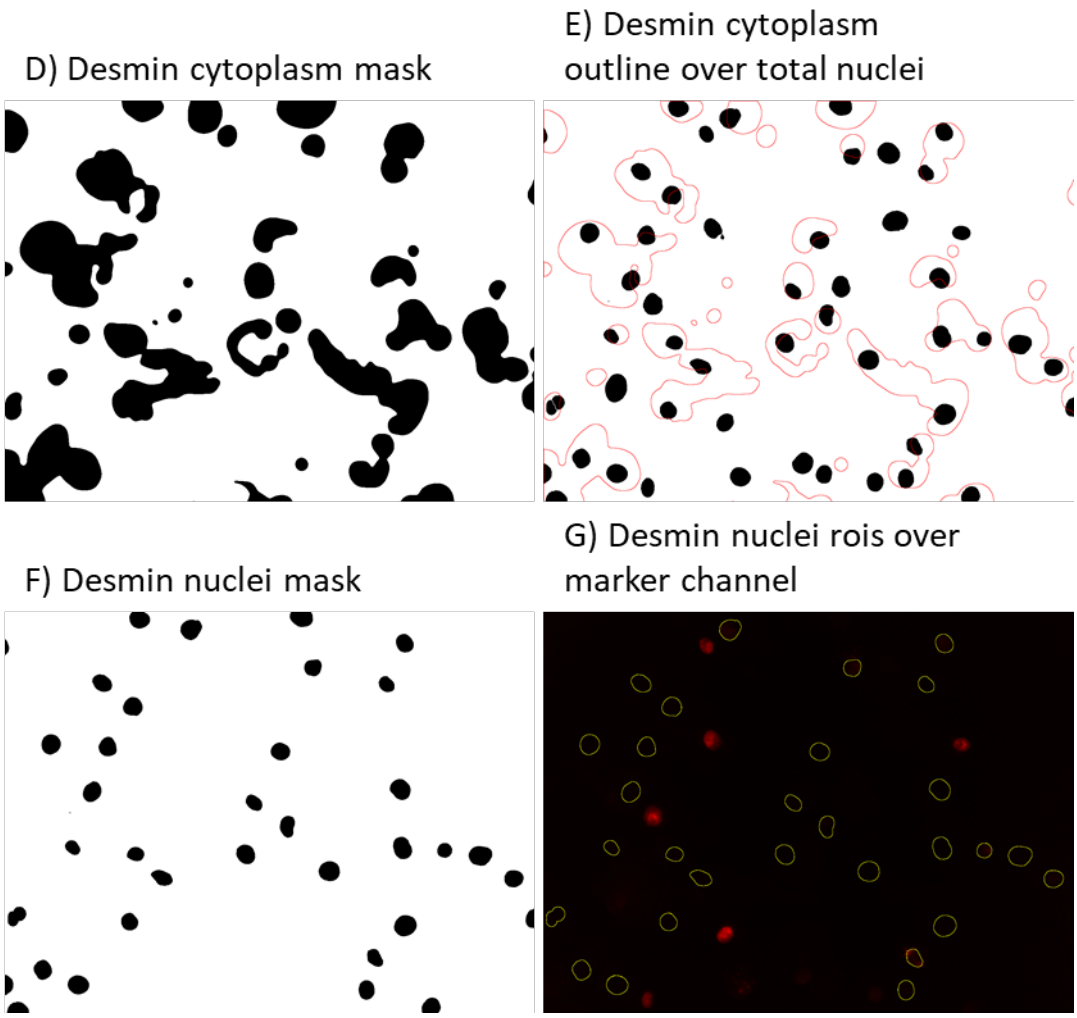

Figure 3.6 Additional steps to only measure marker expression within nuclei with desmin positive cytoplasm.

The steps described in Figure 3.5 are sufficient if the cell population is highly pure however the image used shows a mixed cell population. D) shows the desmin cytoplasm mask created after automated thresholding of the desmin channel E) shows the outline of the desmin mask overlayed on the same all nuclei mask created previously, where it is evident that not all nuclei are within desmin staining regions. F) shows the resulting nuclei mask when those nuclei that are not within desmin stained areas are removed. G) shows that when the ROI are measured in this image the nuclei which were highly expressing the marker were removed suggesting the highly expressing cells were not desmin positive.

3.3.3. Myotube nuclei fusion index Macro

Muscle fibres contain many terminally differentiated myonuclei. This differentiation process can be performed in cell culture with myoblasts differentiating and fusing together to form myotubes, precursors to muscle fibres. The ability of myoblasts to fuse and form myotubes can be measured by observing how many nuclei fuse into myosin heavy chain positive myotubes. Myotube size and number of myonuclei per myotube are also used as measured of differentiation (Yamamoto *et al.*, 2008). However, because myotubes often span more than a single FOV this is hard to perform accurately without imaging the entire cell population (Agley *et al.*, 2012). The number of nuclei within a field of view that are fused or are still individual nuclei is a simple measure that gives a strong reflection of differentiation capacity. Therefore, this program was created to determine the fusion index, the percentage of nuclei within a FOV, that are present in myosin heavy chain positive myotubes.

The logic behind this program was to first detect all nuclei within the field of view and count them, then to remove all nuclei that were not within Myosin heavy chain positive staining areas, and then finally to count the remaining nuclei. Counts of the total number of nuclei detected then the number of nuclei after removing non covered nuclei allows for the determination of fusion index of these cell populations.

A similar table to that described in the cell type population percentage macro was created in the processFolder function to store the total and fused nuclei counts from each image. The creation of the nuclei ROI is the same as described in the cell type population percentage macro (section 3.3.1 &Figure 3.7B), as is the selection of cytoplasmic myosin heavy chain positive myotubes area (section 3.3.1 &Figure 3.7C). Binary reconstruct was again used to remove nuclei not within the myosin heavy chain staining (section 3.3.1 &Figure 3.7D&E). The resulting .csv file contained the ROI manager count for total number of nuclei and number of fused nuclei. This .csv file was then ready for post processing and data analysis as outlined in sections 3.2.3.3 and 3.2.4.

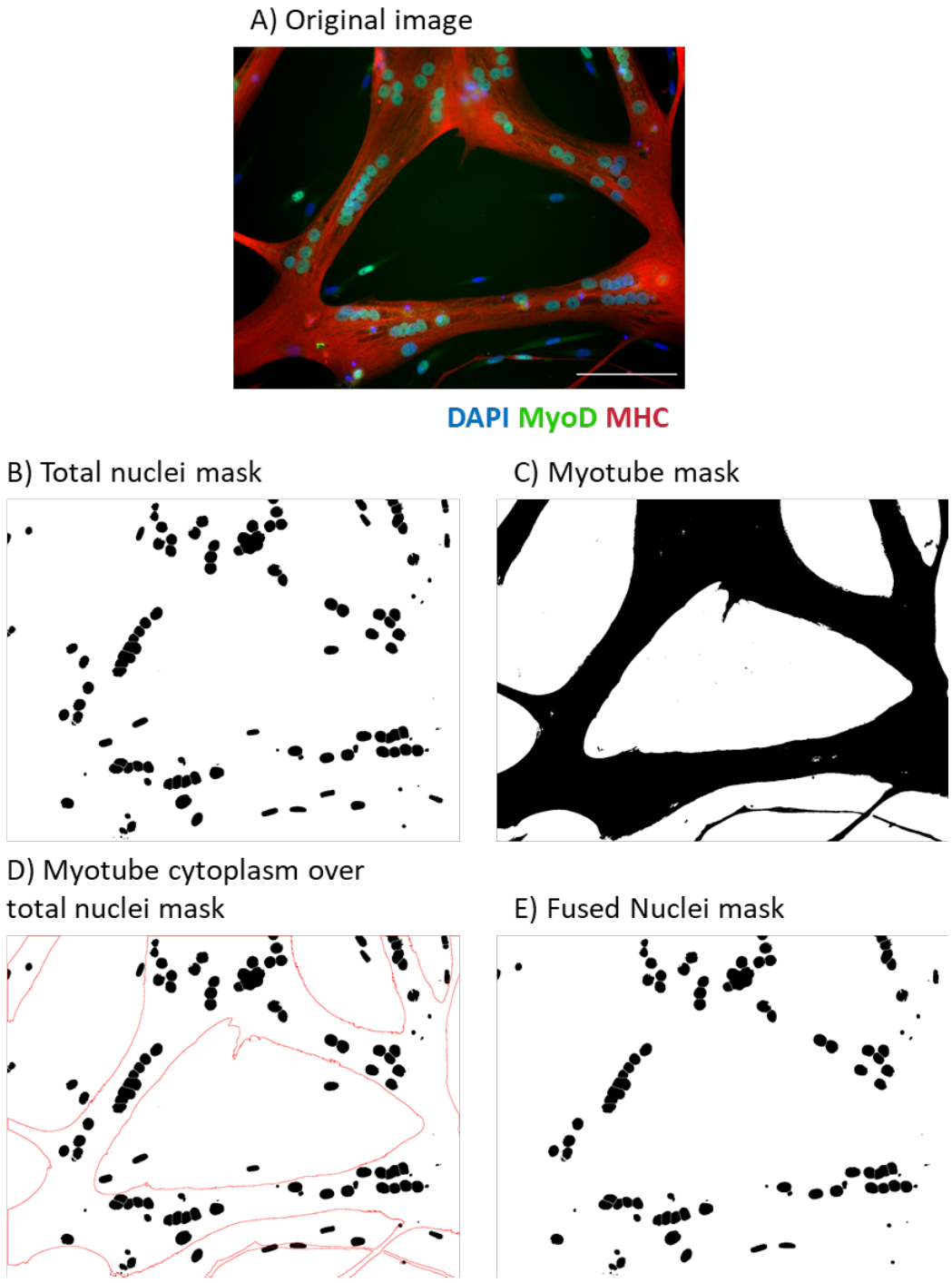

Figure 3.7 Myotube formation assay macro main steps

This macro was developed to determine the number of nuclei fused into myosin heavy chain positive myotubes within a microscopy image. A) the original three colour microscopy image B) The automated threshold of all nuclei within the field of view. C) The automated threshold of myotubes using myosin heavy chain D) Representation of the outlines from the myotube mask overlayed on the total nuclei mask. E) The nuclei mask after binary reconstruct removes nuclei that are not fused.

3.4. Discussion

This chapter describes the successful building of automated image analysis programs for multiple different analyses. Automation of image analysis improves analysis speed and data gathering as well as reduces the influence of subjective bias compared to manual processing of images (Arena *et al.*, 2017). Although manual counts can be performed quickly for certain analyses, such as cell type counts, once the number of images to analyse goes beyond tens of images the time commitment to analyse manually is disproportionately outweighed by macro building. For one study within this thesis 10 fields of view were imaged for each of 9 time point from 6 biopsies for each marker of interest. This one analysis produced 540 images alone, when the 4 different markers were analysed for that series of experiments a total of 2160 images were analysed. Manual counts taking roughly 3 minutes per image would have taken approximately 6,480 minutes. Clicking through each image in a semi-automated program such as using the adobe photoshop protocol or FIJI without a macro would have taken around 5 minutes per image, totalling 10,800 minutes. The automated programs designed in this chapter can analyse 180 images in under 2.5 minutes which would have led to a maximum of 30 minutes to analyse the same 2160 images. The amount of data produced is also order of magnitude greater than a manual count and therefore the performance is only comparable to clicking through FIJI which results in a >3000% speed improvement.

The abundance of raw data and measurements that can be taken and analysed from these programs is huge. By collecting raw fluorescence intensity values, it allows the presentation of the raw data providing transparency to the observer whilst showing the heterogeneity within a sample that is not shown when data is presented as subjective binary counts (Jost & Waters, 2019). Additionally, as the images are saved in their raw file format, they can be reanalysed for different measures indefinitely.

The use of open source software such as FIJI and python allows analysis to be performed from any computer without the need for an expensive software licence such as Adobe Photoshop (Agley *et al.*, 2012). There is also no “blackbox” analysis where images are fed into a program and data is retrieved without the user understanding how that data was collected because the code is freely available. FIJI was also chosen as it has an active online community which was helpful as the binary reconstruct plugin was a suggestion from the community (http://forum.imagej.net/). This collaborative scientific

community has been evidenced by the publication of a specific FIJI plugin, MuscleJ, for analysis of skeletal muscle histology sections, negating the pay to use software (Mayeuf-Louchart *et al.*, 2018).

The FIJI macros developed are only compatible with .zvi files as the individual colour channels take on specific names once split and need to be called to select the windows. However, changing the code to work with other file types, such as Nikon raw data .nd2 files, would not be difficult. The programs also require high quality images to work efficiently. Poor quality images lead to bad thresholding and therefore inaccurate selections and marker expression. Although all possible measures were taken to produce the highest quality images some images had to be removed from analysis due to high levels of background staining preventing accurate detection of nuclei or non-biological debris in the image.

All image acquisition took place on the same widefield fluorescence microscope therefore out of focus fluorescence was present in all images (Pawley, 2006). This also meant that images were taken in two dimensions, whereas cells and myotubes are three dimensional structures. Using a confocal microscope would improve the signal to noise ratio within the image by acquiring optical slices through a sample removing out of focus light (Allen *et al.*, 2013). The optical slides could also be used to observe the 3D structures within the image. Access to an affordable confocal microscope was not possible for this work. The noise induced by out of focus light was present in all images and therefore was likely to be similar for all images that were directly compared and as cells are a thin monolayers the amount of out of focus light may not be a limiting factor (Combs, 2010). It was also minimised by following the image acquisition steps out lined in the methods sections such as using most of the dynamic range of the CCD camera.

One of the main advantages of using image analysis programs is automated segmentation, the separation of image content into ROIs and background. For complex images, such as of tissue structure, it is hard for automated programs to reach the level of human segmentation due to human understanding of the structural biology underlying the image (Berlage, 2005). However, for relatively simplistic image of cultured cells automated segmentation is more accurate, less variable, much faster and, critically, unbiased. Where the automated segmentation did encounter problems was when analysing differentiation capacity of myoblasts into myotubes. Using fusion index to

analyse differentiation capacity may be seen as a simple analysis but without stitching FOV together to capture whole myotubes it is the most accurate measure of differentiation ability (Kandalla *et al.*, 2011). Measurements made on myosegments may not fully reflect the whole myotube and are therefore likely to introduce unknown errors. A macro to count the number of nuclei within each individual myosegment was created, however during testing it was found to be inadequate because it could not distinguish between overlapping myotubes. Additionally, two myosegments in the same FOV could be from the same myotube with an adjoining section outside the FOV. The overlapping on myotubes is a common feature of cultured myotubes which makes the accurate separation of individual myotubes difficult (Duca *et al.*, 1998; Zhu *et al.*, 2007). Additionally, a nucleus might be overlying a myotube, rather than being within the myotube and incorrectly counted as a myonucleus. It may be possible for automated thresholding to separate overlapping myotubes and overlying nuclei if confocal images were taken throughout the whole three-dimensional myotubes allowing for the segmentation of myotubes based on their distribution in the z axis.

In conclusion, fluorescence microscopy is a powerful biological technique with far reaching applications. This chapter demonstrates the development of bespoke image analysis programs that were used throughout this thesis to provide fast, unbiased analysis of hundreds of images. The programs provide more detailed analysis than manual methods allowing for more detailed analysis and highlights further the biological heterogeneity present within cell populations. The knowledge gained from this will provide the basis for further developments in apply fluorescence imaging and image analysis to skeletal muscle research.

Chapter 4: Replicative senescent phenotypes of human skeletal muscle precursor cells

4.1. Introduction

Cellular senescence of myoblasts is one potential mechanism contributing to the age-related decline in skeletal muscle mass and function in humans (Schafer *et al.*, 2005; Sousa-Victor *et al.*, 2014). Whole skeletal muscle tissue from older adults shows increased senescence associated markers, such as p21 protein (Carlson & Conboy, 2007), but skeletal muscle tissue consists of many different cell types which may be differentially expressing these senescent markers. Measuring tissue expression also does not allow the functional assessment of senescent cells. Understanding the senescent phenotype and functioning of skeletal muscle cells *in vitro* could provide cell type specific markers to identify senescent cells both at early passage *in vitro* as well as *in vivo*.

Previous cell culture studies show few differences in senescent marker expression or cell functioning in biopsy extracted cells from different aged donors (Carlson *et al.*, 2009; Pietrangelo *et al.*, 2009; Alsharidah *et al.*, 2013; Barberi *et al.*, 2013; Sousa-Victor *et al.*, 2014; Bigot *et al.*, 2015; García-Prat *et al.*, 2016). This could be an artefact of using cultured cells because measurements of senescent markers do not occur immediately after extraction but after several passages in culture conditions. During these passages senescent cells become a tiny minority population as the proliferative cells divide whilst the senescence cells cannot. After serially passaging cell populations to replicative senescence myoblasts have been shown to have defective cell function and increased senescent marker expression (Renault *et al.*, 2000; Cooper *et al.*, 2003; Bigot *et al.*, 2008; Alsharidah *et al.*, 2013; Baraibar *et al.*, 2016). However, these experiments are often confounded by either using starting populations with low percentages of desmin^{+ve} cells or by the reduction of the cell populations' desmin^{+ve} cell percentages across serial passages.

There are other precursor cell populations present in digested muscle tissue, such as skeletal muscle origin fibroblasts which tend to predominate over all other cell types (Agley *et al.*, 2013, 2015). Whilst it is known that fibroblasts interact with myoblasts to facilitate optimal repair *in vivo* (Murphy *et al.*, 2011), in human primary myoblast cultures the expansion of fibroblasts is often seen as a contaminant. Their expansion can confound myoblast cultures as they notoriously have long proliferative lifespans (Kaji & Matsuo, 1979) and often overrun un-purified myogenic cell populations (Schäfer *et al.*, 2006; Alsharidah *et al.*, 2013).

To identify the senescence phenotype of different human skeletal muscle-derived cells, pure cell populations need to be studied. Replicative senescence is considered the gold standard method for producing populations of senescent cells. However, human skeletal muscle studies have struggled to consistently obtain cultures which comprise pure populations of senescent myoblasts (Decary *et al.*, 1997; Renault *et al.*, 2002*b*; Lorenzon *et al.*, 2004; Alsharidah *et al.*, 2013). The recent development of a CD56 MACS sorting protocol for human myogenic cells has allowed for the purification to 95-99% desmin positive myoblasts after a single sort (Agley *et al.*, 2015). These initially enriched cell populations would thus improve the probability of maintaining high myogenic cell percentages through to replicative senescence. The initial sorting also allows for the investigation of the fibroblast-rich $CD56^{-ve}$ sort fraction and the opportunity to investigate the differences in replicative profiles of the two main skeletal muscle origin precursor cell types. To date no studies have compared the two main cell types isolated from the same human muscle biopsy sample in parallel experiments. This chapter describes a study into the replicative phenotypes of the two main human skeletal muscle-derived precursor populations, myoblasts and fibroblasts.

4.1.1. Aims

To characterise the replicative senescent phenotype of sorted populations of skeletal muscle-derived $CD56^{+ve}$ myoblasts and $CD56^{-ve}$ fibroblasts obtained from the same vastus lateralis muscle biopsy sample. The characterisation was in terms of senescent marker and SASP expression.

It was hypothesised that the two cell types would demonstrate different trajectories towards cell senescence but have similar senescent marker expression at replicative senescence.

4.2. Methods

4.2.1. Participants

Six healthy young (22±1 years) male participants donated muscle biopsy samples from the vastus lateralis as described in the general methods chapter 2 section 2.2.

4.2.2. Cell extraction and culture conditions

The cell extraction, sorting and general cell culture protocols used in this chapter are outlined in Chapter 2, General Methods. Briefly, human skeletal muscle samples were obtained using the Bergström needle technique with applied suction; these samples were then enzymatically digested to extract the mononucleated cell populations. The cells were left to proliferative for seven days after extraction before being sorted using CD56 magnetic beads. The $CD56^{+ve}$ and $CD56^{-ve}$ sort populations were then plated for experimentation simultaneously so that direct comparisons could be made between the cell populations extracted from the same biopsy. Throughout this chapter the $CD56^{+ve}$ fraction will be referred to with the biopsy sample code and (+), e.g. Y01+. The $CD56^{-ve}$ fraction will be referred to with the biopsy sample code and (-), e.g. Y01-.

4.2.3. Handling of purified cell populations

All cell populations were passaged every 72-hours starting after the MACS sort on day seven post biopsy. Passaging of both CD56 sort fractions continued until the $CD56^{+ve}$ cell population either reached replicative senescence, as determined by zero increases in cumulative population doublings (see section 4.2.4), or at a time point when it was assumed that the population has reduced numbers of myogenic expressing cells. High desmin expressing cell numbers were deemed to be lost when a slowing of doubling rate across two passages was followed by an observable increase in doubling rate.

4.2.4. Population doubling time

Cumulative population doublings were calculated for all cell populations across every passage using the following formula; where N1 is the number of cells counted at the end of the passage and N0 is the seeded cell number.

$$\text{Population doublings} = \text{Log2}(N1/N0)/\text{Log2}$$

4.2.5. Determining cell type proportions within the cell populations

Subsets of 20,000 cells from each population were cytospun, as described in the general methods section 2.5, at the end of every 72-hour passage. Passage 1 was started on day 7 after biopsy, post MACS sort. Percentage of desmin expressing cells in the $CD56^{+ve}$, and TE7 expressing cells in the $CD56^{-ve}$, fraction were analysed every other passage by immunocytochemical staining described in the general methods section 2.5.

4.2.6. Senescent marker expression

At the end of each 72-hour passage cytospun samples of 20,000 cells were collected, as described in the general methods section 2.5. Immunocytochemical staining for markers of senescence p16, Ki67 and γH2aX was carried out as described in the general methods section 2.5. They were then analysed as described in the method development chapter 3.3.2. Staining for senescence associated β-Galactosidase was carried out by two different methods, both are described in the general methods 2.5.1.

4.2.7. SASP factor expression

Cell pellets were collected at the end of every passage for mRNA extraction and RT q-PCR as described in the general methods 2.6.

4.2.8. Myotube formation

Myotube differentiation was carried out at early passage and at the time point when cells reached replicative senescence, or when experiments were stopped as described in chapter 2 section 2.5.

4.3. Results

4.3.1. Initial biopsy characteristics

To determine the *in vitro* senescent phenotype of human skeletal muscle derived precursor cells, skeletal muscle biopsies of the vastus lateralis were taken from young healthy male volunteers. The biopsy tissue was enzymatically digested to extract the mono-nucleated cell populations, which were plated in culture and allowed to expand. At 7 days post-extraction, the heterogeneous cell population was sorted using CD56 magnetic beads to select for $CD56^{+ve}$ skeletal muscle precursor cells. The $CD56^{-ve}$ cell population was also retained to investigate the predominant cell population, skeletal muscle origin fibroblasts.

The total number of cells after seven days in culture showed no relationship to the initial biopsy weight. This cell count was attained from the summation of counts from the CD56 positive and negative fractions after MACS sorting prior to plating for experiments therefore providing a visualisation of the total cell population extracted from each biopsy. The number of cells obtained was varied as shown by the standard deviation, $1.48 \times 10^6 \pm 9.56 \times 10^5$ cells (Figure 4.1). The proportion of total cell number that expressed CD56 was relatively constant at 67.27 ± 6.38% for all biopsies (Panel B of Figure 4.1).

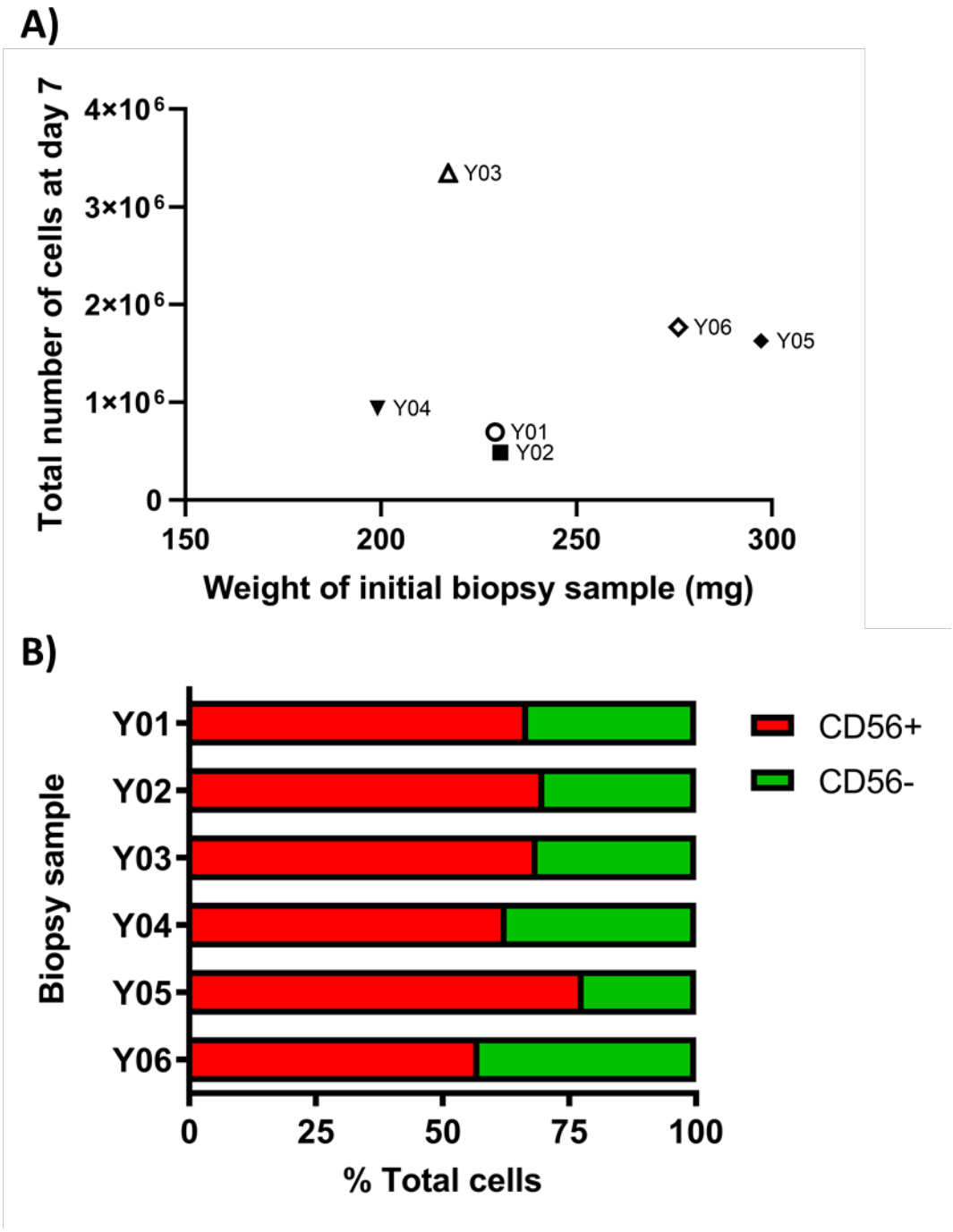

Figure 4.1.Total cell yield 7 day after biopsy and prior to sorting is variable but contains predominantly CD56^{+ve} cells.

After seven days, extracted cell populations were sorted for CD56 via MACS. The post sorted CD56^{+ve} and CD56^{-ve} cell populations were counted and summed to give a total cell number extracted from the biopsy. A) Shows the total cell number (sum of CD56^{+ve} and CD56^{-ve} counts) plotted against the initial biopsy weight. B) Shows the percentage of extracted cells that where CD56^{+ve} myogenic cells and CD56^{-ve} fibrogenic cells from each individual biopsy, calculated as described in the text.

4.4. Skeletal muscle myoblasts results

4.4.1. Replicative myogenic expression within CD56+ve populations

To determine the percentage of myogenic cells within the $CD56^{+ve}$ populations, cells were stained for myogenic marker desmin at selected time points across their replicative lifespans. The CD56 MACS sorting occurred seven days post biopsy and the number of cells isolated was sufficient to determine post sort cell type proportions at ten days in culture post biopsy. Representative images of cells derived from each individual biopsy at early passage (ten days post biopsy) and at the time point at which they reached replicative senescence or were stopped (denoted as late passage) are shown in Figure 4.2. A decrease in the number of desmin positive cells was accompanied by an accumulation of fibroblasts, TE7 positive cells, in three samples and these cell cultures were stopped at this point. Quantification of desmin expression in $CD56^{+ve}$ cells from all six populations show high initial number of desmin positive cells at ten days post biopsy, 97.6 ± 1.7% desmin positive cells (Figure 4.3). Of the six $CD56^{+ve}$ samples three maintained high numbers of desmin positive cells, >90% desmin positive cells, throughout replicative passaging; whereas, three show declining desmin expressing cell numbers, <90% desmin positive cells, from 34 days post biopsy onwards. Interestingly, one of the populations which maintained high desmin expression, Y05+, also seems to increase expression of TE7 within desmin positive cells, something which has not been observed before.

CD56 MACS sorting was attempted in late passage cell populations to remove non myogenic cells. However, it was unsuccessful in that a large population of desmin positive cells were present in the normally fibroblast-dominated $CD56^{-ve}$ fraction. This would suggest that CD56 is not able to select for all myogenic cells at late passage and an unknown subset of myogenic cells were being selected for (Figure 4.4). This meant that CD56 and desmin are not co-myogenic markers at late passage.

The three $CD56^{+ve}$ populations which maintained desmin positivity above 90% were considered to be highly enriched myogenic cell populations and could therefore be used for determination of the myogenic senescent phenotype, provided they also reached proliferative arrest.

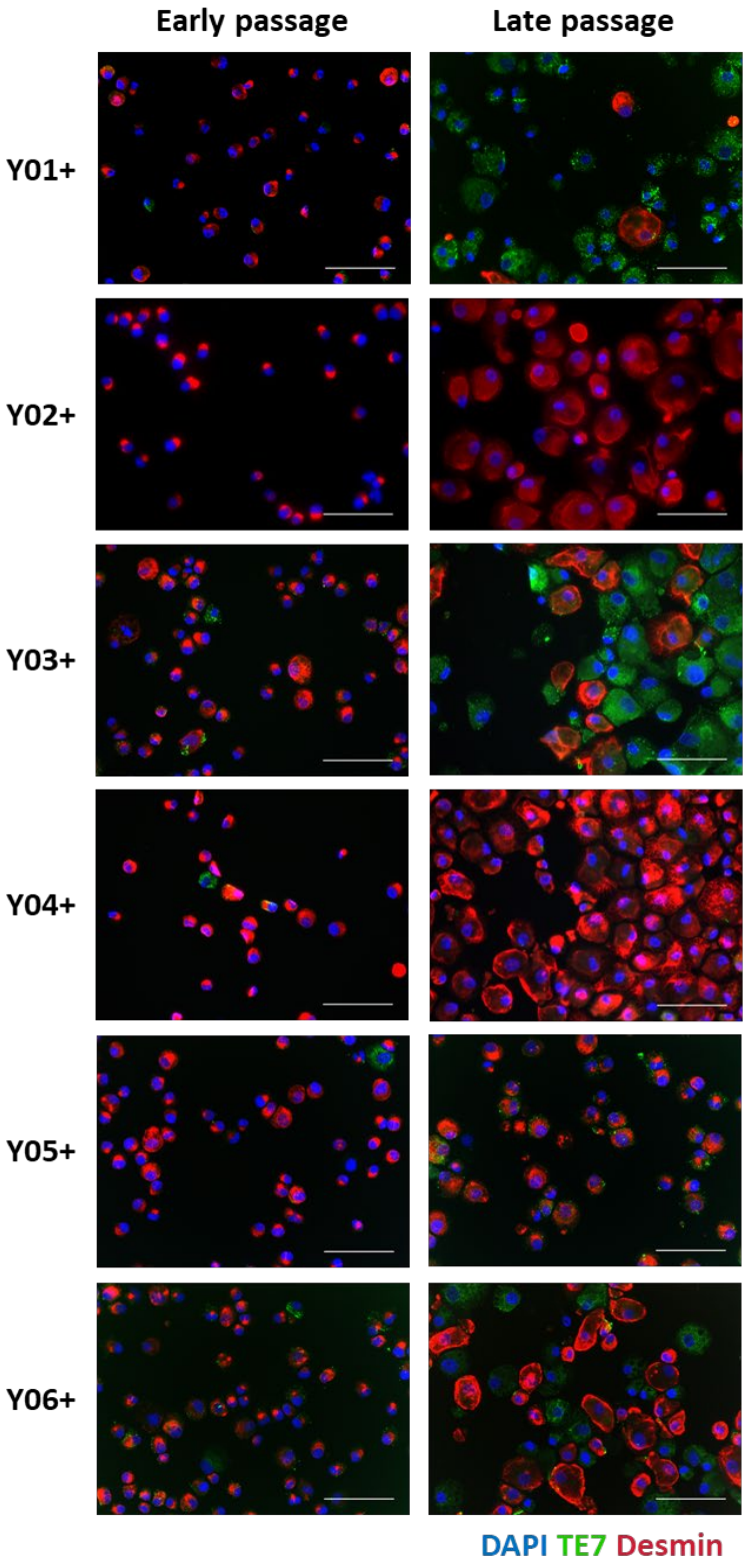

Figure 4.2 Representative images of each individual CD56^{+ve} population at early and late passage. Sub populations of cells (20,000 cells) from each CD56^{+ve} cell population were cytospun at early and late passage and stained for desmin (red), TE7 (green) and DAPI (Blue). Images acquired using a 20x magnification objective, Scale bar = 100 µm.

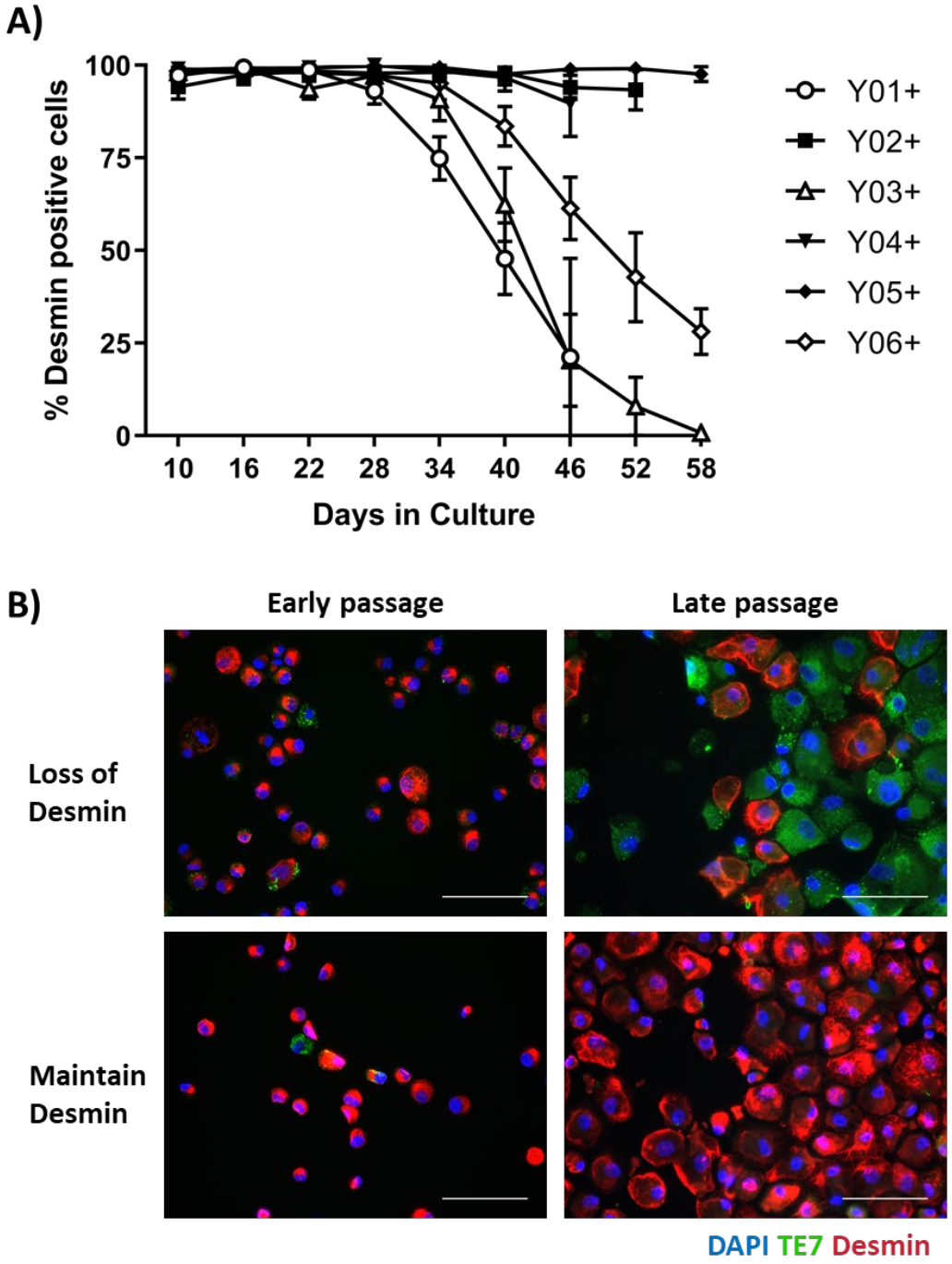

Figure 4.3 Initial CD56 purification does not prevent loss of desmin expressing cells across the replicative lifespan of myoblasts.

Sub populations of cells (20,000 cells) from each CD56+ve population were cytospun at alternate passages across their replicative lifespan and stained for nuclei and desmin to determine myogenic cell proportion by a bespoke automated image analysis program. A) The percentage of desmin positive cells across the replicative lifespan of individual myoblast populations. Data shown as Mean±SD of percentage desmin positive cells per field of view, 10 fields of view per time point, minimum of 100 cells analysed in total per time point. B) Representative images of individual biopsies which maintained and lost desmin expression stained for DAPI (Blue), TE7 (green) and desmin (red). N=6 Images acquired using a 20x magnification objective, Scale bar = 100 µm.

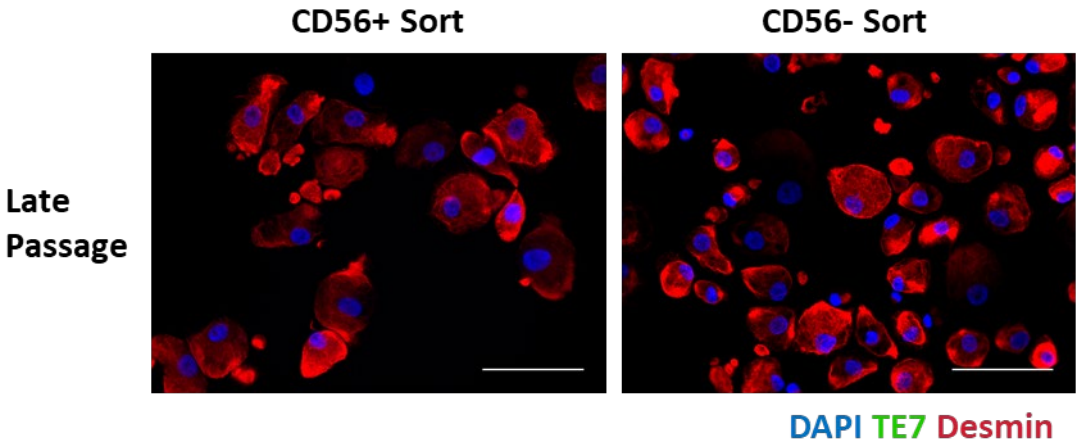

Figure 4.4 CD56 sorting of late passage cells does not positively select for all desmin positive cells.
Representative images showing high numbers of desmin positive cells in both CD56^{+ve} and CD56^{-ve} sort fractions. Images acquired using a 20x magnification objective, Scale bar = 100 µm.

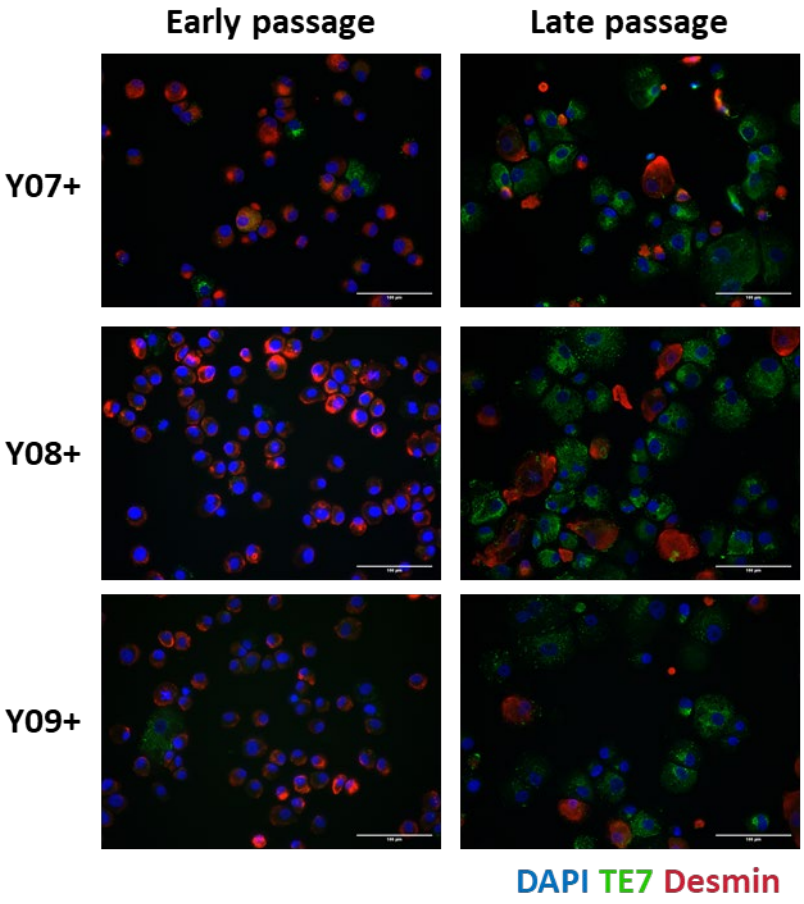

Figure 4.5. Additional CD56^{+ve} cell populations all became overrun with TE7^{+ve} cells.
A further three CD56^{+ve} cell populations extracted and MACS sorted from skeletal muscle biopsies underwent the same passaging experiments. Sub populations of cells (20,000 cells) from these

three additional $CD56^{+ve}$ cell populations were cytospun at early and late passage and stained for desmin (red), TE7 (green) and DAPI (Blue). Images acquired using a 20x magnification objective, Scale bar = 100 µm. All three showed increased numbers of $TE7^{+ve}$ cells after serial passaging.

4.4.2. Replicative potential of CD56+ve cell populations

To monitor the replicative profile of each individual $CD56^{+ve}$ population, cells were passaged every three days and cumulative population doublings were recorded (Figure 4.5). Population doublings were stopped due to reaching proliferative arrest, or when a slowing proliferative rate was followed by an increased proliferative rate which suggested that the cell population had become overrun by another cell type i.e. $TE7^{+ve}$ fibroblasts. The cumulative population doublings of the biopsies which maintained >90% myogenic expression throughout replicative passaging are shown in Figure 4.5A. Of these three biopsies, two reached proliferative arrest, whereas one population, Y05, was still proliferating when it was stopped due to observing a slowing in proliferative rate followed by an increase in proliferative rate indicative of a population which had become overrun with fibroblasts. This cell population, Y05, also showed co-staining of desmin and TE7. Figure 4.5B shows the replicative profile of the $CD56^{+ve}$ populations which did not maintain high desmin expression. Here, two populations were still dividing when experiments where stopped, whereas one, Y06, had reached proliferative arrest.

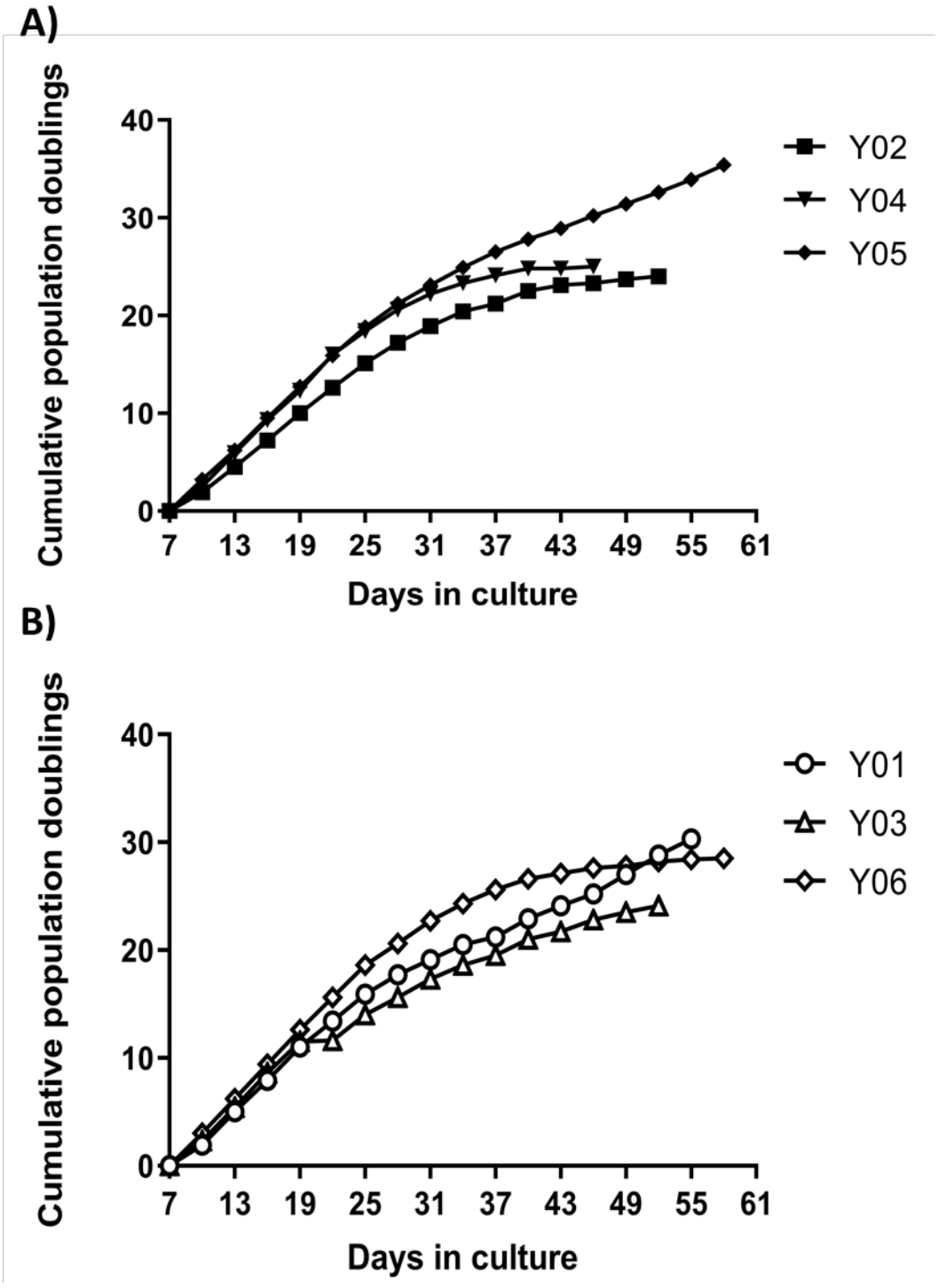

Figure 4.6 Cumulative population doublings for individual CD56^{+ve} cell populations.
Replicative profile of individual biopsies calculated by cumulative population doublings every three days. Population doublings = Log2(N1/N0)/Log2 where N1 is the end of passage cell count and N0 is the number of cells seeded. MACS sorting occurred at day 7 and is used as the initial time point. **A)** Biopsies which maintain high desmin expression. **B)** Biopsies which did not maintain high desmin expression.

4.4.3. Myogenic population senescent marker expression

After combining desmin expression and replicative potential data it is apparent that of the three biopsies which maintained high percentages of desmin expressing cells only two reached proliferative arrest. Therefore, from the initial six starting biopsies only two, Y02 and Y04, had achieved myogenic replicative senescence. Subsequently, these two samples were characterised to obtain the myogenic replicative phenotype. As group statistical analysis cannot be completed with only two samples, statistical analysis was performed using the cell by cell image analysis for each individual cell population at early passage and replicative senescence to determine if there was a significant change in marker expression within each cell population.

To determine the marker expression of myoblasts at replicative senescence, expression of four markers known to be associated with senescence, p16, γH2aX and senescence associated β-Galactosidase (SA β-Gal), and proliferation, Ki67, were assessed. Results for SA β-Gal were not usable for these two biopsies due to technical methodological issues discussed in the methods section 2.5.1.

4.4.3.1. Ki67 expressing cells are rare in senescent myoblast populations

Cells that are undergoing mitosis highly express the protein Ki67, whereas non-dividing cells strongly down regulated its expression (Scholzen & Gerdes, 2000). Therefore, to support the plateaus observed in the cumulative population doubling curves, sub-populations of each cell population were stained for Ki67. Both Y02+ and Y04+ cell populations showed significant reduction in Ki67 expression at replicative senescence ($P < 0.001$, Y02: early passage 761.8±402.2 AU, replicative senescence 367.1±559.6 AU; Y04: early passage 1141.5±783.4 AU, replicative senescence 115.3±172.6 AU, Figure 4.6). Although, both cell populations still retained a very small number of highly Ki67 expressing cells suggesting that not all of the cells had stopped dividing.

4.4.3.2. p16 expression is elevated in senescent myoblast populations

Proliferative arrest as shown by low Ki67 expression is common of many cell populations, not necessarily due to being in a senescent state (Sun & Kaufman, 2018). Different mechanisms of proliferative arrest are associated with expression of specific cell cycle inhibitors (Malumbres *et al.*, 2014). Cellular senescence is often accompanied by increased expression of the cell cycle inhibitor p16. Both senescent myoblast populations showed significant ($P < 0.001$, Y02: early passage 330.7±95.9 AU, late passage 1215.4±277.0 AU; Y04: early passage 272.1±117.3 AU, late passage 440.6±144.8 AU, Figure 4.7) increases in p16 expression, albeit to different extents.

4.4.3.3. γH2aX expression

DNA damage is a potential cause of cellular senescence and therefore is often seen to increase in senescent cells. Double strand breaks in DNA can be observed by staining for γH2aX as the protein is involved in histone repair (Nakamura *et al.*, 2008). Y04+ showed a significantly lower mean fluorescent intensity γH2aX expression at replicative senescence relative to early passage ($P < 0.001$, early passage 757.4±400.3 AU, replicative senescence 232.4±138.5 AU). Whereas, Y02+ showed no statistically significant difference in γH2aX expression ($P = 0.30$, early passage 362.9±205.9 AU, replicative senescence 352.3±67.2 AU Figure 4.8).

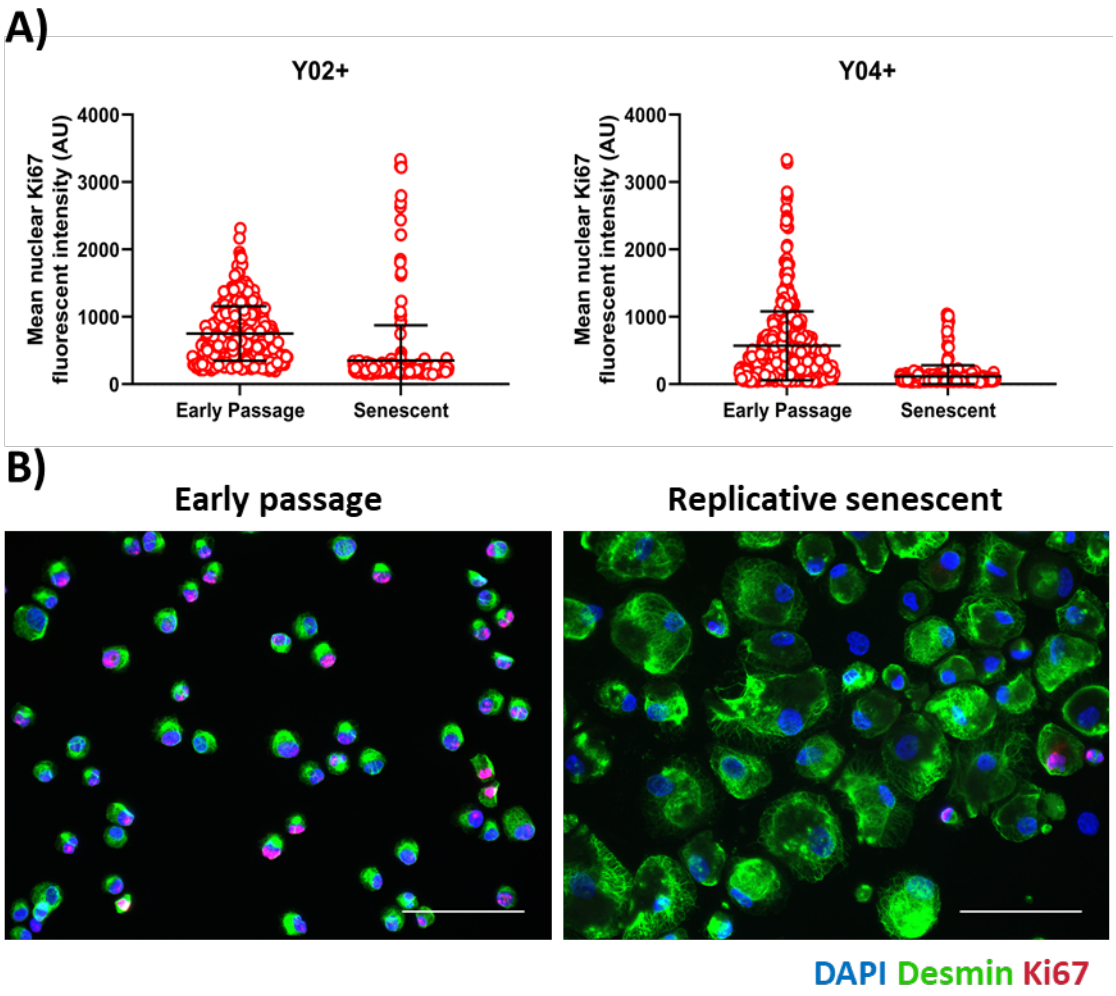

Figure 4.7 Myoblasts express less Ki67 at replicative senescence.
A) Cell by cell mean fluorescent nuclear Ki67 intensity at early passage and replicative senescence for individual myoblast populations which reached myogenic replicative senescence. Each circle represents the mean fluorescent intensity of Ki67 of a single nucleus. Black lines indicate cell population Mean±SD. B) Representative images of Y04+ early passage and replicative senescent cell populations, which maintained myogenicity, stained for DAPI (blue), desmin (green) and Ki67 (red). Scale bar = 100 µm.

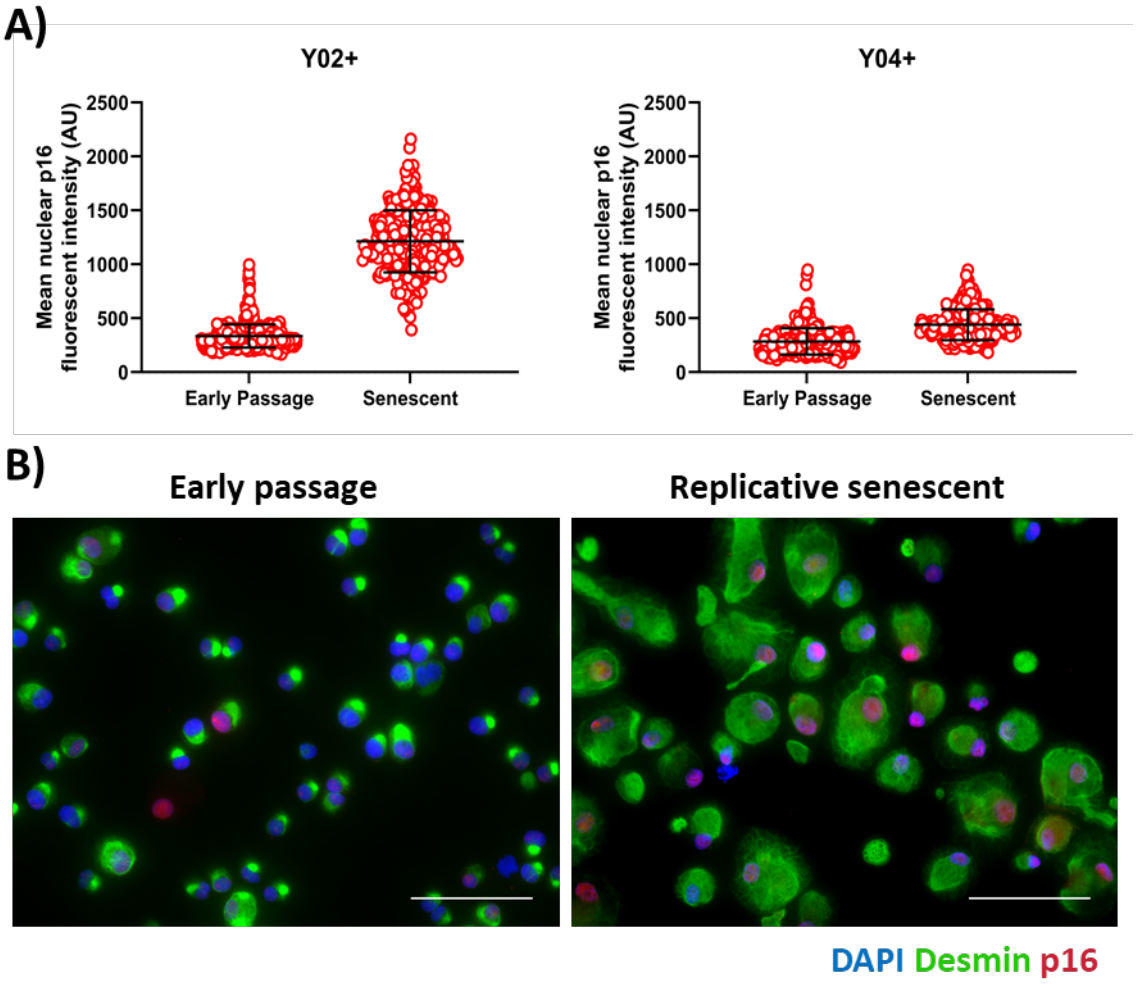

Figure 4.8 Myoblasts express more p16 at replicative senescence.
A) Cell by cell mean fluorescent nuclear p16 intensity at early passage and replicative senescence for individual myoblast populations from the two biopsies which reached myogenic replicative senescence. Each circle represents the mean fluorescent intensity of p16 of a single nucleus. Black lines indicate population Mean±SD. B) Representative images of Y02+ early passage and replicative senescent cell populations, which maintained myogenicity, stained for DAPI (blue), desmin (green) and p16 (red). Scale bar = 100 µm.

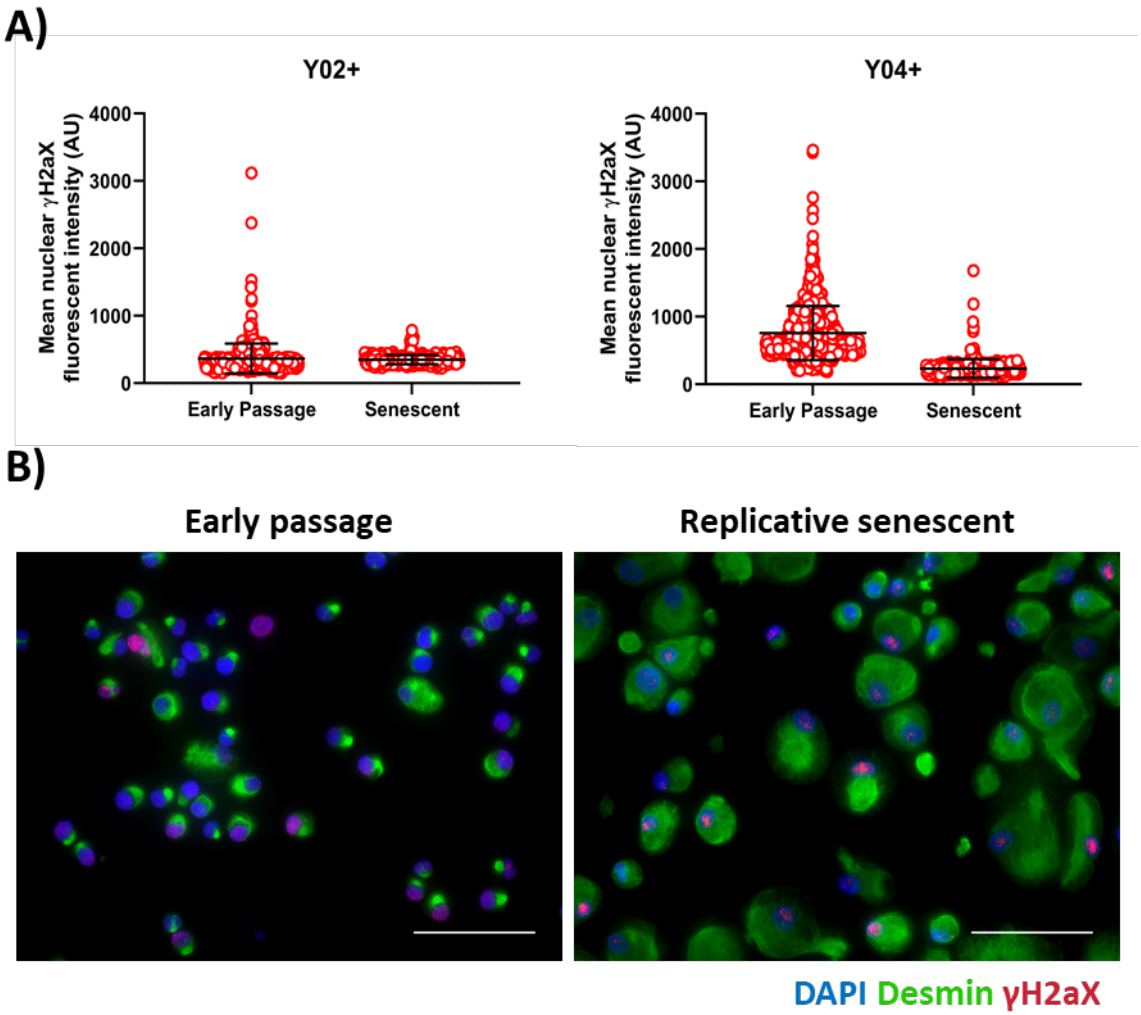

Figure 4.9 γH2aX expression of senescent myoblasts is different between samples.
A) Cell by cell mean fluorescent nuclear γH2aX intensity at early passage and replicative senescence for individual myoblast populations from the two biopsy samples which reached myogenic replicative senescence. Each circle represents the mean fluorescent intensity of γH2aX of a single nucleus. Black lines indicate population Mean±SD. B) Representative images Y02+ of early passage and replicative senescent cell populations, which maintained myogenicity, stained for DAPI (blue), desmin (green) and γH2aX (red). Scale bar = 100 µm.

4.4.4. Myogenic senescence associated secretory phenotype

A characteristic feature of senescent cells is their altered secretome known as the senescence associated secretory phenotype (SASP). The difference in mRNA expression of common SASP factors and senescence associated genes, known to be expressed in other senescent cell types (Coppé *et al.*, 2010*a*; Tchkonia *et al.*, 2010; Xu *et al.*, 2015*b*), were determined at replicative senescence and expressed relative to early passage (10 days after biopsy). In total, twelve senescence associated factors were measured in Y02+ and Y04+ and these factors were grouped as follows. Four showed increases in mRNA expression at replicative senescence compared to early passage in both samples but to different extents, as indicated by the values shown for Y02+ and Y04+ respectively. Specifically, PAI-1 (Y02; ~3 and Y04;~190 fold increase); IGFBP3 (Y02; ~12 and Y04; ~90 fold increase); p16 (~54 and ~27 fold increases); and IL8 (Y02; ~6 and Y04; ~10 fold increase) were increased. A second group of four factors which showed reduced expression at replicative senescence in both Y02+ and Y04+ as indicated in the following results: TGF-β (0.3 fold change in both samples); IL6 (0.5 and 0.99 fold change); MMP (0.7 and 0.9 fold change); and p21 expression was halved in both samples. A further two factors which showed differential changes in expression between the two biopsies: CXCL5 expression was decreased in Y02+, 0.1 fold, but increased by ~10 fold in Y04+. Whereas, IGFBP7 was increased in Y02+, 6 fold, and decreased 0.4 fold in Y04+. The final two SASP factors, TNF-α was below the detection limit of the assay in Y04+ and slightly elevated in Y02+. Whereas β-gal was unchanged in Y02+ and decreased, 0.6 fold in Y04+.

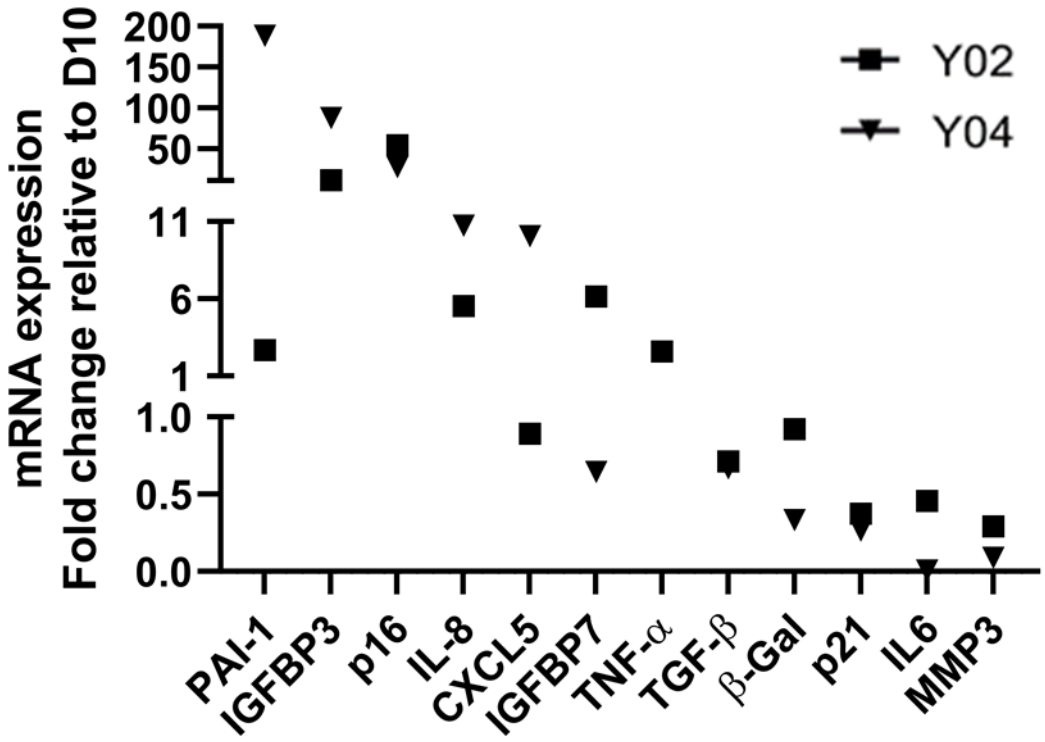

Figure 4.10 Replicative senescent myoblasts have altered mRNA expression of known SASP factors.

Fold change in mRNA expression of known SASP factors was determined by RT-qPCR at replicative senescence, relative to early passage, in both senescent myogenic cell populations. Individual data points are presented as only two samples underwent analysis. SASP factors are ordered from highest mean fold change to lowest mean fold change. As described in the text, factors PAI-1, IGFBP3, p16 and IL-8 were increased in both samples at replicative senescence. CXCL5 and IGFBP7 were both increased in one sample but decreased in the other sample. TGF-β, p21, IL-6 and MMP3 were decreased in both samples. TNF-α was below detection limit in Y04+ and slightly elevated in Y02+. Whereas β-gal was unchanged in Y02+ and decreased in Y04+.

4.4.5. Differentiation is impaired in senescent myoblasts

The role of muscle precursor cells in vivo is to fuse together to form new, or repair damaged, muscle fibres. In vitro, this process can be observed by lowering serum concentration in the media which, coupled with increased seeding density, triggers myoblasts to fuse together to form myotubes. The ability of replicative senescent myoblasts to differentiate into myotubes was investigated by determining the percentage of nuclei incorporated into myotubes after 96 hours of serum removal from the culture medium. The two myogenic senescent populations showed reduced fusion index from 80% fused nuclei in early passage to 50% in replicative senescent cell populations (Figure 4.10). The myotubes formed were also observed to be visibly thinner and contained fewer nuclei per myotube (data not quantified).

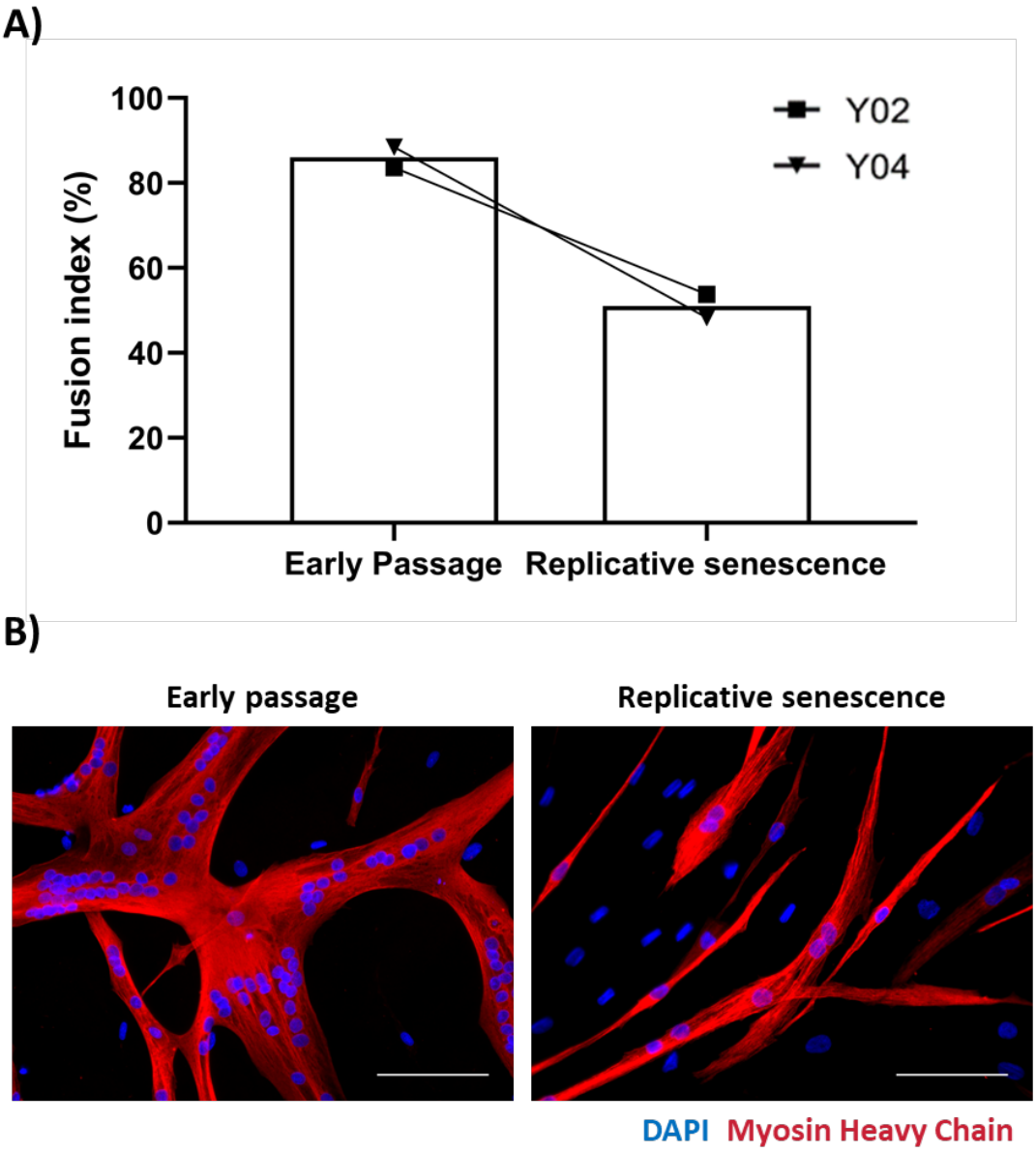

Figure 4.11 Replicative senescence myoblasts fuse less well into myotubes.
Myoblasts at early passage and replicative senescence were induced to differentiate and form myotubes. A) The fusion index, percent of nuclei incorporated into myosin heavy chain positive myotubes, is lower in populations of replicative senescence cells. B) Representative images of biopsies at early passage and late passage directed to differentiate into myotubes and imaged after 96h. Scale bar = 100 µm.

4.5. Fibroblasts

The $CD56^{-ve}$ cell populations from the MACS sort were cultured alongside the $CD56^{+ve}$ cell population from the same biopsy so that they were exposed to the same conditions. Due to the potential for fibroblast populations to take a very long time to reach replicative senescence the $CD56^{-ve}$ were stopped when the $CD56^{+ve}$ population had reached replicative senescence or when the myogenic population was deemed to have been overrun with fibroblasts. The time point at which $CD56^{-ve}$ cell populations were stopped is referred to as late passage in the subsequent results. The same experiments were carried out on the $CD56^{-ve}$ populations as the $CD56^{+ve}$ populations, the results of which are presented below.

4.5.1. Fibrogenic expression within $CD56^{-ve}$ populations

To determine the percentage of fibroblasts within the $CD56^{-ve}$ populations, cells were stained for fibroblast marker TE7 at selected time points across their replicative lifespans. The CD56 MACS sorting occurred seven days post biopsy and the number of cells isolated was sufficient to determine cell type proportions within the population at ten days in culture post biopsy. Representative images of each individual biopsy at early passage (ten days post biopsy) and at the time point at which they were stopped (denoted as late passage) are shown in Figure 4.11; where TE7 expression remained high with serial passaging. Quantification of TE7 expression in $CD56^{-ve}$ cells from all six populations show high initial TE7 expression at 10 days post biopsy accounting for 86.7±9.7% of all cells (Figure 4.12). The number of TE7 expressing cells increased throughout replicative passaging up to 97.8±1.1% when the experiments were stopped. Thus, all $CD56^{-ve}$ populations were determined to be $TE7^{+ve}$ throughout serial passaging and are subsequently referred to as fibroblast cell populations.

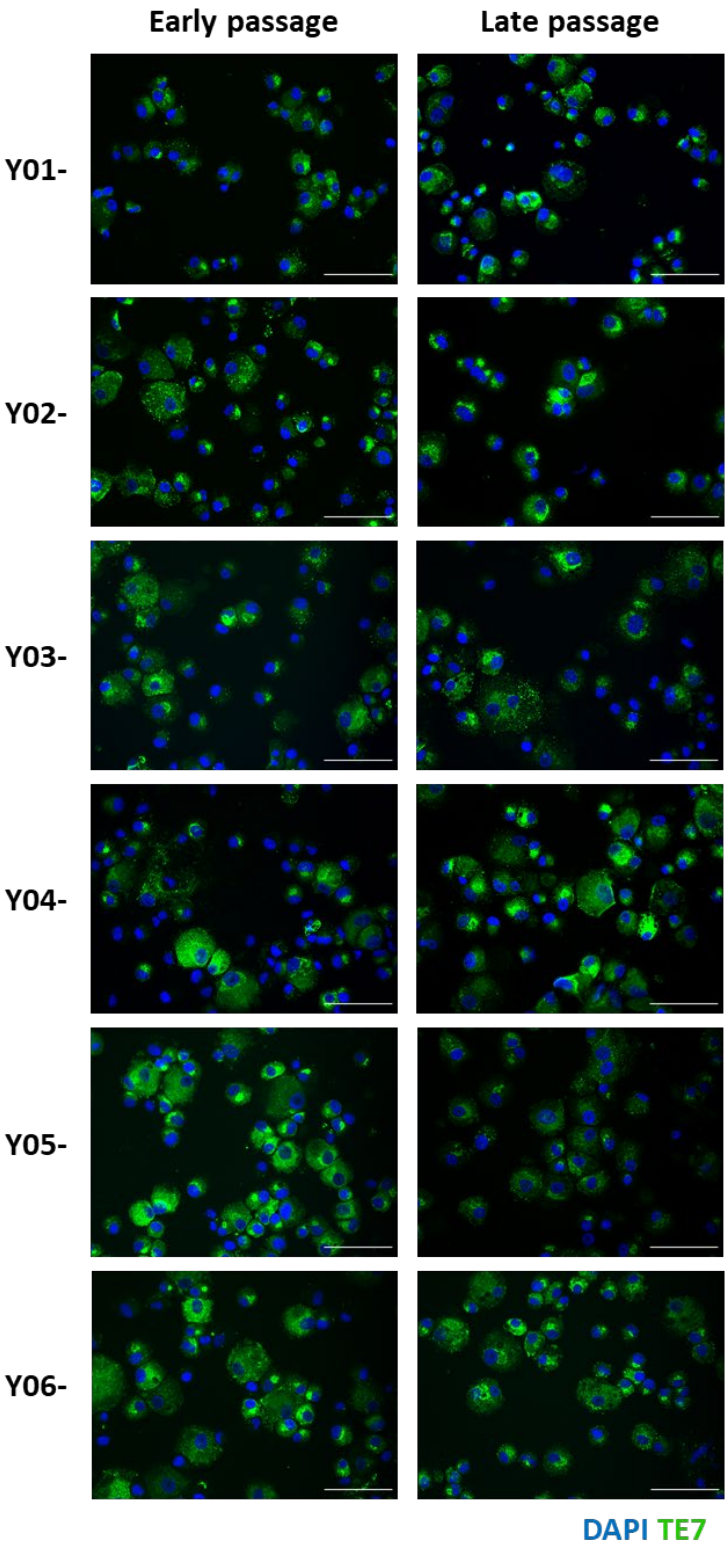

Figure 4.12. Representative images of TE7 stained CD56-ve cell populations at early and late passage.

Sub populations of cells (20,000 cells) from each $CD56^{-ve}$ population were cytospun at early and late passage and stained for DAPI (Blue), TE7 (green) and desmin (red). Images acquired using a 20x magnification objective, scale bar = 100 µm.

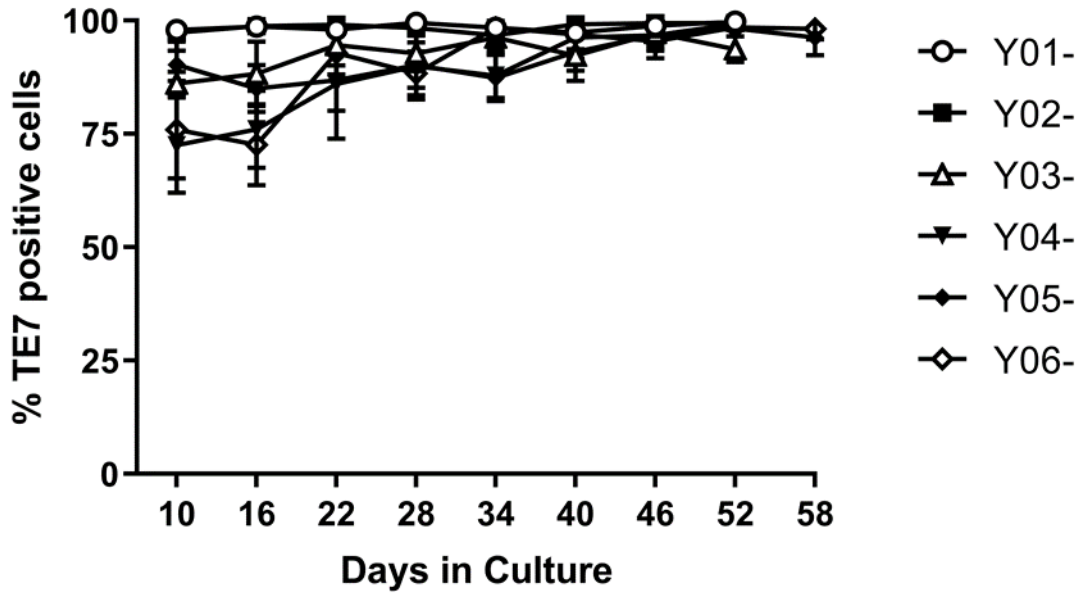

Figure 4.13. The number of TE7 expressing cells increase in CD56^{-ve} populations with serial passaging.

Sub populations of cells (20,000 cells) from each CD56^{-ve} population were cytospun at alternate passages across their replicative lifespan to determine TE7^{+ve} cell proportion by a bespoke automated image analysis program. Data presented as Mean±SD of percentage TE7 positive nuclei per field of view, 10 fields of view per time point, minimum of 100 cells analysed in total per time point. Open symbols represent CD56^{-ve} cell populations with a corresponding CD56^{+ve} cell population which became overrun by fibroblasts.

4.5.2. Replicative potential of fibroblast cell populations

The replicative profile of each individual $CD56^{-ve}/TE7^{+ve}$ fibroblast cell population was monitored by cumulative population doublings every three days in the same way as the $CD56^{+ve}$ populations. The fibroblast population doubling experiments were stopped after the same time in culture as the $CD56^{+ve}$ cell population from the same biopsy. At which point all fibroblast cell populations were still dividing (Figure 4.13), although there was a trend (p=0.052) for slower population doubling times (32.3±7.8 h) at the last recorded passage in the six fibroblast samples, when compared to their early passage rates (22.3±2.1 h). There was also no noticeable difference in characteristics of the $CD56^{-ve}$ cell populations extracted from biopsies which had a $CD56^{+ve}$ population which lost desmin expressing cells compared to those which maintained high percentages of desmin expressing cells (Figure 4.13).

4.5.3. Senescent marker expression within fibroblast cell populations

To determine the marker expression of $CD56^{-ve}/TE7^{+ve}$ fibroblasts after the same time in culture as the $desmin^{+ve}$ myoblasts which had reached replicative senescence, the expression of the same four markers known to be associated with senescent cells, Ki67, p16, γH2aX and SA β-Gal were assessed. As with the $CD56^{+ve}$ populations technical methodologic issues prevented the analysis of all six samples for SA β-Gal, however two fibroblast samples, Y05 and Y06, did provide usable results for SA β-Gal.

4.5.3.1. Ki67 expression is reduced in later passage fibroblasts

The representative images in Figure 4.14 show Ki67 expression in the late passage populations of fibroblasts. The individual cell by cell mean fluorescent intensities indicate that there are still a large proportion of cells with high Ki67 expression in the late passage populations similar to the early passage population, suggesting both early and late passage populations are highly proliferative (Figure 4.15). However, at the whole cell population level mean fluorescent intensity of Ki67 was significantly reduced at late passage compared to early passage (*P = 0.04*, fold change=0.69±0.15, Figure 4.16). Taken with the trend for slower population doubling times at late passage would suggest a slight decrease in the proliferation of the fibroblast cell population.

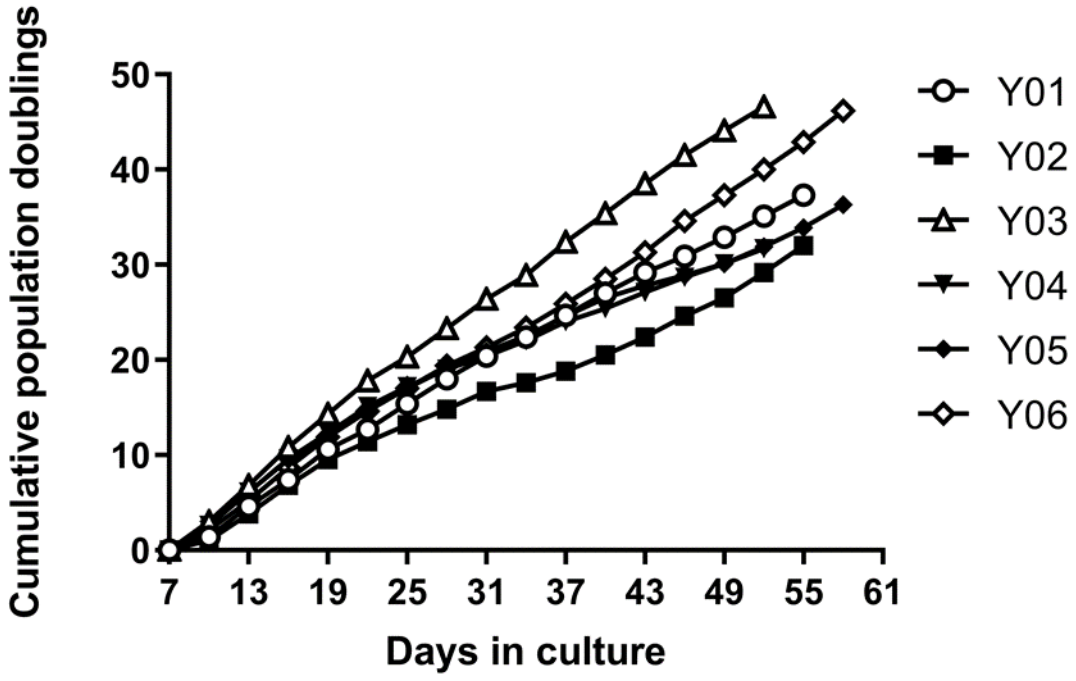

Figure 4.14. Fibroblasts are still highly proliferative after serial passaging when CD56^{+ve} populations have reached replicative senescence or been overrun by fibroblasts.
Replicative profile of individual biopsies calculated by cumulative population doublings every three days. Population doublings = Log2(N1/N0)/Log2 where N1 is the end of passage cell count and N0 is the number of cells seeded. MACS sorting occurred at day 7 and is used as the initial time point. Open symbols represent fibroblast cell populations with a corresponding CD56^{+ve} cell population which became overrun by fibroblasts.

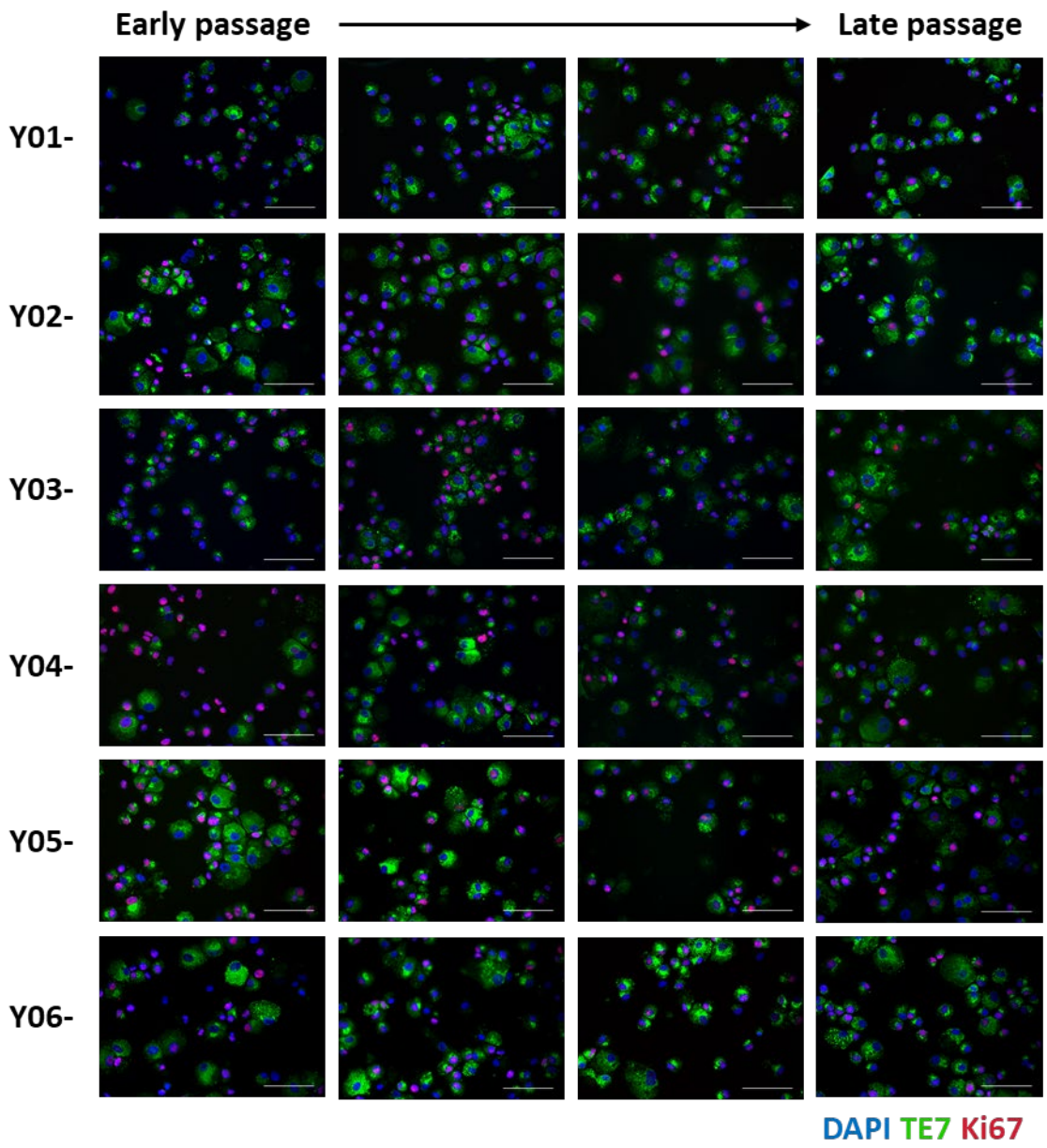

Figure 4.15. Representative images from individual biopsies of Ki67 expression across replicative lifespan of fibroblast cell populations.
Representative images of fibroblast cell populations across serial passages, stained for DAPI (blue), TE7 (green) and Ki67 (red). Images acquired using a 20x magnification objective, Scale bar = 100 µm.

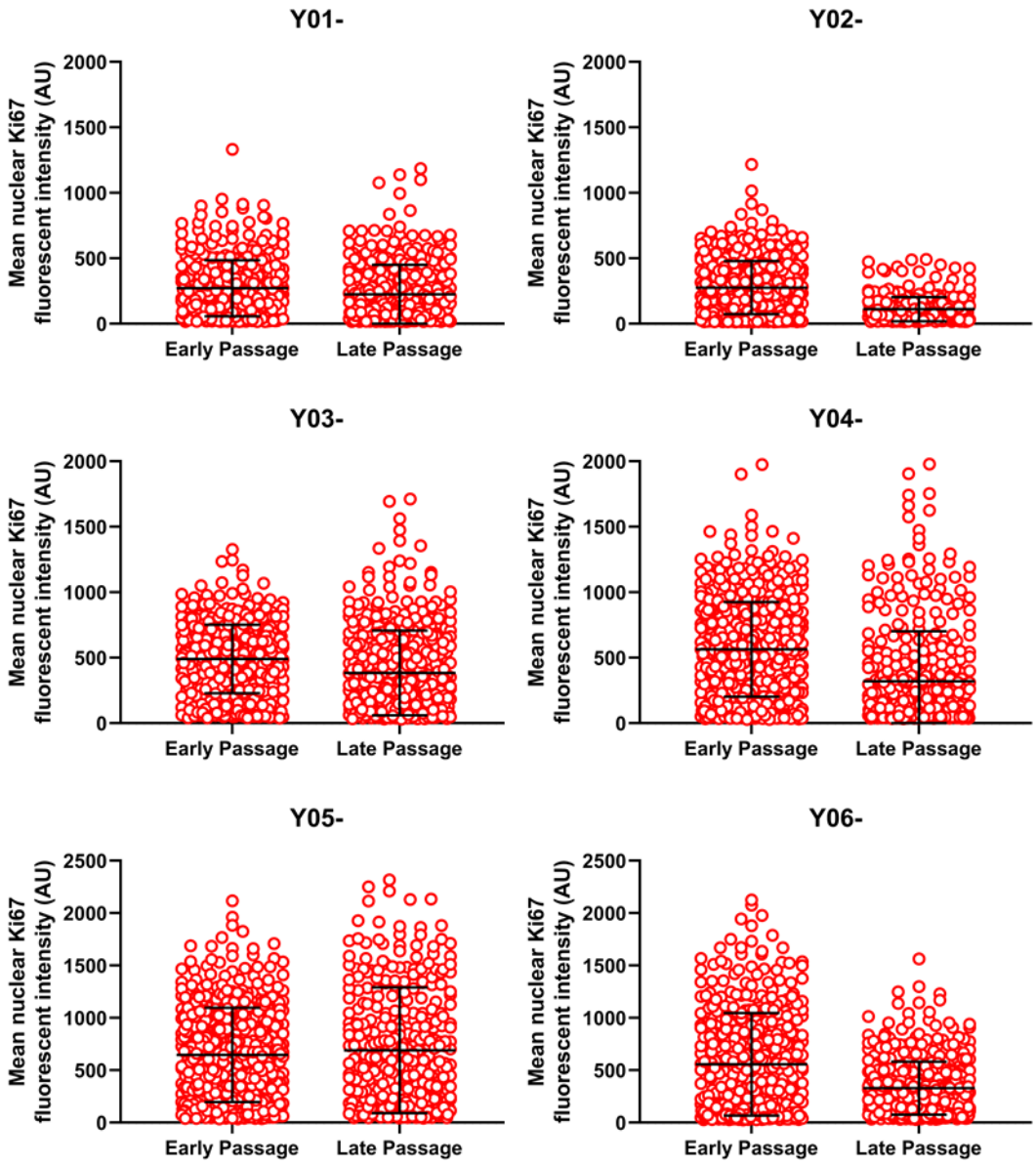

Figure 4.16. Individual cell by cell Ki67 expression at early and late passage for individual fibroblast cell populations.

Cell by cell mean fluorescent nuclear Ki67 intensity at early passage and late passage for individual fibroblast cell populations. Late passage denotes the time point at which the $CD56^{+ve}$ cell population from the same biopsy was stopped. Each circle represents the mean fluorescent intensity of Ki67 of a single nucleus. Black lines indicate population Mean±SD. Statistical analysis was not performed on these individual populations as the same data was used to be analysed in Figure 4.16.

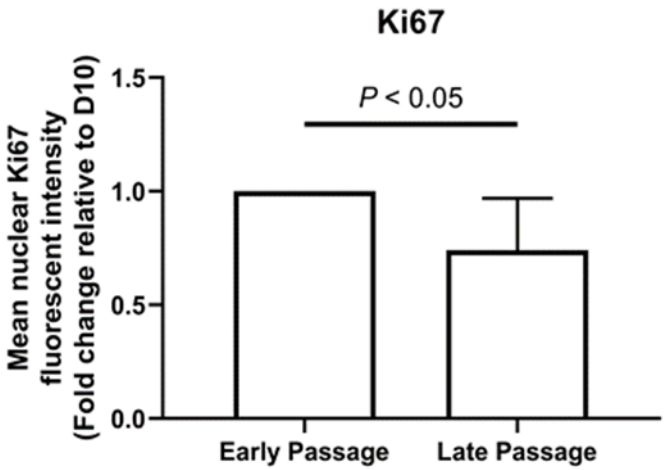

Figure 4.17. Ki67 expression decreases at late passage in Fibroblasts.
Summary of individual mean fluorescent nuclear Ki67 intensity for fibroblast cell populations presented in Figure 4.15. Each individual's cell population mean fluorescent intensity is represented as a fold change from their own early passage population mean. Error bar represents standard deviation between the individuals. N=6, (p = 0.039) paired t-test.

4.5.3.2. p16 expression is unchanged in later passage fibroblasts

Protein levels of the cell cycle inhibitor p16 was unchanged at the cell population level after serial passaging ($p = 0.58$, Figure 4.19). When observing the individual fibroblast cell populations there was only an increase in one sample, Y04, whereas it was either unchanged or slightly lower in the other five samples at late passage (Figure 4.18).

4.5.3.3. γH2aX expression is unchanged in later passage fibroblasts

DNA double strand breaks, as measured by γH2aX expression, was unchanged in late passage fibroblast cells compared to early passage ($p = 0.12$, Figure 4.22). When analysing the individual fibroblast cell populations one sample, Y01, showed an increase in γH2aX expression in contrast to the other samples, which didn't show an increase (Figure 4.21). The cell population with increased γH2aX expression, Y01, was different to the cell population which showed increased p16 expression, Y04, showing difference between cell populations for these senescent markers.

4.5.3.4. Senescence associated β-Galactosidase expression

Because of technical error (Methods section 2.5.1), SA β-Gal could only be analysed in two of the six fibroblast cell populations, Y05 and Y06, both of which had ~10% of cells expressing SA β-Gal at early passage. There was a difference in response to serial passaging between the two samples with one population remaining ~10% positive for SA β-Gal (Y06) whereas, in the other sample (Y05) the percentage of SA β-Gal positive cells increased to ~25% (Figure 4.23). Both populations were therefore lowly expressing SA β-Gal at late passage.

4.5.4. SASP factor expression of later passage fibroblasts

To determine if known SASP factor expression had increased in the fibroblast cell populations after serial passaging, even without reaching replicative senescence, gene expression at the last proliferative time point was measured. For each cell population SASP factor expression was expressed as a fold change relative to the earliest time point measured, 10 days after biopsy, for all six samples. After correcting for multiple tests using

the Bonferroni correction none of the SASP factors were significantly altered at late passage compared to early passage.

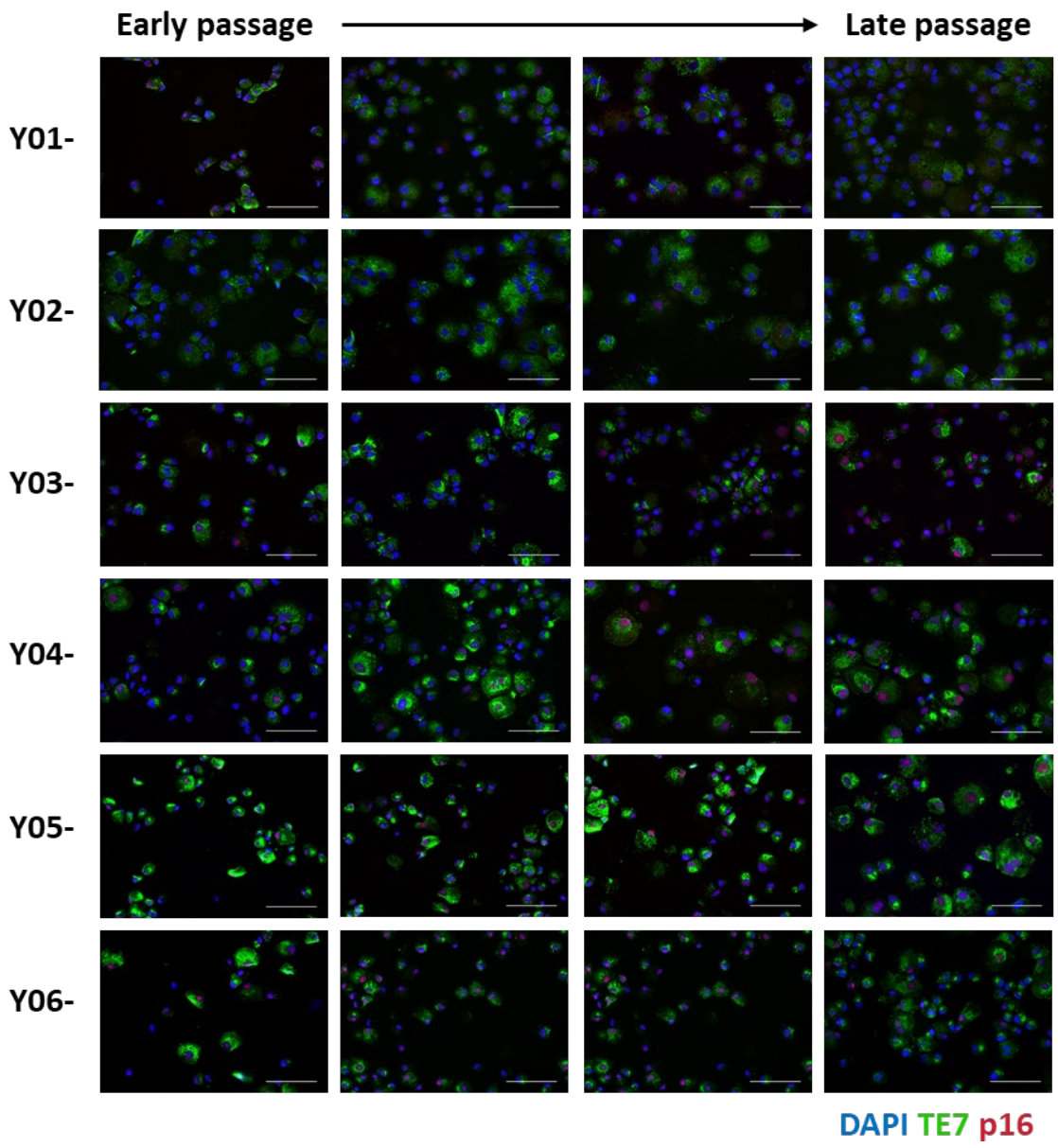

Figure 4.18. Representative images of p16 expression across replicative lifespan of individual fibroblast cell populations.

Representative images of fibroblast cell populations across serial passages, stained for DAPI (blue), TE7 (green) and p16 (red). Images acquired using a 20x magnification objective, Scale bar = 100 µm.

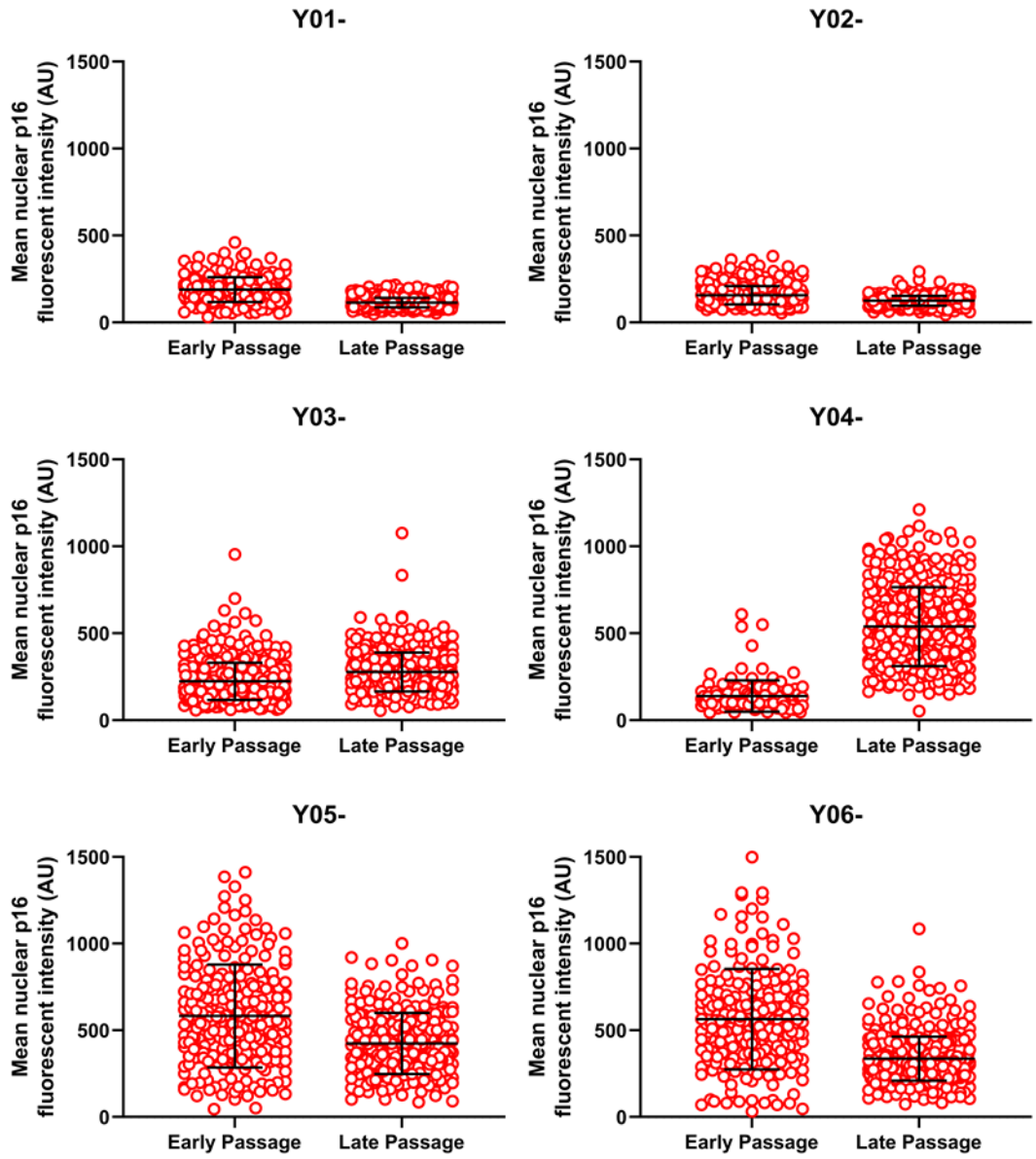

Figure 4.19. Individual cell by cell p16 expression at early and late passage for individual fibroblast cell populations.

Cell by cell mean fluorescent nuclear p16 intensity at early passage and late passage for individual fibroblast cell populations. Late passage denotes the time point at which the $CD56^{+ve}$ cell population from the same biopsy was stopped. Each circle represents the mean fluorescent intensity of p16 of a single nucleus. Black lines indicate population Mean±SD. Statistical analysis was not performed on these individual populations as the same data was used to be analysed in Figure 4.19.

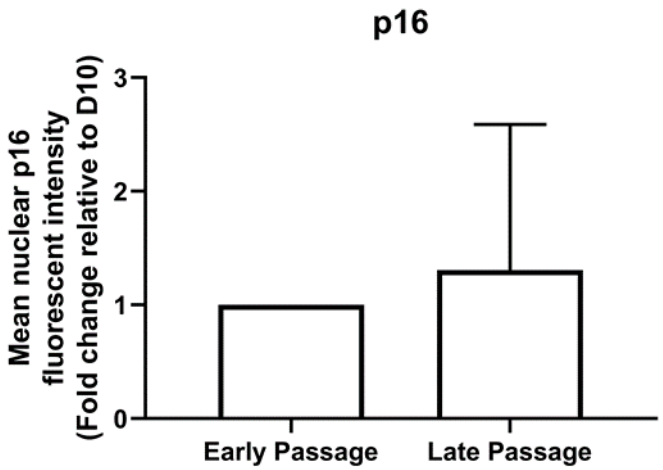

Figure 4.20. Fibroblasts p16 expression trends up at late passage.
Summary of individual mean fluorescent nuclear p16 intensity for fibroblast cell populations presented in Figure 4.18. Each individual's population mean fluorescent intensity is represented as a fold change from their own early passage population mean. Error bar represents standard deviation between the individuals. N=6, non-significant (p = 0.58) paired t-test.

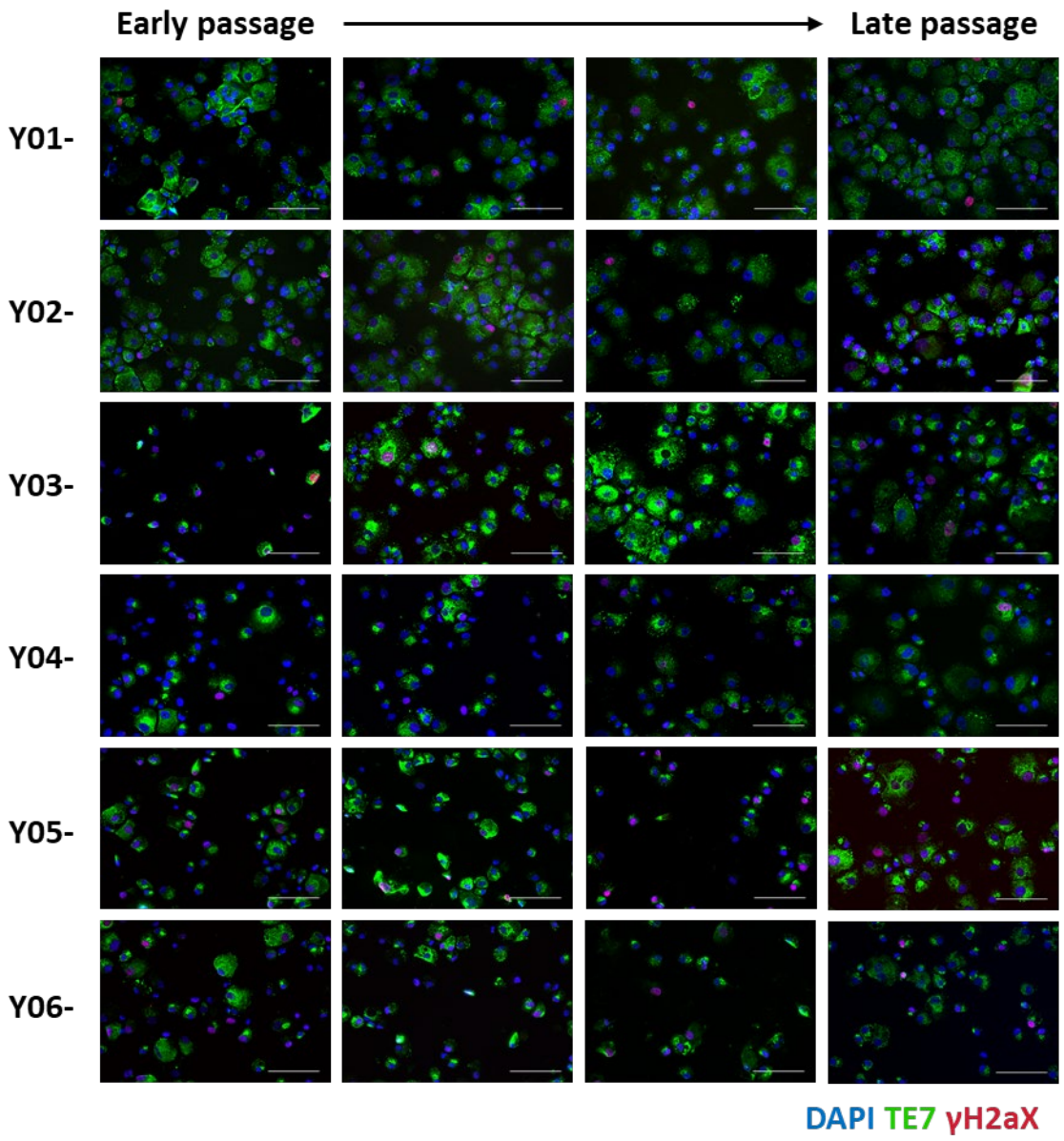

Figure 4.21. Representative images of γH2aX expression across replicative lifespan of individual fibroblast cell populations.

Representative images of fibroblast cell populations across serial passages, stained for DAPI (blue), TE7 (green) and γH2aX (red). Images acquired using a 20x magnification objective, Scale bar = 100 µm.

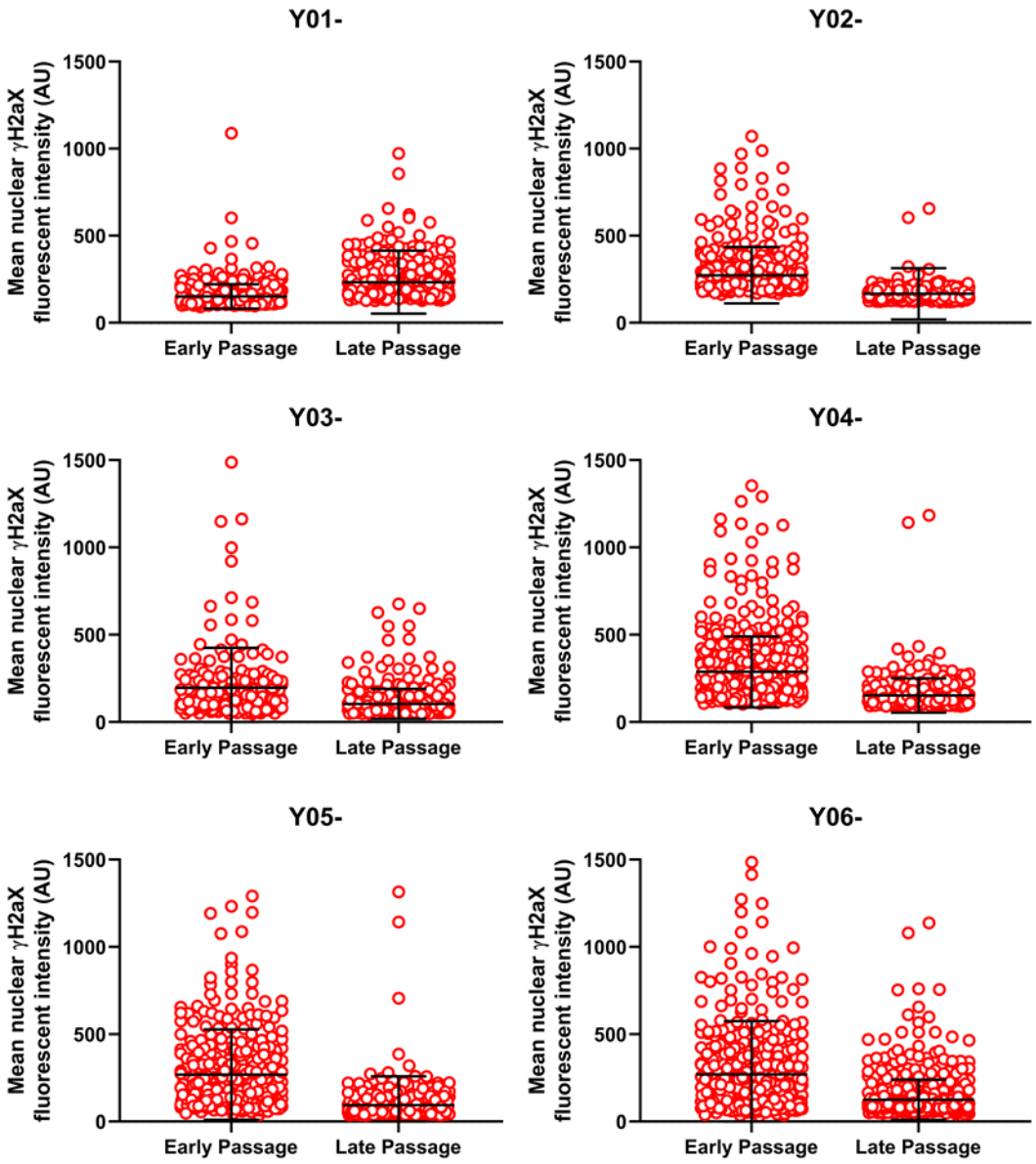

Figure 4.22. Individual cell by cell γH2aX expression at early and late passage for individual fibroblast cell populations.

Cell by cell mean fluorescent nuclear γH2aX intensity at early passage and late passage for individual fibroblast cell populations. Late passage denotes the time point at which the $CD56^{+ve}$ cell population from the same biopsy was stopped. Each circle represents the mean fluorescent intensity of γH2aX of a single nucleus. Black lines indicate population Mean±SD. Statistical analysis was not performed on these individual populations as the same data was used to be analysed in Figure 4.22.

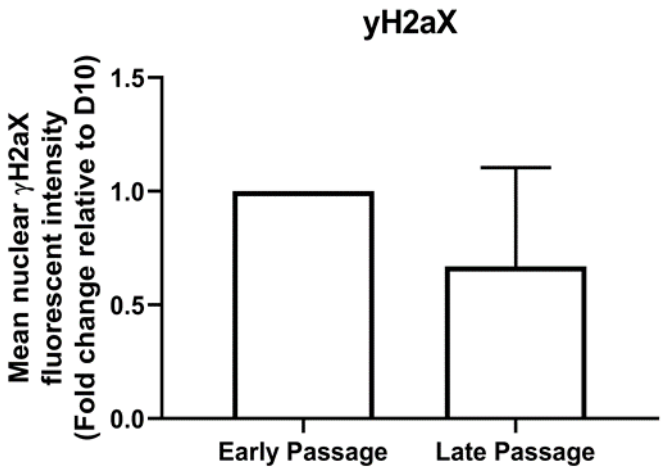

Figure 4.23. Fibroblast γH2aX expression trends down at late passage.
Summary of individual mean fluorescent nuclear γH2aX intensity for fibroblast cell populations presented in Figure 4.21. Each individual's population mean fluorescent intensity is represented as a fold change from their own early passage population mean. Error bar represents standard deviation between the individuals. N=6, non-significant ($p = 0.12$) paired t-test.

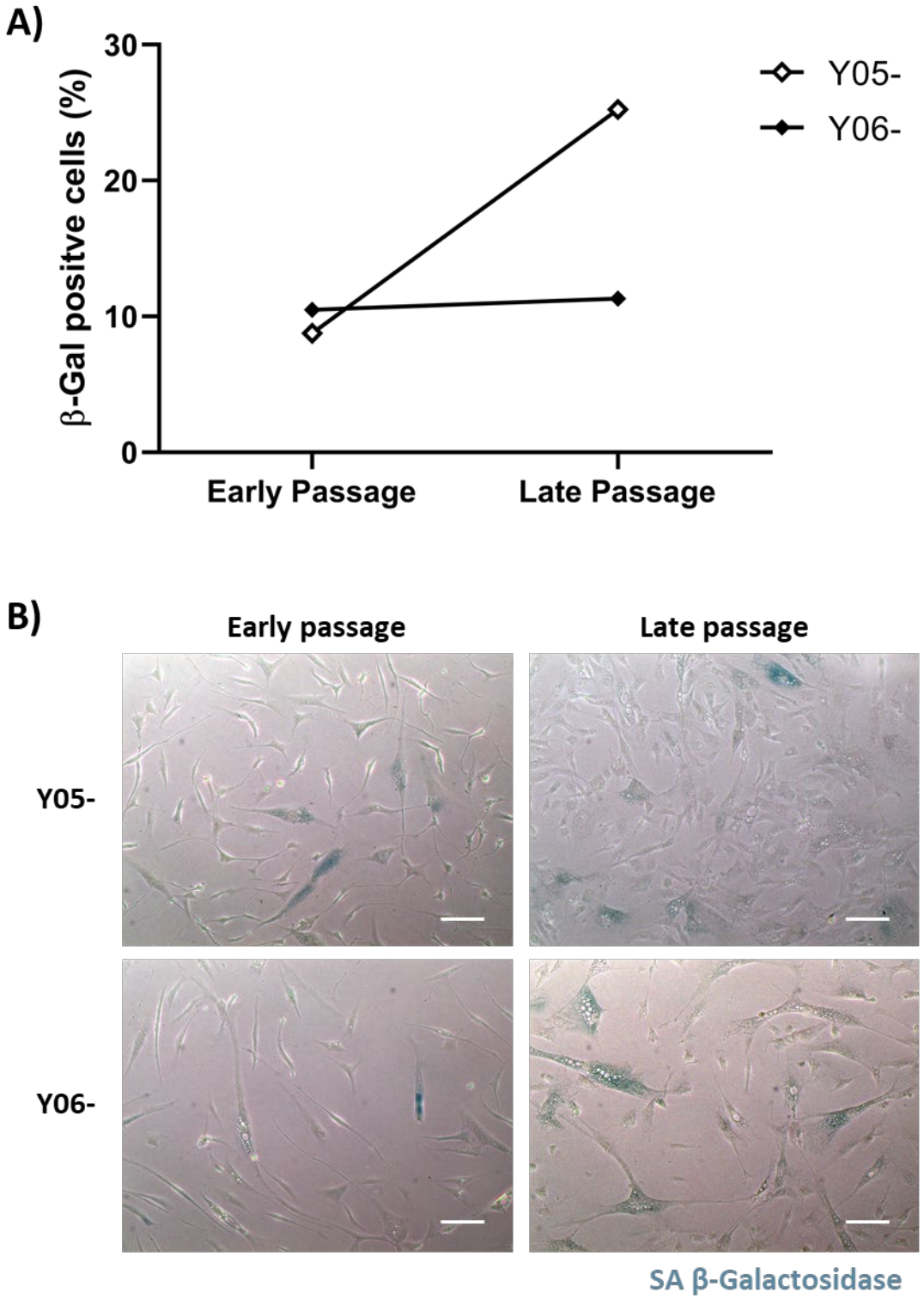

Figure 4.24. Fibroblast cell populations senescence associated β-Galactosidase.
A) Percentage of cells staining positive for SA β-Galactosidase at early and late passage. Each data point represents the mean percentage SA β-Galactosidase positive cells from 10 non overlapping fields of view. **B)** Representative images of early and late passage $CD56^{-ve}$ cell populations stained for SA β-Galactosidase. Images acquired using a 20x magnification objective, Scale bar = 100 µm.

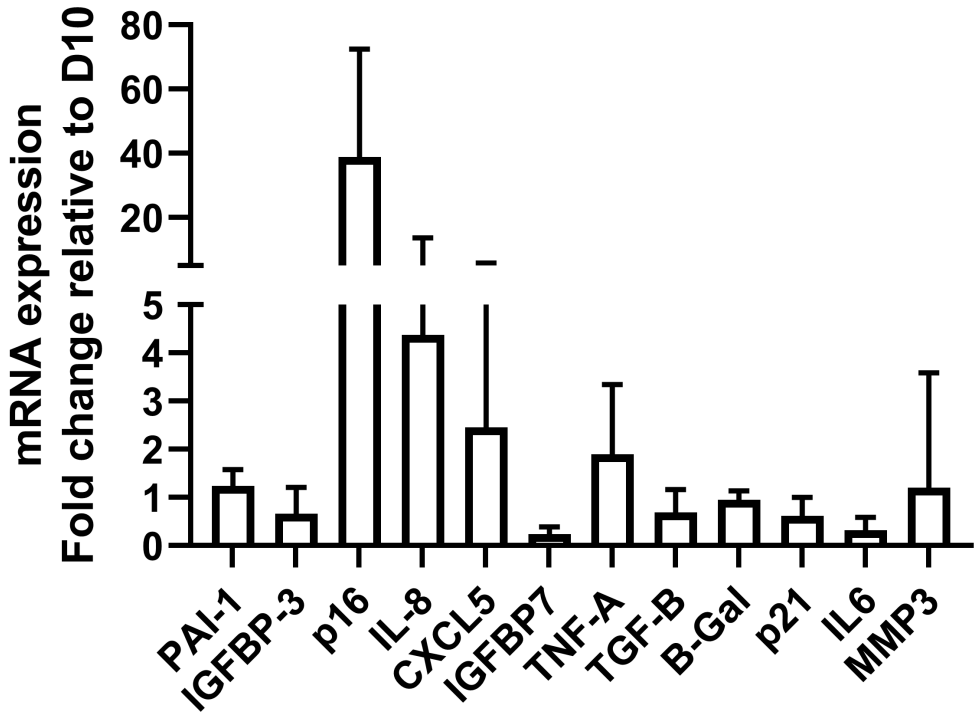

Figure 4.25. SASP factor gene expression changes in fibroblast cell populations after serial passaging.

Fold change in mRNA expression of known SASP factors was determined by RT-qPCR at late passage, relative to early passage, in fibroblast cell populations N=6. Data presented as Mean fold change±SD. Statistical analysis using paired t-tests for individual SASP factors reveals sig. difference for p16, IGFBP7 and IL6 however all three became non-significant after the Bonferroni correction was applied to account for the multiple tests.

4.6. Discussion

The senescent phenotype of the main human skeletal muscle-derived precursor cell populations, myoblasts and fibroblasts are currently not well characterised. The main aim of these experiments was to extensively characterise the senescence phenotype of purified $CD56^{+ve}$ myoblast and $CD56^{-ve}$ skeletal muscle fibroblast cell populations obtained from the same muscle biopsies and exposed to the same time and conditions in culture. The discussion here firstly focused on characterising the myogenic phenotype at replicative senescence before discussing the fibroblasts at the same time point in culture.

4.6.1. Obtaining myoblast enriched cell populations

Of the six original biopsy samples two were deemed to have reached replicative senescence whilst maintaining a high percentage of desmin expressing cells. Previous studies have used cell populations with varying myogenic cell percentages to characterise the phenotype of senescent human muscle cell populations (Renault *et al.*, 2000; Fulle *et al.*, 2005; Schäfer *et al.*, 2006; Alsharidah *et al.*, 2013). This study took a conservative approach and only used myoblast cell populations which had i) achieved replicative senescence and ii) maintained >90% desmin expressing cells throughout their replicative lifespan. Only these two populations undertook senescent phenotypic analysis.

The initial percentage of desmin expressing cells within an extracted cell population from a muscle biopsy can depend on the specific site within the muscle that the sample was taken. There are also unknown effects of the seven days expansion in culture post-extraction that could also influence the percentage of desmin positive cells within the cell population. To standardise and enrich the starting cell population's $desmin^{+ve}$ cell proportion, a MACS sort for the myogenic cell surface marker $CD56^{+ve}$ was performed seven days after the cells were extracted from the biopsy. The pre-sort $desmin^{+ve}$ cell percentage was not directly measured to maximise cell numbers for replicative experiments. However, the pre-sort desmin percentage (67.3 ± 6.4%) was estimated from the proportional difference in population size between the post-sort cell counts of the $CD56^{+ve}$ and $CD56^{-ve}$ cell populations. The $desmin^{+ve}$ cell percentage of the post-sort $CD56^{+ve}$ populations obtained from the six biopsy samples studied was 97.6 ± 1.7%. Thus,

all starting populations were determined to be highly desmin positive and were all used to obtain early passage myogenic phenotypes.

The phenotype of early passage non-senescent myogenic cells is important for providing a reference for comparison with the replicative senescent cell populations. As previous studies have shown there is variability in how long myogenic cell populations take to senesce under culture conditions it is important to obtain the early passage phenotype at as early time point as feasibly possible (Renault *et al.*, 2002*b*; Schafer *et al.*, 2005; Alsharidah *et al.*, 2013). Previous explant studies which wait for accumulation of cells extruded from muscle tissues thus the early extruded cells may undergo multiple rounds of division before early passage measurements are made therefore, they may have more senescent early passage populations (Decary *et al.*, 1997; Renault *et al.*, 2002*b*; Bortoli *et al.*, 2003; Jacquemin *et al.*, 2004; Beccafico *et al.*, 2011). This is also a key issue if trying to compare cumulative population doublings as unknown doublings could have occurred before measurements began.

In this study the time course between cell extraction and starting experiments was standardised across all biopsies to control for proliferation bias. Cells were extracted on the day of the biopsy (day zero) and sorted 7 days later. Thus, all time points are relative to the day of biopsy and cumulative population doublings were all started after the CD56 MACS sorting on day seven post extraction. The early passage phenotype was determined at 10 days after biopsy in all cell populations. At this time point, all cell populations were large enough to undertake a full characterisation, which was not possible for all samples at seven days post biopsy.

To monitor and determine when cell populations had reached a senescent state, cumulative population doublings were measured at every passage across the cell population's replicative lifespan. Of the six $CD56^{+ve}$ cell populations analysed; three reached proliferative arrest, as determined by the time point at which no increase in cumulative population doublings occurred. The other $CD56^{+ve}$ populations were thought to have become overrun by another cell type, most likely to be $TE7^{+ve}$ fibroblasts as seen by Alsharidah *et al.*, (2013), so were stopped at this point. This was due to an observation of a slowing in population doubling rate, suggesting a population was reaching proliferative arrest, but then a subsequent increase in population doubling rate, where

the fibroblasts over ran the culture. PDs are a crude description of population growth because haemocytometer counts are not precise enough to detect very small changes in population number. More accurate cell counts can be obtained using FACS or automatic cell counters, but this may not add that much additional information as serial passaging of cells creates exponential large numbers of cells. From a single cell undergoing the mean cumulative population doublings counted in these experiments would undergo ~25 doublings would create 2^{24} (over 16 x10^6) cells and as shown earlier the average size of starting CD56^{+ve} population was 400,000 cells.

Of the three CD56^{+ve} cell populations to reach replicative senescence only two maintained high percentages of myogenic cells representing a 33.3% success rate of developing replicative senescent populations of desmin positive cells. However, one of the populations, Y05+, which showed a slowing then accelerating pattern in cumulative population doublings turned out to maintain high desmin expression throughout. Interestingly, it was observed that these cells were co-expressing desmin and TE7 which have not previously been observed in this laboratory (Figure 4.2). Concurrent analysis of population cell type proportions would have prevented the premature ending of this sample's replicative experiments. A better understanding of why certain populations seem to be predisposed to overrunning is needed, although it could just be a case of length of culture time allowing the TE7 cell population to increase as is starting to be seen in two of the biopsies which maintained high desmin^{+ve} cell percentages and reached replicative senescence (Figure 4.3A). There is a small trend for declining numbers of desmin expressing cells at the latest time points suggest that a minority cell population may be still dividing that is altering the cell type proportions of the population. This expansion of fibroblasts would suggest that at this time point the myoblasts are not producing a strong senescent bystander effect. If the myoblast population does reach the replicative senescent state, then their SASP has the potential to cause surrounding cells to become senescent (Nelson *et al.*, 2012). However, even though these fibroblasts are in the minority they seem to be able to withstand the senescence inducing environment and over run the senescent myogenic population.

To prevent the loss of desmin positive cells and accumulated TE7 expressing fibroblasts seen in the other three CD56^{+ve} samples it was thought that re-sorting for CD56 would prevent the accumulation of non-myogenic cell types within the CD56^{+ve} cell

populations. However, the results of pilot experiments suggested that there is a loss of CD56 expression with repeated passaging, data not shown. Analysis of the $CD56^{-ve}$ fraction of late passage MACS sorts showed an increased proportion of desmin positive cells (Figure 4.4), as well as, a larger absolute number of cells. Therefore, CD56 was not actively selecting for all myogenic cells across their proliferative lifespan. Another research group have also shown modulation in the expression of CD56 in human primary skeletal muscle cells across time in culture (Meng *et al.*, 2011). They also suggest that there may be cells capable of myogenic linage potential, such as skeletal muscle pericytes within the $CD56^{-ve}$ cell population which may explain the co expression of desmin and TE7 mentioned previously.

The sorting method employed was developed previously to enrich early passage cells for experimentation. It was not specifically designed for long term culture experiments. A single MACS sort using a single marker was chosen as it was the gentlest method for cell separate and could produce highly enriched cell populations without significantly reducing cell yield after a single sort (Agley *et al.*, 2015). Double sorting for the same marker, passing the CD56 positive sort fraction from the first sort through a new column, may further enrich the myogenic cell population at the expense of a lower cell yield (Agley *et al.*, 2015). However, CD56 is not the best marker of skeletal muscle satellite cells or muscle precursor cells; the transcription factor Pax7 is currently agreed to be the best marker, but it is not a viable candidate for MACS cell sorting which requires cell surface markers. Pax7 is also lost as satellite cells become myoblasts therefore Pax7 expressing cells are lost with serial passaging (Olguin & Olwin, 2004). Currently there is no well-established native, cell surface marker, that could be successfully used to purify primary human myoblasts across their replicative life span. Therefore, maintaining high numbers of myogenic cells is still a significant challenge to reliably obtaining replicative senescence populations of myogenic cells. Recently CD82 has been found as a novel marker of human muscle satellite cells and double sorting using both CD56 and CD82 has produced highly enriched myogenic cell populations (Alexander *et al.*, 2016; Uezumi *et al.*, 2016). However, it has yet to be investigated if CD82 expression is maintained throughout the replicative lifespan.

It is clear from the current work that the issues of creating replicative senescent populations are not prevented by initial purification of the cell populations. Of the six

$CD56^{+ve}$ cell populations only two maintained a myogenic phenotype through to proliferative arrest. Three further biopsy samples were taken and treated in the same manner but all three also became overrun with $TE7^{+ve}$ fibroblasts (Figure 4.5).

4.6.2. Replicative senescent phenotype of myoblasts

With only two of six $CD56^{+ve}$ cell populations maintaining high proportions of myogenic cells through to replicative senescence limited conclusions could be drawn about their phenotypic characteristics. As mentioned, a further three $CD56^{+ve}$ samples were subsequently used to increase the statistical power, however all three also became overrun with fibroblasts.

The two myogenic replicative senescent cell populations were analysed for four markers associated with senescence as there is no definitive marker of senescence. The most commonly utilised senescent cell marker is the presence of SA β-Gal (Dimri *et al.*, 1995). Due to technical problems SA β-Gal was unfortunately not assayed correctly for the two samples which reached myogenic replicative senescence (Methods section 2.5.1). Data is only available Y05+ and Y06+. Y05+ was the sample which was mistakenly stopped early during replicative passaging even though it maintained a high myogenic cell percentage. Y06+ reached replicative senescence but failed to maintain a high myogenic cell percentage. Therefore, neither can be reliably used to infer myogenic replicative senescent expression of SA β-Gal.

The other three senescence markers; p16, γH2aX and lack of Ki67 were measured using the automated image analysis program developed in chapter 3. As only two cell populations maintained high proportions of myogenic cells through to replicative senescence the change in senescent marker expression was observed between early and replicative senescence within the individual cell populations. Both populations showed decreased Ki67 protein and increased p16 protein. This is consistent with previous studies looking at senescent cell populations showing increased p16 mRNA (Barberi *et al.*, 2013). However, both cell populations showed lower mean fluorescent intensity of γH2aX at late passage compared to early passage which is different to Alsharidah *et al.*, (2013) who showed that there are more γH2aX positive cells in senescent populations of myogenic cells compared to early passage cells when assessed by binary counting.

Subjective binary counts are often used to determine if a cell is expressing markers such as Ki67, p16 or γH2aX. However, as shown by the individual cell by cell mean fluorescent intensity data for all three markers there is a very heterogenous expression of these markers within a cell population. Thus, using a subjective cut off point for positivity is potentially misleading and easily manipulated. Quantitative analysis can be performed using qPCR or western blot. However, these techniques only determine the overall increase in senescent marker expression within the cell population therefore they lose the cell by cell heterogeneity present within the cell populations. Although the image analysis method employed cannot categorically say a cell population has stopped dividing it is clearly evident that there is a shift in the populations towards an increased number of nuclei with very low mean fluorescent intensity for Ki67 and whole populations shifts for more p16 expression which would be indicative of a population that has reached replicative senescence.

The discrepancy in γH2aX results between ours and previous studies could also be the result of using this more objective analysis method. It is suggested that each γH2aX foci represents a single double strand break and therefore cells with more foci have more DNA damage (Rothkamm *et al.*, 2015). This should also be represented by the mean fluorescent intensity because more bright pixels within the nucleus would increase the mean fluorescent intensity for that nucleus. However, due to the very specific locations of γH2aX expression at the DNA double strand break sites very few pixels expressing γH2aX as a proportion of total nuclear pixel the difference in mean fluorescent intensity may not be seen by the current method. A further development of the program could be to threshold within each nucleus for expression of γH2aX then counting how many individual objects are detected within the nucleus therefore giving an automated number of foci count.

To summarise the increases in p16 expression and decreased Ki67 expression, together with the cells proliferative arrest strengthens the argument that these cell populations have reached replicative senescence. The addition of available SA β-Gal data in support of these markers would further reinforce this statement. However, in the case of these two cell populations increased DNA damage does not seem to be present in the senescent state at the population level.

The key feature of senescent cells is their altered secretory phenotype, their senescence associated secretory phenotype (SASP). The SASP is thought to be mainly pro-inflammatory in nature but with the specific makeup of the SASP being cell type specific (Childs *et al.*, 2014). Within the SASP factors used throughout this thesis PAI-1, IGFBP3, IGFBP7, IL6, IL8, TGF-β, MMP3, CXCL5 and TNF-α are either directly or secondary to the inflammatory SASP (Coppé *et al.*, 2010*a*). Of the factors used as a small prospective marker panel, four, PAI-1, IGFBP3, p16 and IL-8, were shown to be upregulated in both myogenic replicative senescent cell populations. The upregulation of p16 mRNA complements the data found from the protein image analysis method presented. The down regulation of p21 was surprising as it is often associated, alongside p16, as a senescence associated cell cycle inhibitor. However, p21 is upregulated in the DNA damage response and increased DNA damage was not observed in these cell populations. IGFBP3 and IL-8 mRNA expression were upregulated between 8- and 50-fold in both biopsies, whereas PAI-1 was 200-fold upregulated in one biopsy and only slightly in the other, 2-fold. Previous studies have shown TGF-β protein upregulation (in conditioned media) in senescent myoblasts at the early stage of differentiation (Alsharidah *et al.*, 2013). The current study did not show an upregulation of TGF-β mRNA and expression was assessed in proliferative conditions rather than during differentiation initiation.

The functional capacity of the senescent $CD56^{+ve}$ populations was investigated to determine if they were able to undergo full and timely differentiation into myotubes at early and late passage. This has importance in a regenerative tissue such as skeletal muscle which must undergo multiple round of regeneration throughout life. The fusion index results of the current experiments support previous literature in that fewer nuclei are incorporated into myotubes when late passage cells are directed to differentiate than early passage cells (Renault *et al.*, 2000; Bortoli *et al.*, 2005; Alsharidah *et al.*, 2013). The 80% nuclei fusion observed in this study was also seen in previous studies (Alsharidah *et al.*, 2013). The myotubes formed at late passage and therefore at replicative senescence in this study, visibly contained fewer nuclei per myotube and were thinner than those formed by early passage cells.

To summarise, these experiments aimed to characterise the myogenic replicative senescence phenotype. It was observed that initial myogenic cell proportion can be enhanced by $CD56^{+ve}$ sorting however enrichment does not necessarily last through to

replicative senescence. This problem cannot be solved by regular sorting for CD56 because it has been shown that desmin positive cells accumulate in the $CD56^{-ve}$ fraction after later passage sorts suggesting there is modulation of CD56 expression in serially passaged myogenic cells. In the two cell populations which maintained myogenicity and were deemed to reach proliferative arrest by cumulative population doublings analysis; Ki67 expression was significantly reduced, p16 expression was significantly increased and cells were less able to differentiate into myotubes. They also showed some elevated SASP factor mRNA expression. However, only two samples were analysed and therefore further samples must be assayed before valid conclusions can be drawn.

4.6.3. Fibroblasts do not reach replicative senescence in the same time frame as myoblasts from the same biopsy sample

The generation of senescent myogenic cell populations was hard to achieve due to them becoming overrun by skeletal muscle derived $TE7^{+ve}$ fibroblasts. This study also aimed to investigate these skeletal muscle origin fibroblast populations in isolation to determine how their behaviour differs from the myogenic cells extracted from the same biopsies. The $CD56^{-ve}$ population were passaged in parallel to the $CD56^{+ve}$ populations from the same biopsies so that the two cell populations could be compared for proliferative and senescent characteristics.

The predominant cell type in the $CD56^{-ve}$ fraction are $TE7^{+ve}$/Collagen VI^{+ve}/$Fibronectin^{+ve}$ fibroblasts (Agley *et al.*, 2015), sharing the same marker as the cell type which overrun some of the $CD56^{+ve}$ cell populations. The proliferative capacity of these cells is much greater than the $CD56^{+ve}$ cells as all six samples were still highly proliferative at the time point their equivalent myogenic population had reached senescence. In all cases the fibroblast populations achieved more population doublings in the same timespan as their paired $CD56^{+ve}$ populations, with the exception of Y05 which showed similar cumulative population doublings for the two cell types. This is of interest as Y05 was the only myogenic cell population to maintain a high proportion of desmin positive cells and still be proliferative at the time of stopping passaging. As well as, containing cells that co-stained for both myogenic, desmin and fibrogenic, TE7 markers.

The high proliferative rate and capacity of skeletal muscle origin fibroblasts is consistent with that of fibroblasts from other tissues. The original experiments by Hayflick were performed on skin fibroblasts and reached 55-65 population doublings before stopping dividing and other studies have shown similar results with fibroblasts from different tissue sources under culture conditions (Allsopp *et al.*, 1992; Alcorta *et al.*, 1996). The fibroblast populations were not followed to replicative senescence due to the long time to reach proliferative arrest and the labour intensity of the experiments.

The senescent marker expression of the fibroblast cell populations supports the notion that these cell populations are still highly proliferative and not senescent after the same time in culture as $CD56^{+ve}$ cells from the same muscle biopsy. Mean fluorescent intensity of Ki67 protein is varied between the cell populations, but when expressed as fold change from each individual population at early passage, the level of Ki67 expression is significantly reduced. When compared to the myogenic senescent $CD56^{+ve}$ cell populations the fold change is much smaller in the $CD56^{-ve}$ cell populations suggesting they are more proliferative. Similarly, to the $CD56^{+ve}$ samples there is a proportion of cells with very low levels of Ki67 mean fluorescent intensity but in the $CD56^{-ve}$ cell population, there is a much larger proportion with high Ki67 expression.

The $CD56^{-ve}$ cell populations also did not show increased p16 protein expression further suggesting that these cell populations were maintaining a proliferative state. Only one individual sample, Y04, shows an increased p16 expression at late passage with all other samples maintaining similar levels of p16. It is interested to note that there are cells with relatively high expression of p16 in both early and late passage cells suggesting that there may be senescent cells within these populations. This is supported by the SA β-Gal assay, which showed that both samples contained around 10% SA β-Gal positive cells at early passage. However, at late passage Y05- increased to around 25% positive cells whereas Y06- maintained a similar level of around 10%. When combined with the p16 expression data there is not an increase in number of higher expressing cells in Y05- at late passage suggesting that p16 expression and SA β-Gal may not always co-express in senescent cells. Additionally, similarly to the $CD56^{+ve}$ populations, γH2aX mean fluorescent intensity did not increase with serial passaging. The expression of SASP factors were also not significantly altered after serial passaging further suggesting that these cell

populations were not becoming senescent by the time point they were stopped proliferating.

Overall, the $CD56^{-ve}$ cell populations do not show significant upregulation of senescent markers or SASP factor expression which is consistent with the population doublings data suggesting that they are still maintaining a highly proliferative population. Thus, highlighting a difference between the two main progenitor cell populations within human skeletal muscle. This finding also supports the observations that purified myogenic cell populations can become overrun by fibroblasts cells which may be due to their longer replicative capacity of 40-60 population doublings (Hayflick, 1965; Allsopp *et al.*, 1992; Alcorta *et al.*, 1996).

4.7. Conclusions

Both main progenitor cell types in human skeletal muscle, myoblasts and fibroblasts, pose challenges when trying to obtain pure populations of replicative senescent cells. The fibroblasts showed no signs of reaching replicative senescence in the timeframe with which it took their myogenic counterparts to either reach proliferative arrest or be themselves overrun by fibroblasts. The long-term culture of human primary cell populations is expensive and time intensive and with the outlined issues stated above are currently, in the case of myoblasts, unreliable. Replicative senescence was seen by some as the gold standard for senescent cell populations (Campisi, 1997), as they argue it is the most representative of an in vivo phenotype. However, due to the heterogeneity of all in vivo populations and the fact that cells can become senescent via other pathways this is now not thought to be the case (Waaijer *et al.*, 2018). Additionally, these cells are *ex vivo*, maintained in non-physiological conditions and purified populations are not likely to be truly representative of an *in vivo* population. However, if a model could be developed to reliably produce senescent populations of highly pure cells, it may provide important information as to the functioning of senescent cells within skeletal muscle tissue. The next chapter outlines the development and analysis of an induced senescence model which is novel in human primary muscle derived myoblasts and fibroblasts.

Chapter 5: DOX-induced senescent phenotypes of human skeletal muscle precursor cells

5.1. Introduction

The results obtained by attempting to follow myoblasts and fibroblasts to replicative senescence were limited in both cell types but for different reasons. For myoblasts, the experiments showed that only two of the six purified populations could be successfully followed to replicative senescence without "contamination" from fibroblasts. Whereas, in the skeletal muscle derived fibroblast populations there were no signs of any of the cell populations reaching senescence within 60 days of cell culture. Coupling these findings to the expense and labour intensity of culturing cells for this extended period suggests that replicative senescence is not currently a reliable or reproducible model for examining cellular senescence within these human skeletal muscle derived cell populations. In order to overcome these disparate results and allow results with more statistical power to be obtained from all biopsy samples, it was decided to attempt to stress-induced senescence in both cell types to understand the senescent phenotypes of these cell populations.

After a review of the literature, the prime candidate that emerged to be used for such an intervention was the chemotherapy drug Doxorubicin (DOX). This was because DOX has been successfully used to induce senescence in human primary cell populations of other muscle cell types cardiomyocytes, cardiac progenitor cells (hCPCs) and vascular smooth muscle precursor cells (hVSMCs; Piegari *et al.*, 2013; Bielak-Zmijewska *et al.*, 2014; Lewis-McDougall *et al.*, 2019). High doses of DOX can cause apoptosis whereas low doses in the range of 0.1-1 µm have been shown to induce the senescent phenotype (Rebbaa *et al.*, 2003; Eom *et al.*, 2005). The fact that DOX has not been previously documented in skeletal muscle opened new possibilities to investigate the mechanisms of stress-induced senescence underlying the generation of senescent cell populations of skeletal muscle origin.

It has been postulated that DOX induces senescence though many mechanisms but primarily thought direct intercalation into DNA, preventing the synthesis of macro-molecules. DOX has also been shown to cause DNA damage by the generation of free radicals which cause further damage to DNA, as well as, lipid peroxidation and protein carbonyls (De Angelis *et al.*, 2010). DNA is also damaged by the induction of cross-links between DNA, interference with DNA unwinding and strand separation, altered helicase activity and initiation of DNA damage via inhibition of topoisomerase II (Gewirtz, 1999). This DNA damage is initiated immediately after addition of DOX, however, the senescent phenotype takes time to develop which is different depending on DOX dose and treatment length, as well as, depending on the cell type being treated (Thorn *et al.*, 2011).

This chapter describes the application of DOX-induced senescence, to human primary cell populations derived from skeletal muscle; muscle precursor cells (MPCs) and skeletal muscle origin fibroblasts. The aim was to gain further insight into the senescent characteristics of these cell populations. These experiments were carried out on the same biopsy samples concurrently with replicative experiments and are therefore directly comparable with their replicative equivalent.

5.1.1. Aims

(1) To use DOX to induce senescence in purified populations of human primary myogenic precursor cells and skeletal muscle origin fibroblasts obtained from the same muscle biopsy sample.

(2) To compare senescent marker and SASP expression within both cell types

It is hypothesised that treatment with DOX will induce senescent phenotypes in both human primary myogenic precursor cells and skeletal muscle origin fibroblasts. As senescence is a universal cell phenomenon, senescent markers and the SASP will be similarly expressed in both cell types.

5.2. Methods

5.2.1. Participants and muscle biopsies

The participants from whom muscle biopsy samples were obtained and used in this chapter are previously described in the general methods 2.1 and were the same as for experiments in the replicative senescence chapter 4.

5.2.2. Doxorubicin treatment (DOX)

Informed by a dose response study for DOX on human cardiac progenitor cells (Ellison-Hughes lab, 2017; Lewis-McDougall *et al.*, 2019)). A similar pilot experiment was undertaken on the skeletal muscle-derived cells. From the cardiac study a dose of 0.2 µm exposed for 24 hours was initially chosen to investigate DOX-induced senescence in MPCs and fibroblasts.

Following successful induction of senescence by carrying out this pilot study, cellular senescence was induced by incubating myoblasts and skeletal muscle origin fibroblasts (day 22 post biopsy) with DOX (0.2 µM) for 24 hours. After 24 hours Doxorubicin was removed, and cultures were thoroughly washed (PBS x5) before fresh growth medium was added. Induction of senescence was assessed at 1, 4, 7, 10, 14, 21, 28 and 35 days after DOX treatment.

The same markers used to assess replicative senescence were used to assess DOX induced senescence; SA β-Gal, immunostaining for p16, Ki67 and γH2aX alongside, RT q-PCR for SASP factor expression.

5.2.3. Myotube formation assay

The myotube formation assay was undertaken with defrosted aliquots of samples because the usual method employed to perform the myotube assay was not compatible with DOX treatment. The myotube assay is usually performed on cells attached to glass coverslips coated in collagen to help the cells adhere. However, when these cells were treated with DOX they detached from the coverslips therefore were unable to be used for

analysis because the density of cells remaining on the coverslips was too sparse for accurate comparison. Other laboratories perform the myotube formation assay in plastic wells, however, the refractory index of standard laboratory plastics is not high enough to perform the automated cell by cell expression analysis achievable with glass coverslips. There are better quality plastics with better refractory indices that are suitable to obtain the cell by cell data. Two types of these plastic chamber slides were used, one coated in poly-L-lysine the other coated in collagen-IV, to test if DOX treated MPCs remained attached. Representative images from the collagen-IV coated sample shows that the cells remain adherent to the plastic and cells without DOX treatment are able to undergo similar differentiation to those on glass collagen coated glass coverslips.

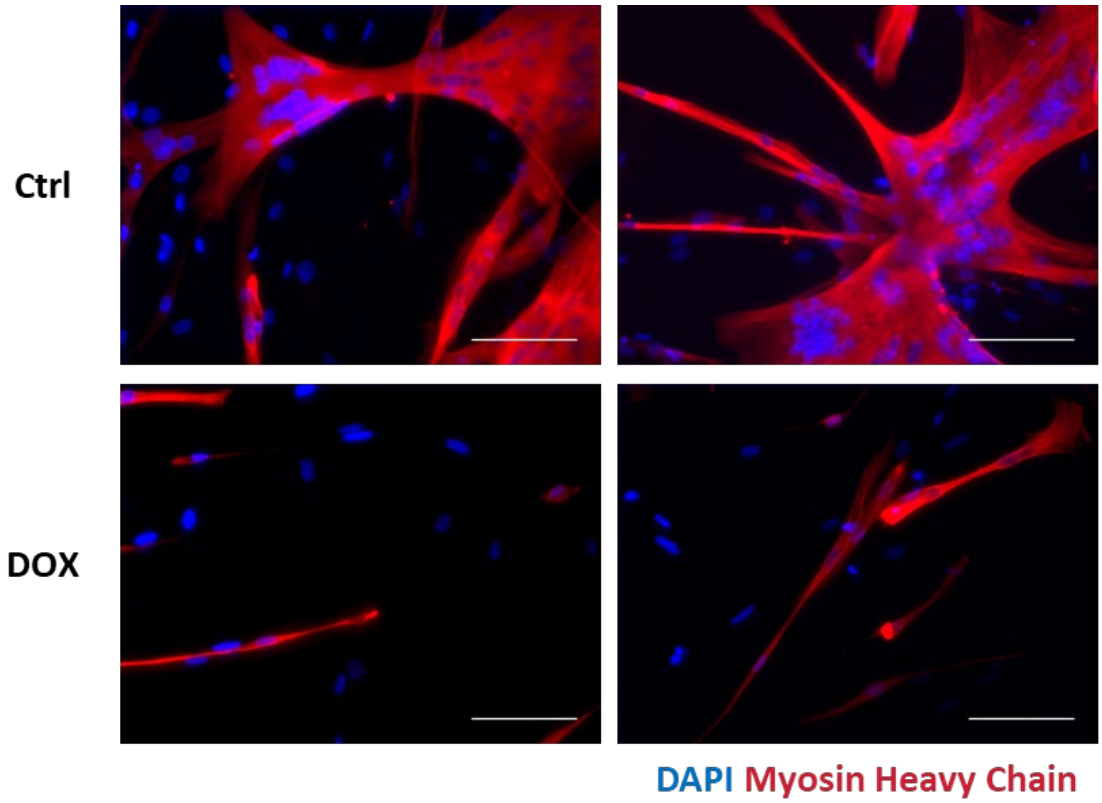

Figure 5.1 Polymer slides can be used to undertake the myogenic differentiation assay using DOX treated myoblasts.
Myoblasts were induced to differentiate four days after DOX treatment or without DOX treatment. After 96h and stained for Stained for DAPI (blue) and Myosin heavy chain (red) Scale bar = 100 µm.

5.3. Results DOX-Induced Myoblast

5.3.1. Desmin expression is maintained after DOX treatment

Desmin expression of $CD56^{+ve}$ myogenic precursor cells was determined before, and at eight time points after DOX treatment. There was a slight, but statistically significant (p=0.025), decrease in the number of desmin positive cells only at 35 days post-DOX treatment, which was 90.8±2.3%, when compared to pre DOX treatment, 96.1±2.8% (Figure 5.2). All time points for all $CD56^{+ve}$ cell populations were considered to be pure desmin populations and could then be analysed for senescent marker expression.

5.3.2. Senescent and proliferation marker expression

5.3.2.1. Ki67 expression is decreased after DOX treatment

Representative images suggest that the number of cells expressing cell cycle protein Ki67 is decreased 24 hours post DOX treatment and very few cells express Ki67 four days after DOX treatment (Figure 5.3). Quantification of Ki67 protein expression shows a significant reduction 24 hours post-DOX treatment relative to pre-DOX treatment (*P = 0.02,* fold change=0.54±0.26, Figure 5.4). A further reduction, relative to pre-DOX treatment, was observed after four days (*P = 0.005,* fold change=0.07±0.02) which was maintained through to 35 days after DOX treatment (*P = 0.01,* fold change=0.11±0.07). Thus, all cell populations were determined to have exited the cell cycle by four days post DOX treatment and did not re-enter the cell cycle before 35 days post-DOX treatment.

5.3.2.2. Delayed increase in p16 expression after DOX treatment

To determine if the cell cycle exit observed was linked with increased senescence-associated cell cycle inhibitors, p16 expression was determined at the same time points. There was a transient, but significant increase in nuclear p16 mean fluorescent intensity 7 days post DOX treatment relative to pre-DOX treatment (*P = 0.02*, fold change=0.07±0.02, Figure 5.6). p16 significantly increased again from 14 days post DOX treatment and remained elevated, relative to pre-DOX treatment, through to D35 post

DOX treatment (*P = 0.008*, D14: fold change=1.89±0.32, D35: fold change=2.04±0.4). Therefore, p16 was not associated with the onset of cell cycle exit but accumulated over time following DOX treatment.

5.3.2.3. Transient DNA damage immediately after DOX treatment

DOX is known to cause DNA damage and this is thought to be the mechanism with which DOX induces senescence (Thorn *et al.*, 2011). DNA damage was investigated by detecting double strand breaks by staining for γH2aX. There was a significant increase in mean nuclear γH2aX mean fluorescent intensity one day after DOX treatment compared to pre DOX treatment (*P = 0.02*, fold change=3.3±1.1, Figure 5.8). This elevated DNA damage returned to pre-DOX treatment levels by four days post DOX treatment and remained unchanged through to D35 post DOX treatment.

5.3.2.4. Senescence associated β-Galactosidase positive cells accumulate after DOX treatment

The DOX treatment experiments were undertaken at the same time as the replicative senescence experiments and therefore, due to the same technical issues (Methods section 2.5.1), SA β-Gal could only be determined in Y05+ and Y06+ cell populations. Both cell populations started with approximately 25% SA β-Gal positive cells at pre-DOX treatment. The percentage of SA β-Gal positive cells was increased 1 day after DOX treatment to approximately 50% and further increased to around 100% by four days post DOX treatment, which was maintained through to D35 post DOX treatment.

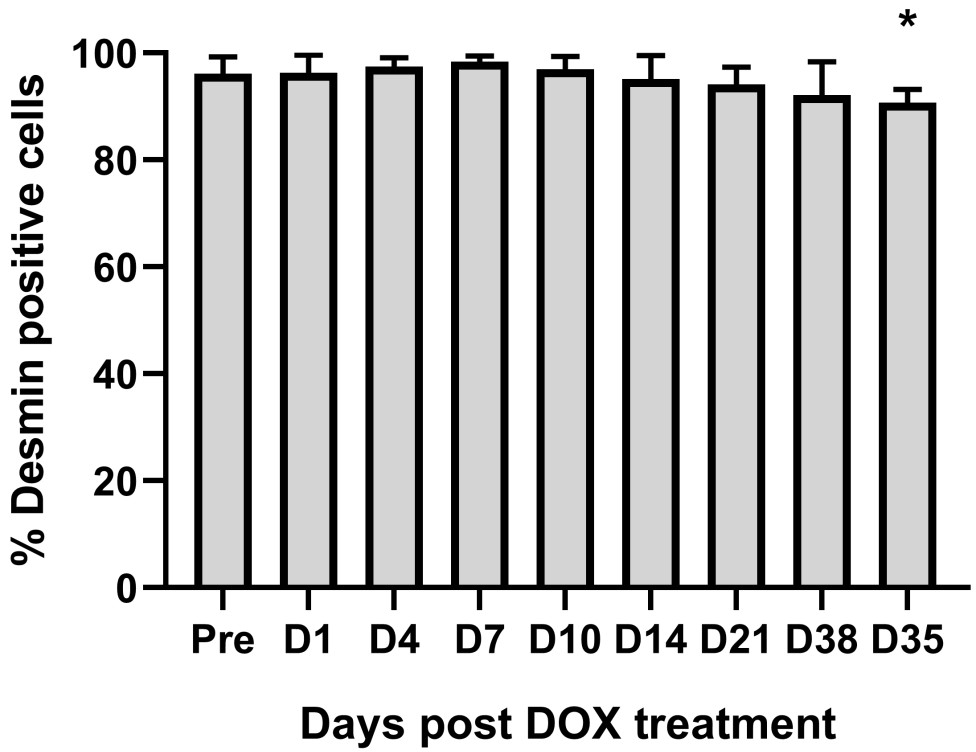

Figure 5.2. Desmin expression is maintained after DOX treatment.
Sub populations of cells (20,000 cells) from each of the 6 individual $CD56^{+ve}$ cell populations were cytospun before, and at eight time points after, DOX treatment and stained for nuclei and desmin to determine percentage of $desmin^{+ve}$ cells by a bespoke automated image analysis program. The percentage of desmin positive cells across the replicative lifespan of individual myoblast populations. Individual cell population means determined from percentage desmin positive cells per field of view, 10 fields of view per time point, minimum of 100 cells analysed in total per time point, N=6 $CD56^{+ve}$ cell populations. Data presented as population Mean±SD. Statistical analysis using one-way RM ANOVA with Dunnett's test for multiple comparisons reveals sig. difference for D35 relative to Pre-DOX treatment *P =0.025.

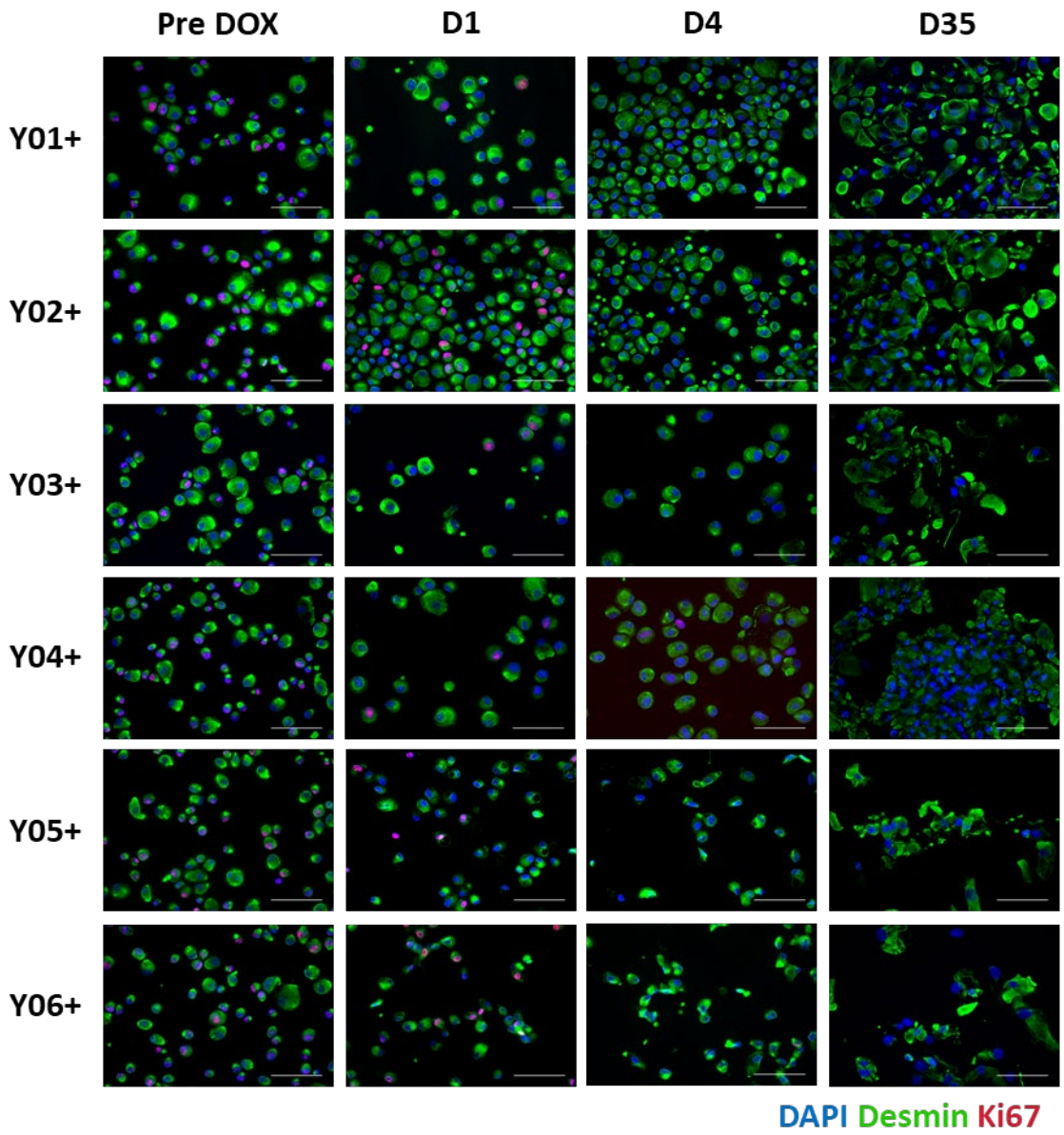

Figure 5.3. Representative images of individual CD56^{+ve} cell populations Ki67 expression across Doxorubicin time course.

Sub populations of cells (20,000 cells) from each CD56^{+ve} cell population were cytospun at different timepoints across the post DOX treatment time course and stained for desmin (green), Ki67 (red) and DAPI (Blue). Scale bar = 100 µm.

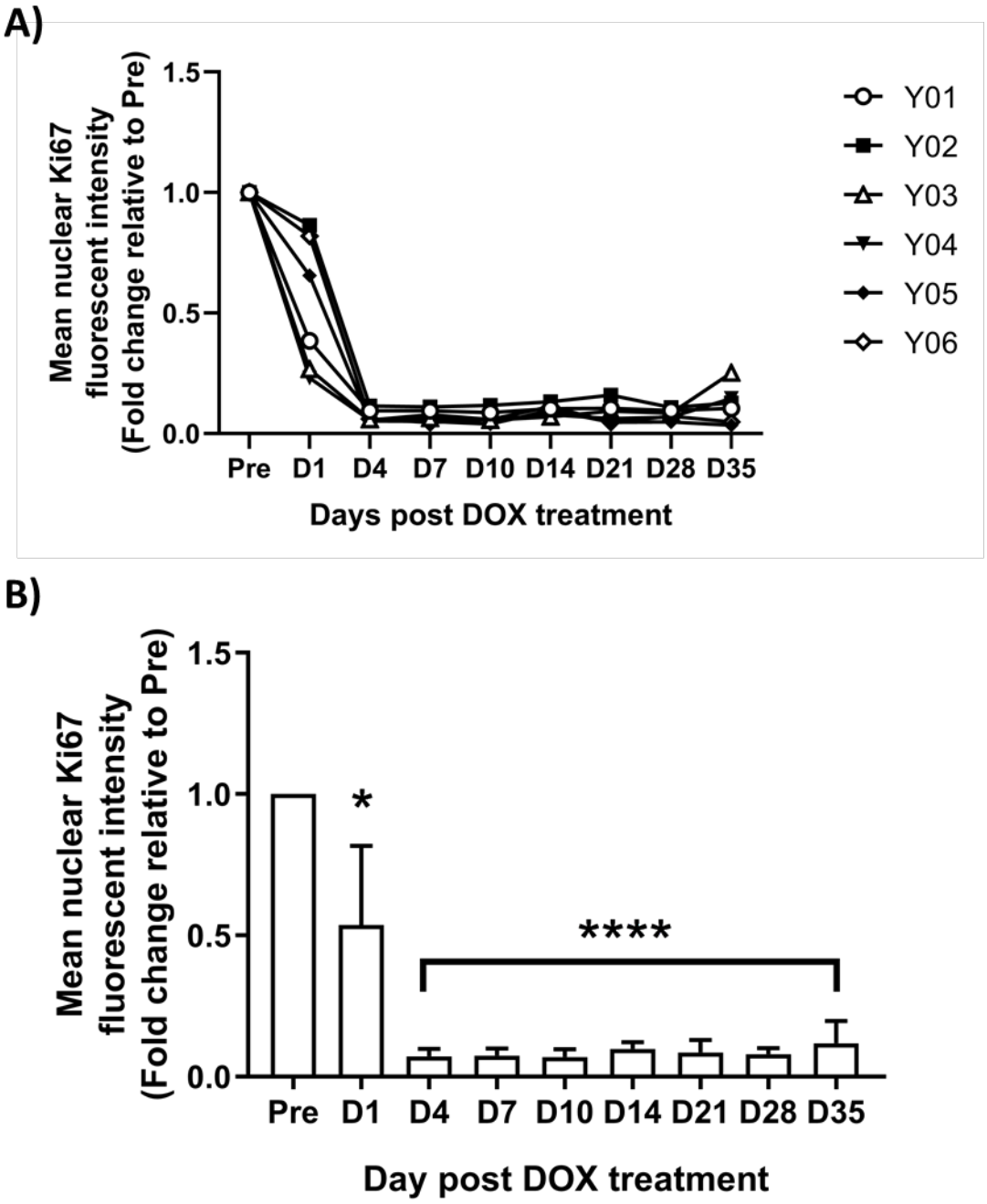

Figure 5.4. Nuclear Ki67 expression decreases across Doxorubicin treatment time course.
A) Individual CD56^{+ve} cell popualtions changes in Ki67 mean fluorescent intensity across the Doxorubicin treatment time course presented as fold change in mean of all individual nuclei Ki67 relative to pre-DOX treatment expression. **B)** Mean of all CD56^{+ve} cell populations mean nuclei Ki67 mean fluorescent intensity presented as fold change from each individual population pre-DOX treatment expression. Statistical analysis (one-way RM ANOVA with Dunnett's test) shows significant differences relative to Pre * *indicates P* <0.05, **** indicates p < 0.001, N=6).

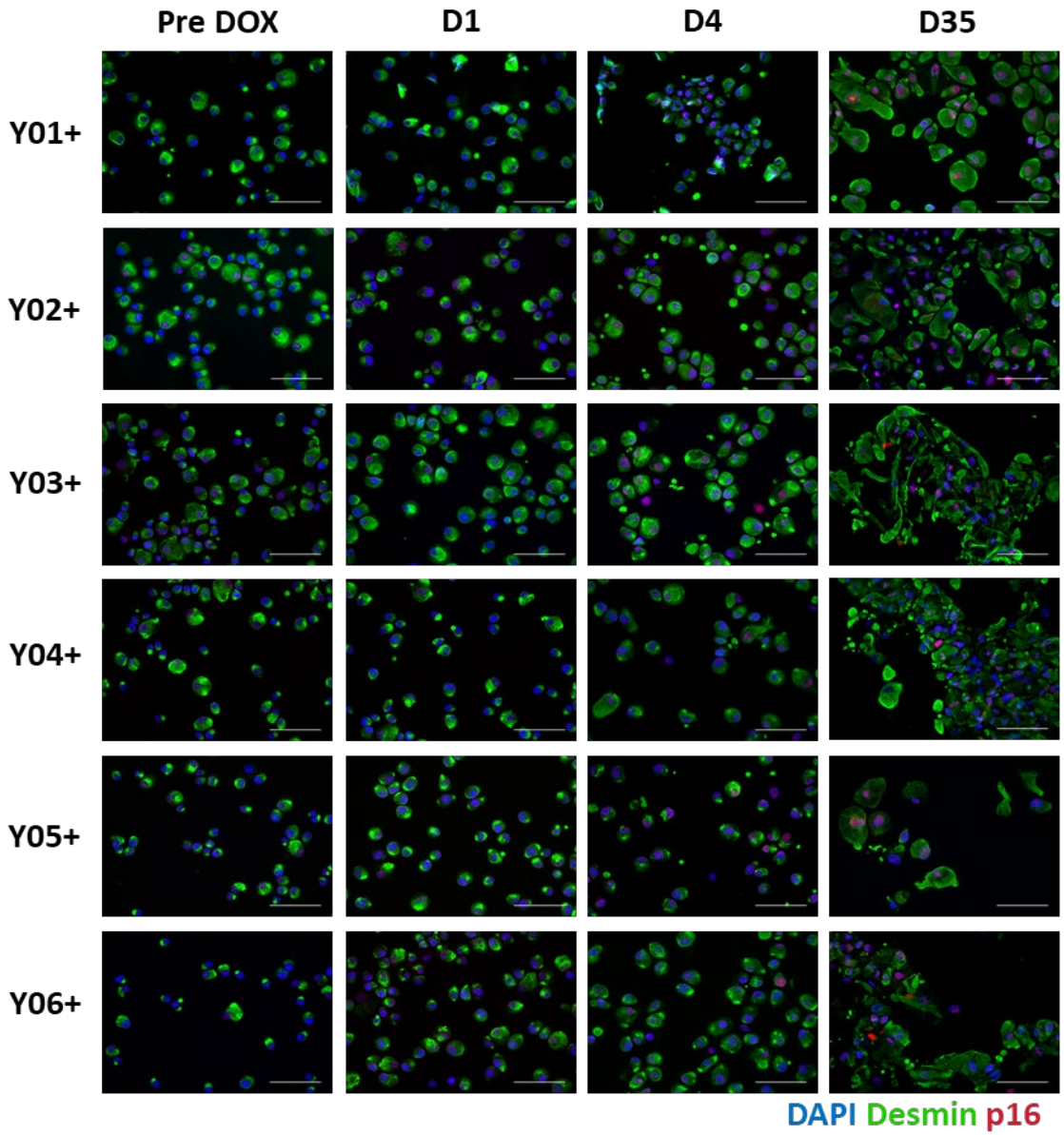

Figure 5.5. Representative images of individual CD56^{+ve} cell populations p16 expression across Doxorubicin time course.

Sub populations of cells (20,000 cells) from each CD56^{+ve} cell population were cytospun at different timepoints across the Doxorubicin time course and stained for desmin (green), p16 (red) and DAPI (Blue). Scale bar = 100 µm.

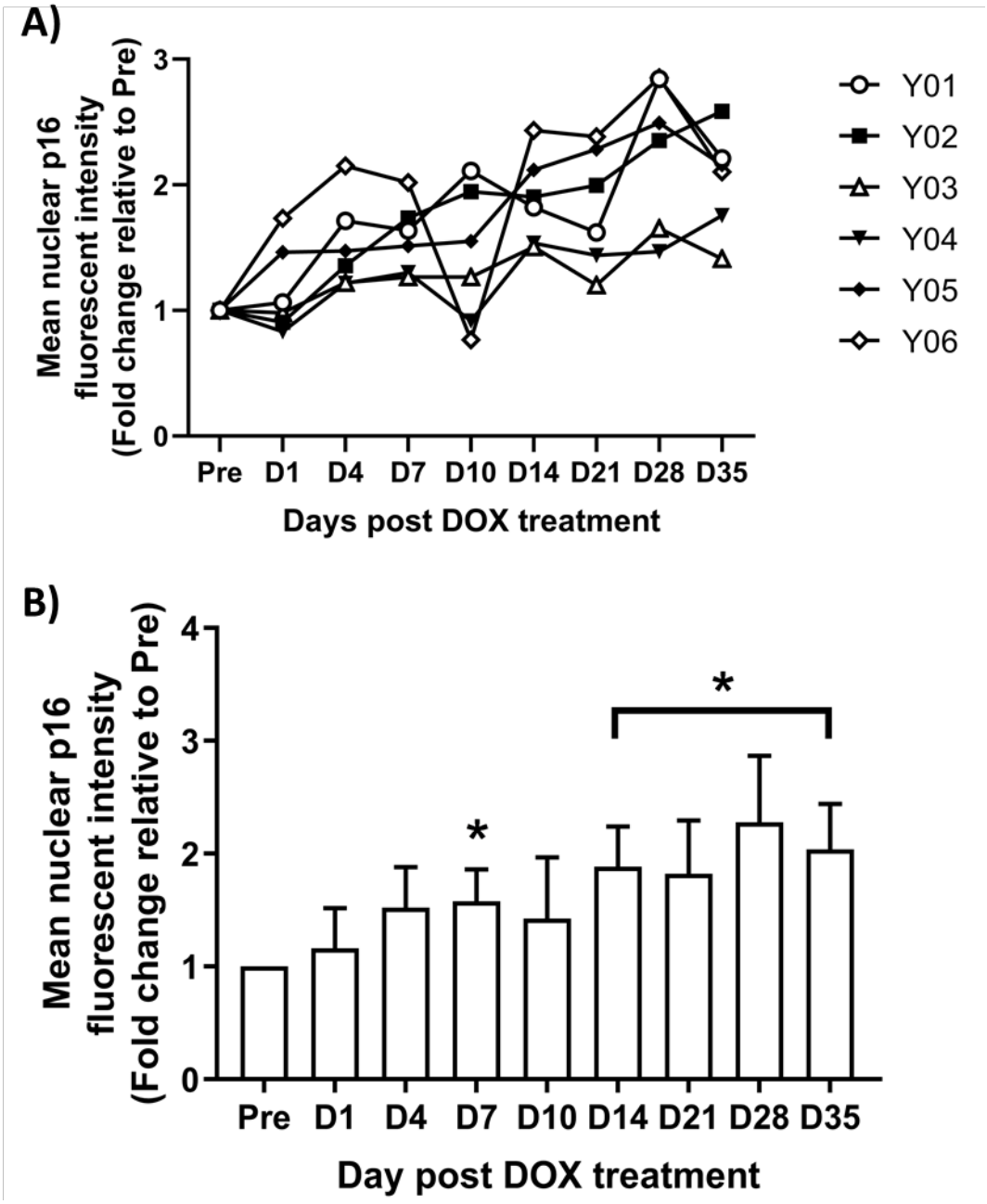

Figure 5.6. Nuclear p16 expression increases after Doxorubicin treatment.
A) Individual $CD56^{+ve}$ cell popualtions changes in p16 mean fluorescent intensity across the Doxorubicin treatment time course presented as fold change in mean of all individual nuclei relative to pre DOX treatment expression. **B)** Mean of all individual nuclei p16 mean fluorescent intensity. * indicate significant different to pre (one-way RM ANOVA with Dunnett's test, P <0.05, N=6).

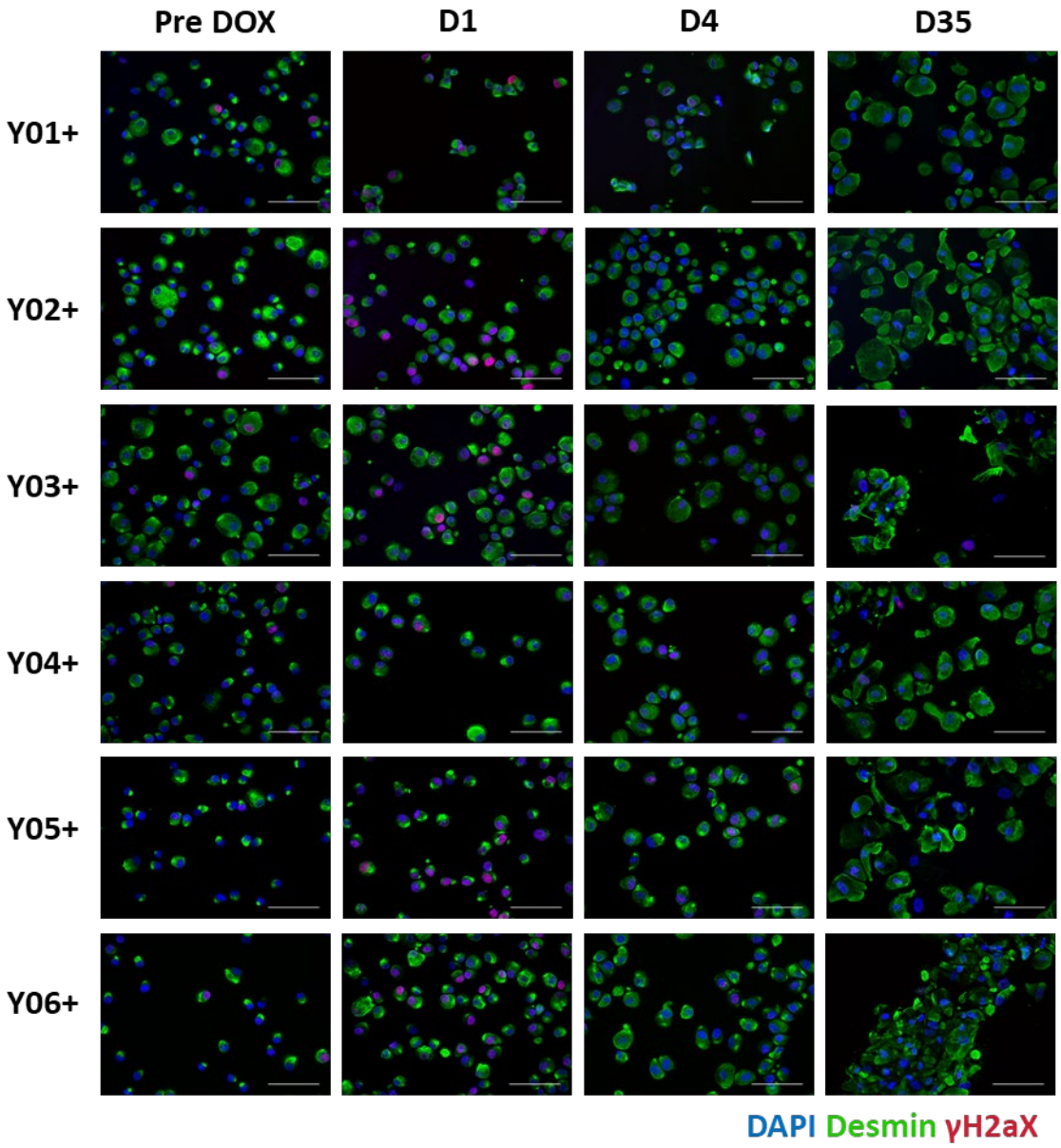

Figure 5.7. Representative images of γH2aX expression across Doxorubicin time course of individual biopsies.

Sub populations of cells (20,000 cells) from each biopsy were cytospun at different timepoints across the Doxorubicin time course and stained for desmin (green), γH2aX (red) and DAPI (Blue). Scale bar = 100 µm.

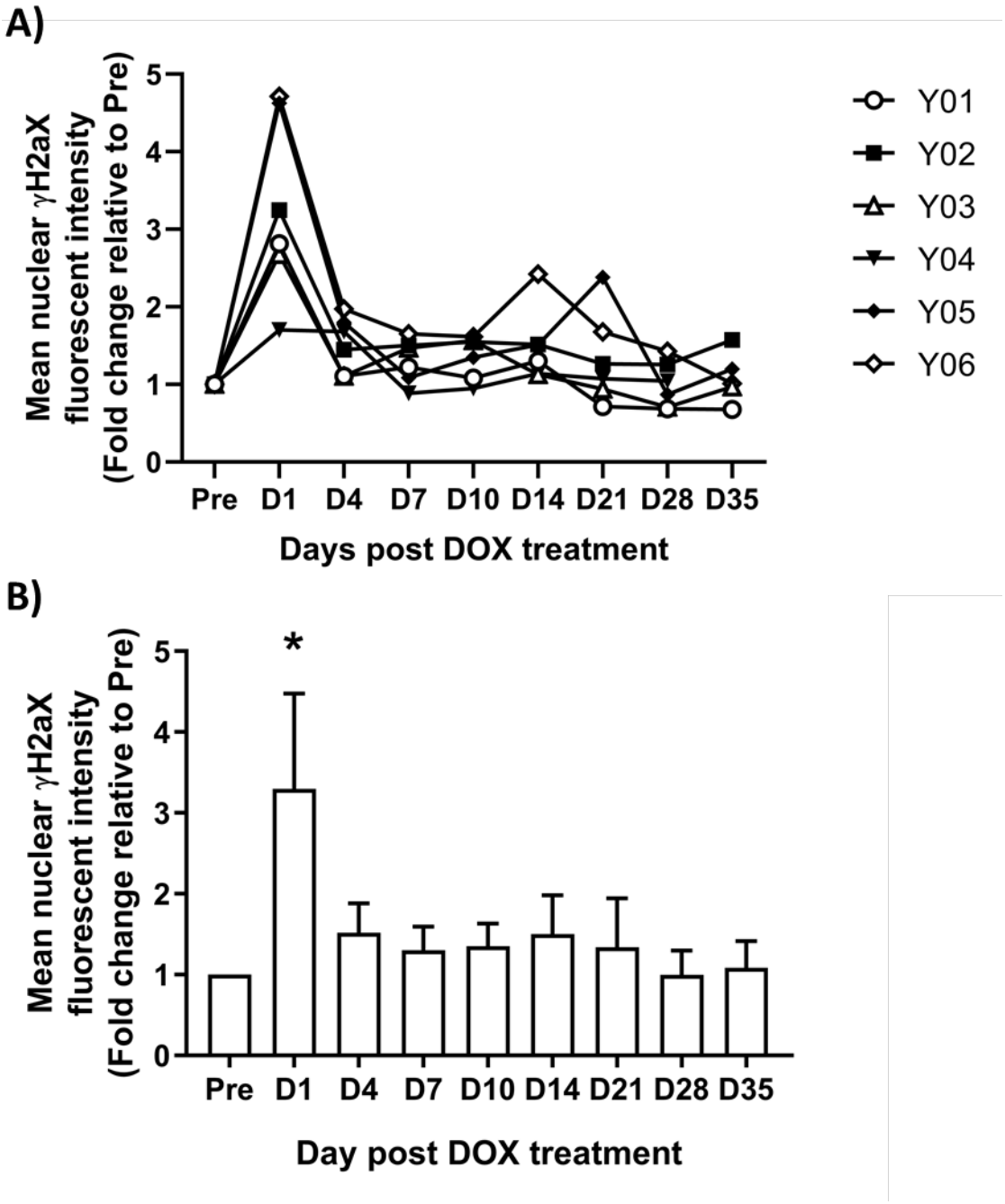

Figure 5.8. Nuclear γH2aX expression transiently increases 24 hours after Doxorubicin treatment. **A)** individual CD56^{+ve} sample γH2aX Mean of all individual nuclei γH2aX mean fluorescent intensity across the Doxorubicin treatment time course. **B)** Mean of all individual nuclei γH2aX mean fluorescent intensity. * indicate significant different to Pre (one-way RM ANOVA with Dunnett's test, *P* <0.05, N=6).

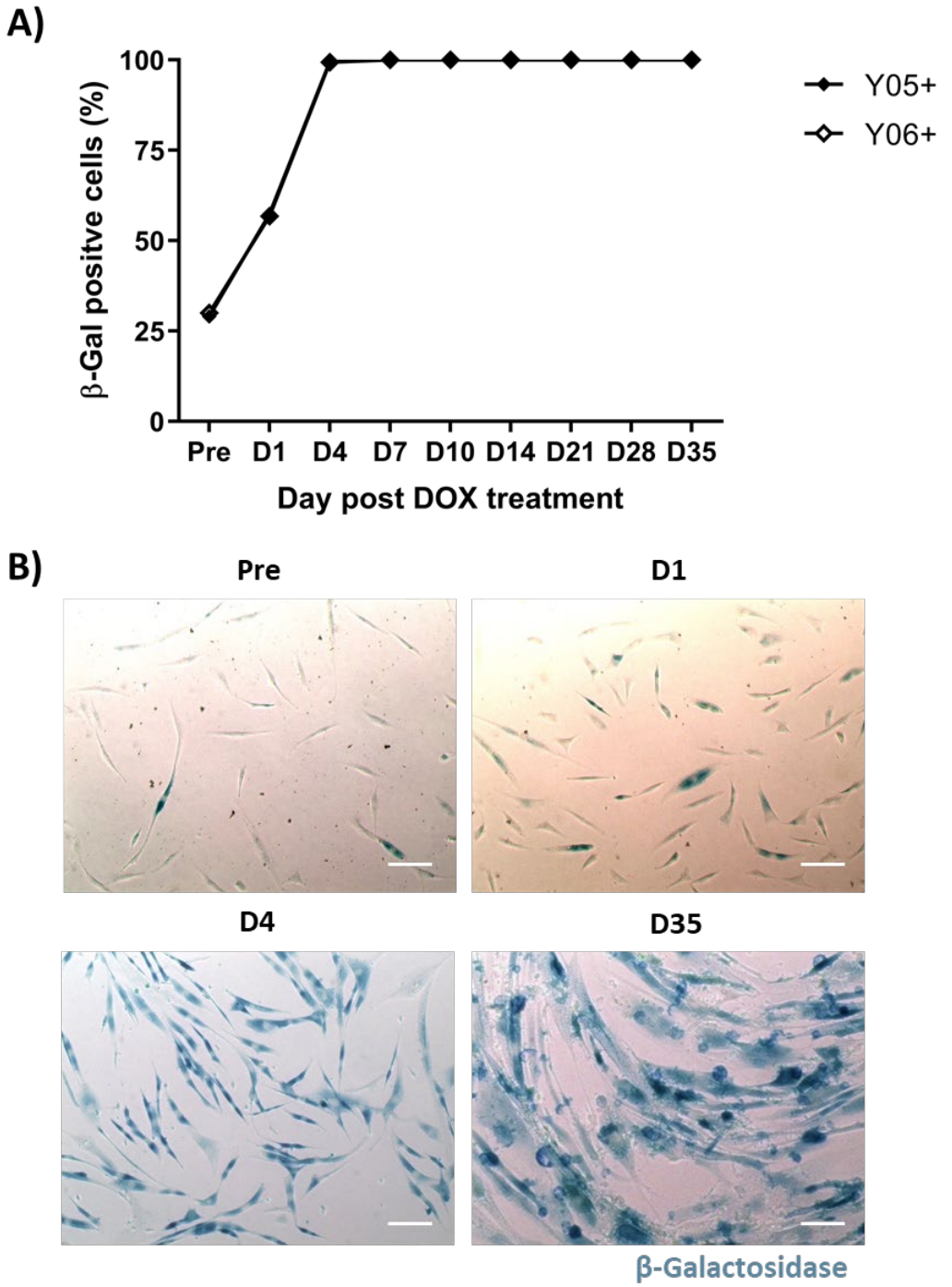

Figure 5.9. Muscle precursor cells express SA β-Gal from four days after DOX treatment.
A) Sub populations of cells (25,000 cells) from Y05+ and Y06+ cell population were plated for SA β-Gal analysis before, and at eight time points after, DOX treatment. The percentage of SA β-Gal positive cells was determined at each time point for the individual myoblast populations. Data shown as individual cell population means determined from percentage SA β-Gal positive cells per field of view, 10 fields of view per time point, minimum of 100 cells analysed in total per time point. Both cell populations responded very similarly and therefore their symbols are overlapping. **B)** Representative images of SA β-Gal positive cells Pre, 1 day, 4 days and 35 days after DOX treatment. Scale bar = 100 µm.

5.3.3. Senescence and SASP factor expression

The fold change in mRNA expression for each of the individual senescence associated and SASP factors over the post DOX time-course relative to each individual $CD56^{+ve}$ cell population pre DOX treatment expression level are presented in Figure 5.10 and Figure 5.11. Figure 5.10 shows the heterogeneity between the individual cell populations whereas Figure 5.11 shows the different expression patterns across the time course of the different SASP factors. As expected from the immunostaining data, statistical significance was seen in the senescence associated cell cycle inhibitors. There was an increase in p21 mRNA from one day post DOX treatment through to 35 days post DOX treatment with the exception of 28 days post DOX treatment. Whereas, p16 mRNA was increased later, from 4 days post DOX treatment through to 35 days post DOX treatment with the exception of 21 days post DOX treatment. IL-8 was significantly increased at 28 days post DOX treatment and β-Gal expression was significantly increased 21 days and 35 days after DOX treatment. IGFBP-3 was significantly decreased at one day but then significantly increases at 21 days post DOX treatment. Two factors, CXCL5 and PAI-1, showed decreases across the time course with CXCL5 significantly reduced from 4 days post DOX through to 35 days post DOX except for 28 days post DOX. Whereas, PAI-1 reduced 4 days post DOX treatment through to 21 days post DOX treatment.

5.3.4. Myotube formation is impaired by DOX treatment

The myogenic differentiation assay couldn't be carried out in parallel with the other analysis due to technical issues mentioned in the methods. Fusion index of myoblasts four days after DOX-treated myoblast populations was significantly lower than untreated cells ($P < 0.01$, 57.8±6.9% reduced to 9.0±3.9% fusion; Figure 5.13). After 35 days in culture, myotube formation had spontaneously occurred without the removal of serum in some cultures. With the removal of serum there was a large variability in fusion between cell populations (23.8±23.1% fusion). However, the morphology of all myotubes post-DOX treatment were thinner and contained fewer nuclei that pre-DOX treated cells (Figure 5.12).

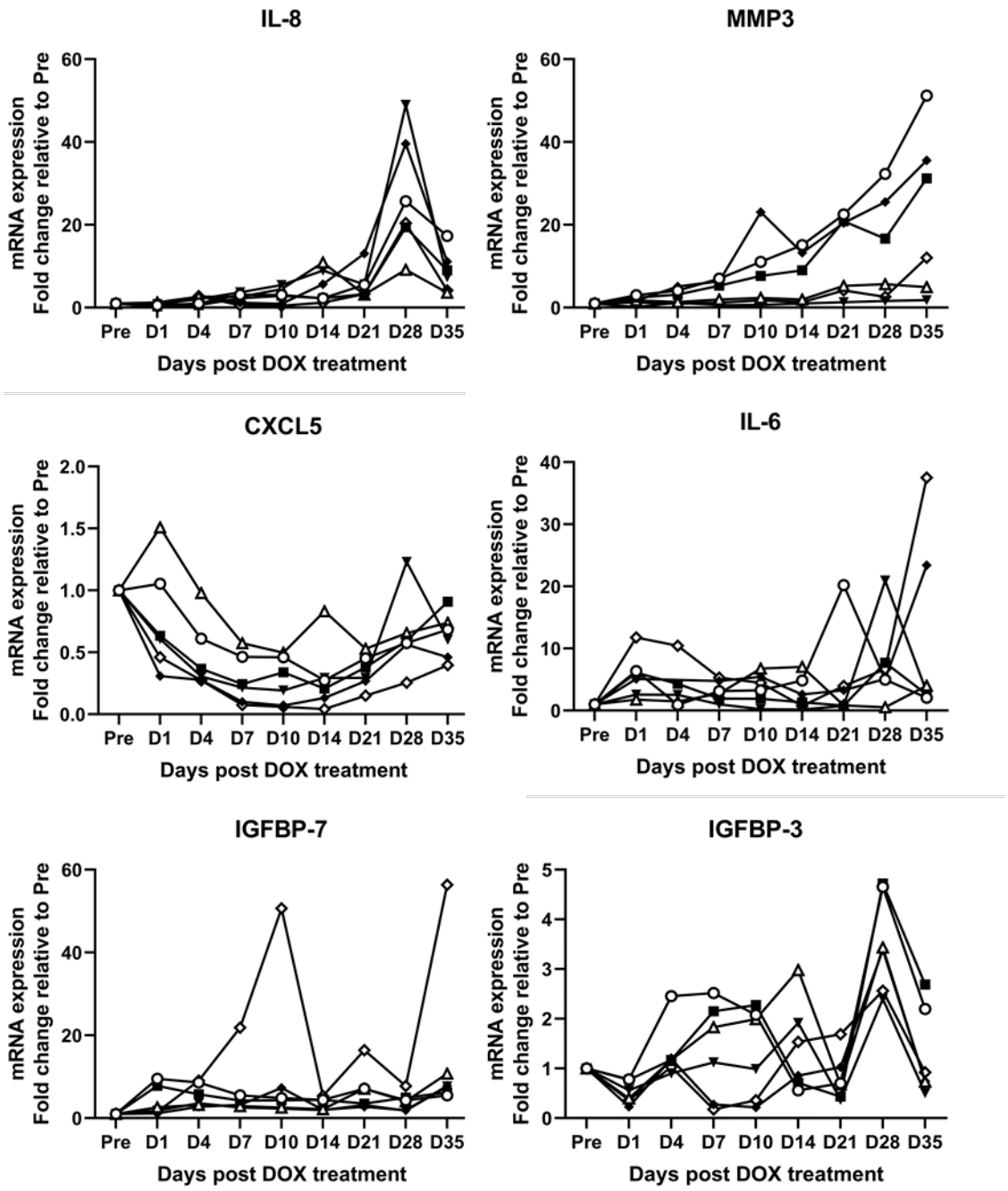

Figure 5.10. Individual myoblast cell populations expression of each SASP factor after DOX treatment.

Individual CD56^{+ve} cell populations mRNA expression of twelve known SASP factors presented as fold change relative to individual populations pre-DOX treatment expression levels across eight time points post DOX treatment. Statistics performed on grouped data in Figure 5.11. Figure continues on next page.

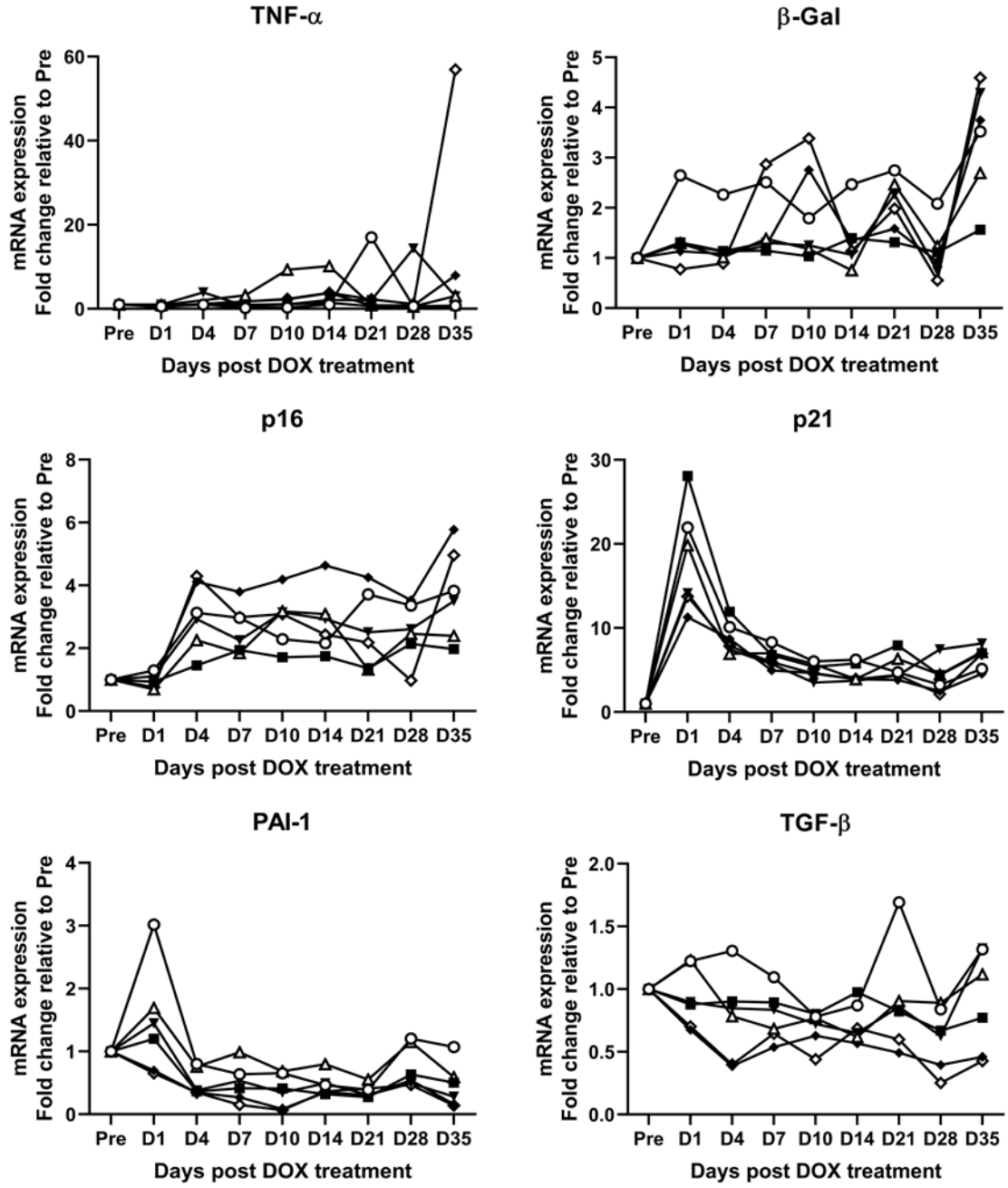

Figure 1.10. continued.

Refer back to figure legend on previous page.

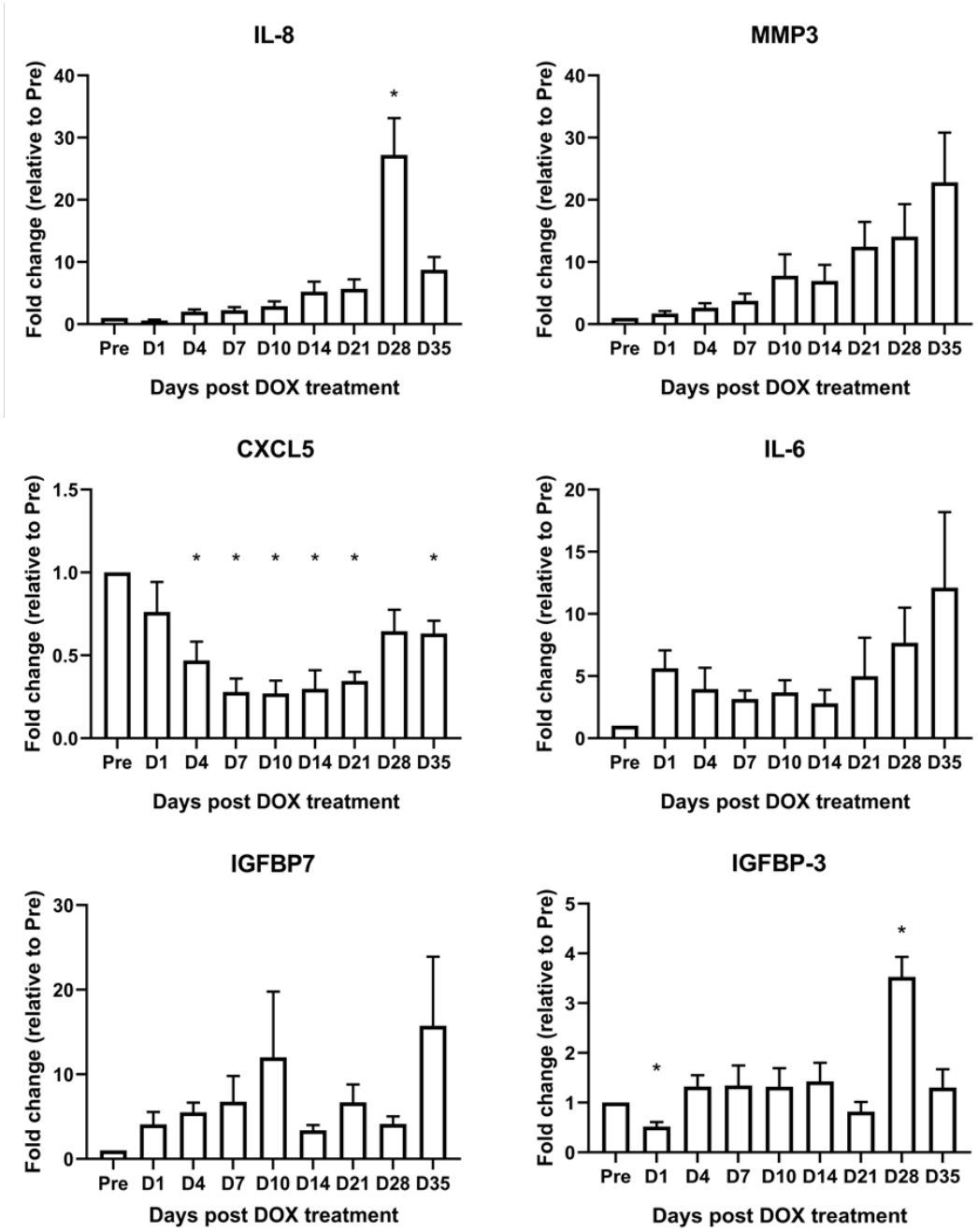

Figure 5.11. Doxorubicin treated myoblasts have altered mRNA expression of known SASP factors.

mRNA expression of twelve known SASP factors presented as mean fold change relative to each individual cell populations pre DOX treatment expression levels across eight time points post DOX treatment. * indicate significant different to Pre (one-way RM ANOVA with Dunnett's test for each SASP factor, *P* <0.05, N=6). Figure continues on next page.

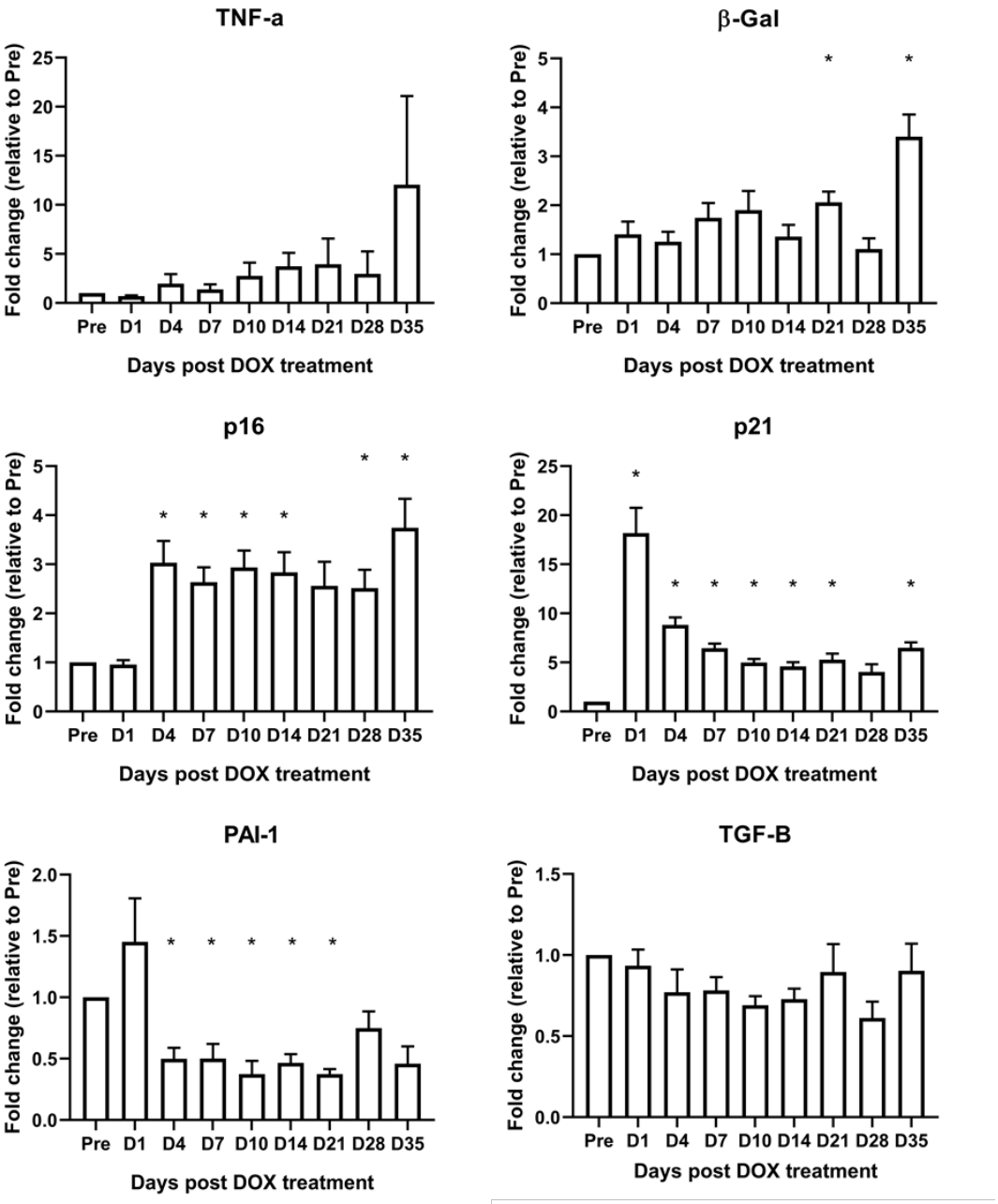

Figure 5.11. continued.
Refer back to figure legend on previous page.

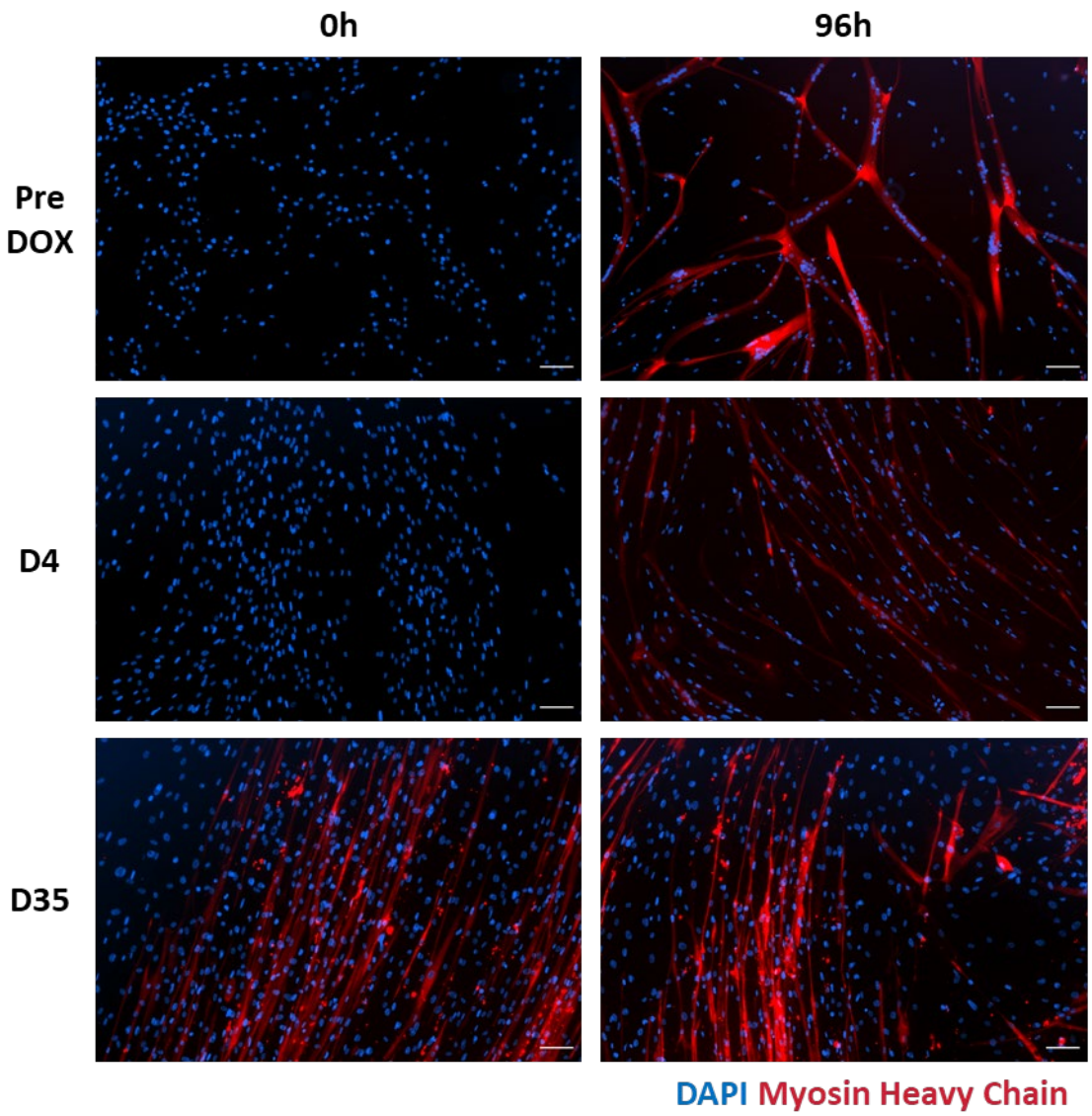

Figure 5.12. Myotube formation is impaired by DOX treatment.
Representative images of DOX treated CD56^{+ve} cell populations before and after being induced to differentiate by serum withdrawal for 96 hours at time points before DOX treatment, four days and 35 days after DOX treatment. Stained for DAPI (blue) and Myosin heavy chain (red) Scale bar = 100 µm.

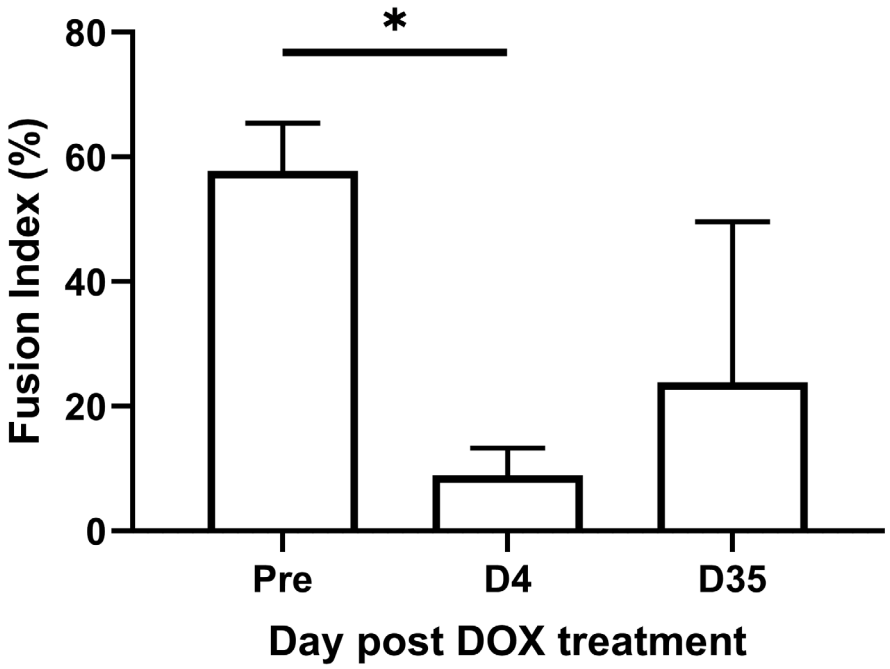

Figure 5.13. DOX treated myoblasts fuse less well into myotubes.
Myoblasts before DOX treatment, four days and 35 days after DOX treatment were induced to differentiate and form myotubes. The fusion index, percent of nuclei incorporated into myosin heavy chain positive myotubes, is lower in populations of DOX treated cells. Data shown as population Mean±SD n=5. Individual cell population means determined from percentage of fused nuclei per field of view, 10 fields of view per time point, minimum of 100 cells analysed in total per time point. * indicate significant different between Pre and D4 (one-way RM ANOVA with Tukey's multiple comparisons test, P <0.05, N=6).

5.4. Results: DOX-induced Fibroblasts

5.4.1. TE7 expression is maintained after DOX treatment

The percentage of TE7 positive cells remained unchanged through to 35 days post DOX treatment (*P = 0.06*). All cell populations were therefore deemed to be pure fibroblasts and could be used for analysis of senescence marker expression.

5.4.2. Senescent and proliferation marker expression

5.4.2.1. Ki67 expression is decreased after DOX treatment

Representative images show that the number of cells expressing cell cycle protein Ki67 was decreased 24 hours after DOX treatment and very few cells expressed Ki67 four days after DOX treatment (Figure 5.15). Quantification of Ki67 protein expression shows a significant reduction 24 hours after DOX treatment relative to pre-DOX treatment (*P < 0.001,* fold change=0.23±0.13, Figure 5.16). A further reduction, relative to pre-DOX treatment, was observed after four days (*P < 0.001,* fold change=0.08±0.02) which was maintained through to 35 days after DOX treatment (*P < 0.001,* fold change=0.16±0.04). Thus, all cell populations were determined to have exited the cell cycle by four days post DOX treatment and did not re-enter the cell cycle before 35 days post DOX treatment.

5.4.2.2. p16 protein levels remains unchanged after DOX treatment

To determine if the cell cycle exit observed was related to increased senescence associated cell cycle inhibitors, p16 expression was determined at the same time points. Representative images show the different expression levels between the individual fibroblast cell populations (Figure 5.17). No significant increase in mean nuclear p16 mean fluorescent intensity was seen at any time point relative to pre-DOX treatment (*P = 0.52*). Therefore, p16 was not associated with the onset of cell cycle exit or senescence induction observed in these fibroblasts cell populations.

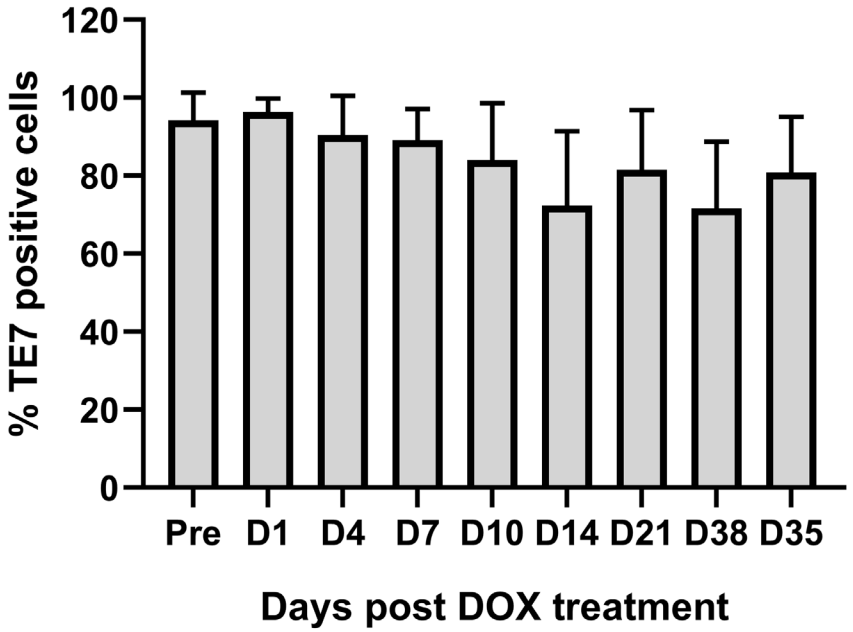

Figure 5.14. TE7 expression is maintained after DOX treatment.
Sub populations of cells (20,000 cells) from each $CD56^{-ve}$ cell population were cytospun before, and at eight time points after, DOX treatment and stained for nuclei and TE7 to determine the percentage of TE7 positive cells across the DOX treatment time course for individual fibroblast populations by a bespoke automated image analysis program. Data shown as population Mean±SD, no significant difference one-way RM ANOVA with Dunnett's test, P <0.05, N=6. Individual cell population means determined from percentage TE7 positive nuclei per field of view, 10 fields of view per time point, minimum of 100 cells analysed in total per time point.

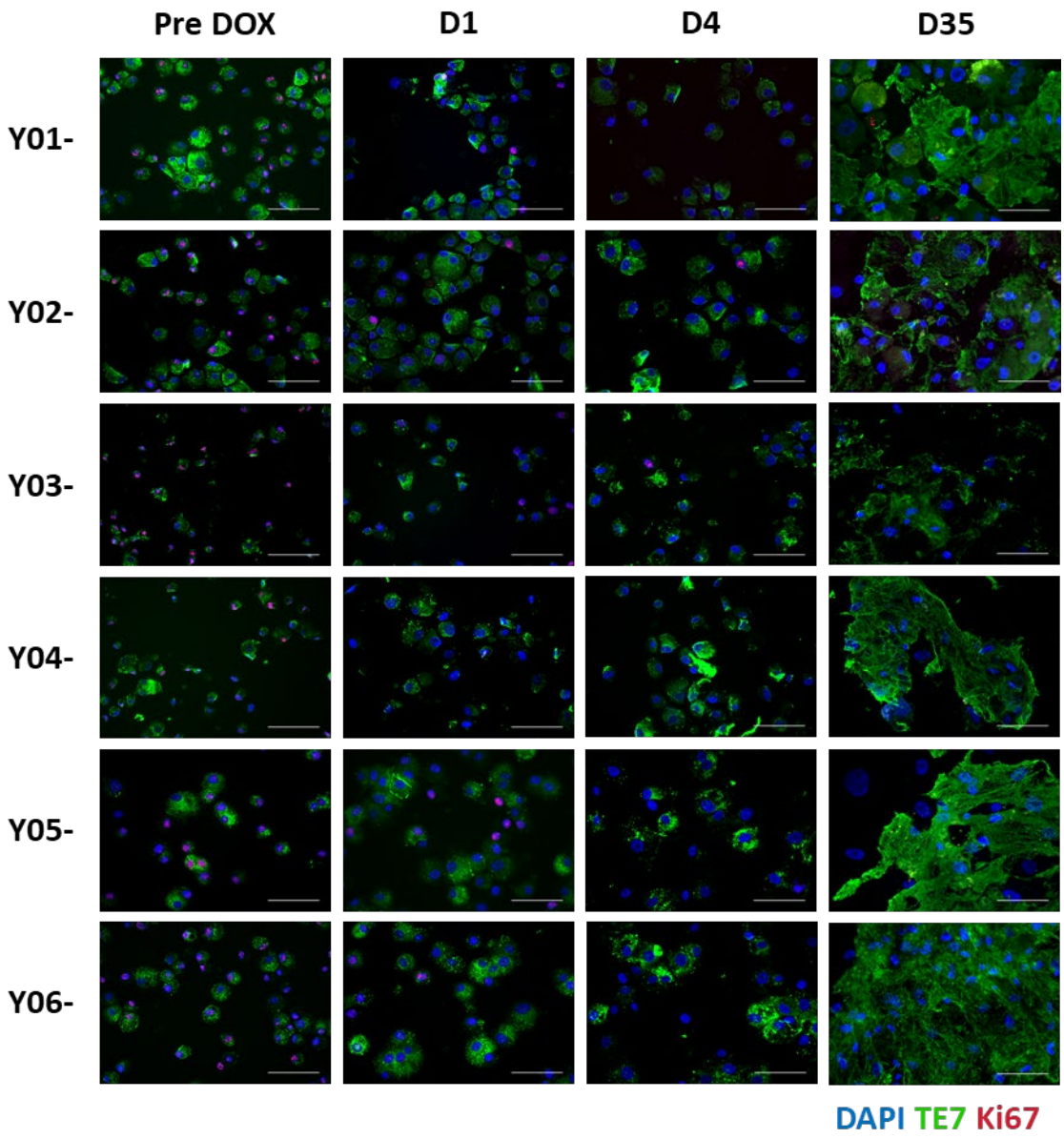

Figure 5.15. Representative images of TE7 expression after DOX treatment.
Sub populations of cells (20,000 cells) from each $CD56^{-ve}$ cell population were cytospun at different timepoints across the Doxorubicin time course and stained for TE7 (green), Ki67 (red) and DAPI (Blue). Scale bar = 100 µm.

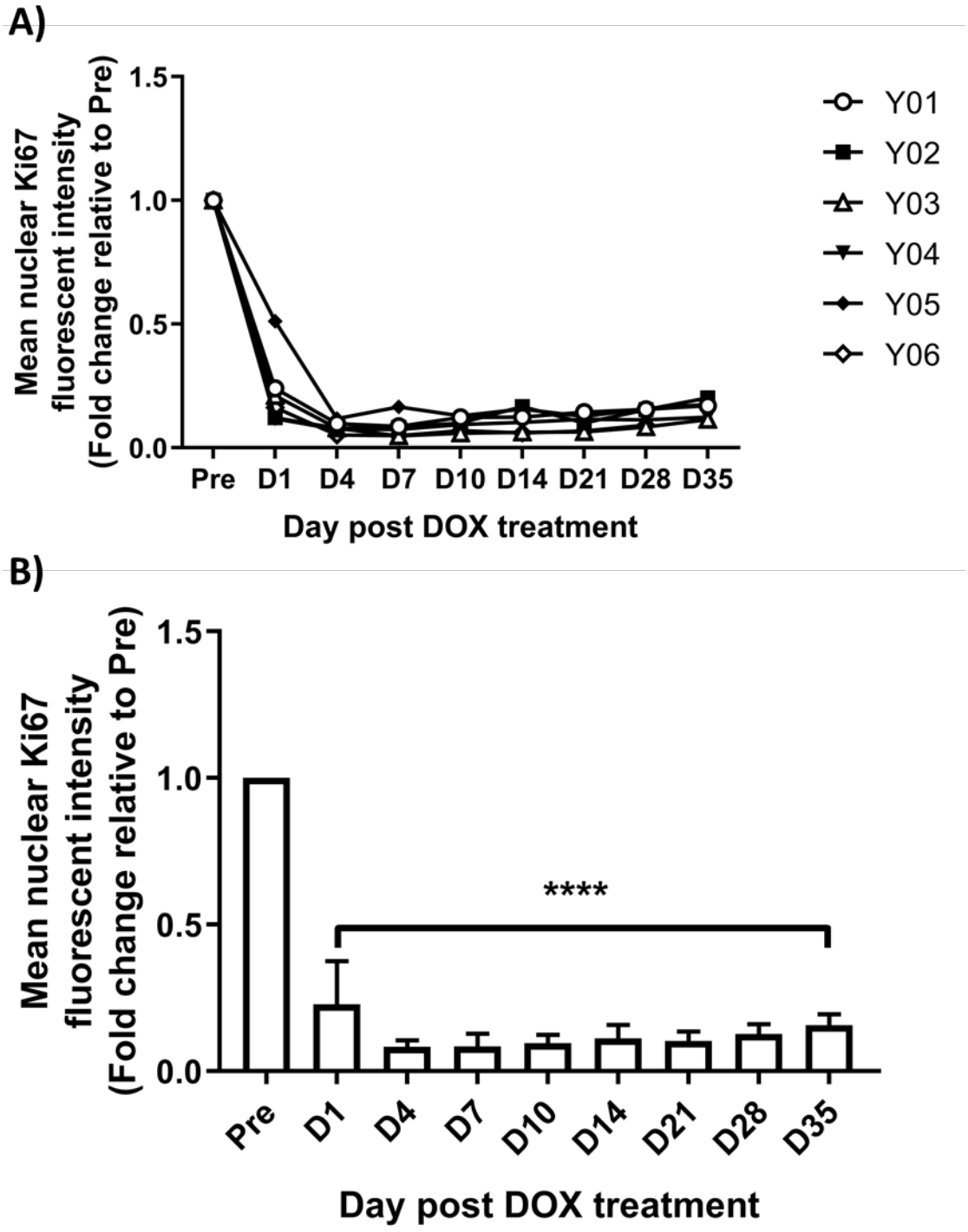

Figure 5.16. Nuclear Ki67 expression decreases across Doxorubicin treatment time course.
A) individual $CD56^{-ve}$ sample Ki67 Mean of all individual nuclei Ki67 mean fluorescent intensity across the Doxorubicin treatment time course. **B)** Mean of all individual nuclei Ki67 mean fluorescent intensity. **** indicate significant different to Pre (one-way RM ANOVA with Dunnett's test, P <0.05, N=6).

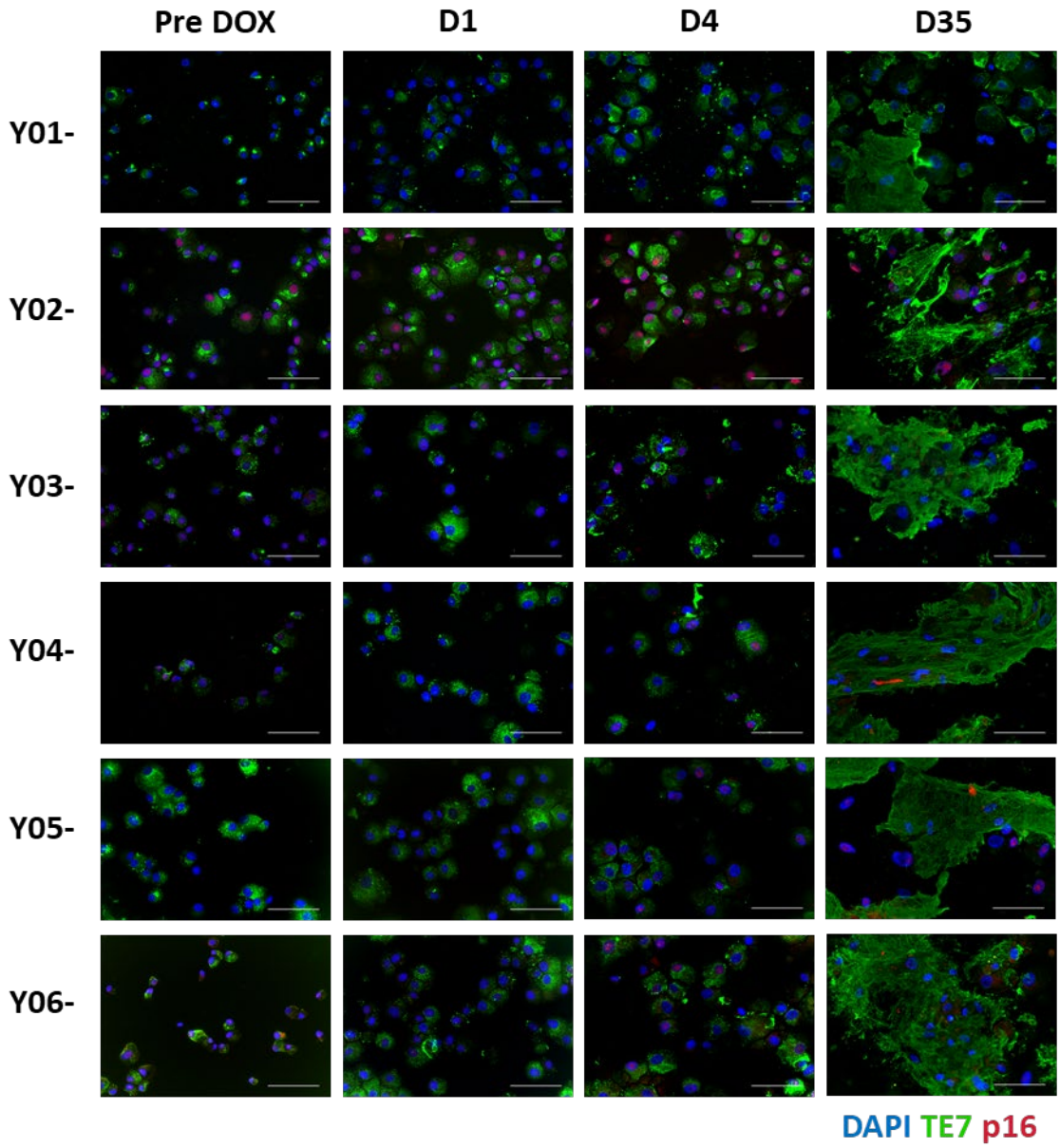

Figure 5.17. Representative images of p16 expression across Doxorubicin time course of individual biopsies.

Sub populations of cells (20,000 cells) from each biopsy were cytospun at different timepoints across the Doxorubicin time course and stained for TE7 (green), p16 (red) and DAPI (Blue). Scale bar = 100 µm.

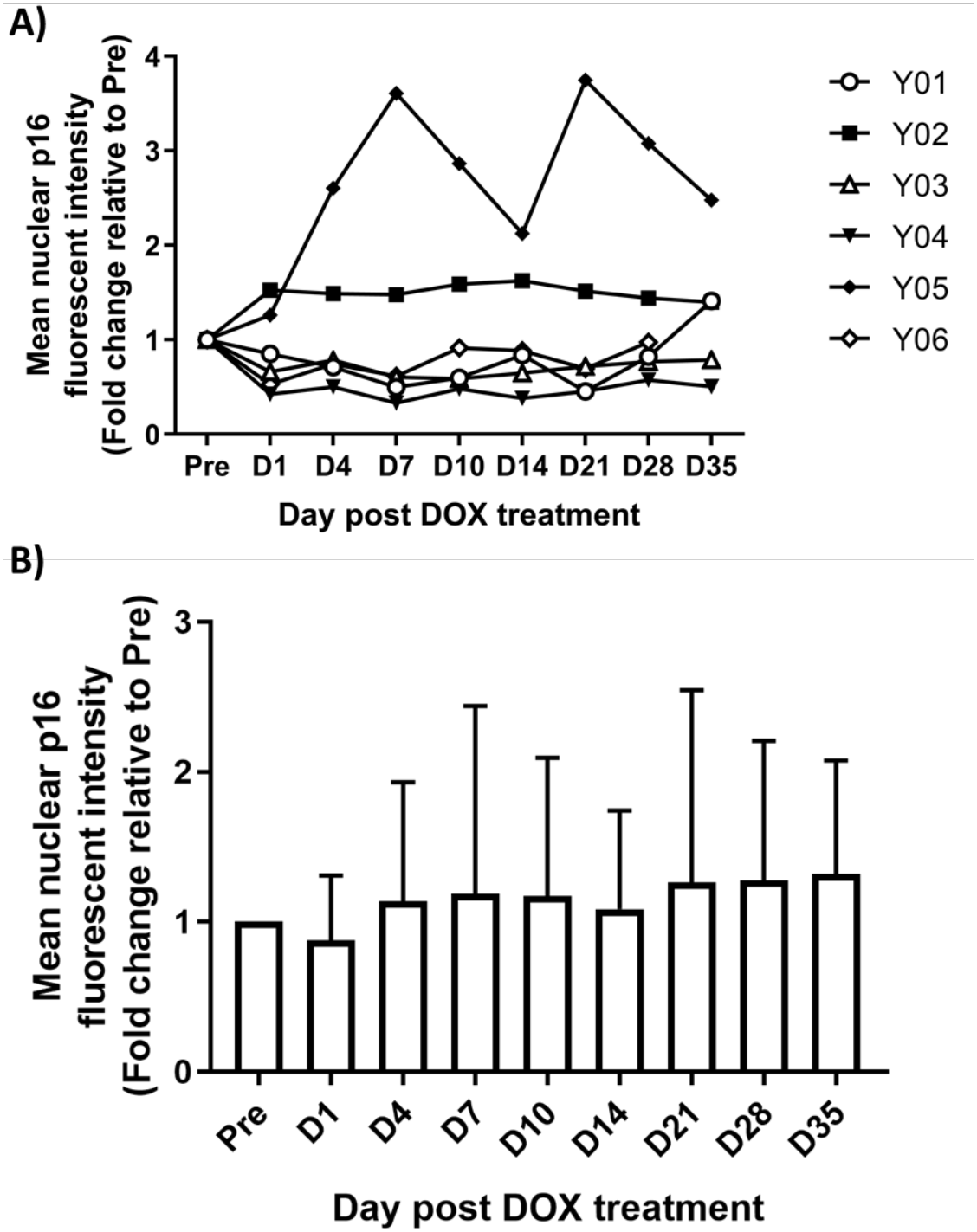

Figure 5.18. Nuclear p16 expression trends to increase across time course after Doxorubicin treatment.

A) individual CD56+ sample p16 Mean of all individual nuclei p16 mean fluorescent intensity across the Doxorubicin treatment time course. **B)** Mean of all individual nuclei p16 mean fluorescent intensity, no significant difference using a one-way RM ANOVA with Dunnett's test, P <0.05, N=6.

5.4.2.3. γH2aX expression is unchanged after DOX treatment

DOX is known to cause DNA damage and this is thought to be the mechanism with which DOX induces senescence (Thorn *et al.*, 2011). DNA damage was investigated by detecting double strand breaks by staining for γH2aX. Representative images suggest an increase in mean nuclear γH2aX mean fluorescent intensity one day after DOX treatment compared to pre-DOX treatment however no statistical significance was found ($p = 0.13$).

5.4.2.4. Senescence Associated β-Galactosidase expression

The DOX treatment experiments were undertaken at the same time as the replicative senescence experiments and therefore, due to the same technical issues (Methods section 2.5.1), SA β-Gal could only be determined in Y05+ and Y06+ fibroblast cell populations. Both cell populations started with around 10% SA β-Gal positive cells at pre-DOX treatment, day 22 after biopsy, thus showing similar expression to replicative passages cells at the same timepoint (Figure 5.21). The percentage of SA β-Gal positive cells was increased to around 50% 4 days after DOX treatment and further increased up to around 100% by seven days after DOX treatment, which was maintained through to D35 post DOX treatment.

5.4.3. Senescence and SASP factor expression

Figure 5.22 and Figure 5.23 show the fold change in mRNA expression for each of the individual senescence associated and SASP factors over the post DOX time-course relative to each individual fibroblast cell population's pre DOX treatment expression level. Figure 5.22 shows the heterogeneity between the individual cell populations whereas Figure 5.23 shows the different expression patterns across the time course of the different SASP factors. The senescence associated cell cycle inhibitor p21 was transiently significantly increased 1 day after DOX treatment returning to baseline within four days. Upregulation of p16 mRNA increased across time reaching significance at 10 and 35 days after DOX treatment. There was also a transient significant increase in TGF-β between 7 and 10 days post DOX treatment. Finally, IGFBP3 expression was significantly reduced 1 day after DOX treatment but this was followed by significant increases 10 days, 14 days and 35 days post DOX treatment (Figure 5.23

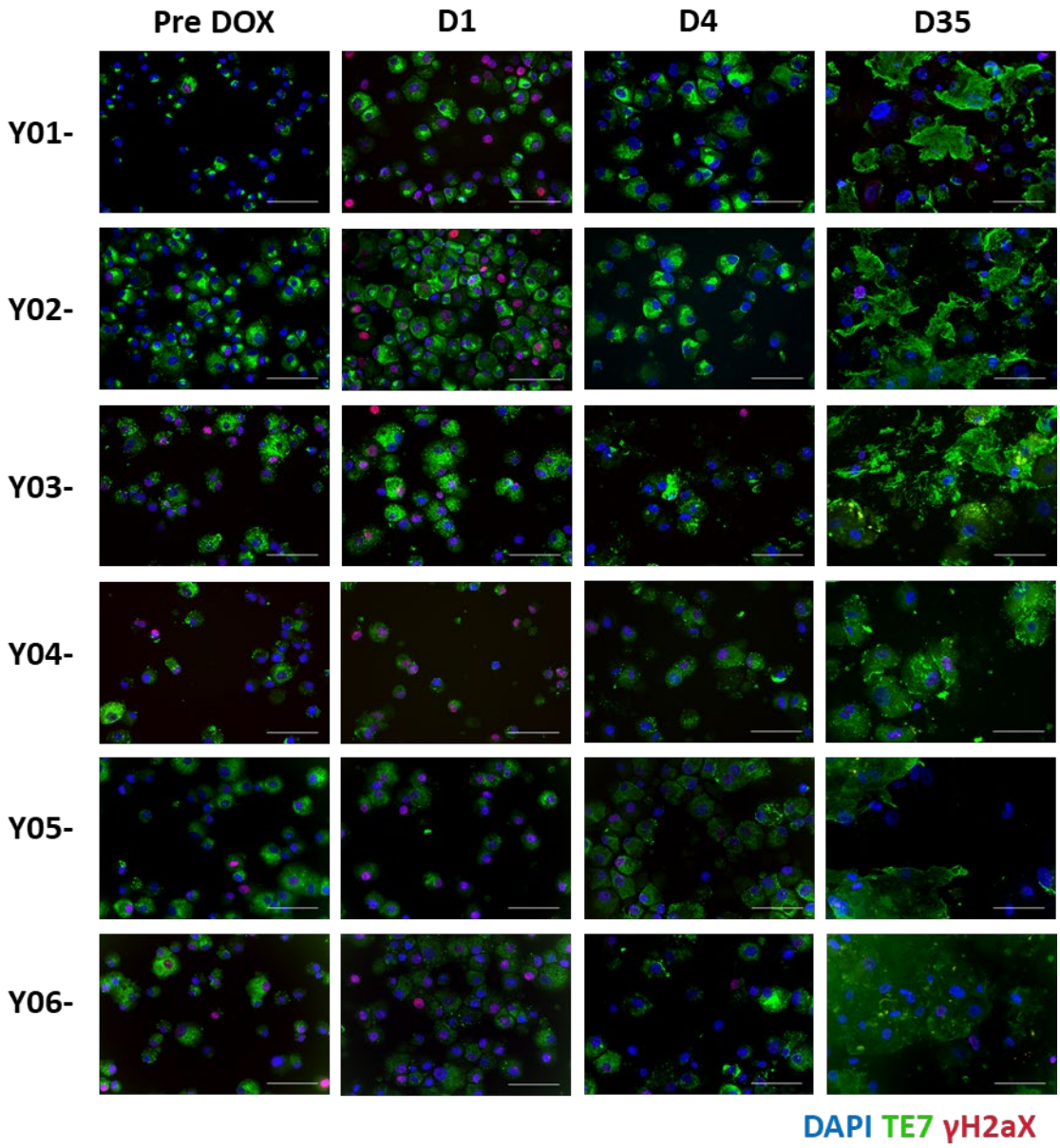

Figure 5.19. Representative images of γH2aX expression across Doxorubicin time course of individual biopsies.

Sub populations of cells (20,000 cells) from each biopsy were cytospun at different timepoints across the Doxorubicin time course and stained for TE7 (green), γH2aX (red) and DAPI (Blue). Scale bar = 100 µm.

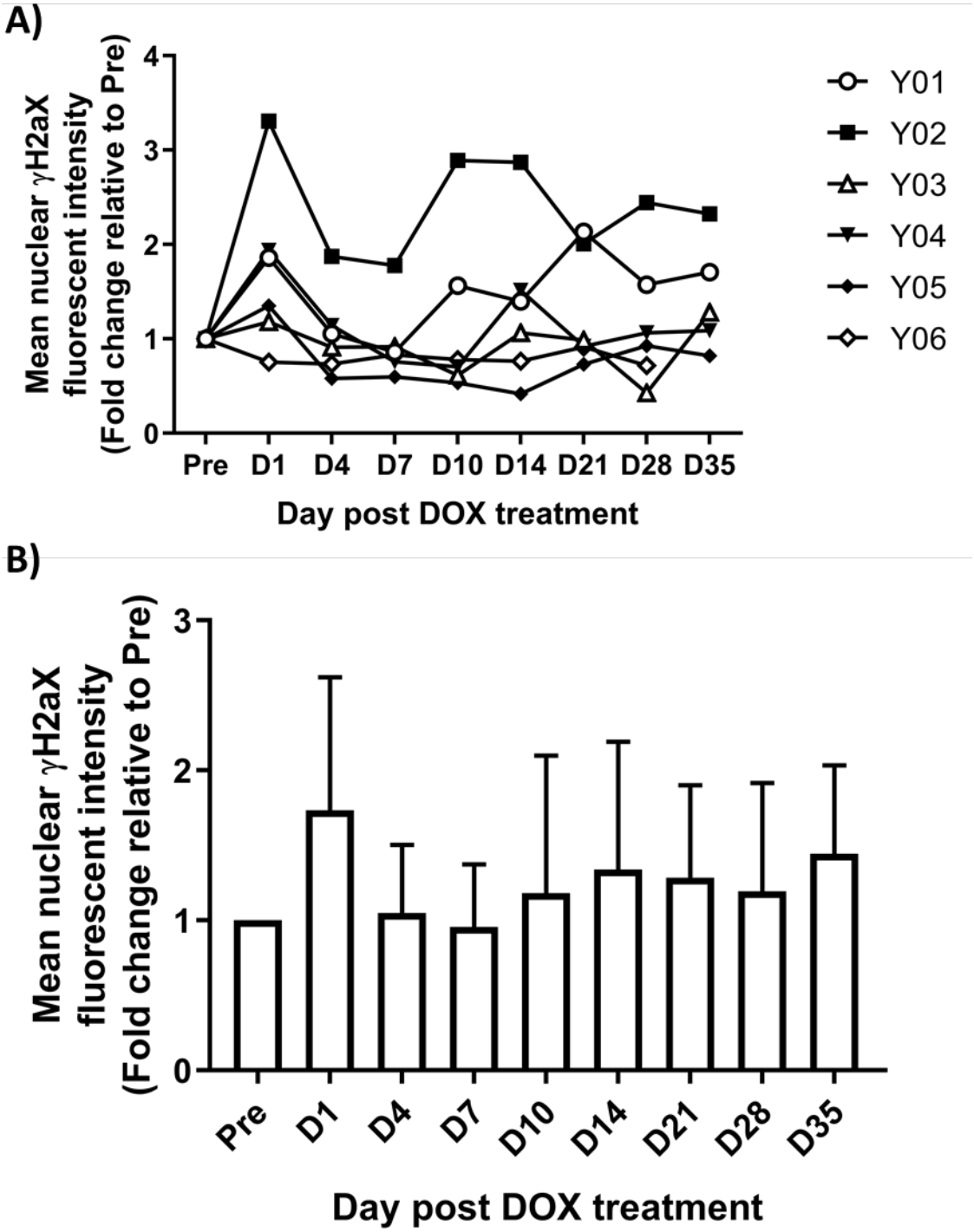

Figure 5.20. Nuclear γH2aX expression transiently increases 24 hours after Doxorubicin treatment.

A) individual CD56^{-ve} cell populations γH2aX Mean of all individual nuclei γH2aX mean fluorescent intensity across the Doxorubicin treatment time course. **B)** Mean of all individual nuclei γH2aX mean fluorescent intensity. No significant difference using a one-way RM ANOVA with Dunnett's test, P <0.05, N=6.

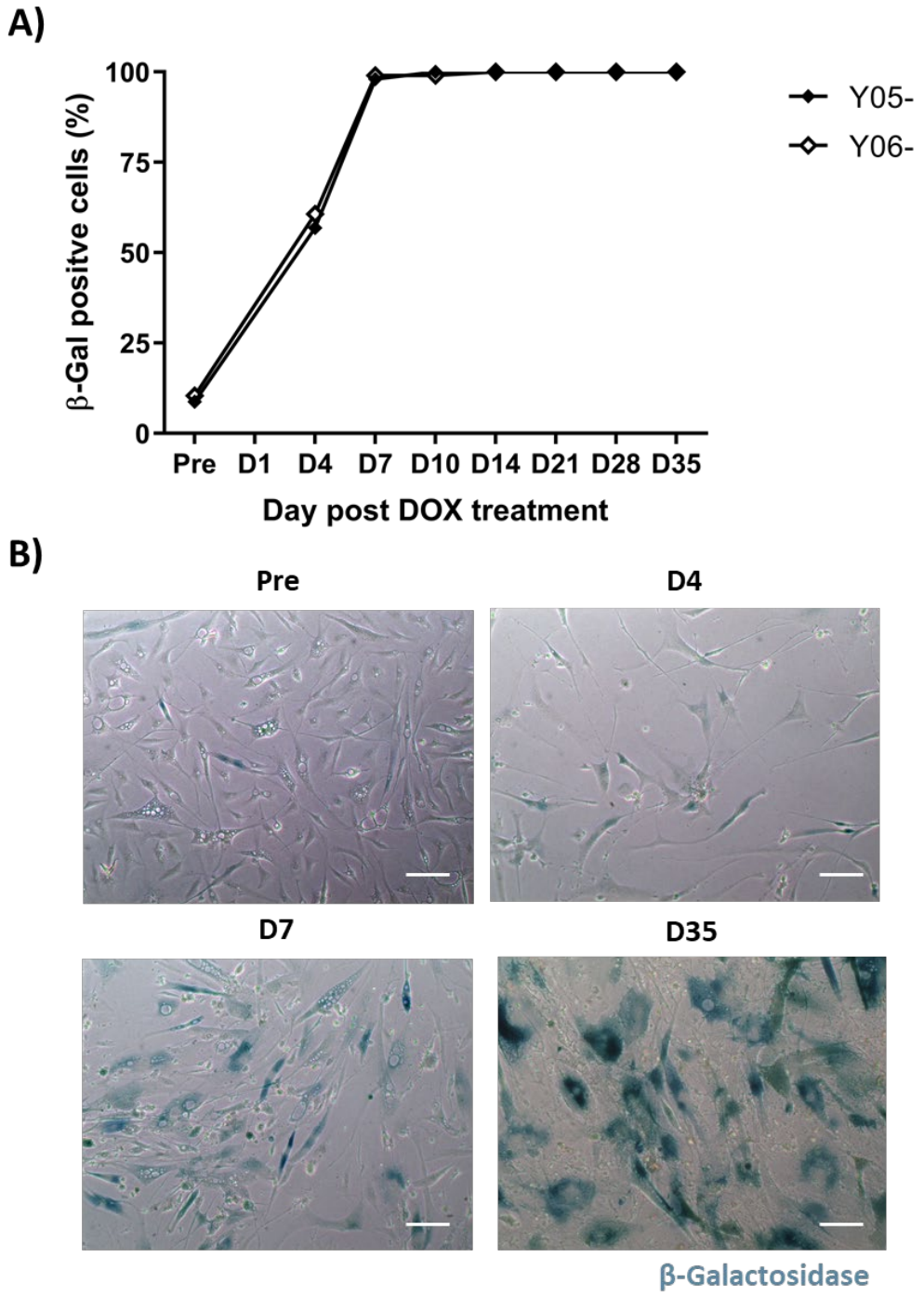

Figure 5.21. Skeletal muscle origin fibroblasts express SA β-Gal from four days after DOX treatment.

A) Sub populations of cells (25,000 cells) from Y05+ and Y06+ cell population were plated for SA β-Gal analysis before, and at eight time points after, DOX treatment. The percentage of SA β-Gal positive cells was determined at each time point for the individual myoblast populations. Data shown as individual cell population means determined from percentage SA β-Gal positive cells per field of view, 10 fields of view per time point, minimum of 100 cells analysed in total per time point. **B)** Representative images of SA β-Gal positive cells Pre, 1 day, 4 days and 35 days after DOX treatment. Scale bar = 100 µm.

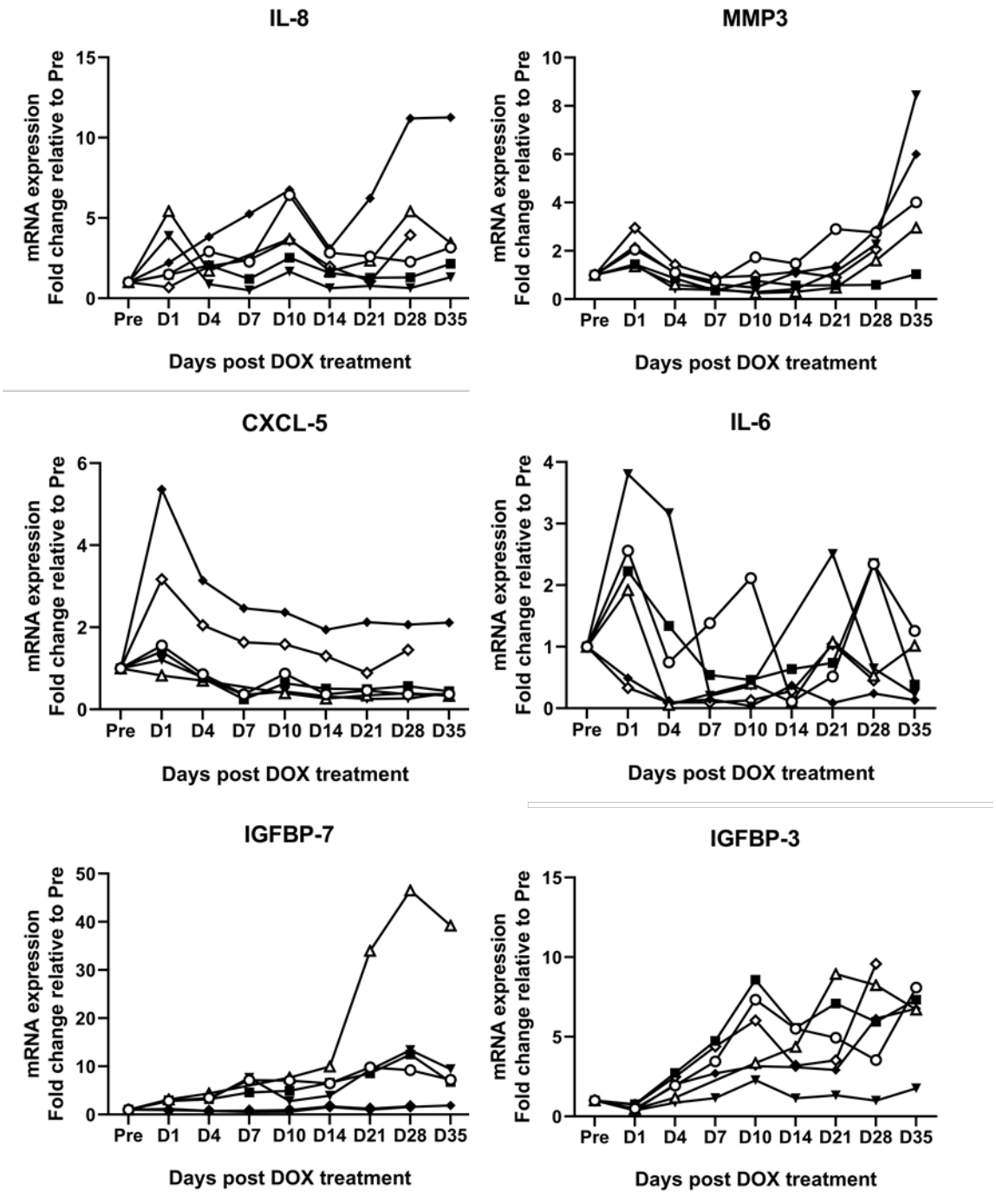

Figure 5.22. Individual fibroblast cell populations expression of each SASP factor after DOX treatment.

Individual CD56^{-ve} cell populations mRNA expression of twelve known SASP factors presented as fold change relative to individual populations pre-DOX treatment expression levels across eight time points post DOX treatment. Statistics performed on grouped data in Figure 5.23. Figure continues on next page.

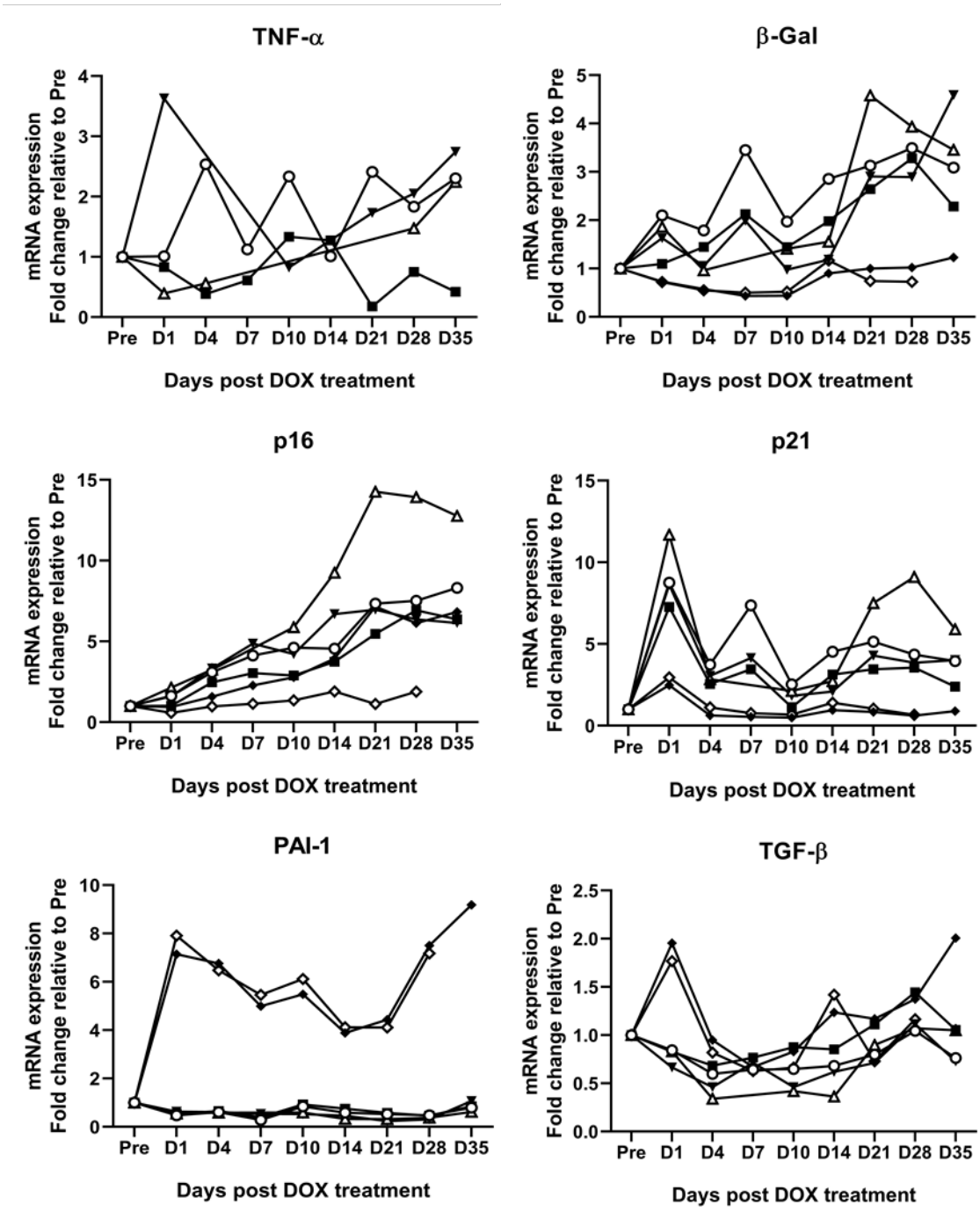

Figure 1.21. continued.

Refer back to figure legend on previous page.

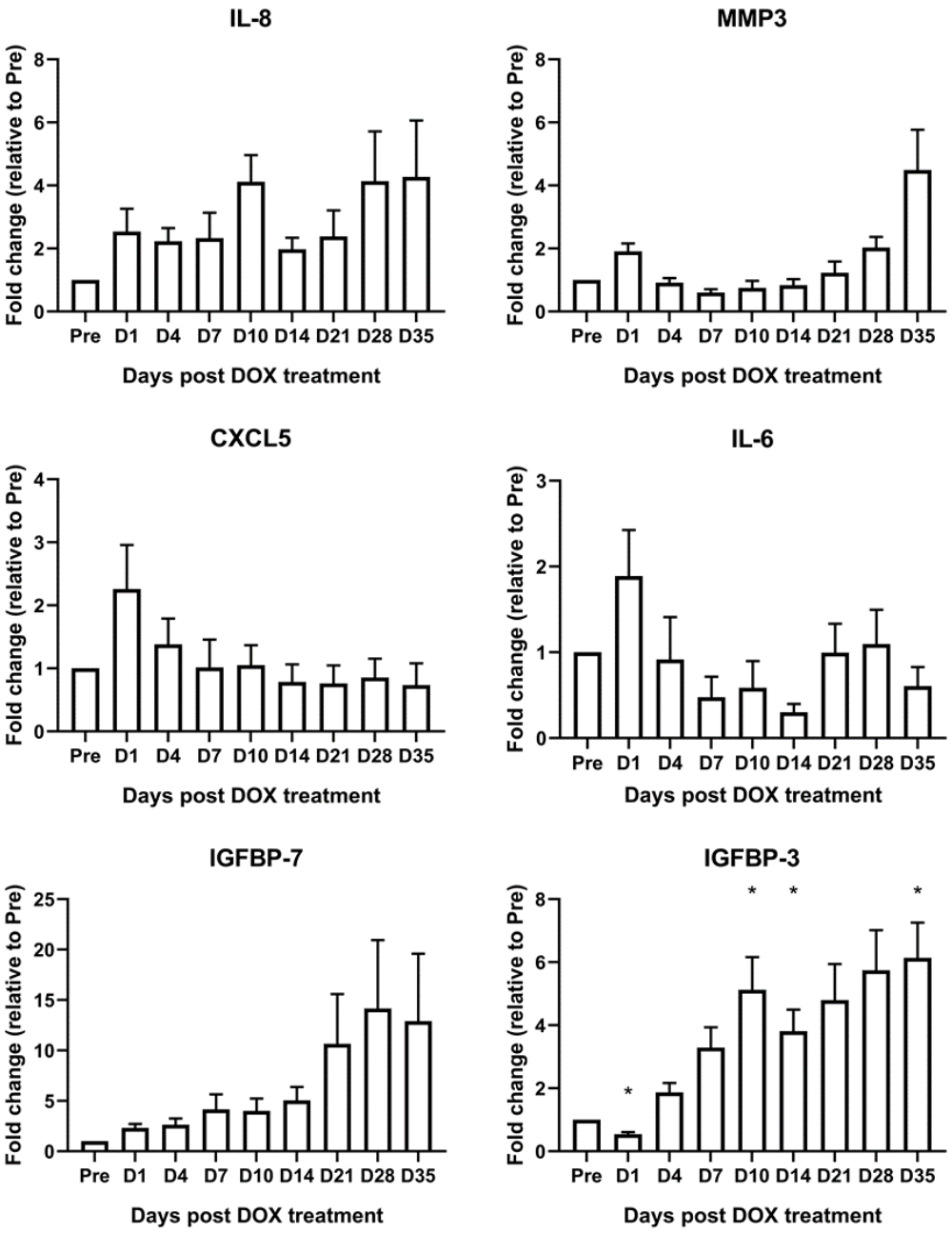

Figure 5.23. Expression of each SASP factor after DOX treatment.

mRNA expression of twelve known SASP factors presented as mean fold change relative to each individual cell populations pre-DOX treatment expression levels across eight time points post DOX treatment. * indicate significant different to Pre (one-way RM ANOVA with Dunnett's test for each SASP factor, P <0.05, N=6). Figure continues on next page.

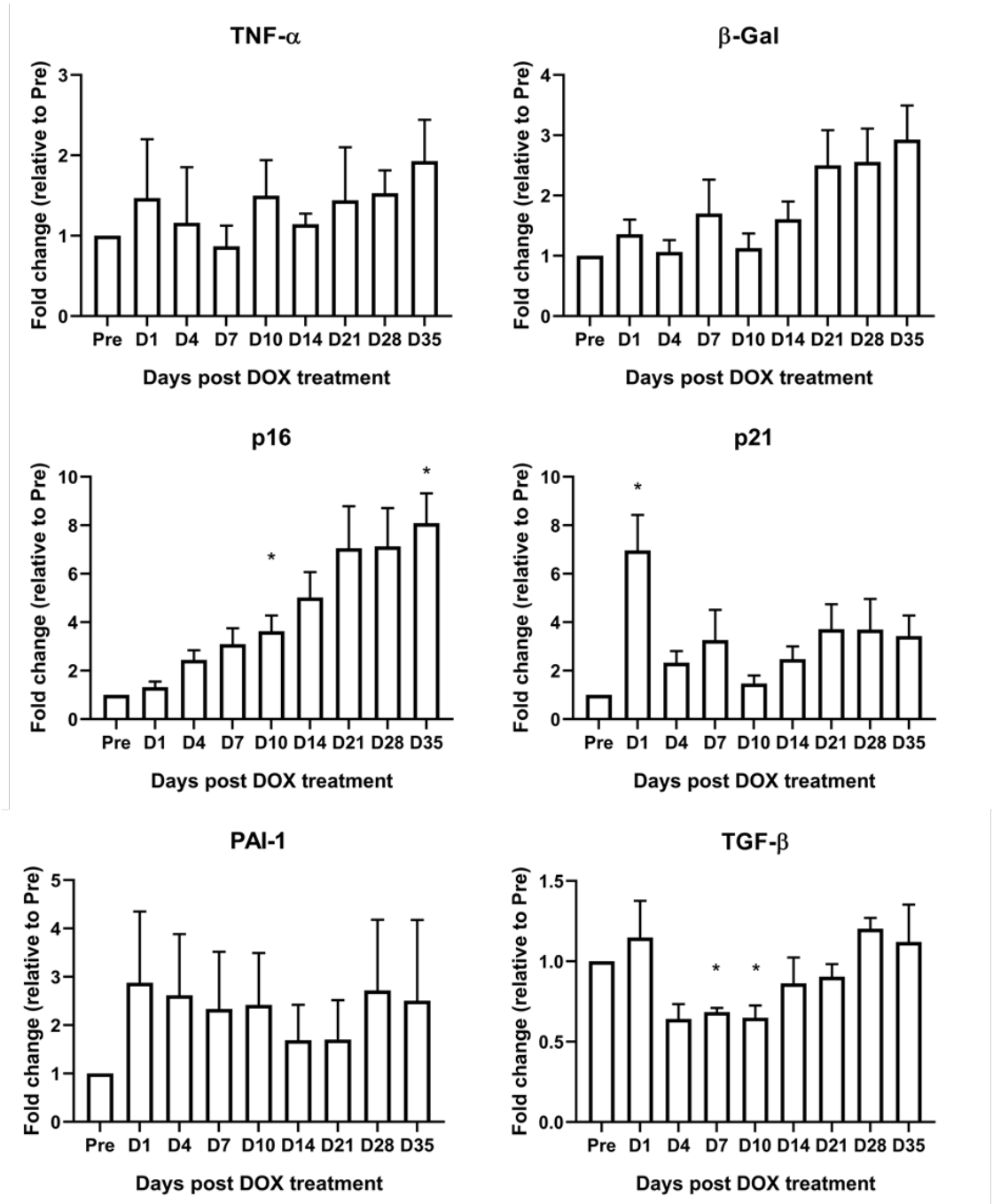

Figure 5.23. continued.
Refer back to figure legend on previous page.

5.5. Myoblasts and Fibroblasts comparison

The individual cells type data presented previously was then compiled to compare the expression differences between the two cell types to determine if there were differences in their response to the identical senescence inducing stimulus, 0.2 µm DOX. Both myoblast cell populations entered senescence more quickly than fibroblasts reaching roughly 100% SA β-Gal positive after four days compared to the two fibroblast cell populations which were 57% and 61% SA β-Gal positive. As SA β-Gal was only analysed in two cell populations statistical analysis could not be undertaken. Both cell types showed similar significant decreases in Ki67 expression after DOX treatment at both four days and 35 days post DOX treatment (N=6, $p > 0.05$). Neither cell type had significant changes in p16 protein expression from pre-DOX samples 4-days after DOX treatment. However, when there was a significant increase in p16 protein expression in MPCs at 35-days post DOX treatment and no significant increase in fibroblasts there was no significant difference between cell types when they were compared ($p = 0.12$). and neither There was a significantly higher increase in γH2aX expression in myoblasts compared to fibroblasts (N=6, $p < 0.001$. Figure 5.24).

The SASP expression of myoblasts and fibroblasts was also compared four and 35 days after DOX treatment. Here, myoblasts showed significantly higher increases in expression of IGFBP7 and IL6 as well as senescence associated marker p21 compared to fibroblasts relative to their pre-DOX treatment expression levels (N=6, $p < 0.05$). After 35 post DOX treatment myoblasts showed significantly elevated expression of MMP3 (N=6 $p < 0.001$).

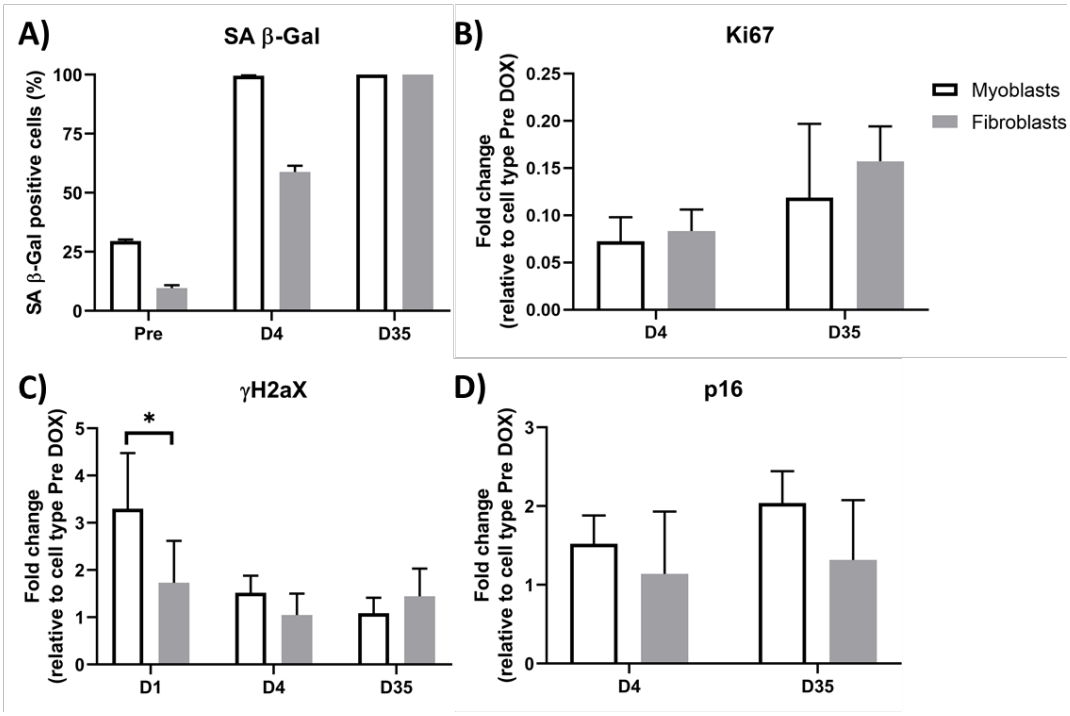

Figure 5.24 Senescent marker comparison of myoblasts and fibroblasts

Data from the cell types graphs presented earlier to show the comparison between the paired myoblast and fibroblasts populations for expression of senescent markers. **A)** The percentage of SA β-Gal positive cells is higher in both myoblasts cell populations compared to the fibroblasts cell populations before DOX treatment and four days after DOX treatment. By 35 days post DOX treatment both cell populations were 100% SA β-Gal positive. Statistical analysis could not be performed as both groups were N=2. **B)** Ki67 fold change relative to pre-DOX treatment for each individual cell type is not significantly different after either four- or 35-days post DOX treatment (N=6, $p > 0.05$). **C)** Fold change increase in γH2aX expression was significantly higher in myoblasts 1 day after Dox treatment compared to fibroblasts before both populations return to pre-DOX treatment levels by four days post DOX treatment (N=6, $p < 0.001$). **D)** There was no significant difference in fold change relative to pre-DOX treatment in p16 expression between myoblasts and fibroblasts (N=6, $p > 0.05$).

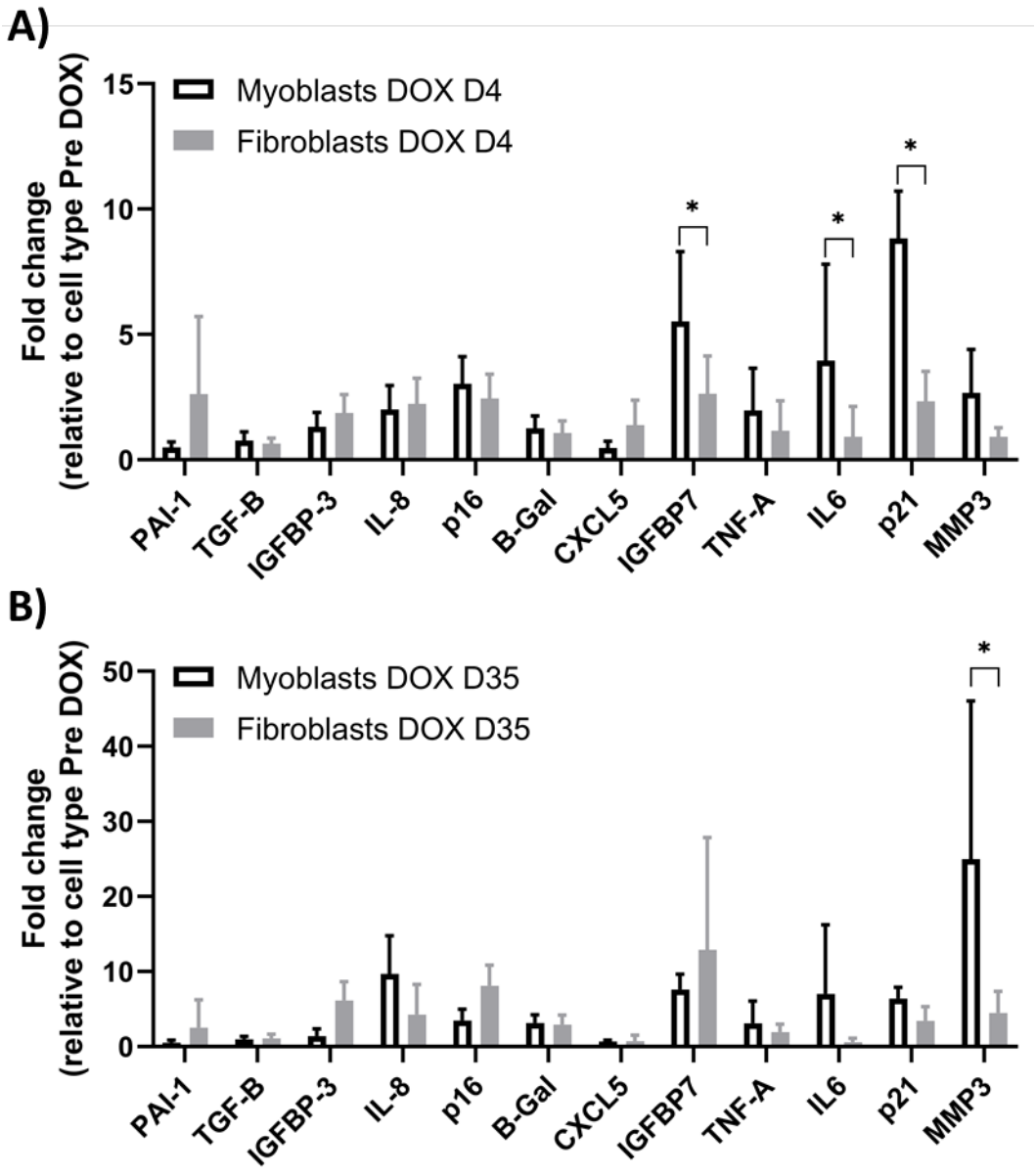

Figure 5.25 SASP expression difference between myoblasts and fibroblasts

Data from the cell types graphs presented earlier to show the comparison between the paired myoblast and fibroblasts populations for expression of a small panel of SASP factors. **A)** Four days after DOX treatment myoblast cell populations have significantly higher fold changed relative to pre-DOX treatment for IGFBP7, IL6 and p21 compared to fibroblasts (N = 6, $p < 0.05$). **B)** 35 days after DOX treatment myoblast cell populations have significantly higher fold changed relative to pre-DOX treatment for MMP3 compared to fibroblasts (N = 6, $p < 0.05$).

5.6. Discussion

The aim of the work undertaken in the chapter was to study senescent phenotypes in human skeletal muscle-derived myoblast and fibroblasts as a result of the induction of senescence with the chemotherapy drug, DOX. It was planned that by using a uniform trigger for the induction of senescence in all cells the limitation of replicative senescence protocols would be removed, and further insight gained.

A previous study used hydrogen peroxide (H_2O_2) to induce senescence in human myoblasts (Renault *et al.*, 2002*c*). Interestingly human myoblasts require very high concentrations (1mM) of H_2O_2 to induce senescence whereas other cell types have been shown to only need 50-200 µM (Chen *et al.*, 2001; Dumont *et al.*, 2001). Human myoblasts treated with H_2O_2 showed reduced cumulative population doublings by 10%, although the cells were treated after ¾ of their normal replicative life span so it could have been shorter if they were treated earlier. Myogenic cell proportion was maintained at 75-80% and cells were myogenin negative confirming that these cells had not been triggered to differentiate, although no marker of senescence was used. When induced to differentiate Myotube formation, in terms of number of nuclei incorporated, was not affected by H_2O_2 treatment. However, after H_2O_2 treatment 33.4% of cells still incorporated BrdU within a 72-hour period suggesting that the treatment had not induced senescence in the whole cell population. Therefore, a more potent inducer of senescence was required.

The results of the present work showed that DOX treatment induces a senescent phenotype in both human skeletal muscle derived MPCs and fibroblasts. Both cell populations were 100% positive for the gold standard senescence marker SA β-Gal within 7 days post DOX treatment and stayed that way throughout the 35 days post DOX treatment. Similar results where shown by Bielak-Zmijewska *et al.*, (2014), who treated hVSMCs with 0.1 µM DOX for one, three and seven days. They showed increases in SA β-Gal positive cells up to around 100% positive by 7 days of treatment. Piegari *et al.*, (2013), using human cardiac progenitor cells, also showed by 7 days post treatment the number of SA β-Gal positive cells had increased to over 75% after 0.1 µM DOX treatment.

Both skeletal muscle origin cell types had very low expression of Ki67 by four days post DOX treatment suggesting the populations were not undergoing cell division. hCPCs also showed a slowing of proliferation with over 50% reduction in BrdU expression after

24 hour DOX treatment but complete proliferative arrest after 48 hours of DOX treatment with 0.1 μM DOX (Piegari *et al.*, 2013). Similar to the skeletal muscle cell populations in the present study, proliferative arrest was maintained 7 days after DOX treatment as shown by low BrdU incorporation and very few cells expressing Ki67 (Piegari *et al.*, 2013). Whereas, hVSMCs ceased to proliferate, as measured by cell counts, immediately after DOX treatment (Bielak-Zmijewska *et al.*, 2014).

Senescence and cell cycle exit is usually associated with the cell cycle inhibitors p16 and p21. Both MPC and fibroblast cell types showed elevated p21 mRNA levels within 24 hours of DOX treatment which was transient for fibroblasts but remained elevated for myoblasts. Whereas upregulation of mRNA expression of p16 was delayed until four, and ten days after DOX treatment in myoblasts and fibroblasts, respectively. Myoblasts also maintained p16 mRNA elevation through to 35 days post DOX treatment, however fibroblasts only reached significance again at 35 days post DOX treatment. When measured at the protein level, from the image analysis data, the delayed upregulation of p16 was confirmed for myoblasts but did not reach significance in the fibroblasts. Interestingly, hVSMCs and hCPCs both showed increased p53, phosphorylated p53 and p16 immediately after 0.1 μM DOX treatment, but only hVSMCs showed transiently increased p21 (Piegari *et al.*, 2013; Bielak-Zmijewska *et al.*, 2014). In the hCPCs p16 expression increased seven days after DOX treatment in terms of overall expression and number of cells staining positive (Piegari *et al.*, 2013). This data taken together would suggest that p21 was more likely to be involved in the initialisation of DOX induced senescence in the skeletal muscle origin and hVSMCs cell types, whilst p16 is more likely involved in the maintenance of the senescent state in all cell types.

DOX induces senescence by causing DNA damage. The transient increase in double strand breaks, as measured by γH2aX, seen in myoblasts, and a trend similar in fibroblasts, suggests that DOX treatment did induce DNA damage. The immediate upregulation of p21 also supports this mechanism, as p21 is the downstream cell cycle inhibitor of the DNA damage response. Interestingly, γH2aX expression returned to baseline within four days post DOX treatment, suggesting that the DNA damage has been repaired and the double stand breaks are no longer present. However, the other senescence markers support these cells being senescent at the population level. The 0.1 μM DOX treated hVSMCs and hCPCs did not show an upregulation of γH2aX but when they were treated with 1 μM DOX

there was a clear elevation in DNA damage (Piegari *et al.*, 2013; Bielak-Zmijewska *et al.*, 2014). Similarly, to the low dose treated hVSMCs, the DNA damage insult never reached significance in the fibroblast populations, the expression of SA β-Gal and lack of Ki67 would suggest that the DOX dose was sufficient to induce a senescent state even without significant increases in DNA double strand breaks.

These findings show that DOX does induce senescence in both myoblast and fibroblast cell populations, but they do not express all the same markers. This is consistent with the finding from other human primary cell types supporting the notion that the induction of senescence may not be identical (Piegari *et al.*, 2013; Bielak-Zmijewska *et al.*, 2014; Xu *et al.*, 2015*a*; Lewis-McDougall *et al.*, 2019). Our results support the notion that SA β-Gal is the strongest marker of senescent cells when used in cell populations that do not normally express it. Ki67 is a strong corroborator of SA β-Gal to confirm that cells are not undergoing division however it does not confirm the cell cycle exit is senescence-related on its own. Cell cycle inhibitor and DNA damage expression are not uniform between the two cell types and are therefore not reliable markers of the senescent state in these cell populations.

This study employed a time course to determine when these cell populations become senescent because it was not known how long after DOX treatment skeletal muscle origin cells would take to develop a senescent phenotype. Using SA β-Gal as the marker would suggest that by four and seven days post DOX treatment, for myoblasts and fibroblasts respectively, these cell populations were senescent. However, if p16 protein was used as the marker then fibroblasts would never be deemed senescent and the myoblasts could only be considered senescent after 14 days post DOX treatment. These discrepancies in senescence marker alignment are often overlooked when investigating the secretory profile of cell populations. Bielak-Zmijewska *et al.*, (2014) observed significant increases in secreted IL6, IL8 and VEGF after three and seven days of DOX treatment, however there was no further follow up and therefore it is unclear whether these markers remained elevated or returned to a baseline measurement over time.

The aim of these experiments was to determine when both cell populations had reached a senescent state and then to investigate their SASP at that time point. However, the inconsistencies in the time course of senescence markers led to examining the mRNA

expression of known SASP factors across the time course. Here, again, temporal fluctuations in SASP factor expression were seen in both cell types. Although, some factors showed similar trends for increased or decreased expression in all cell populations the magnitude of the change was very variable between individuals. Therefore, none of this small panel of SASP factors showed a clear marker characteristic with large temporal and individual variability within and between the cell types.

These results also highlight the issue of selecting a single time point to determine the SASP of a cell population. Both myoblasts and fibroblasts could be considered senescent at multiple time points across the time course employed and the SASP profile would be different depending on which of the time points was chosen. Therefore, drawing conclusion about the SASP profile of a cell type should be interpreted with a lot of caution. Additionally, the interindividual variation in SASP profiles which would not be seen by cell line studies as the genetic diversity of the samples used in high showing that even when cell populations from different individuals are treated in identical conditions their secretory profile is variable. What this study did not investigate was the individual cellular level of SASP factor expression. From the image analysis data, it is clear that there is high variability in cell to cell expression for all markers and therefore there is likely to be cell to cell variability in SASP factor expression as well.

Individual cell SASP has been investigated recently in other fibroblast cell populations. IMR-90 cells, a human foetal lung fibroblast cell line, induced to be senescent after treatment with the cancer therapeutic, bleomycin (50 µm), for 3hrs showed that they could identify senescent cells, however across their transcriptome there were marked differences in expression of key SASP factors such as within the CXCL and interleukin families (Wiley *et al.*, 2017). Another study showed that there was more heterogeneity in populations of replicative senescent HCA2, human foreskin, fibroblasts than when the same cells were induced to become senescent via irradiation at a dosage of 50 Gy (Tang *et al.*, 2019). A hypothesis for this difference in heterogeneity between senescence induction methods could be that within a replicative senescing cell population there is a stochastic element to their senescence induction where cells become senescent at different times across the replicative passaging (Shall & Stein, 1978). Whereas, by inducing a premature senescent state on the cell population, like through DOX, a synchronisation of entering senescence is achieved, thus aligning their senescent

phenotype to a greater extent. However, even when there is synchronisation of entry into senescence there is still variability at both the cell population level as shown by the data presented in this chapter and also the single cell level as shown by the Tang *et al.*, (2019) study. Although there is variability, the overall cell population does show an altered inflammatory profile. Using the small panel of SAP factors assessed here could potentially be useful to identify differences between cell populations extracted from young and old human biopsies without the need for expensive whole transcriptome and secreted proteome analysis.

This study also set out to investigate the functional capacity of senescent MPCs. The ability of MPCs to fuse together to form myotubes was significantly impaired at four days post DOX treatment. The fusion index of untreated cells was lower than that on the early passage replicative cells, 60% compared to 80% fused nuclei. This was because the cells used for the DOX experiments were of a later passage due to the technical issues encountered with the DOX treating cell on glass coverslips. As the results of the replicative senescence chapter and work by Alsharidah *et al.*, (2013) showed there is a decline in fusion index with increased passaging. The fusion index 35 days after DOX treatment was not significantly different to untreated cells. What can be seen from the images is that over 35 days myogenic differentiation and fusion starts to occur without the removal of serum, this, in conjunction with the lower fusion index of the untreated cells could suggest why fusion index in not significantly different between these two time points. Additionally, the visual appearance of the myotubes form 35 days after DOX treatment and thin and spinally without the large number of nuclei per myotube seen in the untreated cells suggesting that thee myotubes formed were of poorer quality. The differentiation capacity of DOX induced hCPCs to differentiate into cardiomyocytes and smooth muscle cells was also impaired 7 days after DOX treatment (Piegari *et al.*, 2013). This would suggest that senescent cells are less able to repair and regenerate than healthy non-senescent cells. This was supported by the finding that hCPCs populations extracted from aged human heart biopsies were more senescent and differentiated less well compared to younger, less senescent cell populations (Lewis-McDougall *et al.*, 2019).

An interesting observation with regards to the fibroblasts populations was that towards the end of the 35 days in culture an extra cellular matrix seems to have been formed. This sheet stained strongly for TE7 suggesting it was a collagen structure being

extruded from the individual cells. There was no apparent over confluence of any of the fibroblast populations, as this connective tissue mesh is a commonly observed structure formed in confluent fibroblasts populations (Agley *et al.*, 2015). After treating the cells with trypsin, the cells detach in sheets which, when disrupted by cytospun prep, causes some nuclei to be detached from the mesh. These nuclei do not co stain with TE7 and are the likely cause of the variability seen in the TE7 analysis. It is thought that these cells have not changed cell lineage as at early time points, they are still TE7 pure before the laying down of the extra cellular connective tissue.

When the two cell types extracted from the same muscle biopsy samples were compared differences in response to the same DOX stimulus were observed. Myoblasts seemed to be more sensitive to the DOX stimuli as shown by the fibroblast cell populations taking longer to reach 100% SA β-Gal positivity whereas the myoblasts reached 100% positivity within four days. The fluorescence images were not taken in the same microscopy session and therefore mean fluorescence intensity could not be directly compared between the two cells types. Therefore, fold change in mean fluorescence intensity relative to each cell type pre-DOX treatment was used for comparison. Myoblasts showed significantly increased DNA damage caused by the treatment as measured by γH2aX one day after DOX treatment supporting the suggestion that myoblasts are more sensitive to the DOX stimulus than fibroblasts. In addition, although there was no difference in reduced expression of Ki67 suggesting that all cells had exited the cell cycle but in combination with the other markers that the fibroblasts were not as quickly entering into a senescent state.

As the myoblasts entered a senescent state after four days it was decided to compare SASP marker expression at this time point and after 35 days when both cell populations had been senescent for a long time. The differences in marker expression between the two cell populations four days after DOX treatment showed a significantly higher expression of IGFBP7 and IL6, as well as, cell cycle inhibitor p21, in myoblasts. However, by 35 days the only significant difference within the SASP factors measured between the two cell types was elevated MMP3 expression from senescent myoblasts. Overall, these results suggest that myoblasts are more sensitive to the DOX induced stimulus that skeletal muscle origin fibroblasts from the same muscle biopsy. If fibroblasts are a more robust cell type than myoblasts this is an area where further research would be

enlightening. The ageing phenotype could be a result of myoblasts accumulating more damage as a result of accumulated stimuli whereas fibroblasts retain function for longer under the same stress thus allowing them to generate more connective tissue in place of myoblasts inability to fully regenerate muscle fibres.

In conclusion, DOX induces senescent phenotypes in both myoblasts and skeletal muscle origin fibroblasts. These cell population are consistently produced without the labour intensity or possibility of reduced cell type proportions. The senescent cells express SA β-Gal, very low Ki67 and increased p16 expression, the latter only in myoblasts populations. Both senescent cell populations show alterations in inflammatory SASP factor expression but there is a high degree of individual and temporal variation. This heterogeneity highlights key issues with defining the SASP of a specific cell type because it is apparent from this study that the SASP is dynamic. However, the successful identification of senescent cells using this collection of markers could potentially help identify differences between human skeletal muscle cell populations extracted from young and old donors. The next chapter applies these markers to determine if differences can be seen in a model of the frailest, old patients undergoing surgery after suffering a hip fracture.

Chapter 6: Senescent characterisation of skeletal muscle precursor cells from old hip fracture patients

6.1. Introduction

With an ageing global population, research into the ageing process is important to understand what strategies may be effective in slowing the progression of ageing and also ameliorating the diseases associated with increasing age. With muscular skeletal disease accounting for 7.5% of the disease burden in those over 60 years of age (Dawson & Dennison, 2016), as well as, the importance of healthy skeletal muscle for maintaining independence and the benefit of physical activity in aged adults (Parise & Yarasheski, 2000; Pollock *et al.*, 2015, 2017). Skeletal muscle is a key tissue for study with regards to potential improvements in the ageing phenotype.

Sarcopenia, defined as an age-related loss of muscle mass among the elderly population, has been associated with various adverse outcomes including frailty, falls and bone fractures (Cooper *et al.*, 2012; Dodds & Sayer, 2015). The rate of muscle cross sectional loss is reported to be 25-33% in the seventh and eighth decades of life, with the rate of decline increasing further into the ninth decade of life (Young *et al.*, 1984; Bassey *et al.*, 1992). Investigating muscle satellite cell functioning in these very old and frail individuals would be the most likely population to find senescence cell burden, if it is indeed an issue within ageing skeletal muscle. This work is needed because the previous studies to investigate age-related senescence within human skeletal muscle precursor cell populations have only found limited differences when comparing otherwise healthy older adults (Alsharidah *et al.*, 2013; Barberi *et al.*, 2013; Bigot *et al.*, 2015).

As very few differences were seen between young and aged individuals it could also be that in otherwise healthy individual's senescence is not an issue for skeletal muscle precursor cells. Alsharidah *et al.*, (2013) used non-diseased otherwise healthy older adults whereas, Barberi *et al.*, (2013) included a group of masters athletes, as well as, normal aged older adults, as they expected to see differences between the exercisers and non-

exercisers. Neither study underwent further characterisation of these otherwise healthy older donors. Beyond age and sex nothing is known about their physiological health apart from them not being master athletes. The participants used could have been anything from extremely frail or sarcopenic through to recreationally active individuals.

To investigate whether senescence is an issue in older skeletal muscle this study set out to use old hip fracture patients as a population suggested to be representative of the frailest and the worst-case scenario for aged muscle, which would theoretically be the most likely to be high in senescent cells. A further characterised phenotype was proposed to offer cell type specific factors that may be able to identify senescent cells from young and old donor skeletal muscle derived cell populations and therefore determine if senescence is involved in the ageing skeletal muscle phenotype. Therefore, this study used the same proliferative/senescence marker panel as the previous chapters to determine if there are differences in MPCs isolated from young donor and old hip fracture patients.

6.1.1. Aims and Hypothesis

To compare the senescent phenotype of human primary myogenic cells from old hip fracture patients and young donor cell populations after limited time in cell culture. This is through proliferative/senescent markers, SASP factor expression and capacity for myogenic differentiation.

It was hypothesised that old hip fracture patient myogenic cell populations would have a higher senescent cell burden with increased SA β-Gal, increased expression of p16, γH2AX and SASP factors, as well as, impaired myogenic fusion, compared to their young donor counterparts.

6.2. Methods

6.2.1. Participants

Young healthy males (n=9, 22±2 years) volunteered to provide muscle biopsies as described in the general methods (Section 2.1). Old hip fracture patients (N=6, 2 Male, 82

± 8 years) were recruited by a collaborating orthopaedic surgeon at the Guy's and St Thomas' Foundation Trust. The muscle tissue donated by the hip fracture patients was muscle tissue routinely removed from the proximal end of the vastus lateralis during their surgical procedure which is normally disposed of. All participants were briefed on experimental procedures, including potential discomfort or risks, and provided written consent. This study received ethical approval from the UK National Health Service Ethics Committee and the London Research Ethics Committee (REC number: 16/LO/1707). Co-sponsorship was awarded by King's College London and Guy's and St Thomas' Foundation Trust. All procedures complied with the human tissue act.

6.2.2. Human primary muscle derived cells

The cell extraction, MACS sorting and cell culture techniques used were the same as described in the general methods (Chapter 2). Hip fracture patient cells were initially expanded and frozen down at various time points after biopsy. They were then defrosted, and experiments were performed at the earliest passage when enough cells were available for all experiments. Stored samples from the young biopsies described in the previous work where used for these experiments along with 3 others which were discussed in Chapter 4 when attempting to increase the replicative senescence n numbers.

6.2.3. Experimental assays

All experimental methods have been described previously for senescent marker and SASP factor expression, as well as, the differentiation assay.

6.3. Results

6.3.1. Hip fracture cells were slow to expand

The hip fracture patient muscle samples were originally expanded for different lengths of time to reach critical mass to freeze down efficiently. Once defrosted, they each also took different amounts of time to expand again to sufficient number for experimental

plating. The number of days post biopsy when hip fracture cells were defrosted and the days post biopsy when experimental plating took place are shown in Figure 6.1. It was observed that all hip fracture cell populations took longer to expand than expected compared to the rate of young cells as shown by the number of days required to expand for experimental plating. Once hip fracture cell populations had expanded sufficiently, they were plated for all possible experiments which was 30±5 days post biopsy. However, not all hip fracture cell populations expanded sufficiently to be used for all experiments. The samples used for each experiment are described in the relevant sections. Frozen samples from young cell populations were chosen to match the same time under culture conditions as the hip fracture patients' cells to provide the closest match between the different aged donors. The young cell populations used ranged from 28 to 31 days post biopsy (30.5±1).

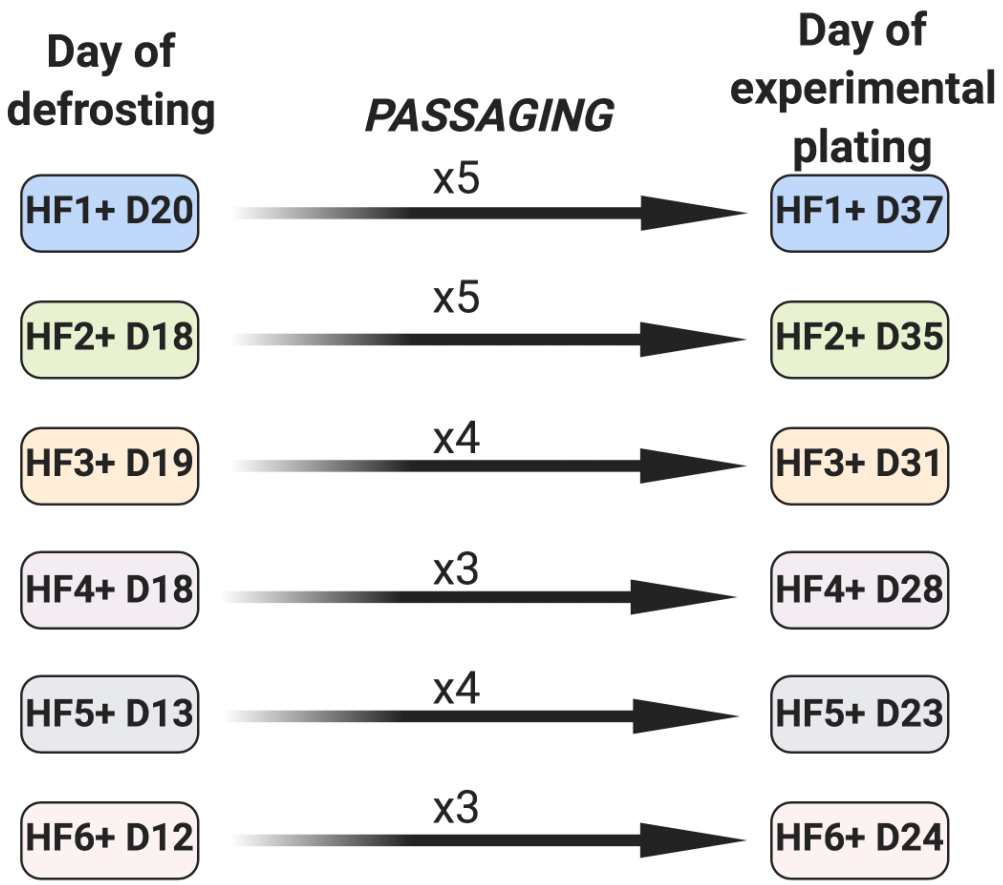

Figure 6.1. Days in culture required to sufficiently expand hip fracture cell populations for all experiments.

Hip fracture patients were expanded after initial extraction then frozen for later experiments. On defrosting each hip fracture cell populations took different lengths of time to expand sufficiently to undergo experiments. The left-hand column indicates the number of days post biopsy that each cell population was cryogenically stored. The right-hand column indicates the days in culture post biopsy when each individual cell population was plated for experiments, Mean±SD = 30±5 days post biopsy.

6.3.2. Variability in desmin expression

Desmin expression was assessed at the first passage after defrosting and populations with low numbers of desmin positive cells were resorted to try to enrich the cell populations. However, the $CD56^{+ve}$ sort fractions were always small and the negative fractions contained many desmin positive cells. It was decided to recombine the sort populations so that experiments could be plated at the earliest possible time point. The percentage of desmin positive cells within hip fracture patients' cell populations at the time point of experimental plating (30±5 days post biopsy), along with the desmin expression of the young cell populations after comparable time in culture (30.5±1 days post biopsy), are shown in Figure 6.3 and representative images of each sample at time of experimentation are shown in Figure 6.2.

6.3.3. Hip fracture patients have more SA β-Gal expressing than young donors after similar time in culture

At the earliest time point possible (30±5 days post biopsy), sub populations of hip fracture patient myogenic cells (25,000 cells) were analysed for expression of SA β-Gal and compared with young myogenic cell populations after a similar time in culture (30.5±1 days post biopsy). For this analysis if cell populations with low desmin cell percentages were removed there would not be sufficient sample numbers for statistical analysis. It was also not possible to only count desmin positive SA β-Gal cells as co-staining of desmin with SA β-Gal was not performed. Therefore, it was decided to use all cell populations, irrespective of their desmin cell percentage, and to refer to these mixed cell populations as muscle-derived cell populations instead of myoblasts. The number of SA β-Gal positive cells was significantly higher in the hip fracture muscle derived cell populations (76.5±10.7%) compared to the young muscle derived cells (28.2±4.7%, $p < 0.001$, Figure 6.4).

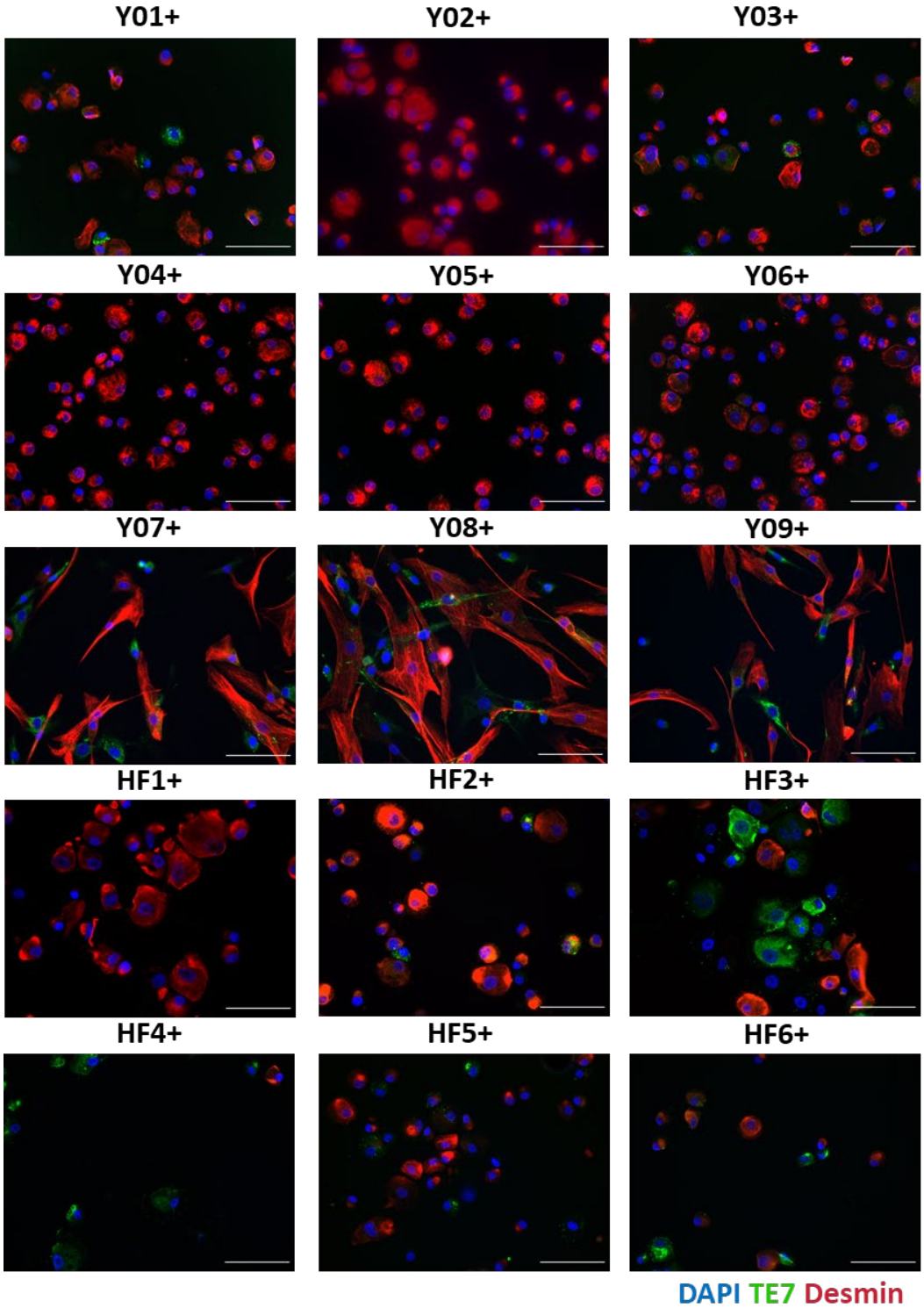

Figure 6.2. Representative images of myogenic expression at time of plating for each individual cell population.

Sub populations of cells (20,000 cells) from each cell population were either cytospun or plated onto glass coverslips at time of experimental plating (young; 30.5±1 days post biopsy and hip fracture patients; 30±5 days post biopsy) and stained for desmin (red), TE7 (green) and DAPI (Blue). Images acquired using a 20x magnification objective, Scale bar = 100 µm.

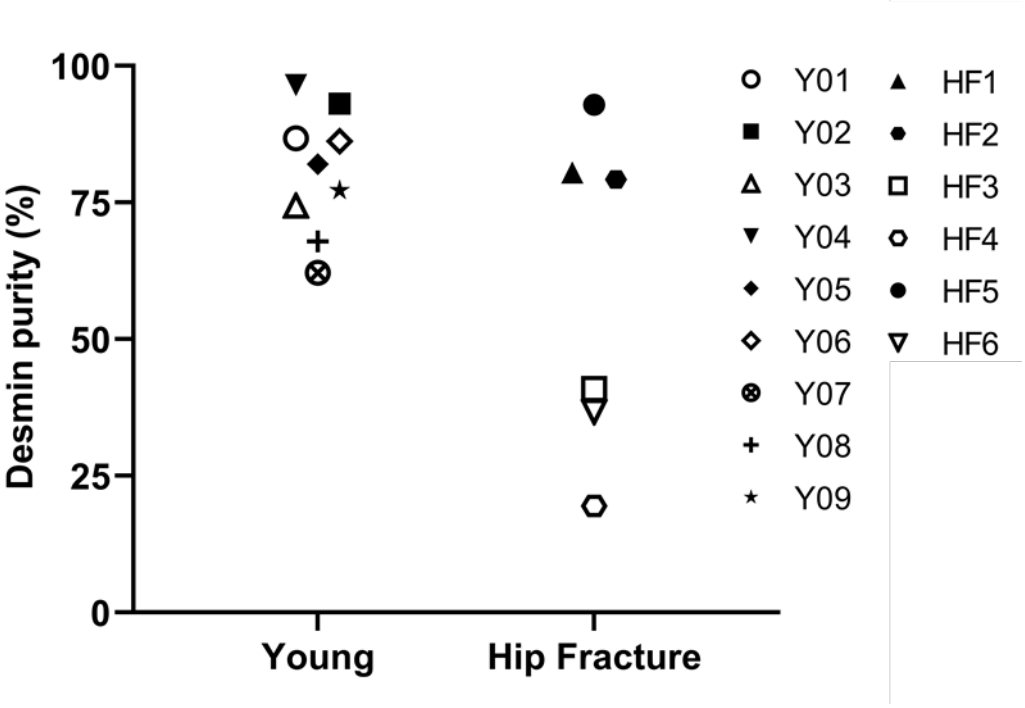

Figure 6.3. Desmin expression quantification of the cell populations at time of experimental plating.

Sub populations of cells (20,000 cells) from each cell population were either cytospun or plated onto glass coverslips at time of experimental plating (30±5 days post biopsy) and stained for nuclei and desmin to determine the percentage of desmin positive cells by a bespoke automated image analysis program. Data shown as mean of percentage desmin positive cells per field of view, 10 fields of view per time point, minimum of 100 cells analysed per individual cell population.

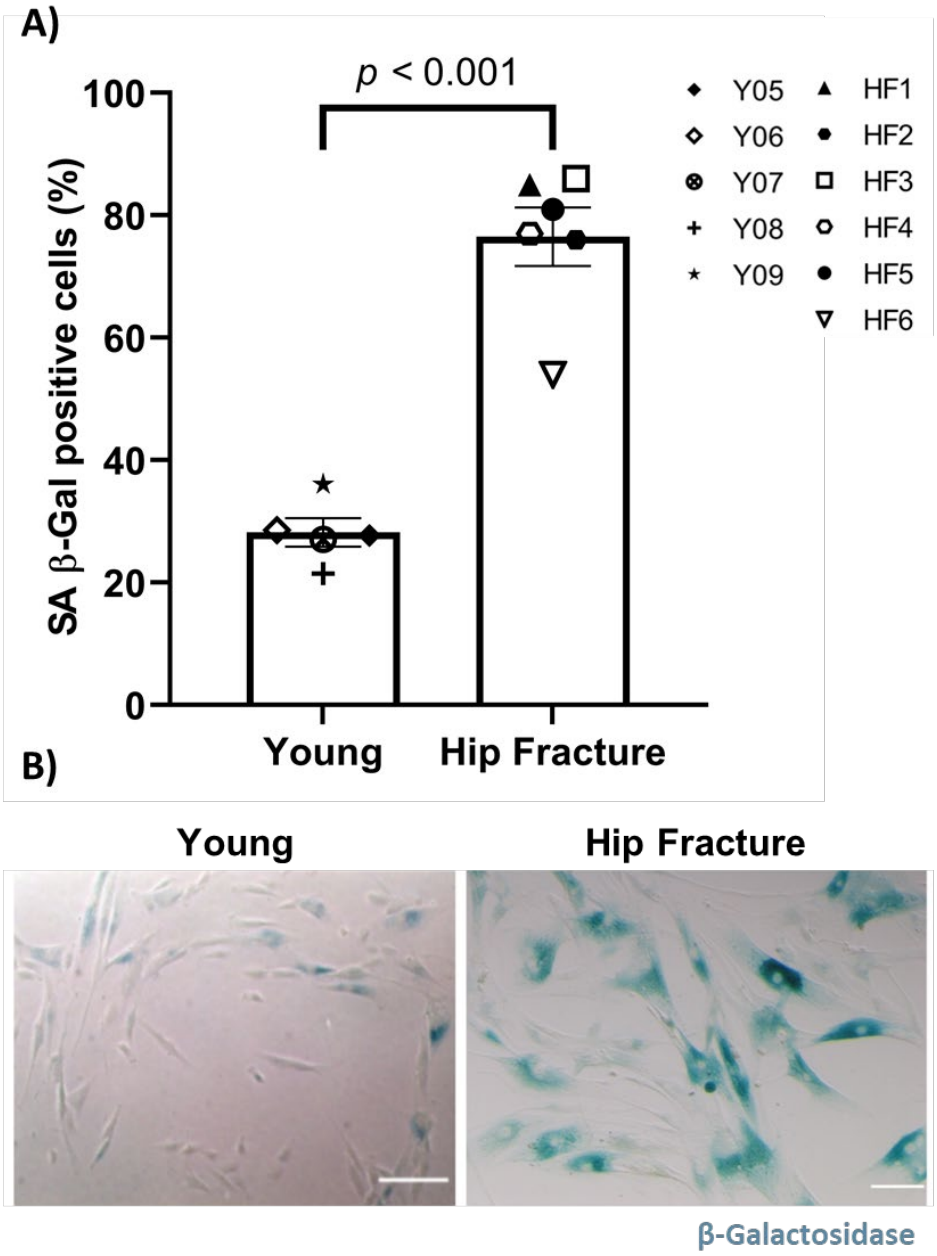

Figure 6.4 Hip fracture patients myogenic cell populations contain more SA β-gal positive cells compared to young cell populations.

A) Sub populations of cells (25,000 cells) from young and hip fracture cell population were plated for SA β-Gal analysis after the same time in culture (young 30.5±1 and hip fracture patients 30±5 days post biopsy). The percentage of SA β-Gal positive cells was determined at each time point for the individual myoblast populations. Data shown as mean of individual cell population determined from percentage SA β-Gal positive cells per field of view, 10 fields of view, minimum of 100 cells analysed in total per individual cell population. Data was compared by unpaired t-test with Welch's correction which does not assume equal variances between groups which showed a significant difference between the two groups ($p < 0.001$). B) Representative images of SA β-Gal positive cells from young and hip fracture patients after the same time in culture 30±x days post biopsy. Scale bar = 100 μm.

6.3.4. No difference in p16 protein between young donors and hip fracture patients

The expression of cell cycle inhibitor p16 within desmin positive cells was determined at the time of experimental plating using immunocytochemistry, analysed by a bespoke automated image analysis program described in Chapter 3. There was no significant difference (p = 0.11) in p16 mean fluorescent intensity between young donors (565.6±250.2 AU) and hip fracture patients (791.0±136.2 AU) desmin^{+ve} cells (Figure 6.5). There was also no observable pattern in p16 expression between populations with high and low numbers of desmin positive cells within either young or hip fracture patient cell populations (Figure 6.5).

6.3.5. Trend for higher γH2aX in hip fracture patient myoblasts compared to young donors

The expression of DNA damage marker γH2aX within desmin positive cells was also determined at the time of experimental plating using the same methods as described for p16 expression. Here, there was a statistical trend (p = 0.064) for higher γH2aX mean fluorescent intensity in hip fracture patients (483.9±144.1 AU), compared to young donor (308.3±121.6 AU) desmin^{+ve} cells after a similar time in culture (Figure 6.6). Again, no difference was observed for γH2aX expression between populations with high and low numbers of desmin positive cells within either young or hip fracture patient cell populations (Figure 6.6).

6.3.6. Hip fracture patients cells do not show impaired differentiation capacity

Four of the hip fracture patients had sufficient cells to undergo the differentiation assay (HF1, HF2, HF5 and HF6). However, one of these samples HF6 was only 40% desmin positive at the time of plating and was therefore excluded from the fusion index analysis. The remaining three high desmin expressing hip fracture cell populations (HF1, HF2 and HF5) underwent the differentiation assay and where analysed for fusion index after seven days (144 hours). The young cells were assayed during the replicative senescence

experiments presented earlier and therefore were only differentiated for 96 hours at early passage, 16 days post biopsy, as per that experimental protocol. There was no difference (p = 0.42) in fusion index between the hip fracture patient myogenic cells which were differentiated for 144 hours (81.7±7.8%) compared to young donor myogenic cells which were only differentiated for 96 hours (84.8±4.0%, Figure 6.7).

6.3.7. Different expression levels of SASP factors between culture aged young and hip fracture patient myogenic cell populations

Three of the hip fracture patients had sufficient cells to undergo the differentiation assay (HF2, HF5 and HF6). Although, HF6 was only 40% desmin positive at the time of plating due to low N numbers it was included so that statistical analysis could be performed. The hip fracture patient cell populations were analysed for expression of eight known senescent markers and SASP factors using qRT-PCR. They were compared with young donor cell populations after similar time in culture. This time point was 28 days post biopsy which was the closest time point that had RNA samples from all young cell populations. A final group of early passage, 10 days post biopsy, young myogenic cells were also included to determine if differences were due to culture age of cells or if there were differences between the age of the cell population donor. Data is presented as fold change relative to young D10 as this is the cell population least likely to be senescent as shown by the data presented in chapter 4. Hip fracture patient mRNA expression of CXCL5 (13.8±12.5 fold change) and IL8 (20.4±14.9 fold change) was significantly higher than both young D10 ($p < 0.001$) and Young D28 ($p < 0.01$). Young D28 were not significantly elevated compared to young D10 for either CXCL5 or IL8. The mRNA expression of p16 was significantly higher in both hip fracture patients (fold change 45.2±11.8, $p < 0.001$) as well as, young D28 (fold change 31.6±12.6, $p < 0.001$) compared to young D10 (fold change 1.2±0.6). Hip fracture patients also expressed significantly more p16 mRNA than young D28 (p = 0.003, Figure 6.8).

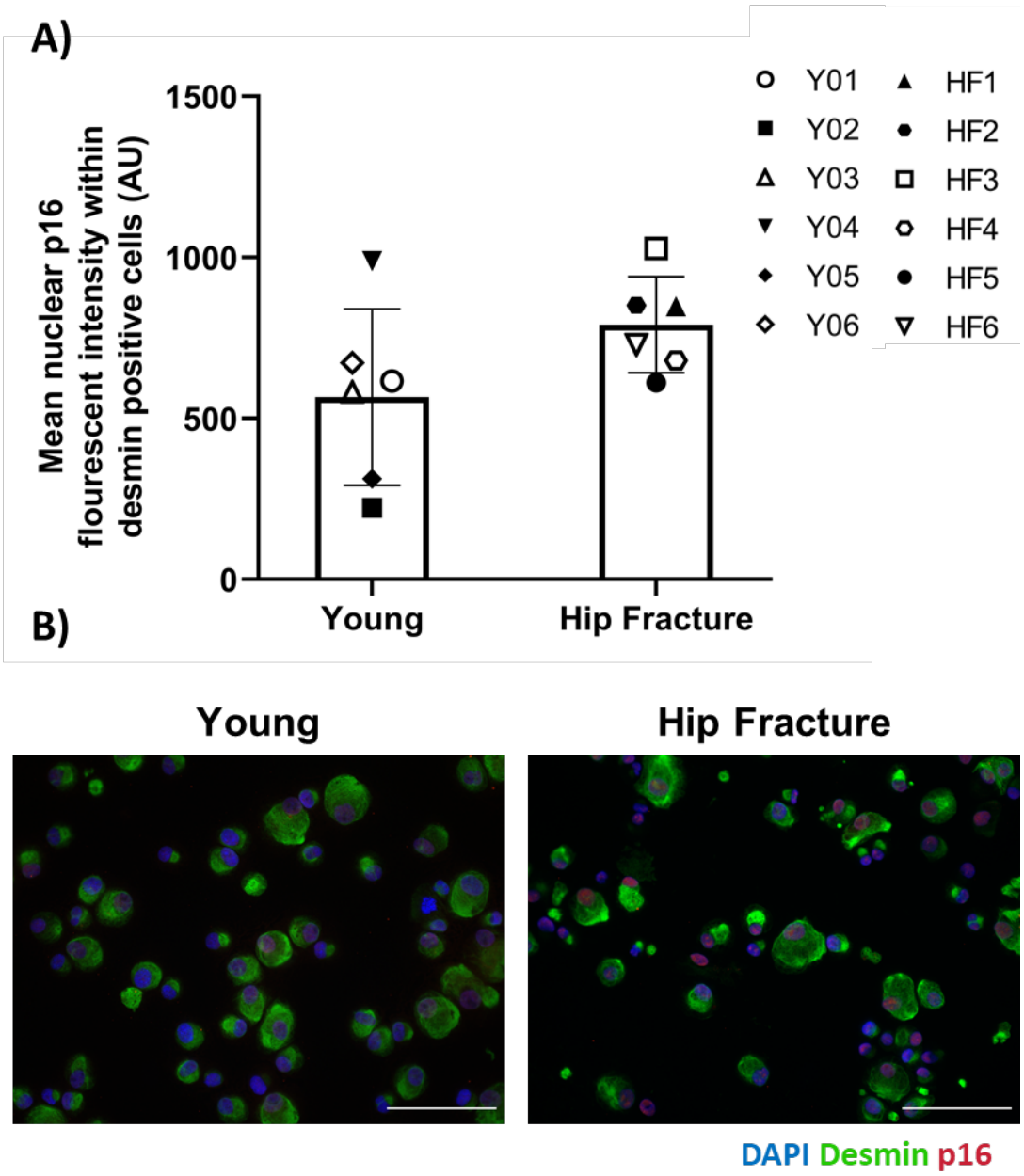

Figure 6.5. No significant increase in nuclear p16 expression in desmin positive hip fracture cells. A) Individual cell populations p16 mean fluorescent intensity presented as mean of all desmin positive individual nuclei. Data was compared by unpaired t-test with Welch's correction which does not assume equal variances between groups which showed no significant difference between the two groups (p = 0.1). B) Representative images of young and hip fracture patient cell populations stained for nuclei (blue), desmin (green) and p16 (red).

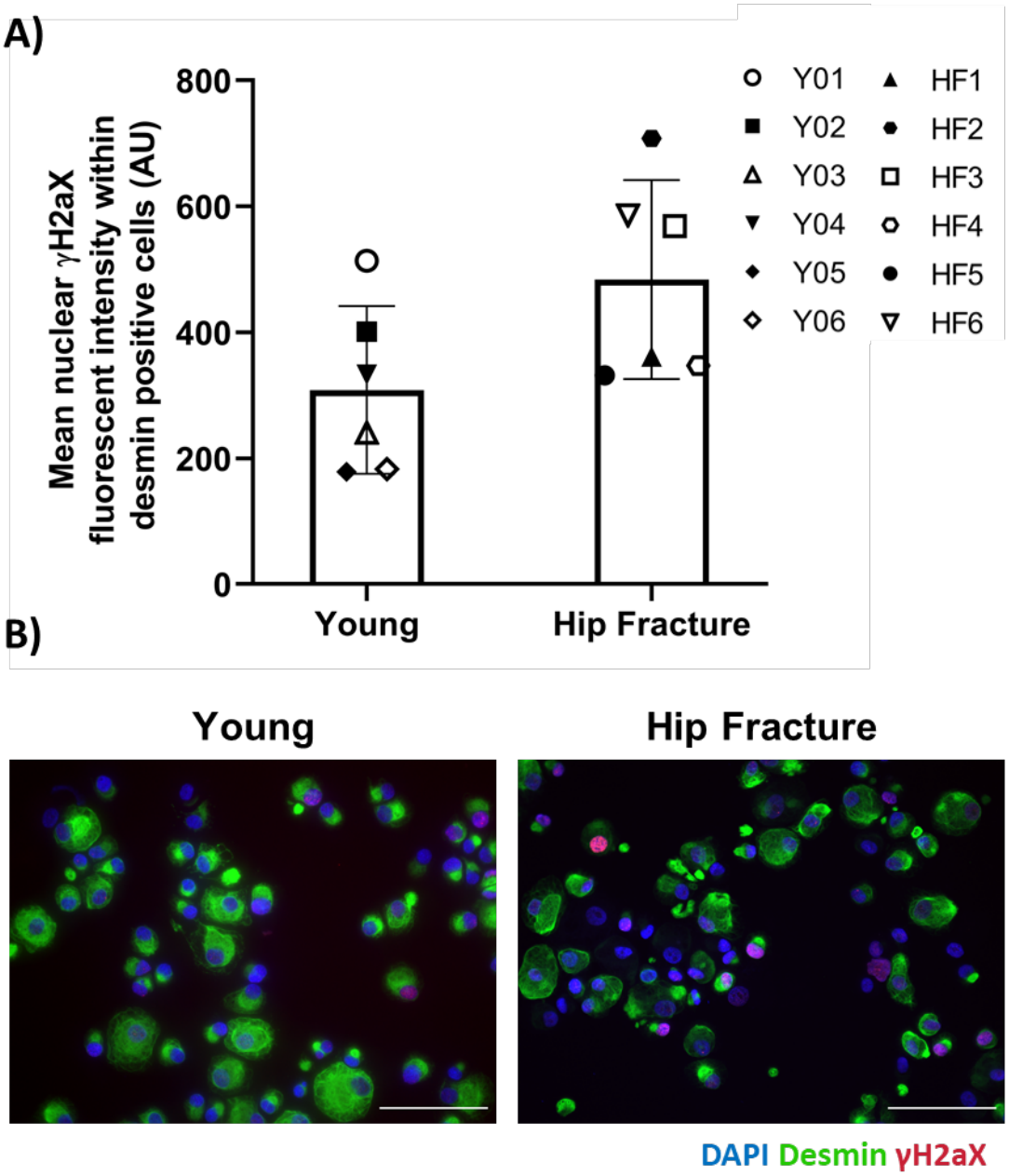

Figure 6.6. Statistical trend for increased γH2aX expression in desmin positive hip fracture cells. A) Individual cell populations γH2aX mean fluorescent intensity presented as mean of all desmin positive cells. Data was compared by unpaired t-test with Welch's correction which does not assume equal variances between groups which showed a trend for higher γH2aX expression in hip fracture patient desmin positive cells (p = 0.064). B) Representative images of young and hip fracture patient cell populations stained for nuclei (blue), desmin (green) and γH2aX (red).

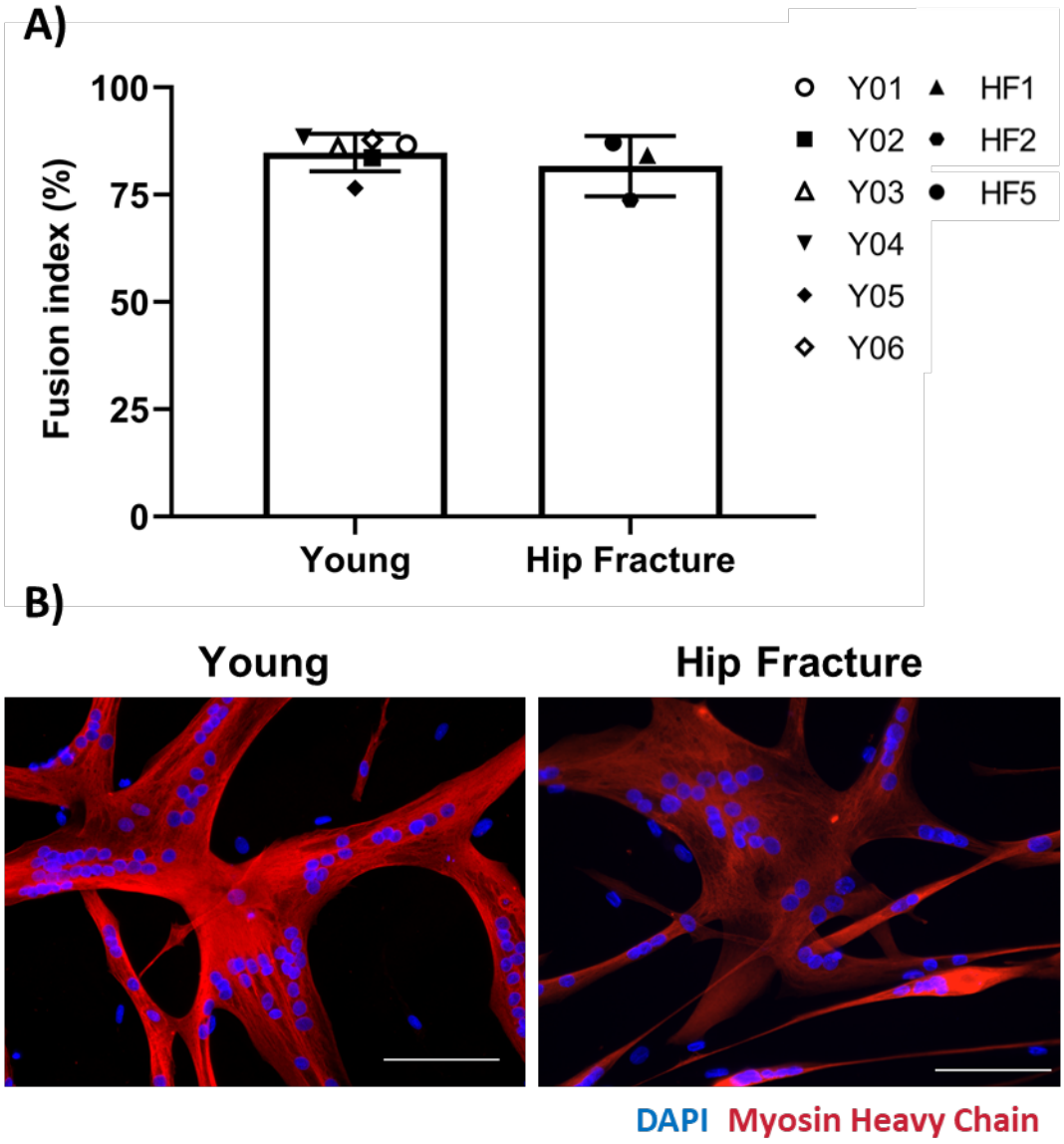

Figure 6.7. No significant difference in fusion index between hip fracture and young myogenic cells.

A) Myoblasts from young donors and hip fracture patients were induced to differentiate and form myotubes. Young myoblasts (n=6) were at early passage (16 days post biopsy) and were imaged 96h after differentiation induction. Hip fracture myoblasts (n=3) were induced to differentiate at the earliest time point possible after defrosting (30±5 days post biopsy) and were imaged 144h after differentiation induction. Data was compared by unpaired t-test with Welch's correction which does not assume equal variances between groups which showed no significant difference in fusion index between young and hip fracture patient cells (p = 0.42). B) Representative images of young and hip fracture patient myoblasts directed to differentiate into myotubes and imaged after 96h young, and 144h hip fracture patients showing nuclei (blue) and myosin heavy chain (red). Scale bar = 100 µm.

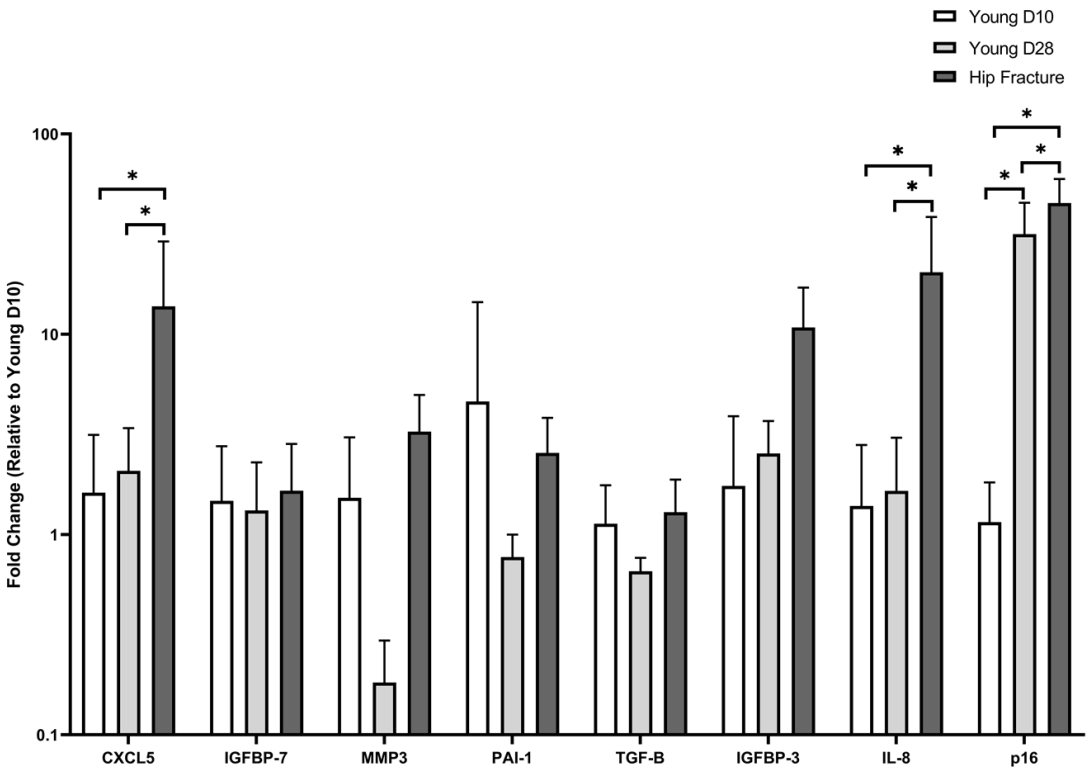

Figure 6.8. Significant differences in SASP factor expression between hip fracture patients and young cell populations after similar time in culture

mRNA expression of eight known SASP factors presented as population mean fold change relative to young D10, early passage young donor myoblasts. * indicate significant difference between the two compared groups (two-way ANOVA with Tukey's multiple comparisons test for differences between group for each SASP factor, P <0.05, Young D10 and Young D28 N=6, Hip fracture N=3).

6.4. Discussion

The aim of this study was to investigate the senescent characteristics of skeletal muscle derived cells isolated from hip fracture patients' in comparison to young donor myoblasts. This study shows that skeletal muscle derived cells, of which a high proportion were desmin^{+ve} MPCs, extracted from hip fracture patients demonstrated higher levels of SA β-Gal, but not other senescent markers, p16 and γH2AX, after comparable time in culture with myoblasts extracted from young donors.

Hip fracture patients' MPCs displayed variability in desmin expression over time in culture and in their ability to proliferate as a cell population. All cell populations went through the CD56 MACS sorting process in order to isolate and expand the CD56^{+ve} myoblast population before being frozen down. After thawing and expanding for experimental plating three of the six hip fracture myoblast populations maintained high desmin expression (93-79% at time of experimental plating) and the other three had much lower desmin expression (20-41% at time of experimental plating). Similarly, to the replicative senescent work in chapter 4, re-sorting of these low desmin expressing cell populations with CD56 magnetic beads was attempted but the negative fractions contained high levels of desmin positive myoblasts. Therefore, the positive and negative fractions were recombined, and these samples were only used for analysis where desmin positivity could be analysed alongside another marker, i.e. immunocytochemical analysis of desmin positive cells for senescent marker expression. This loss of desmin expression does not seem to be associated with age as similar results were shown in the young replicative senescence experiments to a similar extent. As discussed previously the use of an additional sorting marker such as CD82 may improve the myogenic cell enrichment as CD56 expression has been shown to fluctuate across the replicative lifespan of myogenic cells (Meng *et al.*, 2011). This study did not focus on the CD56^{-ve} fractions, which would contain the fibroblasts from these hip fracture patients, but a comparison between the fibroblasts of young and hip fracture patients would be of interest to determine if there are differences in behaviour of these cell populations.

As the hip fracture patients were defrosted their proliferative rate was not measured because it would not be comparable to the young proliferative experiments which were never frozen. However, by observing how long it took to expand these cell populations it

is of interest to note the potential differences in the proliferative rate of hip fracture patient MPCs, which should be investigated on freshly cultured cells without freezing. This unexpectedly slow proliferation prevented the comparison of the cell populations at early passage as the mean number of days in culture before experimental plating was 30±5 days post biopsy. Therefore, young donor cell populations which had been in culture for a similar amount of time as the hip fracture patients' cells were chosen for comparison to provide the most like-for-like comparison. The time points for the young samples varied between 28 and 31 days post biopsy with a mean of 30.5±1 days post biopsy. When comparing the senescent phenotype of hip fracture patients to young donor myoblasts at this comparable point in culture, the hip fracture populations displayed increased expression of SA β-Gal but not p16 or γH2AX. When investigating myogenic fusion index, hip fracture myoblasts did not exhibit impaired differentiation capacity. Lastly, when investigating the mRNA expression of a small panel of senescence markers and SASP factors, a general trend for increased expression of SASP factors was seen in hip fracture cells, compared to both young early passage and after comparable time in culture.

SA β-Gal is considered the gold standard, most commonly used, method of detecting senescent cells *in vitro* (Dimri *et al.*, 1995). Human myoblasts passaged to replicative senescence from healthy and Duchenne muscular dystrophy patients have been shown to express SA β-Gal (Nehlin *et al.*, 2011; Renna *et al.*, 2014) and it was shown to be the clearest senescent marker in DOX-treated MPCs in Chapter 5. In this study, hip fracture patients cell populations were shown to have much higher numbers of SA β-Gal positive cells compared to young cell populations after similar time in culture. This is different to the results of Bigot *et al.*, (2015) who found both young and old human myogenic cell populations had roughly 20% SA β-Gal positive cells. The age of the old participants in the Bigot *et al.*, (2015) ranged from 72 to 80 years old, which was slightly younger than the participants used in the current study (82 ± 8 years). It is possible that the older donors in the current study having higher expression of SA β-Gal could be supporting in human, for the first time, the findings of Sousa-Victor *et al.*, (2014) who demonstrated a significant increase in SA β-Gal expression in geriatric mice, compared to old mice which were not significantly increased over young mice. However, this difference in results may also be explained by the later time point, 30±5 days post biopsy, for comparison used in the present study. Bigot *et al.*, (2015) measured SA β-Gal before 12 population doublings and

within the first half of the cell population life span. Within this study it is likely that SA β-Gal was measured later in the proliferative lifespans considering the young samples reached senescence within 60 days in the replicative senescence experiments. Measuring at this later time point could mean that some of the hip fracture cell populations had reached, or were close to reaching, replicative senescence. This would also explain the slow proliferative rates observed in these cell populations. Additionally, this could suggest that these hip fracture patients have shortened replicative capacity compared to young donor cells, which would be of interest as this has not been previously shown in adult human myogenic cell populations (Alsharidah *et al.*, 2013; Barberi *et al.*, 2013; Bigot *et al.*, 2015). A noticeably shortened replicative capacity would support a possible role for cellular senescence within skeletal muscle ageing. Although, these cell populations were able to expand in culture which would suggest that they are still able to function and therefore any reduction in their proliferative capacity may not be limiting their *in vivo* ability to supply sufficient new myonuclei to regenerate muscle. Overall this preliminary finding supports the premise of this study that hip fracture patients would be the most likely population to exhibit senescent characteristics.

Although SA β-Gal is the gold standard marker of senescence it is not definitive (Kirkland & Tchkonia, 2017). The expression of p16 is often associated with senescent cell populations (Tchkonia *et al.*, 2010; Barberi *et al.*, 2013) and was shown to be elevated at both mRNA and protein level in DOX-induced senescent myoblasts and in replicative senescent myogenic cell populations. In the current study there was no significant difference in p16 protein expression between young and old hip fracture patients after similar time in culture even though there was striking differences in the expression of SA β-Gal. There was however a significant elevation of p16 mRNA in hip fracture cells compared to young after the same time in culture, which was above the significant increase both cell populations showed over early passage young cells (Figure 6.8). Upregulation of RNA always precedes protein expression as it must be present for its translation into the protein. However, RNA is not always translated into protein and therefore the discrepancy between the results could be due to the degradation of the RNA before being translated. More likely is the association with p16 being upregulated in deeply senescent cells as shown by the slow increase in p16 expression after DOX treatment. In those experiments SA β-Gal expression preceded the increase in p16.

Therefore, if these cell populations where left for longer in culture the protein expression of p16 may also have increased. As young early passage cells were not stained for p16 under the same experimental conditions, in the current experiments it is not known if both young and hip fracture patients at similar in culture expressed higher levels of p16 protein when compared to the young early passage.

Immunocytochemistry was also used to determine γH2aX expression within the nucleus of desmin positive cells in young and hip fracture patient cells at comparable times in culture. Here, a statistical trend for increased mean nuclear fluorescence intensity of γH2aX in hip fracture patient myoblasts was seen. Similarly to SA β-Gal and p16, a previous study did not show a difference in γH2aX between young and old adults but did see increased expression in senescent cells (Alsharidah *et al.*, 2013). However, in the replicative senescence study in this thesis only one of the replicative senescent myogenic cell populations showed a significant increase in γH2aX. Therefore, it should be remembered that γH2aX is a generic marker of DNA damage, an increase in which is associated with, but not specific to senescent cells therefore it cannot be used as a senescence marker in isolation (Nakamura *et al.*, 2008). The trend for increased γH2aX expression could be the result of using an older population of aged adults in the present study which might be revealing that very late in life skeletal muscle cell populations are starting to show the signs of senescence burden. Or that the later time point in culture than the Alsharidah *et al.*, (2013) study could also be confounding the results as γH2aX is increased as cells progress towards replicative senescence. Cells reaching replicative senescence start to have uncapped DNA ends as their telomeres reach critically short lengths initiating the DNA damage response, including increased γH2aX expression, eventually leading to proliferative arrest and cellular senescence (Nakamura *et al.*, 2008; d'Adda di Fagagna, 2008).

Overall, the combined results of the markers used have, for the first time, shown differences in senescence marker expression between young and old adult human myoblasts by using very old hip fracture patient myoblasts. It is unclear from the current experiments if this is due to the age of the donor or differences in response to the culture environment due to the relative late time point used for comparison, around 30 days in culture post biopsy. Having a higher burden of senescent cells can impair tissue functioning especially in a regenerative tissue such as skeletal muscle as it reduces the

available pool of proliferative cells to generate new myonuclei (Bigot *et al.*, 2008). Senescent cells can also impact surrounding cells by their alter secretory phenotype, their SASP (Nelson *et al.*, 2012).

Senescent cells synthesise and secrete a number of proinflammatory cytokines, chemokines, GFs, and proteases, collectively termed the SASP factors (Coppé *et al.*, 2010*a*). The SASP has been shown to be very specific to the individual even when exposed to the same induction stimulus such as DOX treatment as shown in chapter 5. In the present study, mRNA expression of a small panel of SASP factors was investigated, namely: CXCL5, IGFBP-7, MMP3, PAI-1, TGF-β, IGFBP-3, IL-8. This sub panel of the previously used SASP factors included those which showed significant changes and, in the case of TGF-β, shown previously to be increased in senescent myoblasts (Alsharidah *et al.*, 2013). Only three of the hip fracture populations had sufficient cells to undergo RNA analysis, one of which was only 40% desmin positive and therefore may not provide the most reliable SASP prolife of myogenic cells. However, due to the low n number it was retained for this preliminary analysis so allow for statistical analysis to be performed. Significantly, increased expression in hip fracture muscle derived cell populations was observed for CXCL5, and IL-8 compared to young cells after the same time in culture and young early passage cells. Significant increases over young cells after the same time in culture suggest that this effect is due to the cell origin and not just due to exposure to culture conditions. CXCL-5 is involved in the DDR, being upregulated during replicative exhaustion, telomere disruption and oncogenic stress (Coppé *et al.*, 2010*b*). This would support the results of increased senescent markers showing increased SA β-Gal, p16 and a trend for increased γH2aX. IL-8 is a proinflammatory cytokine, initiating an immune response at the secretory cells location (Acosta *et al.*, 2008). There was also a statistical trend for increased IGFBP-3 mRNA expression in hip fracture patients compared to early passage young muscle derived cells. IGFBP-3 has been demonstrated to inhibit cell division through its interaction with IGF-1 (Kelley *et al.*, 1996), and has been shown to interact with the DDR pathway thereby contributing to induction of cellular senescence (Elzi *et al.*, 2012; Ozcan *et al.*, 2016).

Caution should be applied when interpreting these SASP results due to the inclusion of one low desmin positive cell population together with only two other cell populations. The variability in the cell type SASP shown even after the same DOX stimuli (chapter 5) as

well as the interindividual variability suggest that looking at specific SASP factors expression could be misleading. Overall, there is a general trend for an increased inflammatory SASP in hip fracture patients, but this must be investigated further including more participants and more SASP factors.

Even though the hip fracture patients were showing signs of being more senescent and having an increased SASP than young donor cell populations they did not exhibit an impairment in differentiation capacity which has been shown in previous studies (Renault *et al.*, 2000; Alsharidah *et al.*, 2013; Barberi *et al.*, 2013). Senescent myotubes have been reported to be thinner and contain fewer nuclei compared to early passage myotubes, as well as the total number of nuclei fusing being lower (Bigot *et al.*, 2008); these traits were not observed in the current study as can be seen in Figure 6.7. Observing no difference in fusion index is similar to previous studies who showed early passage young and old donor cells have a similar fusion index (Alsharidah *et al.*, 2013; Barberi *et al.*, 2013). However, a more recent study has shown impaired fusion capacity in old donor myoblasts compared to young when they limited fusion index to nuclei within myotubes containing more than 3 myonuclei (Bechshøft *et al.*, 2019). However, the number of myogenin positive cells was not different between the age groups suggesting that the final fusion stage of differentiation may be impaired in older adults. This was supported by lower expression of myogenic fusion protein myomaker (Bechshøft *et al.*, 2019). Conversely, Bigot *et al.*, (2015) have shown that older donor myoblasts show higher fusion into myotubes and a lower number of Pax7 positive, undifferentiated, reserve cells. This preliminary study only investigated fusion index and therefore conclusions cannot be drawn on the mechanisms behind the fusion results observed. There are also inconsistencies in the methodology of comparison used due to using pre-existing young differentiation data. The old hip fracture patients were differentiated for seven days because previous work has suggested that differentiation may not be impaired but delayed so the decision was made to extend the differentiation process to seven days instead of stopping after four days, which was when the young cells were analysed for fusion index. However, a previous study have allowed senescent cells to differentiate for seven days and still see marked impairment of fusion index (Alsharidah *et al.*, 2013). Overall, it is of interest to observe no impaired myogenic fusion of hip fracture patients even though they express higher levels of senescent markers. It is not clear if this is due to inherent factors within these aged hip fracture cell

populations or from allowing the cells longer to differentiate making up for any delay in activation of the myogenic programme. It would be of interest to determine the phenotype of the, unfused, reserve cells in these cell populations to determine if retaining fusion competence is at the expense of maintaining a larger cell population which retains proliferative potential.

This study set out to use a more well-defined population of older people than previous studies with hospital patients undergoing hip fracture surgery donate muscle tissue removed during their surgery. It also attempted to get the oldest participants possible and the age criteria was set to 70+ years for recruitment. However, no further information is available on the phenotype or lifestyle of the hip fracture patients as ethical approval was not granted for access to patient records for these participants. These hip fracture patients may have had underlying conditions such as cancer, diabetes, or heart disease which directly, or through their prescribed treatments could be affecting the myogenic cells investigated. It could also be possible for a hip fracture patient to be a highly active individual who fractured their hip by falling off their bike and were not frail. Furthermore, the distribution of cell types throughout skeletal muscle is not homogeneous, for example there are more connective tissue cells towards the tendinous ends of muscles (Gillies & Lieber, 2011). Therefore, the specific site from which the muscle biopsy is taken may affect the proportions of the extracted cell population. In this thesis all of the young participant muscle biopsies samples were taken from the mid belly of the *vastus lateralis* to standardise the biopsy location. However, as the hip fracture patient samples were taken from the site of their operation, they originated from the proximal end of the *vastus lateralis* which is likely to contain more connective tissues cells. Therefore, these results must be taken in the context of preliminary results as we are unsure if the effects are truly due to differences in the cell populations.

The slow proliferation of the hip fracture cell populations prevented early passage comparisons suggesting that the cells compared are well on their trajectory to replicative senescence. As this trajectory is highly individual the different time course to senescence could be confounding the results obtained. However, even with these limitations the result of this pilot study suggests that there may be an aged population of human who do experience signs of senescence within skeletal muscle cell populations. This warrants further investigation to understand where these differences are and if they are also

present in other aged people or if they are unique to the trauma involved with something as severe as a hip fracture.

Chapter 7: General discussion

Cellular senescence is a key feature of ageing tissues in both animal models and humans therefore the importance of studying cellular senescence is that it provides insights into how cellular behaviour and function is altered in ageing tissues. Targeting senescence has tremendous potential to significantly improve healthspan and alleviate age-associated dysfunctions, frailty and tissue fibrosis (Borghesan *et al.*, 2020). The removal of senescent cells has been shown to improve both the healthspan and life span of mice in both genetic knock out models as well as free living animals treated with senolytic drugs (Kirkland & Tchkonia, 2017). Studies of *in vitro* senescent cells have shown the inherent heterogeneity of senescent cell populations depending on intrinsic and extrinsic factors including cell type, senescence inducer, tissue of origin, and environmental conditions. Although cellular senescence has been consistently shown in many tissues, the findings within post mitotic such as skeletal muscle are both under researched and unclear (Tuttle *et al.*, 2020). Therefore, using a human primary cell culture system this thesis set out to: 1) characterise the senescent phenotype of human primary $CD56^{+ve}$ skeletal muscle precursor cells and the $CD56^{-ve}$ skeletal muscle origin fibroblasts after CD56 MACS sorting 2) to investigate this senescent myogenic phenotype within a very old, and likely frail, population of patients undergoing hip fracture surgery to determine if senescence was present within aged myogenic cell populations 3) additionally, automated image analysis programmes were developed for the quantification of the immunofluorescence staining in order to help address these aims.

7.1. Overview of findings

7.1.1. Image analysis programs

Determining expression of markers is often performed manually using binary classifications as positive or negative based on human observation. This form of analysis, although simple, is subject to observer bias and misses a lot of biological information within an image (Lee & Kitaoka, 2018). Using image analysis programs allows individual pixel values to be quantified within specific regions of interest and therefore gives a better

representation of the marker expression level within the cell population. The automation of these programs decreases the analyse time substantially as well as removing bias and improving the reliability of data acquired. Therefore, automated image analysis programs were developed to analyse different image types throughout this thesis.

The image analysis programs developed were to:

1) Count the number of cells which expressed a certain cell type marker, e.g. desmin as a marker of myoblasts or TE7 as a marker of fibroblasts
2) Analyse the pixel intensities of a marker, e.g. cell cycle inhibitor p16, within regions of interest which define each individual nucleus within an image
3) Analyse the pixel intensities of a marker, e.g. cell cycle inhibitor p16, within regions of interest which define each individual nucleus of a given cell type, as defined by a cell type specific marker such as desmin for myoblasts or TE7 for fibroblasts, within an image
4) Count the number of nuclei incorporated within myotubes as a percentage of the total number of nuclei within a field of view

These automated image analysis programs were successfully used throughout this thesis showing significant changes in marker expression and fusion index across all research questions. Further improvements to the methods to analyse three dimensional myotube formation to try to separate overlapping myotubes allowing accurate myotube volume measures are under way, as well as, further automation on the output data restructuring into the same workflow to allow ease of use for other researchers.

7.1.2. Replicative senescence

Previous studies investigating senescence within human primary skeletal muscle cells have been hampered by issues of myogenic expression of the cell populations extracted from muscle biopsies (Schafer *et al.*, 2005; Alsharidah *et al.*, 2013). This study employed a CD56 MACS sort in order to enrich, to greater than 95% desmin expression, the myogenic cell population before passaging to replicative senescence to try to prevent the issues of variable desmin expression. The purification of myogenic cell populations from the other precursor cell populations in skeletal muscle allowed both for a better understanding of the phenotype of these myogenic cells but also the opportunity to investigate the characteristics of the other precursor cell populations from the same

tissue origin. This study allowed for the first investigation and comparison of the $CD56^{-ve}$, predominantly $TE7^{+ve}$ fibroblasts, cell populations from the same muscle biopsy as the $CD56^{+ve}$ myoblasts.

The main findings were that:

1) CD56 purification does not prevent the accumulation of fibroblasts within highly enriched desmin positive cell cultures
2) The two myogenic cell populations that reached replicative senescence were not identical in phenotype at replicative senescence
3) $CD56^{-ve}/TE7^{+ve}$ fibroblasts do not reach replicative senescence within the same time frame as myoblasts from the same muscle biopsy, maintaining high proliferative activity and low senescent marker expression

What was of most interest was the vastly different behaviours of the two different cell populations from the same biopsies under cell culture conditions. The $TE7^{+ve}$ fibroblasts were the most proliferative of the $CD56^{-ve}$ cell populations becoming roughly 100% pure across time in culture. They also showed no signs of approaching cellular senescence when the myogenic cell populations from the same biopsies were either senescent or themselves becoming overrun with fibroblasts. This difference in replicative capacity could be due to the myoblasts having undergone more divisions *in vivo* than the fibroblasts therefore reducing their telomere length and proliferative potential *ex vivo*. Or it could be due to the fibroblasts being more resistant to the stresses of the artificial culture environment such as, higher than physiological oxygen tension, the potential effect of the culture environment are discussed further later in this discussion. Another possible explanation is that the fibroblast cell population are maintained by another stem cell population external to skeletal muscle providing fibroblasts which have undergone fewer divisions than the satellite cells which themselves are thought to not have a significant replenishment from an external adult stem cell source. The discrepancy between replicative capacity and virality of the skeletal muscle origin fibroblasts highlights that all cell populations within skeletal muscle must be considered when evaluating the effecting of ageing on this tissue.

It was also of interest to note that CD56 sorting became less effective at purifying desmin positive cells over time in culture. CD56 has been shown to stay present even through terminal differentiation of human primary myoblasts (Agley *et al.*, 2015) but has

been shown to vary in expression over time in culture (Meng *et al.*, 2011). With the recent discovery of CD82 as another marker of myogenic cells it should be investigated to see if it also fluctuates over serial passaging (Alexander *et al.*, 2016). Future work to develop a method for late passage purification of myoblasts would be of great benefit to senescence research as it would be able to prevent the overrunning of fibroblasts seen in the current work. Sorting based on markers such as desmin or PAX7 would require either permeabilisation of the cell populations, preventing the use of the sorted cells for further culture experiments, whereas, the genetic manipulation of these markers to express GFP, which would allow the sorting of live cells, requires altering the genetic makeup of the cells potentially causing unknown affects to the cells.

Overall, these replicative senescence experiments have highlighted differences in proliferative capacity of the two main human muscle precursor cell populations however the technical challenges associated with generating senescent populations of these cells types mean that currently other methods are required to analyse the senescent phenotype of these cell populations. The next set of experiment sort to address these issues.

7.1.3. DOX induced senescence

To circumvent the problems observed with the replicative method of senescence induction a premature induction of senescence was used on the same cell populations. Both myoblasts and fibroblasts were treated with DOX to induce an accelerated senescent phenotype in the same cell populations. DOX was chosen as it had been successfully developed and utilised for use with other type of human muscle cell populations such as cardiac and smooth muscle (Piegari *et al.*, 2013; Bielak-Zmijewska *et al.*, 2014; Lewis-McDougall *et al.*, 2019). These senescent cell poulations could then be characterised and compared to investigate the differing senescent cell phenotypes from the same tissue.

The main findings were that:

1) Both myoblasts and fibroblasts are induced to become senescent after DOX treatment
2) The most consistent marker of cellular senescence was SA β-Gal in combination with the lack of Ki67.

3) Although the entry into senescence was more heterogenous with DOX treatment there was still large variability both between and within cell types in regard to SASP factor expression
4) difference senescent profile between myoblasts and fibroblasts from the same muscle sample

Treating both cell populations with DOX was successful in generating populations of senescent cells which maintain their cell type purity across time allowed for the senescent phenotyping of these cell populations. Of the markers used in this study, SA β-Gal was the clearest marker of senescent as both cell types do not express the marker when still proliferative. However, the cell cycle inhibitor most frequently associated with cellular senescence, p16, was less clear as a marker of senescence. The expression of p16 did not demark every senescent cell and was only upregulated after extended time in cell culture, much later than expression of SA β-Gal and loss of Ki67. These results, in combination with the early increase in p21 expression would suggest that p21 is involved in the instigation of the senescent state whereas p16 is more a marker of deep senescence. Although, further work with these specific cells types is needed to confirm this finding.

The variability in SASP factor expression from the same cell type of different individual highlights important issues regarding the use of cell lines in human research. Using cell lines, genetic clones of a single cell, masks much of the variability seen when using heterogenous populations of cells from different individuals (discussed further in section 7.3). This work also highlights issues with understanding the *in vivo* secretion of senescent cells marked as senescent via markers such as SA β-Gal. This work shows that the expression of these senescent markers does not determine that cell's specific secretory profile. This is further complicated by the differences in SASP factor expression between the two different cell types from the same tissue. This is important for understanding which cell types are causing the elevated tissue levels of SASP factors in older muscle as skeletal muscle consists of multiple cell types which could become senescent and it would be unclear which cells were responsible for the elevated SASP factors.

7.1.4. Hip fracture patients

With most previous human primary cell culture studies finding no differences in senescence burden within muscle precursor cell populations between young and old participants it was thought that senescence may not be an issue in this cell type within healthy other humans. However, the findings of Sousa-Victor *et al.*, (2014) showing an increased senescent burden in "geriatric" adults it was thought that there may be cases where the very old and frail may have increased senescence burden which have not be identified when younger, healthier groups of older people have been investigated. This study therefore aimed to investigate a population of very old and likely frail individuals who were undergoing hip fracture surgery to determine if in extreme cases senescence started to become apparent.

The main findings were that:

1) Hip fracture patient cells took longer to expand after defrosting than cells from healthy young donors
2) Hip fracture patients had higher senescent markers and elevated SASP factor expression compared to young cells at early passage and after similar times in culture
3) Even with higher senescent cell burden hip fracture patients' myoblasts still retain the ability to differentiate to the same level as young early passage cells

This study must be considered as a pilot study due to the limitations of the cells being used having undergone culture expansion. This expansion brings in many other potential contributing factors beyond the inherent differences in the cell populations such as, resistance to culture stresses or variability in freeze thaw effects on cell populations. However, considering these limitations, cell populations from old hip fracture patients showed elevated senescence markers compared to those from young individuals after similar time under culture conditions. Interestingly, myogenic differentiation did not seem to be impaired in these patients even though they had increased numbers of senescent cells. An interesting hypothesis to explore further is the difference in fusion between young and old donor cells, as Bigot *et al.*, (2015) suggest that cells from older donors fuse more readily than young reducing the reserve cell population. The authors suggest that these reserve cells are indicative of the cells which will replenish the satellite cell population *in vivo*. This would provide an explanation for the reduction in satellite cell

number seen with increasing age. The next step with the current study should investigate the makeup of the non-fused cell population and determine if they are indeed more satellite cell like and if they are reduced in older individuals. Having shown differences between old hip fracture patients and young healthy individuals opens important questions about whether these differences are due to the lifestyle habits or the trauma of suffering a hip fracture. Therefore, there are many potentially interesting avenues of investigation brought to light by these preliminary results which require further investigation.

7.2. Senescent marker panels

This study utilised a small panel of senescence associated markers however they are not an exhaustive list of senescence associated markers. It is becoming more apparent that senescent cells exhibit a wide range of expression changes that are not categorically expressed in all cells deemed to be senescent (Kirkland & Tchkonia, 2017). Therefore, it is commonplace to use multiple markers to identify senescent cells. This is further highlighting the diversity of classifying cellular senescence. Due to the many ways of a cell entering a senescent state it is likely that there is not a clear phenotype but a general pattern of expression changes most clearly identifiable by a change in secretory profile to become more inflammatory in nature. However, it has also been shown that some cells expressing senescent markers do not have an elevated inflammatory SASP further confusing the phenotype. This varied expression was also seen in both cell types investigated in the current work. Now that populations of senescent cells have been generated from these two cell types further characterisation of their senescence associated marker expression could further characterise their cell type specific senescence marker expression. However, what is apparent from the current work is that the senescent marker expression may not be heterogenous across the same cell population or between different individual donors. Using a wider panel of senescence associated makers may lead to better understand of the variability in marker expression within a cell population and therefore identify more targeted cell type markers.

7.3. Investigating the Senescence Associated Secretory Phenotype

One of the most prominent features of senescent cells is their altered secretory phenotype, the SASP (Coppé *et al.*, 2008). The chronic expression of SASP factors can lead to tissue dysregulation and start a cycle of inducing senescence in neighbouring cells (Adams, 2009). Careful investigation into the components of SASPs and their mechanism of action, may improve our understanding of the pathological backgrounds of age-associated diseases (Byun *et al.*, 2015). Studies of SASP expression of different cell types have suggested that there may be common senescence-associated gene signatures but that there are cell type, tissue, senescence inducer and environmental conditions that can influence the makeup of the SASP (Maciel-Barón *et al.*, 2016; Hernandez-Segura *et al.*, 2017; Casella *et al.*, 2019; Basisty *et al.*, 2020). It was therefore thought to be important to try to understand the makeup of the SASP from the main human skeletal muscle cell types as it may lead to the discovery of novel cell type specific factors or biomarkers of senescence. For example, a previous study found that senescence human myoblasts had increased levels of secreted TGF-β which was sufficient to inhibit the differentiation of non-senescent myoblasts (Alsharidah *et al.*, 2013). The work presented in this thesis has added further evidence of the heterogeneity within the SASP, showing that even when induced to become senescent via the same stimulus there is large variation between individual donors, between difference cell types from the same tissue, as well as, within different cells of the cell types. This phenotypic heterogeneity has led to suggestions that there may be different subsets of senescent cells with a population which will require single cell technologies to fully understand (Borghesan *et al.*, 2020). The DOX induced senescence protocol developed can be used to generate SASP producing senescent cells for both myoblasts and fibroblasts to investigate individual cell differences. The DOX method also allows for investigation of the effect of SASP section from senescent skeletal muscle origin fibroblasts on the functioning of non-senescent myoblasts and *vice versa.*

7.4. Benefits and limitations of a cell culture model for human cellular senescence

This thesis utilised a human primary cell culture model to investigate senescence within purified cell populations. The addition of MACS sorting allows for a system where cell type specific senescent cells can be investigated allowing for a better understanding of cell type differences when using bulk analysis techniques such as RNA and protein expression. Using impure cell populations clouds cell type specific expression as has been shown by the studies presented in this thesis showing differential expression of SASP factors between the two main skeletal muscle precursor cell populations.

Human primary cell populations also show the differences within a cell type extracted from the same donor. This work highlights the importance of using human primary cell populations in culture conditions as they demonstrate the heterogeneity between different individuals, as well as, within an individual cell population. Cell lines are favoured for their ease of use however, using sub clones of clonal populations drastically reduces the cell to cell variability. Cell lines have also been immortalised changing a key *in vivo* characteristic which may also affect their functioning under culture conditions.

The use of cell culture also has the benefit of understanding the effect of senescence on cellular function. Studies which characterise cellular markers, such as histological studies or RNA seq, are unable to assess functional behaviour of the cells therefore miss the most important measure of the effect on the cell. For example, the discrepancy in fusion index between induced senescent cells having poor fusion whereas hip fracture patient myoblasts with increased senescence do not seem to have impaired fusion shows a functional difference even though both populations express the same senescent markers. These differences allow for mechanistic manipulation of the cells to either return the cells to functioning states or prevent their impact on the functioning of local healthy cells. Cell culture systems also allow for the manipulation of cellular processes and pathways to determine the effect of certain compounds, such as high levels of SASP factors. These experiments could potentially uncover treatments that could potentially slow the progression of age-related muscle loss. Thus, prolonging the functional independence of older people and potentially help with satellite cell exhaustion conditions such as muscular dystrophies.

Although there are many benefits to using human primary cell culture, there are limitations to all cell culture systems. A specific limitation to skeletal muscle cell culture is that satellite cells are usually in a quiescent state within their anatomical niche *in vivo*. The function of the satellite cell anatomical niche is to maintain cellular quiescence by preventing satellite cells from being exposed to signal which could cause them to activate or become damaged unnecessarily. Cells under culture conditions have been removed from this niche environment and have become activated. The length of time in culture has been shown to alter the transcriptome of satellite cell populations (Charville *et al.*, 2015). With suggestion that these changes are started immediately after extraction, during the enzymatic isolation process (Machado *et al.*, 2017). The cell extraction and sorting protocol employed throughout this thesis incubates all cells extracted from the biopsy for 7 days before starting any experiment and therefore changes in the transcriptome are likely to have started. What is interested is that previous studies have suggested that this length of time in culture is one of the causes of showing no difference between young and old cells however the current study using hip fracture patients show that some differences may be retained. The cell culture studies may also be limited by the fact that culture conditions aim to provide the optimal growth environment for cells. cell culture may remove intrinsic differences between young and old in vivo cell populations is that the culture environment is a “youthful environment”, so old cells are free from extrinsic circulating factors which are present in the aged circulation. A youthful environment, fresh media, could alter the phenotype of these cells as would be suggested by the findings of Conboy *et al.*, (2005) that old cells behave like young cells in a youthful environment. Several studies have shown that changes to the circulatory environment are, at least in part, responsible for the impaired regenerative potential in aged muscle. Mouse models have shown that rejuvenating the environment within which old muscles are exposed improves their regenerative function. Autografting elderly extensor digitorum longus muscle into young animals showed better improvement in muscle mass and force generation than when young muscles were transplanted into old animals (Carlson & Faulkner, 1989). Whereas, Conboy *et al.*, (2005) conjoined the circulatory systems of young and old mice, termed heterochronic parabiosis, and showed that the young circulatory environment improved the old mouse muscle regeneration. The new muscle in the old mice was from the old mice's satellite cells not the young animal suggesting an improved rejuvenation in the old satellite cells not just replacement with donors from the young animal. However, this artificial culture environment is very

different even to the young *in vivo* environment where the cells are protected in the niche. This is strikingly obvious by the fact that all cultured cells are in an activated state whereas in vivo they are predominantly quiescent. They rapidly down regulate PAX7 and commit to the myogenic lineage and are known as myogenic precursor cells.

A further issue surrounding the cell culture system used is that of oxygen tension. The system used in the present thesis maintains cells under atmospheric oxygen tension, 21% oxygen. This oxygen tension is much higher than these cells would be exposed to in vivo which is suggested to fluctuate from anoxic through to 4% oxygen (Keeley & Mann, 2019). The hyperoxic conditions in the current cell culture system have been shown to affect cellular behaviour. Specifically, with regards to senescence, SASP factor expression has been shown to differ at different oxygen tensions adding yet another variable to understanding the phenotype of senescent cells.

Although there are many limitations to cell culture studies their use is invaluable to understanding cellular function. It has often been suggested that cell culture systems do not translate well into human interventions very efficiently. However, developments are being made to try to make culture systems more physiologically relevant. The culturing of cells at tissue specific "physioxic" conditions, alongside 3D culturing utilising biomaterials and the development of co-culture systems are all allowing for more physiologically relevant manipulations of cells which are more likely to behave like in vivo cell populations. However, whilst these developments are moving the cell culture field towards more physiological conditions there will always be effects of removing cells from their native integrative environment into a model system. These limitations must always be considered however they do not outweigh the benefits of using cell culture systems in conjunction with other methodologies.

7.5. Future directions

This work has shown that artificially induced senescent cells share some commonalities to senescent cells from a population of very old, and likely frail, humans. However, although there was a general trend for senescent cells to express similar markers there was a large inter individual, as well as, cell to cell variability in SASP expression within the cell populations. The variability observed is very likely to be representative of the inherent *in vivo* biological variability due to the multitude of intrinsic

and extrinsic stimuli individual cells are exposed to. This biological variability is greatly reduced by using genetically identical cell lines or littermate animal models. To develop a greater understanding of the complex interactions within the human physiological system the biological variability needs to be present in the model systems. The first major step towards this would be to physiologically characterise the individuals from which the cell populations are extracted. Having a better understanding of the overall physiological environment from which the cells are taken is more likely to yield interpretable results.

One of the key overlapping factors of frailty and sarcopenia is low physical activity levels of the individuals, which is an important factor when considering rate of muscle functionality decline (Fried *et al.*, 2001; Dennison *et al.*, 2017; Harridge & Lazarus, 2017). There is still a clear decline in muscle function in highly active master athletes, however, the magnitude of muscle function decline is slower than that of sedentary individuals (Pollock *et al.*, 2015; Seals *et al.*, 2016). Having shown a significantly increased senescent burden in cells from hip fracture patients, a population likely to be sedentary, understanding if a lack of physical activity is involved in the senescent phenotype of these patients by comparing their cellular function to masters athletes would provide important insight into human physiological ageing.

The current study along with previous studies have used very minimal characterisation of the people from which their cell populations are extracted (Lazarus & Harridge, 2010). Often just using an age bracket and generic criteria of “otherwise healthy”. A deep physiological phenotyping of these individual will provide a much better context of the environment from which these cells are extracted. Skeletal muscle is a key effected tissue from the benefits of physical activity and therefore understanding the physical activity and muscle quality of the muscle from which these samples are taken would provide potentially important insight into the ageing and physical activity interaction with regards to skeletal muscle loss. Specifically, within the context of cellular senescence, exercise is already hypothesised to be a potential senolytic and therefore this study lays the foundations for potential experiments investigate the effects of exercise within these hip fracture patient populations to reduce senescent burden.

Alongside this physiological characterisation of the individual donors, the cell populations should be characterised as immediately as possible to determine the in vivo phenotype. A very recent study employed single cell RNA seq on all extracted nuclei from

tissue samples of human skeletal muscle (Rubenstein *et al.*, 2020). This technique provides the best in vivo characterisation of all cell types within skeletal muscle. This small-scale study has identified 11 mono-nuclear cells types within skeletal muscle. Applying this technology on physiological characterised individual of different aged would yield key information about the ageing and physical activity interaction within the make-up of cell populations within skeletal muscle. However, as discussed previously these techniques are unable to assess function of these cell populations even if they do determine expression differences between groups. Therefore, using this technology alongside cell culture of the same cell populations will provide a greater understanding of *in vivo* population phenotype, as well as, the cell populations functional behaviour. Having this single cell phenotype will also allow for a better understanding of what effects the cell culture environment is having on the transcriptome of the extracted cells. This will provide a reference transcriptome to determine the best cell culture parameters to best retain the cells *in vivo* phenotype and therefore better optimise the cell culture models for translational findings. Work is currently underway to develop an immediate isolation extraction protocol to yield sufficient cells to undertake this analysis from physiological characterise young and old individual of differing physical activity levels.

The development of the DOX induced senescence model has allowed for the probing of the mechanisms underpinning he senescent phenotype and functional impairments of senescent cells such as, the inhibition of myogenic differentiation. Generating senescent cell populations is important due to the limitation of extracting senescent cells from *in vivo* populations which are quickly overrun by proliferating cells after the extraction process. Previous work in the Harridge laboratory has characterised the Wnt-β-catenin signalling pathway in healthy young human primary cells and showed that interfering with this pathway impaired differentiation (Agley *et al.*, 2017). Therefore, investigating this signalling pathway within the context of senescence would provide a logical first step into probing the resulting impairment in differentiation. The populations of artificially generated senescent cells can also be co-cultured with otherwise healthy cells or myotubes to determine the effect of the myogenic SASP on healthy cell function. This work would provide important information about the ageing process and how the senescent bystander effect and inflammageing in the microenvironment may be affecting both satellite cell and muscle fibre maintenance. Finally, senolytic drugs can be tested to see their efficacy at removing senescent cells within human primary skeletal muscle origin

cells and then compared with the effects of exercised human serum at removing senescent cells to help understand if exercise may in itself act like a senolytic agent.

7.6. Final conclusions

The age-related decline in skeletal muscle mass and function is inevitable being observed in even the most highly active of individuals. This phenomenon is an integrative physiological problem with multiple causal mechanisms. The present work aimed to further investigate what, if any, role the process of cellular senescence was a contributing factor within the main cell populations which regenerate skeletal muscle, myoblasts and fibroblasts. It aimed to provide a better characterisation of the senescent phenotype of the main cell types within skeletal muscle and has shown a chronologically aged human population who show signs of increased senescence. This study also highlighted the heterogeneity within cell populations deemed to be senescent. When using only a small panel of markers interindividual and cell to cell variability was shown in senescent phenotype. What ageing research in humans in general is lacking is the use of highly characterised individuals in studies. This work showed that using very old hip fracture patients successfully identified higher senescence in this likely to be frail population. Having a worst-case scenario population thus allows for differences to be determined and allow for physiological intervention to be tested. Such as the lifelong involvement in exercise training. The use of highly active master athlete would provide an exercise continuum with frail hip fracture patients through to these master athletes allowing for a whole body physiological, down to an individual cell to cell, characterisation of how physical activity in interacting with the inherent ageing process. The integration of methodologies such as single cell RNA seq and human primary cell culture on highly characterised donor cell populations will provide much needed clarity to answering the questions of ageing within skeletal muscle.

References

Acosta JC, O'Loghlen A, Banito A, Guijarro M V, Augert A, Raguz S, Fumagalli M, Da Costa M, Brown C, Popov N, Takatsu Y, Melamed J, d'Adda di Fagagna F, Bernard D, Hernando E & Gil J (2008). Chemokine Signaling via the CXCR2 Receptor Reinforces Senescence. *Cell* **133,** 1006–1018.

Adams PD (2009). Healing and Hurting: Molecular Mechanisms, Functions, and Pathologies of Cellular Senescence. *Mol Cell* **36,** 2–14.

Agley CC, Lewis FC, Jaka O, Lazarus NR, Velloso C, Francis-West P, Ellison-Hughes GM & Harridge SDR (2017). Active GSK3β and an intact β-catenin TCF complex are essential for the differentiation of human myogenic progenitor cells. *Sci Rep* **7,** 1–16.

Agley CC, Rowlerson AM, Velloso CP, Lazarus NL & Harridge SDR (2015). Isolation and Quantitative Immunocytochemical Characterization of Primary Myogenic Cells and Fibroblasts from Human Skeletal Muscle. *J Vis Exp*1–14.

Agley CC, Rowlerson AM, Velloso CP, Lazarus NR & Harridge SDR (2013). Human skeletal muscle fibroblasts, but not myogenic cells, readily undergo adipogenic differentiation. *J Cell Sci* **126,** 5610–5625.

Agley CC, Velloso CP, Lazarus NR & Harridge SDR (2012). An Image Analysis Method for the Precise Selection and Quantitation of Fluorescently Labeled Cellular Constituents: Application to the Measurement of Human Muscle Cells in Culture. *J Histochem Cytochem* **60,** 428–438.

Alcorta D a, Xiong Y, Phelps D, Hannon G, Beach D & Barrett JC (1996). Involvement of the cyclin-dependent kinase inhibitor p16 (INK4a) in replicative senescence of normal human fibroblasts. *Proc Natl Acad Sci U S A* **93,** 13742–13747.

Alexander MS, Rozkalne A, Colletta A, Estrella E, Kunkel LM, Correspondence EG, Spinazzola JM, Johnson S, Rahimov F, Meng H, Lawlor MW & Gussoni E (2016). CD82 Is a Marker for Prospective Isolation of Human Muscle Satellite Cells and Is Linked to Muscular Dystrophies. **19,** 800–807.

Allbrook DB, Han MF & Hellmuth AE (1971). Population of Muscle Satellite Cells in Relation to Age and Mitotic Activity. *Pathology* **3,** 233–243.

Allen JR, Ross ST & Davidson MW (2013). Sample preparation for single molecule localization microscopy. *Phys Chem Chem Phys* **15,** 18771–18783.

Allsopp RC, Vaziri H, Patterson C, Goldstein S, Younglai E V., Futcher AB, Greider CW & Harley CB (1992). Telomere length predicts replicative capacity of human fibroblasts. *Proc Natl Acad Sci U S A* **89,** 10114–10118.

Alsharidah M, Lazarus NR, George TE, Agley CC, Velloso CP & Harridge SDR (2013). Primary human muscle precursor cells obtained from young and old donors produce similar proliferative, differentiation and senescent profiles in culture. *Aging Cell* **12,** 333–344.

De Angelis A, Piegari E, Cappetta D, Marino L, Filippelli A, Berrino L, Ferreira-Martins J, Zheng H, Hosoda T, Rota M, Urbanek K, Kajstura J, Leri A, Rossi F & Anversa P (2010). Anthracycline cardiomyopathy is mediated by depletion of the cardiac stem cell pool and is rescued by restoration of progenitor cell function. *Circulation* **121,** 276–292.

De Angelis L, Berghella L, Coletta M, Lattanzi L, Zanchi M, Cusella-De Angelis MG, Ponzetto C & Cossu G (1999). Skeletal myogenic progenitors originating from embryonic dorsal aorta coexpress endothelial and myogenic markers and contribute to postnatal muscle growth and regeneration. *J Cell Biol* **147,** 869–877.

Arena ET, Rueden CT, Hiner MC, Wang S, Yuan M & Eliceiri KW (2017). Quantitating the cell: turning images into numbers with ImageJ. *Wiley Interdiscip Rev Dev Biol*; DOI: 10.1002/wdev.260.

Asakura A (2012). Skeletal Muscle-derived Hematopoietic Stem Cells: Muscular Dystrophy Therapy by Bone Marrow Transplantation. *J Stem Cell Res Ther*; DOI: 10.4172/2157-7633.s11-005.

Asfour HA, Allouh MZ & Said RS (2018). Myogenic regulatory factors: The orchestrators of myogenesis after 30 years of discovery. *Exp Biol Med* **243,** 118–128.

Baker DJ, Childs BG, Durik M, Wijers ME, Sieben CJ, Zhong J, Saltness RA, Jeganathan KB, Casaclang Verzosa G, Pezeshki A, Khazaie K, Miller JD & Van Deursen JM (2016). Naturally occurring p16 Ink4a -positive cells shorten healthy lifespan. *Nature* **530,** 184–189.

Baker DJ, Wijshake T, Tchkonia T, LeBrasseur NK, Childs BG, van de Sluis B, Kirkland JL &

van Deursen JM (2011). Clearance of p16Ink4a-positive senescent cells delays ageing-associated disorders. *Nature* **479,** 232–236.

Baraibar MA, Hyzewicz J, Rogowska-Wrzesinska A, Bulteau A-L, Prip-Buus C, Butler-Browne G & Friguet B (2016). Impaired energy metabolism of senescent muscle satellite cells is associated with oxidative modifications of glycolytic enzymes. *Aging (Albany NY)* **8,** 3375–3389.

Barberi L, Scicchitano BM, De Rossi M, Bigot A, Duguez S, Wielgosik A, Stewart C, McPhee J, Conte M, Narici M, Franceschi C, Mouly V, Butler-Browne G & Musarò A (2013). Age-dependent alteration in muscle regeneration: the critical role of tissue niche. *Biogerontology* **14,** 273–292.

Basisty N, Kale A, Jeon OH, Kuehnemann C, Payne T, Rao C, Holtz A, Shah S, Sharma V, Ferrucci L, Campisi J & Schilling B (2020). A proteomic atlas of senescence-associated secretomes for aging biomarker development. *PLoS Biol* **18,** e3000599.

Bassey EJ, Fiatarone MA, O'Neill EF, Kelly M, Evans WJ & Lipsitz LA (1992). Leg extensor power and functional performance in very old men and women. *Clin Sci* **82,** 321–327.

Beccafico S, Puglielli C, Pietrangelo T, Bellomo R, Mediche S & Studi CC (2007). Age-Dependent Effects on Functional Aspects in Human Satellite Cells. **352,** 345–352.

Beccafico S, Riuzzi F, Puglielli C, Mancinelli R, Fulle S, Sorci G & Donato R (2011). Human muscle satellite cells show age-related differential expression of S100B protein and RAGE. *Age (Omaha)* **33,** 523–541.

Bechshøft CJLL, Jensen SM, Schjerling P, Andersen JL, Svensson RB, Eriksen CS, Mkumbuzi NS, Kjaer M & Mackey AL (2019). Age and prior exercise in vivo determine the subsequent in vitro molecular profile of myoblasts and nonmyogenic cells derived from human skeletal muscle. *Am J Physiol Physiol* **316,** C898–C912.

Begley LA, Kasina S, Mehra R, Adsule S, Admon AJ, Lonigro RJ, Chinnaiyan AM & Macoska JA (2008). CXCL5 promotes prostate cancer progression. *Neoplasia* **10,** 244–254.

Bergström J (1962). Muscle electrolytes in man. *Scand J Clin Lab Investig* **14,** 511–513.

Berlage T (2005). Analyzing and mining image databases. *Drug Discov Today* **10,** 795–802.

Bielak-Zmijewska A, Wnuk M, Przybylska D, Grabowska W, Lewinska A, Alster O, Korwek Z, Cmoch A, Myszka A, Pikula S, Mosieniak G & Sikora E (2014). A comparison of replicative senescence and doxorubicin-induced premature senescence of vascular smooth muscle cells isolated from human aorta. *Biogerontology* **15,** 47–64.

Bigot A, Duddy WJ, Ouandaogo ZG, Negroni E, Mariot V, Ghimbovschi S, Harmon B, Wielgosik A, Loiseau C, Devaney J, Dumonceaux J, Butler-Browne G, Mouly V & Duguez S (2015). Age-Associated Methylation Suppresses SPRY1, Leading to a Failure of Re-quiescence and Loss of the Reserve Stem Cell Pool in Elderly Muscle. *Cell Rep* **13,** 1172–1182.

Bigot A, Jacquemin V, Debacq-Chainiaux F, Butler-Browne GS, Toussaint O, Furling D & Mouly V (2008). Replicative aging down-regulates the myogenic regulatory factors in human myoblasts. *Biol Cell* **100,** 189–199.

Biressi S, Tagliafico E, Lamorte G, Monteverde S, Tenedini E, Roncaglia E, Ferrari S, Ferrari S, Cusella-De Angelis MG, Tajbakhsh S & Cossu G (2007). Intrinsic phenotypic diversity of embryonic and fetal myoblasts is revealed by genome-wide gene expression analysis on purified cells. *Dev Biol* **304,** 633–651.

Bjornson CRR, Cheung TH, Liu L, Tripathi P V., Steeper KM & Rando TA (2012). Notch signaling is necessary to maintain quiescence in adult muscle stem cells. *Stem Cells* **30,** 232–242.

Blackburn EH, Epel ES & Lin J (2015). Human telomere biology: A contributory and interactive factor in aging, disease risks, and protection. *Science (80-)* **350,** 1193–1198.

Blanco-Bose WE, Yao CC, Kramer RH & Blau HM (2001). Purification of mouse primary myoblasts based on α7 integrin expression. *Exp Cell Res* **265,** 212–220.

Blasco MA (2005). Telomeres and human disease: Ageing, cancer and beyond. *Nat Rev Genet* **6,** 611–622.

Blasco MA, Lee HW, Hande MP, Samper E, Lansdorp PM, DePinho RA & Greider CW (1997). Telomere shortening and tumor formation by mouse cells lacking telomerase RNA. *Cell* **91,** 25–34.

Blau HM & Webster C (1981). Isolation and characterization of human muscle cells. *Proc*

Natl Acad Sci U S A **78,** 5623–5627.

Bodnar AG, Ouellette M, Frolkis M, Holt SE, Chiu CP, Morin GB, Harley CB, Shay JW, Lichtsteiner S & Wright WE (1998). Extension of life-span by introduction of telomerase into normal human cells. *Science (80-)* **279,** 349–352.

Boldrin L, Muntoni F & Morgan JE (2010). Are human and mouse satellite cells really the same? *J Histochem Cytochem* **58,** 941–955.

Bolte S & Cordelieres FP (2006). A guided tour into subcellular colocalisation analysis in light microscopy. *J Microsc* **224,** 13–232.

Boppart MD, Burkin DJ & Kaufman SJ (2006). α 7 β 1 -Integrin regulates mechanotransduction and prevents skeletal muscle injury. *Am J Physiol - Cell Physiol* **290,** 1660–1665.

Borghesan M, Hoogaars WMH, Varela-Eirin M, Talma N & Demaria M (2020). A Senescence-Centric View of Aging: Implications for Longevity and Disease. *Trends Cell Biol*1–15.

Bortoli S, Renault V, Eveno E, Auffray C, Butler-Browne G & Piétu G (2003). Gene expression profiling of human satellite cells during muscular aging using cDNA arrays. *Gene* **321,** 145–154.

Bortoli S, Renault V, Mariage-Samson R, Eveno E, Auffray C, Butler-Browne G & Piétu G (2005). Modifications in the myogenic program induced by in vivo and in vitro aging. *Gene* **347,** 65–72.

Brack AS & Rando TA (2007). Intrinsic changes and extrinsic influences of myogenic stem cell function during aging. *Stem Cell Rev* **3,** 226–237.

Breen L & Phillips SM (2011). Skeletal muscle protein metabolism in the elderly: Interventions to counteract the “anabolic resistance” of ageing. *Nutr Metab* **8,** 68.

Broccoli D, Young JW & De Lange T (1995). Telomerase activity in normal and malignant hematopoietic cells. *Proc Natl Acad Sci U S A* **92,** 9082–9086.

Brooke MH & Kaiser KK (1970). Three “myosin adenosine triphosphatase” systems: the nature of their pH lability and sulfhydryl dependence. *J Histochem Cytochem* **18,** 670–672.

Brooks NE & Myburgh KH (2014). Skeletal muscle wasting with disuse atrophy is multi-dimensional: The response and interaction of myonuclei, satellite cells and signaling pathways. *Front Physiol* **5 MAR,** 1–14.

Brooks S V. & Faulkner JA (1990). Contraction-induced injury: Recovery of skeletal muscles in young and old mice. *Am J Physiol - Cell Physiol*.

Buckingham M & Relaix F (2007). The role of Pax genes in the development of tissues and organs: Pax3 and Pax7 regulate muscle progenitor cell functions. *Annu Rev Cell Dev Biol* **23,** 645–673.

Buckingham M & Relaix F (2015). PAX3 and PAX7 as upstream regulators of myogenesis. *Semin Cell Dev Biol* **44,** 115–125.

Byun HO, Lee YK, Kim JM & Yoon G (2015). From cell senescence to age-related diseases: Differential mechanisms of action of senescence-associated secretory phenotypes. *BMB Rep* **48,** 549–558.

Calado RT & Young NS (2008). Telomere maintenance and human bone marrow failure. *Blood* **111,** 4446–4455.

Campisi J (1997). The biology of replicative senescence. *Eur J Cancer Part A* **33,** 703–709.

Campisi J (2013). Aging, Cellular Senescence, and Cancer. *Annu Rev Physiol* **75,** 685–705.

Campisi J & d'Adda di Fagagna F (2007). Cellular senescence: when bad things happen to good cells. *Nat Rev Mol Cell Biol* **8,** 729–740.

Caremani M, Melli L, Dolfi M, Lombardi V & Linari M (2015). Force and number of myosin motors during muscle shortening and the coupling with the release of the ATP hydrolysis products. *J Physiol* **593,** 3313–3332.

Carlson BM (1973). The Regeneration of Skeletal Muscle - A Review. *Am J Anat*.

Carlson BM & Faulkner J a (1989). Muscle transplantation between young and old rats: age of host determines recovery. *Am J Physiol* **256,** C1262–C1266.

Carlson ME & Conboy IM (2007). Loss of stem cell regenerative capacity within aged niches. *Aging Cell* **6,** 371–382.

Carlson ME, Suetta C & Conboy MJ (2009). Molecular aging and rejuvenation of human muscle stem cells. *EMBO Mol Med* **1,** 381–391.

Carosio S, Berardinelli MG, Aucello M & Musarò A (2011). Impact of ageing on muscle cell regeneration. *Ageing Res Rev* **10,** 35–42.

Carrel A & Ebeling AH (1921). Age and multiplication of fibroblasts. *J Exp Med* **34,** 599–623.

Casella G, Munk R, Kim KM, Piao Y, De S, Abdelmohsen K & Gorospe M (2019). Transcriptome signature of cellular senescence. *Nucleic Acids Res* **47,** 7294–7305.

Chang HY, Chi JT, Dudoit S, Bondre C, Van De Rijn M, Botstein D & Brown PO (2002). Diversity, topographic differentiation, and positional memory in human fibroblasts. *Proc Natl Acad Sci U S A* **99,** 12877–12882.

Charville GW, Cheung TH, Yoo B, Santos PJ, Lee GK, Shrager JB & Rando TA (2015). Ex vivo expansion and in vivo self-renewal of human muscle stem cells. *Stem Cell Reports* **5,** 621–632.

Chen QM, Prowse KR, Tu VC, Purdom S & Linskens MHK (2001). Uncoupling the senescent phenotype from telomere shortening in hydrogen peroxide-treated fibroblasts. *Exp Cell Res* **265,** 294–303.

Cheung TH, Quach NL, Charville GW, Liu L, Park L, Edalati A, Yoo B, Hoang P & Rando TA (2012). Maintenance of muscle stem-cell quiescence by microRNA-489. *Nature* **482,** 524–528.

Childs BG, Baker DJ, Kirkland JL, Campisi J, van Deursen JM & Deursen JM Van (2014). Senescence and apoptosis: dueling or complementary cell fates? *EMBO Rep* **15,** 1–15.

Clase KL, Mitchell PJ, Ward PJ, Dorman CM, Johnson SE & Hannon K (2000). FGF5 stimulates expansion of connective tissue fibroblasts and inhibits skeletal muscle development in the limb. *Dev Dyn* **219,** 368–380.

Collins CA, Olsen I, Zammit PS, Heslop L, Petrie A, Partridge TA & Morgan JE (2005). Stem cell function, self-renewal, and behavioral heterogeneity of cells from the adult muscle satellite cell niche. *Cell* **122,** 289–301.

Collins M, Renault V, Grobler LA, St. Clair Gibson A, Lambert MI, Derman EW, Butler-Browne GS, Noakes TD & Mouly V (2003). Athletes with exercise-associated fatigue have abnormally short muscle DNA telomeres. *Med Sci Sports Exerc* **35,** 1524–1528.

Comai G & Tajbakhsh S (2014). *Molecular and cellular regulation of skeletal myogenesis*, 1st edn. Elsevier Inc.

Combs CA (2010). Fluorescence microscopy: A concise guide to current imaging methods. *Curr Protoc Neurosci*1–19.

Conboy IM, Conboy MJ, Wagers AJ, Girma ER, Weissman IL & Rando TA (2005). Rejuvenation of aged progenitor cells by exposure to a young systemic environment. *Nature* **433,** 760–764.

Cooper C, Dere W, Evans W, Kanis JA, Rizzoli R, Sayer AA, Sieber CC, Kaufman JM, Abellan Van Kan G, Boonen S, Adachi J, Mitlak B, Tsouderos Y, Rolland Y & Reginster JYL (2012). Frailty and sarcopenia: Definitions and outcome parameters. *Osteoporos Int* **23,** 1839–1848.

Cooper RN, Tajbakhsh S, Mouly V, Cossu G, Buckingham M & Butler-Browne GS (1999). In vivo satellite cell activation via Myf5 and MyoD in regenerating mouse skeletal muscle. *J Cell Sci* **112 (Pt 1,** 2895–2901.

Cooper RN, Thiesson D, Furling D, Di Santo JP, Butler-Browne GS & Mouly V (2003). Extended amplification in vitro and replicative senescence: key factors implicated in the success of human myoblast transplantation. *Hum Gene Ther* **14,** 1169–1179.

Coppé J-P, Desprez P-Y, Krtolica A & Campisi J (2010*a*). The Senescence-Associated Secretory Phenotype: The Dark Side of Tumor Suppression. *Annu Rev Pathol*99–118.

Coppé J-P, Patil CK, Rodier F, Sun Y, Muñoz DP, Goldstein J, Nelson PS, Desprez P-Y & Campisi J (2008). Senescence-Associated Secretory Phenotypes Reveal Cell-Nonautonomous Functions of Oncogenic RAS and the p53 Tumor Suppressor. *PLoS Biol* **6,** e301.

Coppé JP, Patil CK, Rodier F, Krtolica A, Beauséjour CM, Parrinello S, Hodgson JG, Chin K, Desprez PY & Campisi J (2010*b*). A human-like senescence-associated secretory phenotype is conserved in mouse cells dependent on physiological oxygen. *PLoS One*; DOI: 10.1371/journal.pone.0009188.

Cornelison DDW & Wold BJ (1997). Single-cell analysis of regulatory gene expression in quiescent and activated mouse skeletal muscle satellite cells. *Dev Biol* **191,** 270–283.

Cottle BJ, Lewis FC, Shone V & Ellison-Hughes GM (2017). Skeletal muscle-derived

interstitial progenitor cells (PICs) display stem cell properties, being clonogenic, self-renewing, and multi-potent in vitro and in vivo. *Stem Cell Res Ther* **8,** 158.

Crown AL, He XL, Holly JMP, Lightman SL & Stewart CEH (2000). Characterisation of the IGF system in a primary adult human skeletal muscle cell model, and comparison of the effects of insulin and IGF-I on protein metabolism. *J Endocrinol* **167,** 403–415.

Cruz-Jentoft A, Landi F & Topinkova E (2010). Understanding sarcopenia as a geriatric syndrome. **13,** 1–7.

Cruz-Jentoft AJ et al. (2019). Sarcopenia: Revised European consensus on definition and diagnosis. *Age Ageing* **48,** 16–31.

d'Adda di Fagagna F (2008). Living on a break: cellular senescence as a DNA-damage response. *Nat Rev Cancer* **8,** 512–522.

D'Antona G, Lanfranconi F, Pellegrino MA, Brocca L, Adami R, Rossi R, Moro G, Miotti D, Canepari M & Bottinelli R (2006). Skeletal muscle hypertrophy and structure and function of skeletal muscle fibres in male body builders. *J Physiol* **570,** 611–627.

Dawson A & Dennison E (2016). Measuring the musculoskeletal aging phenotype. *Maturitas* **93,** 13–17.

Decary S, Ben Hamida C, Mouly V, Barbet JP, Hentati F & Butler-Browne GS (2000). Shorter telomeres in dystrophic muscle consistent with extensive regeneration in young children. *Neuromuscul Disord* **10,** 113–120.

Decary S, Mouly V & Butler-Browne GS (1996). Telomere length as a tool to monitor satellite cell amplification for cell-mediated gene therapy. *Hum Gene Ther* **7,** 1347–1350.

Decary S, Mouly V, Hamida CBEN, Sautet A, Barbet JP & Butler-Browne GS (1997). Replicative potential and telomere length in human skeletal muscle: implications for satellite cell-mediated gene therapy. *Hum Gene Ther* **1438,** 1429–1438.

Delmonico MJ, Harris TB, Lee JS, Visser M, Nevitt M, Kritchevsky SB, Tylavsky FA & Newman AB (2007). Alternative definitions of sarcopenia, lower extremity performance, and functional impairment with aging in older men and women. *J Am Geriatr Soc* **55,** 769–774.

Dennison EM, Sayer AA & Cooper C (2017). Epidemiology of sarcopenia and insight into possible therapeutic targets. *Nat Rev Rheumatol* **13,** 340–347.

Dimri GP, Lee XH, Basile G, Acosta M, Scott C, Roskelley C, Medrano EE, Linskens M, Rubelj I, Pereirasmith O, Peacocke M & Campisi J (1995). A Biomarker That Identifies Senescent Human-Cells in Culture and in Aging Skin in-Vivo. *Proc Natl Acad Sci U S A* **92,** 9363–9367.

Dodds R & Sayer AA (2015). Dodds 2015 Sarcopenia and frailty. *Clin Med (Northfield Il)* **15,** s88–s91.

Di Donna S, Mamchaoui K, Cooper RN, Seigneurin-Venin S, Tremblay J, Butler-Browne GS & Mouly V (2003). Telomerase can extend the proliferative capacity of human myoblasts, but does not lead to their immortalization. *Mol Cancer Res* **1,** 643–653.

Duca KA, Chiu KP, Sullivan T, Berman SA & Bursztajn S (1998). Nuclear clustering in myotubes: A proposed role in acetylcholine receptor mRNA expression. *Biochim Biophys Acta - Mol Cell Res* **1401,** 1–20.

Dumont P, Royer V, Pascal T, Dierick JF, Chainiaux F, Frippiat C, De Magalhaes JP, Eliaers F, Remacle J & Toussaint O (2001). Growth kinetics rather than stress accelerate telomere shortening in cultures of human diploid fibroblasts in oxidative stress-induced premature senescence. *FEBS Lett* **502,** 109–112.

Dunnett CW (1955). A Multiple Comparison Procedure for Comparing Several Treatments with a Control. *J Am Stat Assoc* **50,** 1096–1121.

Elzi DJ, Lai Y, Song M, Hakala K, Weintraub ST & Shiio Y (2012). PAI-1 - Insulin-like growth factor binding protein 3 cascade regulates stress-induced senescence. *Pnas* **109,** 12052–12057.

Eom Y-WW, Kim MA, Park SS, Goo MJ, Kwon HJ, Sohn S, Kim W-HH, Yoon G & Choi KS (2005). Two distinct modes of cell death induced by doxorubicin: Apoptosis and cell death through mitotic catastrophe accompanied by senescence-like phenotype. *Oncogene* **24,** 4765–4777.

Eren M, Boe AE, Murphy SB, Place AT, Nagpal V, Morales-Nebreda L, Urich D, Quaggin SE, Scott Budinger GR, Mutlu GM, Miyata T & Vaughan DE (2014). PAI-1-regulated extracellular proteolysis governs senescence and survival in Klotho mice. *Proc Natl*

Acad Sci U S A **111,** 7090–7095.

Faget D V., Ren Q & Stewart SA (2019). Unmasking senescence: context-dependent effects of SASP in cancer. *Nat Rev Cancer* **19,** 439–453.

Fitts RH (2008). The cross-bridge cycle and skeletal muscle fatigue. *J Appl Physiol* **104,** 551–558.

Franceschi C & Campisi J (2014). Chronic inflammation (Inflammaging) and its potential contribution to age-associated diseases. *Journals Gerontol - Ser A Biol Sci Med Sci* **69,** S4–S9.

Freitas-Rodríguez S, Folgueras AR & López-Otín C (2017). The role of matrix metalloproteinases in aging: Tissue remodeling and beyond. *Biochim Biophys Acta - Mol Cell Res* **1864,** 2015–2025.

Freund A, Orjalo A V, Desprez PY & Campisi J (2010). Inflammatory networks during cellular senescence: causes and consequences. *Trends Mol Med* **16,** 238–246. Available at: http://www.ncbi.nlm.nih.gov/pubmed/20444648 [Accessed May 21, 2017].

Fridman AL & Tainsky MA (2008). Critical pathways in cellular senescence and immortalization revealed by gene expression profiling. *Oncogene* **27,** 5975–5987.

Fried LP, Tangen CM, Walston J, Newman AB, Hirsch C, Gottdiener J, Seeman T, Tracy R, Kop WJ, Burke G & McBurnie MA (2001). Frailty in Older Adults: Evidence for a Phenotype. *Journals Gerontol Ser A Biol Sci Med Sci* **56,** M146–M157.

Frontera WR & Ochala J (2015). Skeletal muscle: a brief review of structure and function. *Calcif Tissue Int* **96,** 183–195.

Fukada S, Uezumi A, Ikemoto M, Masuda S, Segawa M, Tanimura N, Yamamoto H, Miyagoe-Suzuki Y & Takeda S (2007). Molecular signature of quiescent satellite cells in adult skeletal muscle. *Stem Cells* **25,** 2448–2459.

Fulle S, Di Donna S, Puglielli C, Pietrangelo T, Beccafico S, Bellomo R, Protasi F & Fanò G (2005). Age-dependent imbalance of the antioxidative system in human satellite cells. *Exp Gerontol* **40,** 189–197.

García-Plazaola JI, Fernández-Marín B, Duke SO, Hernández A, López-Arbeloa F & Becerril

JM (2015). Autofluorescence: Biological functions and technical applications. *Plant Sci* **236,** 136–145.

García-Prat L, Martínez-Vicente M, Perdiguero E, Ortet L, Rodríguez-Ubreva J, Rebollo E, Ruiz-Bonilla V, Gutarra S, Ballestar E, Serrano AL, Sandri M & Muñoz-Cánoves P (2016). Autophagy maintains stemness by preventing senescence. *Nature* **529,** 37–42.

Gautel M & Djinović-Carugo K (2016). The sarcomeric cytoskeleton: from molecules to motion. *J Exp Biol* **219,** 135–145.

Gewirtz DA (1999). A critical evaluation of the mechanisms of action proposed for the antitumor effects of the anthracycline antibiotics adriamycin and daunorubicin. *Biochem Pharmacol* **57,** 727–741.

Gibson MC & Schultz E (1983). Ily an Accurate Reflection of the Change in the Abso- Lute Number of Satellite Cells. 574–580.

Gillies AR & Lieber RL (2011). Structure and function of the skeletal muscle extracellular matrix. *Muscle and Nerve* **44,** 318–331.

Goh Q, Song T, Petrany MJ, Cramer AA, Sun C, Sadayappan S, Lee SJ & Millay DP (2019). Myonuclear accretion is a determinant of exercise-induced remodeling in skeletal muscle. *Elife*; DOI: 10.7554/eLife.44876.

Goodpaster T, Legesse-Miller A, Hameed MR, Aisner SC, Randolph-Habecker J & Coller HA (2008). An immunohistochemical method for identifying fibroblasts in formalin-fixed, paraffin-embedded tissue. *J Histochem Cytochem* **56,** 347–358.

Gorgoulis V et al. (2019). Cellular Senescence: Defining a Path Forward. *Cell* **179,** 813–827.

Grounds MD, Garrett KL, Lai MC, Wright WE & Beilharz MW (1992). Identification of skeletal muscle precursor cells in vivo by use of MyoD1 and myogenin probes. *Cell Tissue Res* **267,** 99–104.

Gundersen K (2016). Muscle memory and a new cellular model for muscle atrophy and hypertrophy. *J Exp Biol* **219,** 235–242.

Günther S, Kim J, Kostin S, Lepper C, Fan C-MM & Braun T (2013). Myf5-Positive Satellite Cells Contribute to Pax7-Dependent Long-Term Maintenance of Adult Muscle Stem

Cells. *Cell Stem Cell* **13,** 590–601.

Guo K, Wang J, Andrés V, Smith RC & Walsh K (1995). MyoD-induced expression of p21 inhibits cyclin-dependent kinase activity upon myocyte terminal differentiation. *Mol Cell Biol* **15,** 3823–3829.

Halevy O, Novitch BG, Spicer DB, Skapek SX, Rhee J, Hannon GJ, Beach D & Lassar AB (1995). Correlation of terminal cell cycle arrest of skeletal muscle with induction of p21 by MyoD. *Science (80-)* **267,** 1018–1021.

Hampel B, Wagner M, Teis D, Zwerschke W, Huber LA & Jansen-Dürr P (2005). Apoptosis resistance of senescent human fibroblasts is correlated with the absence of nuclear IGFBP-3. *Aging Cell* **4,** 325–330.

Haniffa MA, Collin MP, Buckley CD & Dazzi F (2009). Mesenchymal stem cells: The fibroblasts' new clothes? *Haematologica* **94,** 258–263.

Harper S (2014). Economic and social implications of aging societies. *Science (80-)* **346,** 587–591.

Harridge SDR, Bottinelli R, Canepari M, Pellegrino MA, Reggiani C, Esbjörnsson M & Saltin B (1996). Whole-muscle and single-fibre contractile properties and myosin heavy chain isoforms in humans. *Pflugers Arch Eur J Physiol* **432,** 913–920.

Harridge SDR & Lazarus NR (2017). Physical Activity, Aging, and Physiological Function. *Physiology*; DOI: 10.1152/physiol.00029.2016.

Hayflick L (1965). The limited in vitro lifetime of human diploid cell strains. *Exp Cell Res* **37,** 614–636.

Hayflick L (1998). How and why we age. *Exp Gerontol* **33,** 639–653.

Hayflick L & Moorhead PS (1961). The serial cultivation of human diploid cell strains. *Exp Cell Res* **25,** 585–621.

Heredia JE, Mukundan L, Chen FM, Mueller AA, Deo RC, Locksley RM, Rando TA & Chawla A (2013). Type 2 innate signals stimulate fibro/adipogenic progenitors to facilitate muscle regeneration. *Cell* **153,** 376–388.

Hernández-Hernández JM, García-González EG, Brun CE & Rudnicki MA (2017). The myogenic regulatory factors, determinants of muscle development, cell identity and

regeneration. *Semin Cell Dev Biol* **72,** 10–18.

Hernandez-Segura A, de Jong T V., Melov S, Guryev V, Campisi J & Demaria M (2017). Unmasking Transcriptional Heterogeneity in Senescent Cells. *Curr Biol* **27,** 2652-2660.e4.

Hernandez-Segura A, Nehme J & Demaria M (2018). Hallmarks of Cellular Senescence. *Trends Cell Biol* **28,** 436–453.

Hines WC, Su Y, Kuhn I, Polyak K & Bissell MJ (2014). Sorting out the FACS: A devil in the details. *Cell Rep* **6,** 779–781.

Huang LWM-JJ (1995). Image thresholding by minimizing the measure of fuzziness. *Pattern Recognit*.

Hubackova S, Krejcikova K, Bartek J & Hodny Z (2012). IL1-and TGFβ-Nox4 signaling, oxidative stress and DNA damage response are shared features of replicative, oncogene-induced, and drug-induced paracrine "Bystander senescence." *Aging (Albany NY)* **4,** 932–951.

Hughes VA, Frontera WR, Wood M, Evans WJ, Dallal GE, Roubenoff R & Fiatarone Singh MA (2001). Longitudinal muscle strength changes in older adults: influence of muscle mass, physical activity, and health. *J Gerontol A Biol Sci Med Sci* **56,** B209-17.

Huxley AF (1957). Muscle structure and theories of contraction. *Prog Biophys Biophys Chem* **7,** 255–318.

Huxley AF & Simmons RM (1971). Proposed mechanism of force generation in striated muscle. *Nature* **233,** 533–538.

Itahana K, Campisi J & Dimri GP (2004). Mechanisms of cellular senescence in human and mouse cells. *Biogerontology* **5,** 1–10.

Ito Y, Kayama T & Asahara H (2012). A systems approach and skeletal myogenesis. *Comp Funct Genomics*; DOI: 10.1155/2012/759407.

Jacquemin V, Furling D, Bigot A, Butler-Browne G. S & Mouly V (2004). IGF-1 induces human myotube hypertrophy by increasing cell recruitment. *Exp Cell Res* **299,** 148–158.

Jankowski R, Deasy B & Huard J (2002). Muscle-derived stem cells. *Gene Ther* **9,** 642–647.

Janssen I, Heymsfield SB, Wang Z & Ross R (2000). Skeletal muscle mass and distribution in 468 men and women aged 18-88 yr. *J Appl Physiol* **89,** 81–88.

Joe AWB, Yi L, Natarajan A, Le Grand F, So L, Wang J, Rudnicki MA & Rossi FMV (2010). Muscle injury activates resident fibro/adipogenic progenitors that facilitate myogenesis. *Nat Cell Biol* **12,** 153–163.

Jones D, Round J & Haan A de (2004). *Skeletal muscle from molecules to movement*. Elsevier Ltd.

Jost AP-T & Waters JC (2019). Designing a rigorous microscopy experiment: Validating methods and avoiding bias. *J Cell Biol*jcb.201812109.

Kadi F, Charifi N, Denis C & Lexell J (2004). Satellite cells and myonuclei in young and elderly women and men. *Muscle Nerve* **29,** 120–127.

Kadi F, Ponsot E, Piehl-Aulin K, MacKey A, Kjaer M, Oskarsson E & Holm L (2008). The effects of regular strength training on telomere length in human skeletal muscle. *Med Sci Sports Exerc* **40,** 82–87.

Kaji K & Matsuo M (1979). Doubling potential and calendar time of human diploid cells in vitro. *Exp Gerontol* **14,** 329–334.

Kandalla PK, Goldspink G, Butler-Browne G & Mouly V (2011). Mechano Growth Factor E peptide (MGF-E), derived from an isoform of IGF-1, activates human muscle progenitor cells and induces an increase in their fusion potential at different ages. *Mech Ageing Dev* **132,** 154–162.

Kang MK (1998). Replicative Senescence of Normal Human Oral Keratinocytes Is Associated with the Loss of Telomerase Activity without shortening of Telomeres. *Cell growth Differ* **9,** 85–95.

Kardon G, Harfe BD & Tabin CJ (2003). A Tcf4-positive mesodermal population provides a prepattern for vertebrate limb muscle patterning. *Dev Cell* **5,** 937–944.

Katz B (1961). The Terminations of the Afferent Nerve Fibre in the Muscle Spindle of the Frog. *Philos Trans R Soc London* **243,** 221–240.

Kawamura M, Toiyama Y, Tanaka K, Saigusa S, Okugawa Y, Hiro J, Uchida K, Mohri Y, Inoue Y & Kusunoki M (2012). CXCL5, a promoter of cell proliferation, migration and

invasion, is a novel serum prognostic marker in patients with colorectal cancer. *Eur J Cancer* **48,** 2244–2251.

Keeley TP & Mann GE (2019). Defining physiological normoxia for improved translation of cell physiology to animal models and humans. *Physiol Rev* **99,** 161–234.

Kennedy BK, Berger SL, Brunet A, Campisi J, Cuervo AM, Epel ES, Franceschi C, Lithgow GJ, Morimoto RI, Pessin JE, Rando TA, Richardson A, Schadt EE, Wyss-Coray T & Sierra F (2014). Geroscience: Linking aging to chronic disease. *Cell* **159,** 709–713.

Kirkland JL & Tchkonia T (2017). Cellular Senescence: A Translational Perspective. *EBioMedicine* **21,** 21–28.

Korhonen MT, Mero AA, Alln M, Sipila S, Hakkinen K, Liikavainio T, Viitasalo JT, Haverinen MT & Suominen H (2009). Biomechanical and skeletal muscle determinants of maximum running speed with aging. *Med Sci Sports Exerc* **41,** 844–856.

Kortlever RM, Higgins PJ & Bernards R (2006). Plasminogen activator inhibitor-1 is a critical downstream target of p53 in the induction of replicative senescence. *Nat Cell Biol* **8,** 877–884.

Krishnamurthy J, Torrice C, Ramsey MR, Kovalev GI, Al-Regaiey K, Su L & Sharpless NE (2004). Ink4a/Arf expression is a biomarker of aging. *J Clin Invest* **114,** 1299–1307.

Krizhanovsky V, Xue W, Zender L, Yon M, Hernando E & Lowe SW (2008). Implications of cellular senescence in tissue damage response, tumor suppression, and stem cell biology. *Cold Spring Harb Symp Quant Biol* **73,** 513–522.

Kuang S, Kuroda K, Le Grand F & Rudnicki MA (2007). Asymmetric self-renewal and commitment of satellite stem cells in muscle. *Cell* **129,** 999–1010.

Kuilman T, Michaloglou C, Mooi WJ & Peeper DS (2010). The essence of senescence. *Genes Dev* **24,** 2463–2479.

Kuilman T, Michaloglou C, Vredeveld LCWW, Douma S, van Doorn R, Desmet CJ, Aarden LA, Mooi WJ & Peeper DS (2008). Oncogene-Induced Senescence Relayed by an Interleukin-Dependent Inflammatory Network. *Cell*

Kuilman T & Peeper DS (2009). SMS-ing cellular stress. ; DOI: 10.1038/nrc2560.

Kyo S, Takakura M, Kohama T & Inoue M (1997). Telomerase activity in human

endometrium. *Cancer Res* **57,** 610–614.

Larsen BD, Rampalli S, Burns LE, Brunette S, Dilworth FJ & Megeney LA (2010). Caspase 3/caspase-activated DNase promote cell differentiation by inducing DNA strand breaks. *Proc Natl Acad Sci U S A* **107,** 4230–4235.

Larsson L, Grimby G & Karlsson J (1979). Muscle strength and speed of movement in relation to age and muscle morphology. *J Appl Physiol Respir Environ Exerc Physiol* **46,** 451–456.

Lazarus NR & Harridge SDR (2010). Exercise, Physiological Function, and the Selection of Participants for Aging Research. *J Gerontol Med Sci* **65,** 851–854.

Lazarus NR & Harridge SDR (2017). Declining performance of master athletes: silhouettes of the trajectory of healthy human ageing? *J Physiol* **595,** 2941–2948.

Lee BY, Han JA, Im JS, Morrone A, Johung K, Goodwin EC, Kleijer WJ, DiMaio D & Hwang ES (2006). Senescence-associated β-galactosidase is lysosomal β-galactosidase. *Aging Cell* **5,** 187–195.

Lee JY & Kitaoka M (2018). A beginner's guide to rigor and reproducibility in fluorescence imaging experiments. *Mol Biol Cell* **29,** 1519–1525.

Lees H, Walters H & Cox LS (2016). Animal and human models to understand ageing. *Maturitas* **93,** 18–27.

Leikina E, Gamage DG, Prasad V, Goykhberg J, Crowe M, Diao J, Kozlov MM, Chernomordik L V. & Millay DP (2018). Myomaker and Myomerger Work Independently to Control Distinct Steps of Membrane Remodeling during Myoblast Fusion. *Dev Cell* **46,** 767-780.e7.

Lemos DR, Babaeijandaghi F, Low M, Chang CK, Lee ST, Fiore D, Zhang RH, Natarajan A, Nedospasov SA & Rossi FMV (2015). Nilotinib reduces muscle fibrosis in chronic muscle injury by promoting TNF-mediated apoptosis of fibro/adipogenic progenitors. *Nat Med* **21,** 786–794.

Lepper C, Partridge TA & Fan C-M (2011). An absolute requirement for Pax7-positive satellite cells in acute injury-induced skeletal muscle regeneration. *Development* **138,** 3639–3646.

Lewis-McDougall FC, Ruchaya PJ, Domenjo-Vila E, Shin Teoh T, Prata L, Cottle BJ, Clark JE, Punjabi PP, Awad W, Torella D, Tchkonia T, Kirkland JL & Ellison-Hughes GM (2019). Aged-senescent cells contribute to impaired heart regeneration. *Aging Cell* **18,** 1–15.

Lewis FC, Henning BJ, Marazzi G, Sassoon D, Ellison GM & Nadal-Ginard B (2014). Porcine Skeletal Muscle-Derived Multipotent PW1 pos /Pax7 neg Interstitial Cells: Isolation, Characterization, and Long-Term Culture. *Stem Cells Transl Med* **3,** 702–712.

Lewis WH & Lewis MR (1917). Behavior of cross striated muscle in tissue cultures. *Am J Anat* **22,** 169–194.

Lopez-Otin C, Blasco MA, Partridge L, Serrano M & Kroemer G (2013). The hallmarks of aging. *Cell* **153,** 1194–1217.

Lorenzon P, Bandi E, de Guarrini F, Pietrangelo T, Schäfer R, Zweyer M, Wernig A & Ruzzier F (2004). Ageing affects the differentiation potential of human myoblasts. *Exp Gerontol* **39,** 1545–1554.

Machado L, Lima JE De, Fabre O, Proux C, Szegedi A, Varet H, Ingerslev LR, Barrès R, Mourikis P, Esteves de Lima J, Fabre O, Proux C, Legendre R, Szegedi A, Varet H, Ingerslev LR, Barrès R, Relaix F & Mourikis P (2017). In Situ Fixation Redefines Quiescence and Early Activation of Skeletal Muscle Stem Cells. *Cell Rep* **21,** 1982–1993.

Maciel-Barón LA, Morales-Rosales SL, Aquino-Cruz AA, Triana-Martínez F, Galván-Arzate S, Luna-López A, González-Puertos VY, López-Díazguerrero NE, Torres C & Königsberg M (2016). Senescence associated secretory phenotype profile from primary lung mice fibroblasts depends on the senescence induction stimuli. *Age (Omaha)* **38,** 1–14.

Mahdy MAA (2018). Skeletal muscle fibrosis : an overview. *Cell Tissue Res*; DOI: 10.1007/s00441-018-2955-2.

Malaquin N, Martinez A & Rodier F (2016). Keeping the senescence secretome under control: Molecular reins on the senescence-associated secretory phenotype. *Exp Gerontol* **82,** 39–49.

von Maltzahn J, Chang NC, Bentzinger CF & Rudnicki MA (2012). Wnt signaling in

myogenesis. *Trends Cell Biol* **22,** 602–609.

von Maltzahn J, Jones AE, Parks RJ & Rudnicki MA (2013). Pax7 is critical for the normal function of satellite cells in adult skeletal muscle. *Proc Natl Acad Sci* **110,** 16474–16479.

Malumbres M et al. (2014). Cyclin-dependent kinases. *Genome Biol* **15,** 122.

Martin N, Beach D & Gil J (2014). Ageing as developmental decay: insights from p16INK4a. *Trends Mol Med* **20,** 667–674.

Mathew SJ, Hansen JM, Merrell AJ, Murphy MM, Lawson JA, Hutcheson DA, Hansen MS, Angus-Hill M & Kardon G (2011). Connective tissue fibroblasts and Tcf4 regulate myogenesis. *Development* **138,** 371–384.

Mauro A (1961). SATELLITE CELL OF SKELETAL MUSCLE FIBERS. *J Biophys Biochem Cytol* **9,** 493–495.

Maxwell S. & Delaney H. . (1990). *DESIGNING EXPERIMENTS AND ANALYZING DATA: A Model Comparison Perspective*.

Mayeuf-Louchart A, Hardy D, Thorel Q, Roux P, Gueniot L, Briand D, Mazeraud A, Bouglé A, Shorte SL, Staels B, Chrétien F, Duez H & Danckaert A (2018). MuscleJ: a high-content analysis method to study skeletal muscle with a new Fiji tool. *Skelet Muscle* **8,** 25.

McHugh D & Gil J (2018). Senescence and aging: Causes, consequences, and therapeutic avenues. *J Cell Biol* **217,** 65–77.

McKinnell IW, Ishibashi J, Le Grand F, Punch VGJ, Addicks GC, Greenblatt JF, Dilworth FJ & Rudnicki MA (2008). Pax7 activates myogenic genes by recruitment of a histone methyltransferase complex. *Nat Cell Biol* **10,** 77–84.

McNeal AS, Liu K, Nakhate V, Natale CA, Duperret EK, Capell BC, Dentchev T, Berger SL, Herlyn M, Seykora JT & Ridky TW (2015). CDKN2B loss promotes progression from benign melanocytic nevus to melanoma. *Cancer Discov* **5,** 1072–1085.

Meng J, Adkin CF, Xu S wen, Muntoni F & Morgan JE (2011). Contribution of human muscle-derived cells to skeletal muscle regeneration in dystrophic host mice. *PLoS One*; DOI: 10.1371/journal.pone.0017454.

Metter EJ, Conwit R, Tobin J & Fozard JL (1997). Age-associated loss of power and strength in the upper extremities in women and men. *Journals Gerontol - Ser A Biol Sci Med Sci* **52,** 267–276.

Millay DP, O'Rourke JR, Sutherland LB, Bezprozvannaya S, Shelton JM, Bassel-Duby R & Olson EN (2013). Myomaker is a membrane activator of myoblast fusion and muscle formation. (Supp). *Nature* **499,** 301–305.

Mitchell KJ, Pannerec A, Cadot B, Parlakian A, Besson V, Gomes ER, Marazzi G, Sassoon DA, Pannérec A, Cadot B, Parlakian A, Besson V, Gomes ER, Marazzi G & Sassoon DA (2010). Identification and characterization of a non-satellite cell muscle resident progenitor during postnatal development. *Nat Cell Biol* **12,** 257–266.

Montarras D, L'Honoré A & Buckingham M (2013). Lying low but ready for action: ThMontarras D, L'Honoré A & Buckingham M (2013). Lying low but ready for action: The quiescent muscle satellite cell. FEBS J 280, 4036–4050.e quiescent muscle satellite cell. *FEBS J* **280,** 4036–4050.

Moore DR, Churchward-Venne TA, Witard O, Breen L, Burd NA, Tipton KD & Phillips SM (2015). Protein ingestion to stimulate myofibrillar protein synthesis requires greater relative protein intakes in healthy older versus younger men. *Journals Gerontol - Ser A Biol Sci Med Sci* **70,** 57–62.

Morgan JE, Prola A, Mariot V, Pini V, Meng J, Hourde C, Dumonceaux J, Conti F, Relaix F, Authier FJ, Tiret L, Muntoni F & Bencze M (2018). Necroptosis mediates myofibre death in dystrophin-deficient mice. *Nat Commun*; DOI: 10.1038/s41467-018-06057-9.

Moss F & Leblond CP (1970). Nature of dividing nuclei in skeletal muscle of growing rats. *J Cell Biol* **44,** 459–462.

Mourikis P, Sambasivan R, Castel D, Rocheteau P, Bizzarro V & Tajbakhsh S (2012). A critical requirement for notch signaling in maintenance of the quiescent skeletal muscle stem cell state. *Stem Cells* **30,** 243–252.

Muir AR, Kanji AH & Allbrook D (1965). The structure of the satellite cells in skeletal muscle. *J Anat* **99,** 435–444.

Mukund K & Subramaniam S (2019). Skeletal muscle: A review of molecular structure and

function, in health and disease. *Wiley Interdiscip Rev Syst Biol Med*1–46.

Murphy MM, Lawson JA, Mathew SJ, Hutcheson DA & Kardon G (2011). Satellite cells, connective tissue fibroblasts and their interactions are crucial for muscle regeneration. *Development* **138,** 3625–3637.

Murray MP, Duthie EH, Gambert SR, Sepic SB & Mollinger LA (1985). Age-related differences in knee muscle strength in normal women. *Journals Gerontol* **40,** 275–280.

Nabeshlma Y, Hanaokat K, Hayasakat M, Esuml E & Li S (1993). Myogenin gene disruption muscle defect. **364,** 8–11.

Nakamura AJ, Chiang YJ, Hathcock KS, Horikawa I, Sedelnikova OA, Hodes RJ & Bonner WM (2008). Both telomeric and non-telomeric DNA damage are determinants of mammalian cellular senescence. *Epigenetics Chromatin* **1,** 1–12.

Ndip A, Jude EB & Boulton AJM (2016). CHAPTER 8 Inflammation in Type 2 Diabetes. **1,** 164–179.

Nehlin JO, Just M, Rustan AC & Gaster M (2011). Human myotubes from myoblast cultures undergoing senescence exhibit defects in glucose and lipid metabolism. *Biogerontology* **12,** 349–365.

Nelson G, Wordsworth J, Wang C, Jurk D, Lawless C, Martin-Ruiz C & von Zglinicki T (2012). A senescent cell bystander effect: senescence-induced senescence. *Aging Cell* **11,** 345–349.

Olguin HC & Olwin BB (2004). Pax-7 up-regulation inhibits myogenesis and cell cycle progression in satellite cells: a potential mechanism for self-renewal. *Dev Biol* **275,** 375–388.

Orjalo A V, Bhaumik D, Gengler BK, Scott GK & Campisi J (2009). Cell surface-bound IL-1 is an upstream regulator of the senescence-associated IL-6/IL-8 cytokine network. *Proc Natl Acad Sci* **106,** 17031–17036.

Otsu N (1979). A Threshold Selection Method from Gray-Level Histograms. *IEEE Trans Syst Man Cybern* **9,** 62–66.

Overend TJ, Cunningham DA, Paterson DH & Smith WDF (1992). Physiological responses

of young and elderly men to prolonged exercise at critical power. *Eur J Appl Physiol Occup Physiol* **64,** 187–193.

Page-McCaw A, Ewald AJ & Werb Z (2007). Matrix metalloproteinases and the regulation of tissue remodelling. *Nat Rev Mol Cell Biol* **8,** 221–233.

Parise G & Yarasheski KE (2000). The utility of resistance exercise training and amino acid supplementation for reversing age-associated decrements in muscle protein mass and function. *Curr Opin Clin Nutr Metab Care* **3,** 489–495.

Parrinello S, Coppe J-P, Krtolica A & Campisi J (2005). Stromal-epithelial interactions in aging and cancer: senescent fibroblasts alter epithelial cell differentiation. *J Cell Sci* **118,** 485–496.

Passerieux E, Rossignol R, Letellier T & Delage JP (2007). Physical continuity of the perimysium from myofibers to tendons: Involvement in lateral force transmission in skeletal muscle. *J Struct Biol* **159,** 19–28.

Pawley JB (2006). *Handbook Of Biological Confocal Microscopy*ed. Pawley JB. Springer US, Boston, MA. Available at: http://link.springer.com/10.1007/978-0-387-45524-2.

Pearson S., Young A, Macaluso A, Devito G, Nimmo M., Cobbold M & Harridge SD. (2002). Muscle function in elite master weightlifters. *Med Sci Sports Exerc* **34,** 1199–1206.

Piegari E, De Angelis A, Cappetta D, Russo R, Esposito G, Costantino S, Graiani G, Frati C, Prezioso L, Berrino L, Urbanek K, Quaini F & Rossi F (2013). Doxorubicin induces senescence and impairs function of human cardiac progenitor cells. *Basic Res Cardiol*; DOI: 10.1007/s00395-013-0334-4.

Pietrangelo T, Puglielli C, Mancinelli R, Beccafico S, Fanò G & Fulle S (2009). Molecular basis of the myogenic profile of aged human skeletal muscle satellite cells during differentiation. *Exp Gerontol* **44,** 523–531.

Pilling D, Fan T, Huang D, Kaul B & Gomer RH (2009). Identification of markers that distinguish monocyte-derived fibrocytes from monocytes, macrophages, and fibroblasts. *PLoS One* **4,** 31–33.

Pogogeff IA & Murray MR (1945). Regeneration of adult mammalian skeletal muscle in vitro. *Science (80-)* **101,** 174.

Pogogeff IA & Murray MR (1946). FORM AND BEHAVIOR OF ADULT MAMMALIAN SKELETAL MUSCLE IN VITRO. *Anat Rec* **95,** 321–335.

Pollock RD, Carter S, Velloso CP, Duggal N a., Lord JM, Lazarus NR & Harridge SDR (2015). An investigation into the relationship between age and physiological function in highly active older adults. *J Physiol* **593,** 657–680.

Pollock RD, O'Brien K, Duggal NA, Daniels L, Nielson K, Rowlerson A, Philip A, Lazarus NR, Lord JM & Harridge SDR (2017). Properties of the vastus lateralis muscle in relation to age and physiological function in highly active older individuals aged 55 - 79 years. *Under Rev Aging Cell*; DOI: 10.1111/acel.12735.

Ponsot E, Lexell J & Kadi F (2008). Skeletal muscle telomere length is not impaired in healthy physically active old women and men. *Muscle and Nerve* **37,** 467–472.

Rebbaa A, Zheng X, Chou PM & Mirkin BL (2003). Caspase inhibition switches doxorubicin-induced apoptosis to senescence. *Oncogene* **22,** 2805–2811.

Rebbeck RT, Karunasekara Y, Board PG, Beard NA, Casarotto MG & Dulhunty AF (2014). Skeletal muscle excitation-contraction coupling: Who are the dancing partners? *Int J Biochem Cell Biol* **48,** 28–38.

Renault V, Piron-Hamelin G, Forestier C, DiDonna S, Decary S, Hentati F, Saillant G, Butler-Browne G. & Mouly V (2000). Skeletal muscle regeneration and the mitotic clock. *Exp Gerontol* **35,** 711–719.

Renault V, Rolland E, Thornell LE, Mouly V & Butler-Browne G (2002*a*). Distribution of satellite cells in the human vastus lateralis muscle during aging. *Exp Gerontol* **37,** 1513–1514.

Renault V, Thorne L-E, Eriksson P-O, Butler-Browne G & Mouly V (2002*b*). Regenerative potential of human skeletal muscle during aging. *Aging Cell* **1,** 132–139.

Renault V, Thornell L-E, Butler-Browne G & Mouly V (2002*c*). Human skeletal muscle satellite cells: aging, oxidative stress and the mitotic clock. *Exp Gerontol* **37,** 1229–1236.

Renna LV V., Cardani R, Botta A, Rossi G, Fossati B, Costa E & Meola G (2014). Premature senescence in primary muscle cultures of myotonic dystrophy type 2 is not associated with p16 induction. *Eur J Histochem* **58,** 275–286.

Roberts AI, Lee L, Schwarz E, Groh V, Spies T, Ebert EC & Jabri B (2001). Cutting Edge: NKG2D Receptors Induced by IL-15 Costimulate CD28-Negative Effector CTL in the Tissue Microenvironment. *J Immunol* **167,** 5527–5530.

Rodgers JT, King KY, Brett JO, Cromie MJ, Charville GW, Maguire KK, Brunson C, Mastey N, Liu L, Tsai C-R, Goodell M a & Rando T a (2014). mTORC1 controls the adaptive transition of quiescent stem cells from G0 to G(Alert). *Nature* **509,** 393–396.

Rodier F, Coppé J-P, Patil CK, Hoeijmakers WAM, Muñoz DP, Raza SR, Freund A, Campeau E, Davalos AR & Campisi J (2009). Persistent DNA damage signalling triggers senescence-associated inflammatory cytokine secretion. *Nat Cell Biol* **11,** 973–979.

Rolland Y, CZERWINSKI S, KAN GA VAN, MORLEY JE, CESARI M, ONDER G, WOO J, BAUMGARTNER R, PILLARD F, BOIRIE Y, CHUMLEA WMC & VELLAS B (2008). SARCOPENIA: ITS ASSESSMENT, ETIOLOGY, PATHOGENESIS, CONSEQUENCES AND FUTURE PERSPECTIVES. *J Nutr Heal Aging* **12,** 433–450.

Roman W, Martins JP, Carvalho FA, Voituriez R, Abella JVG, Santos NC, Cadot B, Way M & Gomes ER (2017). Myofibril contraction and crosslinking drive nuclear movement to the periphery of skeletal muscle. *Nat Cell Biol* **19,** 1189–1201.

Rosenberg IH (1997). Symposium : Sarcopenia : Diagnosis and Mechanisms Sarcopenia : Origins and Clinical Relevance. *J Nutr* **127,** 990–991.

Roth SM, Martel GF, Ivey FM, Lemmer JT, Metter EJ, Hurley BF & Rogers MA (2000). Skeletal muscle satellite cell populations in healthy young and older men and women. *Anat Rec* **260,** 351–358.

Rothkamm K, Barnard S, Moquet J, Ellender M, Rana Z & Burdak-Rothkamm S (2015). DNA damage foci: Meaning and significance. *Environ Mol Mutagen* **56,** 491–504.

Royal Statistical Society (2019). Remark AS R94 : A Remark on Algorithm AS 181 : The W-test for Normality Author (s): Patrick Royston Source : Journal of the Royal Statistical Society . Series C (Applied Statistics), Vol . 44 , No . 4 Published by : Wiley for the Royal Statistical Soc. **44,** 547–551.

Rubenstein AB, Smith GR, Raue U, Begue G, Minchev K, Ruf-Zamojski F, Nair VD, Wang X, Zhou L, Zaslavsky E, Trappe TA, Trappe S & Sealfon SC (2020). Single-cell transcriptional profiles in human skeletal muscle. *Sci Rep* **10,** 229.

Sabourin LA, Girgis-gabardo A, Seale P, Asakura A & Rudnicki MA (1999). Reduced Differentiation Potential of Primary. *Cell* **144,** 631–643.

Sajko S, Kubínová L, Cvetko E, Kreft M, Wernig A & Erzen I (2004). Frequency of M-cadherin-stained satellite cells declines in human muscles during aging. *J Histochem Cytochem* **52,** 179–185.

Sajko Š, Kubínová L, Kreft M, Dahmane R, Wernig A & Eržen I (2002). Improving Methodological Strategies for Satellite Cells Counting in Human Muscle During Ageing. *Image Anal Stereol* **21,** 7–12.

Sakuma K & Yamaguchi A (2012). Sarcopenia and age-related endocrine function. *Int J Endocrinol*; DOI: 10.1155/2012/127362.

Sambasivan R, Yao R, Kissenpfennig A, Wittenberghe L Van, Paldi A, Gayraud-morel B, Guenou H, Malissen B, Tajbakhsh S, Galy A, Sambasivan R, Yao R, Kissenpfennig A & Wittenberghe L Van (2011). Pax7-expressing satellite cells are indispensable for adult skeletal muscle regeneration. *Development* **138,** 4333.

Schafer R, Erzen I & Wernig A (2005). Age Dependence of the Human Skeletal Muscle Stem Cell in Forming Muscle Tissue. *Artif Organs* **30,** 130–140.

Schäfer R, Knauf U, Zweyer M, Högemeier O, de Guarrini F, Liu X, Eichhorn HJ, Koch FW, Mundegar RR, Erzen I & Wernig A (2006). Age dependence of the human skeletal muscle stem cell in forming muscle tissue. *Artif Organs* **30,** 130–140.

Scharner J & Zammit PS (2011). The muscle satellite cell at 50: The formative years. *Skelet Muscle* **1,** 1–13.

Schindelin J, Rueden CT, Hiner MC & Eliceiri KW (2015). The ImageJ ecosystem: An open platform for biomedical image analysis. *Mol Reprod Dev* **82,** 518–529.

Schmalbruch H & Hellhammer U (1976). The number of satellite cells in normal human muscle. *Anat Rec* **185,** 279–287.

Scholzen T & Gerdes J (2000). The Ki-67 protein: From the known and the unknown. *J Cell Physiol* **182,** 311–322.

Sciorati C, Rigamonti E, Manfredi AA & Rovere-Querini P (2016). Cell death, clearance and immunity in the skeletal muscle. *Cell Death Differ* **23,** 927–937.

Seale P (2000). Pax7 Is Required for the Specification of Myogenic Satellite Cells. *Cell* **102,** 777–786.

Seale P & Rudnicki MA (2000). A new look at the origin, function, and "stem-cell" status of muscle satellite cells. *Dev Biol* **218,** 115–124.

Seals DR, Justice JN & Larocca TJ (2016). Physiological geroscience: Targeting function to increase healthspan and achieve optimal longevity. *J Physiol* **594,** 2001–2024.

Serrano M (2014). Senescence helps regeneration. *Dev Cell* **31,** 671–672.

Shall S & Stein W (1978). A Mortalization Theory for the Control of Cell Proliferation and for the Origin of Immortal Cell Lines. *J Theor Biol* **76,** 219–231.

Shay JW & Bacchetti S (1997). A survey of telomerase activity in human cancer. *Eur J Cancer Part A* **33,** 787–791.

Shay JW & Wright WE (2000). Hayflick, his limit, and cellular ageing. *Nat Rev Mol Cell Biol* **1,** 72–76.

Shea KL, Xiang W, LaPorta VS, Licht JD, Keller C, Basson MA & Brack AS (2010). Sprouty1 Regulates Reversible Quiescence of a Self-Renewing Adult Muscle Stem Cell Pool during Regeneration. *Cell Stem Cell* **6,** 117–129.

Sherwood RI, Christensen JL, Conboy IM, Conboy MJ, Rando TA, Weissman IL & Wagers AJ (2004). Isolation of adult mouse myogenic progenitors: functional heterogeneity of cells within and engrafting skeletal muscle. *Cell* **119,** 543–554.

Shippen-Lentz D & Blackburn EH (1990). Functional evidence for an RNA template in telomerase. *Science (80-)* **247,** 546–552.

Snijders T, Nederveen JP, McKay BR, Joanisse S, Verdijk LB, van Loon LJC & Parise G (2015). Satellite cells in human skeletal muscle plasticity. *Front Physiol*; DOI: 10.3389/fphys.2015.00283.

Snijders T, Verdijk LB & van Loon LJC (2009). The impact of sarcopenia and exercise training on skeletal muscle satellite cells. *Ageing Res Rev* **8,** 328–338.

Snow MH (1977). The effects of aging on satellite cells in skeletal muscles of mice and rats. *Cell Tissue Res* **185,** 399–408.

Sousa-Victor P, Gutarra S, García-Prat L, Rodriguez-Ubreva J, Ortet L, Ruiz-Bonilla V, Jardí

M, Ballestar E, González S, Serrano AL, Perdiguero E & Muñoz-Cánoves P (2014). Geriatric muscle stem cells switch reversible quiescence into senescence. *Nature* **506,** 316–321.

Spalding KL, Bhardwaj RD, Buchholz BA, Druid H & Frisén J (2005). Retrospective birth dating of cells in humans. *Cell* **122,** 133–143.

Spaulding C, Guo W & Effros RB (1999). Resistance to apoptosis in human CD8+ T cells that reach replicative senescence after multiple rounds of antigen-specific proliferation. *Exp Gerontol* **34,** 633–644.

Stein GH, Drullinger LF, Soulard A & Dulić V (1999). Differential Roles for Cyclin-Dependent Kinase Inhibitors p21 and p16 in the Mechanisms of Senescence and Differentiation in Human Fibroblasts. *Mol Cell Biol* **19,** 2109–2117.

Sun X & Kaufman PD (2018). Ki-67: more than a proliferation marker. *Chromosoma* **127,** 175–186.

Sutermaster BA & Darling EM (2019). Considerations for high-yield, high-throughput cell enrichment: fluorescence versus magnetic sorting. *Sci Rep* **9,** 1–9.

Swann JB & Smyth MJ (2007). Review series Immune surveillance of tumors. *J Clin Invest* **117,** 1137–1146.

Tang H, Geng A, Zhang T, Wang C, Jiang Y & Mao Z (2019). Single senescent cell sequencing reveals heterogeneity in senescent cells induced by telomere erosion. *Protein Cell* **10,** 370–375.

Tapscott SJ (2005). The circuitry of a master switch: Myod and the regulation of skeletal muscle gene transcription. *Development* **132,** 2685–2695.

Tchkonia T, Morbeck DE, Von Zglinicki T, Van Deursen J, Lustgarten J, Scrable H, Khosla S, Jensen MD & Kirkland JL (2010). Fat tissue, aging, and cellular senescence. *Aging Cell* **9,** 667–684.

Tchkonia T, Zhu Y, van Deursen J, Campisi J & Kirkland JL (2013). Cellular senescence and the senescent secretory phenotype: therapeutic opportunities. *J Clin Invest* **123,** 966–972.

Thorn CF, Oshiro C, Marsh S, Hernandez-Boussard T, McLeod H, Klein TE & Altman RB

(2011). Doxorubicin pathways. *Pharmacogenet Genomics* **21,** 440–446.

Tominaga K (2015). The emerging role of senescent cells in tissue homeostasis and pathophysiology. *Pathobiol Aging Age-related Dis* **5,** 27743.

Turgeon MO, Perry NJS & Poulogiannis G (2018). DNA damage, repair, and cancer metabolism. *Front Oncol*; DOI: 10.3389/fonc.2018.00015.

Tuttle CSL, Waaijer MEC, Slee-Valentijn MS, Stijnen T, Westendorp R & Maier AB (2020). Cellular senescence and chronological age in various human tissues: A systematic review and meta-analysis. *Aging Cell* **19,** 1–11.

Uezumi A, Fukada SI, Yamamoto N, Takeda S & Tsuchida K (2010). Mesenchymal progenitors distinct from satellite cells contribute to ectopic fat cell formation in skeletal muscle. *Nat Cell Biol* **12,** 143–152.

Uezumi A, Nakatani M, Ikemoto-Uezumi M, Yamamoto N, Morita M, Yamaguchi A, Yamada H, Kasai T, Masuda S, Narita A, Miyagoe-Suzuki Y, Takeda S, Fukada S ichiro, Nishino I & Tsuchida K (2016). Cell-Surface Protein Profiling Identifies Distinctive Markers of Progenitor Cells in Human Skeletal Muscle. *Stem Cell Reports* **7,** 263–278.

Vandervoort AA (2002). Aging of the human neuromuscular system. *Muscle and Nerve* **25,** 17–25.

Verdijk LB, Koopman R, Schaart G, Meijer K, Savelberg HHCM & van Loon LJC (2007). Satellite cell content is specifically reduced in type II skeletal muscle fibers in the elderly. *Am J Physiol Endocrinol Metab* **292,** E151-7.

Waaijer M, Tuttle C, Slee-Valentijn M, Stijnen T, Westendorp R & Maier A (2018). CELLULAR SENESCENCE AND CHRONOLOGICAL AGE IN VARIOUS HUMAN TISSUES: A SYSTEMATIC REVIEW AND META-ANALYSIS. *Innov Aging* **2,** 94–94.

Wagatsuma A (2007). Adipogenic potential can be activated during muscle regeneration. *Mol Cell Biochem* **304,** 25–33.

Wagner M, Hampel B, Bernhard D, Hala M, Zwerschke W & Jansen-Dürr P (2001). Replicative senescence of human endothelial cells in vitro involves G1 arrest, polyploidization and senescence-associated apoptosis. *Exp Gerontol* **36,** 1327–1347.

Wajapeyee N, Serra RW, Zhu X, Mahalingam M & Green MR (2008). Oncogenic BRAF

Induces Senescence and Apoptosis through Pathways Mediated by the Secreted Protein IGFBP7. *Cell* **132,** 363–374.

Wang YX, Dumont N a & Rudnicki M a (2014). Muscle stem cells at a glance. *J Cell Sci* **127,** 4543–4548.

Waters JC (2009). Accuracy and precision in quantitative fluorescence microscopy. *J Cell Biol* **185,** 1135–1148.

Waters JC & Wittmann T (2014). Concepts in quantitative fluorescence microscopy. In *Methods in Cell Biology*, 1st edn., pp. 1–18. Elsevier Inc. Available at: http://dx.doi.org/10.1016/B978-0-12-420138-5.00001-X.

Weintraub H, Tapscott SJ, Davis RL, Thayer MJ, Adam MA, Lassar AB & Miller AD (1989). Activation of muscle-specific genes in pigment, nerve, fat, liver, and fibroblast cell lines by forced expression of MyoD. *Proc Natl Acad Sci U S A* **86,** 5434–5438.

Wiley CD, Flynn JM, Morrissey C, Lebofsky R, Shuga J, Dong X, Unger MA, Vijg J, Melov S & Campisi J (2017). Analysis of individual cells identifies cell-to-cell variability following induction of cellular senescence. *Aging Cell*1–8.

Wilkinson DJJ, Piasecki M & Atherton PJJ (2018). The age-related loss of skeletal muscle mass and function: Measurement and physiology of muscle fibre atrophy and muscle fibre loss in humans. *Ageing Res Rev* **47,** 123–132.

Wosczyna MN & Rando TA (2018). A Muscle Stem Cell Support Group: Coordinated Cellular Responses in Muscle Regeneration. *Dev Cell* **46,** 135–143.

Wright WE, Piatyszek MA, Rainey WE, Byrd W & Shay JW (1996). Telomerase activity in human germline and embryonic tissues and cells. *Dev Genet* **18,** 173–179.

Xu M et al. (2018). Senolytics improve physical function and increase lifespan in old age. *Nat Med* **24,** 1246–1256.

Xu M, Palmer AK, Ding H, Weivoda MM, Pirtskhalava T, White TA, Sepe A, Johnson KO, Stout MB, Giorgadze N, Jensen MD, LeBrasseur NK, Tchkonia T & Kirkland JL (2015*a*). Targeting senescent cells enhances adipogenesis and metabolic function in old age. *Elife* **4,** e12997.

Xu M, Tchkonia T, Ding H, Ogrodnik M, Lubbers ER, Pirtskhalava T, White TA, Johnson KO,

Stout MB, Mezera V, Giorgadze N, Jensen MD, LeBrasseur NK & Kirkland JL (2015*b*). JAK inhibition alleviates the cellular senescence-associated secretory phenotype and frailty in old age. *Proc Natl Acad Sci U S A* **112,** E6301–E6310.

Xu X, Wilschut KJ, Kouklis G, Tian H, Hesse R, Garland C, Sbitany H, Hansen S, Seth R, Knott PD, Hoffman WY & Pomerantz JH (2015*c*). Human Satellite Cell Transplantation and Regeneration from Diverse Skeletal Muscles. *Stem Cell Reports* **5,** 419–434.

Xue W, Zender L, Miething C, Dickins RA, Hernando E, Krizhanovsky V, Cordon-Cardo C & Lowe SW (2007). Senescence and tumour clearance is triggered by p53 restoration in murine liver carcinomas. *Nature* **445,** 656–660.

Yablonka-Reuveni Z, Rudnicki MA, Rivera AJ, Primig M, Anderson JE & Natanson P (1999*a*). The transition from proliferation to differentiation is delayed in satellite cells from mice lacking MyoD. *Dev Biol* **210,** 440–455.

Yablonka-Reuveni Z, Seger R & Rivera a J (1999*b*). Fibroblast growth factor promotes recruitment of skeletal muscle satellite cells in young and old rats. *J Histochem Cytochem* **47,** 23–42.

Yamamoto DL, Csikasz RI, Li Y, Sharma G, Hjort K, Karlsson R & Bengtsson T (2008). Myotube formation on micro-patterned glass: Intracellular organization and protein distribution in C2C12 skeletal muscle cells. *J Histochem Cytochem* **56,** 881–892.

Yang W & Hu P (2018). Skeletal muscle regeneration is modulated by inflammation. *J Orthop Transl*1–8.

Yin H, Price F & Rudnicki MA (2013). Satellite cells and the muscle stem cell niche. *Physiol Rev* **93,** 23–67.

Yokoyama T, Takano K, Yoshida A, Katada F, Sun P, Takenawa T, Andoh T & Endo T (2007). DA-Raf1, a competent intrinsic dominant-negative antagonist of the Ras-ERK pathway, is required for myogenic differentiation. *J Cell Biol* **177,** 781–793.

Yoshimoto S, Loo TM, Atarashi K, Kanda H, Sato S, Oyadomari S, Iwakura Y, Oshima K, Morita H, Hattori M, Honda K, Ishikawa Y, Hara E & Ohtani N (2013). Obesity-induced gut microbial metabolite promotes liver cancer through senescence secretome. *Nature* **499,** 97–101.

Young A, Stokes M & Crowe M (1984). Size and strength of the quadriceps muscles of old

and young women. *Eur J Clin Invest* **14,** 282–287.

Zammit PS (2006). Pax7 and myogenic progression in skeletal muscle satellite cells. *J Cell Sci* **119,** 1824–1832.

Zammit PS (2017). Function of the myogenic regulatory factors Myf5, MyoD, Myogenin and MRF4 in skeletal muscle, satellite cells and regenerative myogenesis. *Semin Cell Dev Biol* **72,** 19–32.

Zammit PS, Heslop L, Hudon V, Rosenblatt JD, Tajbakhsh S, Buckingham ME, Beauchamp JR & Partridge TA (2002). Kinetics of myoblast proliferation show that resident satellite cells are competent to fully regenerate skeletal muscle fibers. *Exp Cell Res* **281,** 39–49.

Zammit PS, Partridge TA & Yablonka-Reuveni Z (2006). The skeletal muscle satellite cell: the stem cell that came in from the cold. *J Histochem Cytochem* **54,** 1177–1191.

Von Zglinicki T (2002). Oxidative stress shortens telomeres. *Trends Biochem Sci* **27,** 339–344.

Von Zglinicki T, Martin-Ruiz CM & Saretzki G (2005). Telomeres, cell senescence and human ageing. *Signal Transduct* **5,** 103–114.

Zhu CH, Mouly V, Cooper RN, Mamchaoui K, Bigot A, Shay JW, Di Santo JP, Butler-Browne GS & Wright WE (2007). Cellular senescence in human myoblasts is overcome by human telomerase reverse transcriptase and cyclin-dependent kinase 4: Consequences in aging muscle and therapeutic strategies for muscular dystrophies. *Aging Cell* **6,** 515–523.